PhD Thesis Defense

A Cut-Cell-Free Isogeometric Framework Based on the Shifted Boundary Method for Embedded and Multipatch Discretizations

Candidate: **Nicolò Antonelli**

Supervisors: Prof. Riccardo Rossi
Prof. Rubén Zorrilla

PhD Program: Structural Analysis

Universitat Politècnica de Catalunya
Barcelona, 2026

Gecko
Design for IGA-type discretization workflows

Summary

- Introduction & Motivations
- Publication I: SBM-IGA for Poisson (2D/3D)
- Publication II: SBM-IGA + VMS for Stokes, and viscoplastic fluids
- Publication III: Gap–SBM for nonconforming multipatch coupling
- Wrap-up: contributions, limitations, and future work

ELSEVIER
Computer Methods in Applied Mechanics and Engineering
Volume 430, 1 October 2024, 117228

The Shifted Boundary Method in Isogeometric Analysis

Nicolò Antonelli [a b], Ricky Aristio [c], Andrea Gorgi [a b], Rubén Zorrilla [a b], Riccardo Rossi [a b], Guglielmo Scovazzi [d], Roland Wüchner [c]

ELSEVIER
Computer Methods in Applied Mechanics and Engineering
Volume 447, 1 December 2025, 118386

Isogeometric analysis for non-Newtonian viscoplastic fluids: challenges for non-smooth solutions

Nicolò Antonelli [a b], Andrea Gorgi [a b], Rubén Zorrilla [a b], Riccardo Rossi [a b]

ELSEVIER
Computer Methods in Applied Mechanics and Engineering
Volume 456, 1 July 2026, 118913

Isogeometric multipatch coupling with arbitrary refinement and parametrization using the Gap–Shifted Boundary Method

Nicolò Antonelli [a b], Andrea Gorgi [a b], Rubén Zorrilla [a b], Riccardo Rossi [a b]

The thesis is organized around three publications that build one coherent cut-cell-free story.

- **Publication I: SBM-IGA for Poisson (2D/3D)**

Dirichlet penalty-free
Neumann limitations
Condition number analysis

ELSEVIER
Computer Methods in Applied Mechanics and Engineering
Volume 430, 1 October 2024, 117228

The Shifted Boundary Method in Isogeometric Analysis

Nicolò Antonelli [a b], Ricky Aristio [c], Andrea Gorgi [a b], Rubén Zorrilla [a b], Riccardo Rossi [a b], Guglielmo Scovazzi [d], Roland Wüchner [c]

ELSEVIER
Computer Methods in Applied Mechanics and Engineering
Volume 447, 1 December 2025, 118386

Isogeometric analysis for non-Newtonian viscoplastic fluids: challenges for non-smooth solutions

Nicolò Antonelli [a b], Andrea Gorgi [a b], Rubén Zorrilla [a b], Riccardo Rossi [a b]

ELSEVIER
Computer Methods in Applied Mechanics and Engineering
Volume 456, 1 July 2026, 118913

Isogeometric multipatch coupling with arbitrary refinement and parametrization using the Gap–Shifted Boundary Method

Nicolò Antonelli [a b], Andrea Gorgi [a b], Rubén Zorrilla [a b], Riccardo Rossi [a b]

The thesis is organized around three publications that build one coherent cut-cell-free story.

- **Publication II: SBM-IGA + VMS for Stokes, and viscoplastic fluids**

Extention to Stokes fluids
Bingham fluids benchmarks
Limitations for non-smooth solutions

Computer Methods in Applied Mechanics and Engineering
Volume 447, 1 December 2025, 118386

Isogeometric analysis for non-Newtonian viscoplastic fluids: challenges for non-smooth solutions

Nicolò Antonelli [a b], Andrea Gorgi [a b], Rubén Zorrilla [a b], Riccardo Rossi [a b]

Computer Methods in Applied Mechanics and Engineering
Volume 430, 1 October 2024, 117228

The Shifted Boundary Method in Isogeometric Analysis

Nicolò Antonelli [a b], Ricky Aristio [c], Andrea Gorgi [a b], Rubén Zorrilla [a b], Riccardo Rossi [a b], Guglielmo Scovazzi [d], Roland Wüchner [c]

Computer Methods in Applied Mechanics and Engineering
Volume 456, 1 July 2026, 118913

Isogeometric multipatch coupling with arbitrary refinement and parametrization using the Gap–Shifted Boundary Method

Nicolò Antonelli [a b], Andrea Gorgi [a b], Rubén Zorrilla [a b], Riccardo Rossi [a b]

The thesis is organized around three publications that build one coherent cut-cell-free story.

- **Publication III: Gap–SBM for nonconforming multipatch coupling**

Penalty-free Gap-SBM coupling
Comparison vs. Body-fitted coupling
Allows local h- or p- refinement
Condition number analysis

ELSEVIER
Computer Methods in Applied Mechanics and Engineering
Volume 456, 1 July 2026, 118913

Isogeometric multipatch coupling with arbitrary refinement and parametrization using the Gap–Shifted Boundary Method

Nicolò Antonelli [a b], Andrea Gorgi [a b], Rubén Zorrilla [a b], Riccardo Rossi [a b]

ELSEVIER
Computer Methods in Applied Mechanics and Engineering
Volume 430, 1 October 2024, 117228

The Shifted Boundary Method in Isogeometric Analysis

Nicolò Antonelli [a b], Ricky Aristio [c], Andrea Gorgi [a b], Rubén Zorrilla [a b], Riccardo Rossi [a b], Guglielmo Scovazzi [d], Roland Wüchner [c]

ELSEVIER
Computer Methods in Applied Mechanics and Engineering
Volume 447, 1 December 2025, 118386

Isogeometric analysis for non-Newtonian viscoplastic fluids: challenges for non-smooth solutions

Nicolò Antonelli [a b], Andrea Gorgi [a b], Rubén Zorrilla [a b], Riccardo Rossi [a b]

Introduction: FEM and IGA

- In standard FEM, geometry and solution approximation are built with different representations

- In IGA, the same spline basis functions are used CAD geometry and analysis ⇒ exact geometry representation at the analysis level

- IGA provides high-order and highly continuous approximation spaces; compared to FEM, IGA can achieve higher accuracy **per degree of freedom**

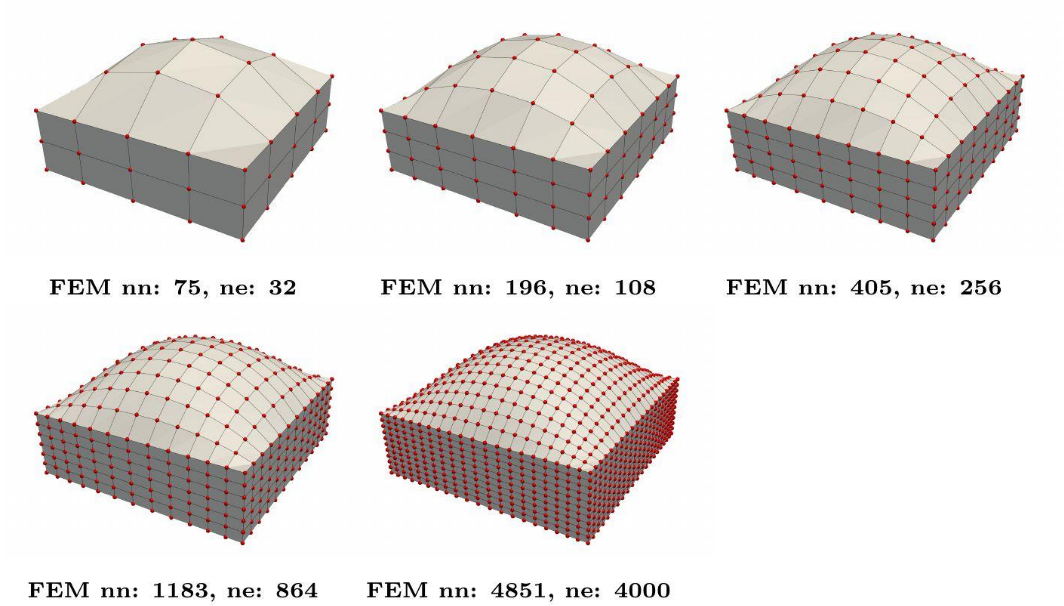

IGA vs. FEM. Image taken from [1]

[1] W. Fukuda. 3D-IGA Mesh vs. 3D-FEM Mesh. 2025.

Introduction: FEM and IGA

- In standard FEM, geometry and solution approximation are built with different representations
- In IGA, the same spline basis functions are used CAD geometry and analysis ⇒ exact geometry representation at the analysis level
- IGA provides high-order and highly continuous approximation spaces; compared to FEM, IGA can achieve higher accuracy **per degree of freedom**

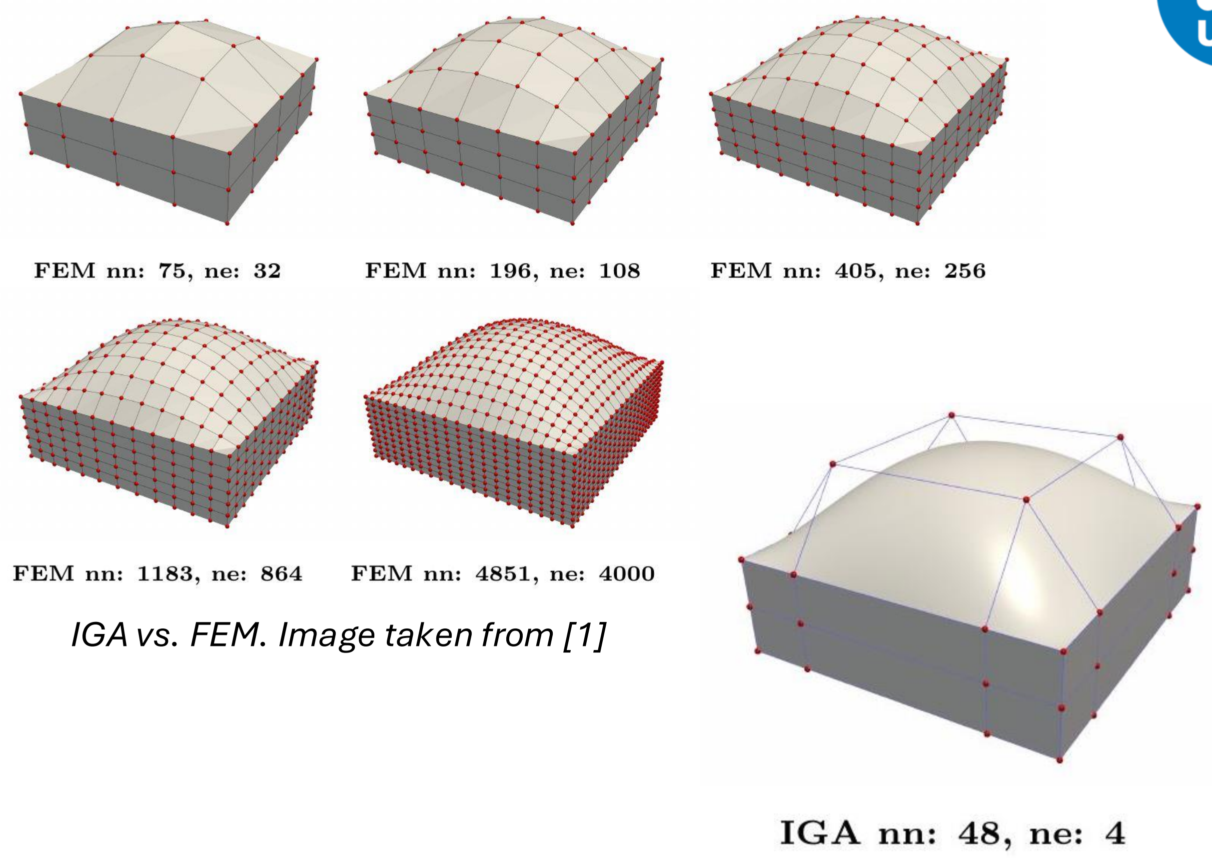

IGA vs. FEM. Image taken from [1]

[1] W. Fukuda. 3D-IGA Mesh vs. 3D-FEM Mesh. 2025.

Introduction: FEM and IGA

- In standard FEM, geometry and solution approximation are built with different representations
- In IGA, the same spline basis functions are used CAD geometry and analysis ⇒ exact geometry representation at the analysis level
- IGA provides high-order and highly continuous approximation spaces; compared to FEM, IGA can achieve higher accuracy **per degree of freedom**

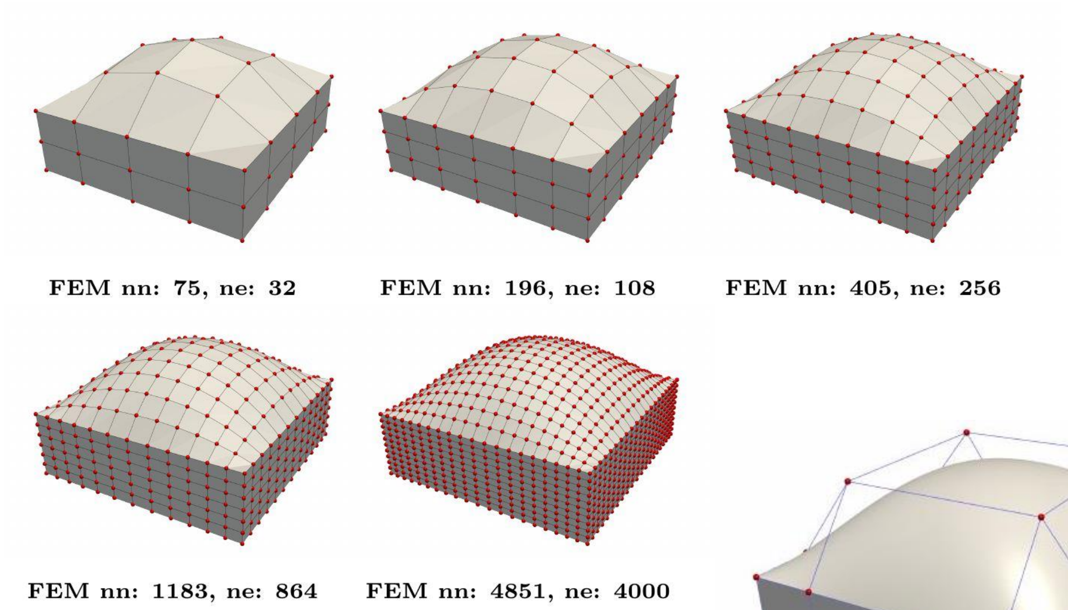

IGA vs. FEM. Image taken from [1]

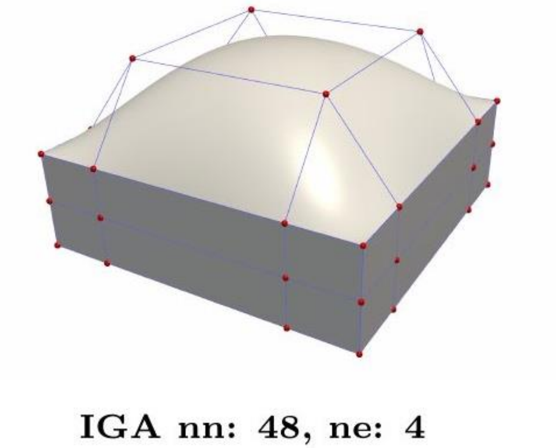

[1] W. Fukuda. 3D-IGA Mesh vs. 3D-FEM Mesh. 2025.

Industrial CAD geometry makes analysis-suitable parameterizations the main bottleneck for standard IGA

- CAD are mainly defined by Boundary Representation (B-Rep) modelling (not body-fitted)
- Complex CAD models are inherently multipatch and often non-watertight

As a result, constructing analysis-suitable volumetric multipatch parametrizations requires substantial human intervention and remains costly and fragile

New family of embedded methods started to appear: FCM, IBRA, QueSO, …

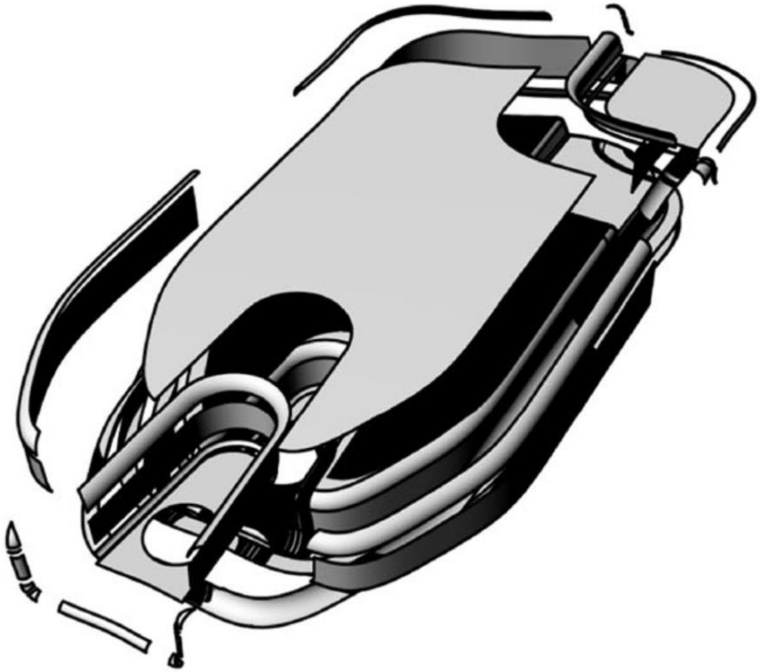

Multipatch model. Image taken from [2]

[2] Realization of CAD-integrated shell simulation based on isogeometric B-Rep analysis. T. Teschemacher , A. M. Bauer , T. Oberbichler, M. Breitenberger, R. Rossi, R. Wüchner and K.-U. Bletzinger, 2018.

Industrial CAD geometry makes analysis-suitable parameterizations the main bottleneck for standard IGA

- CAD are mainly defined by Boundary Representation (B-Rep) modelling (not body-fitted)
- Complex CAD models are inherently multipatch and often non-watertight

As a result, constructing analysis-suitable volumetric multipatch parametrizations requires substantial human intervention and remains costly and fragile

New family of embedded methods started to appear: FCM, IBRA, QueSO, ...

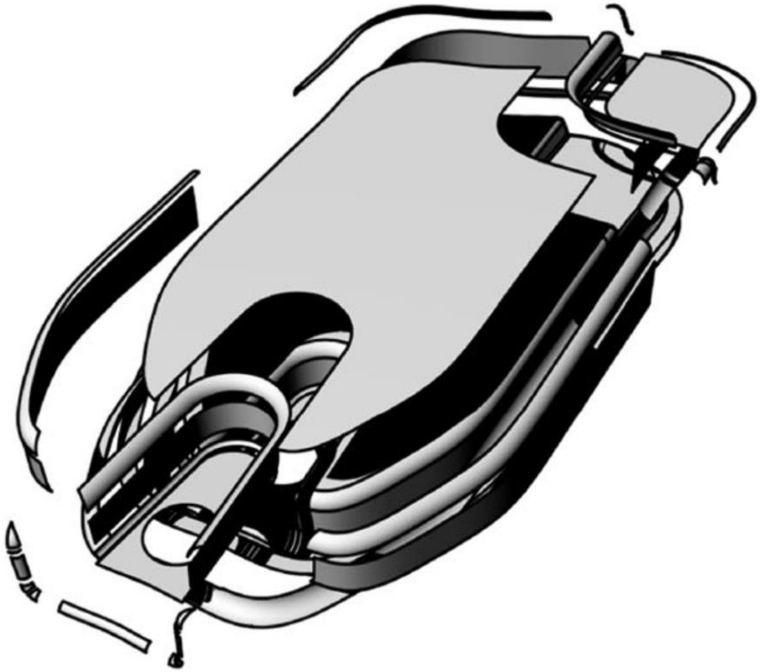

Multipatch model. Image taken from [2]

[2] Realization of CAD-integrated shell simulation based on isogeometric B-Rep analysis. T. Teschemacher , A. M. Bauer , T. Oberbichler, M. Breitenberger, R. Rossi, R. Wüchner and K.-U. Bletzinger, 2018.

Industrial CAD geometry makes analysis-suitable parameterizations the main bottleneck for standard IGA

- CAD are mainly defined by Boundary Representation (B-Rep) modelling (not body-fitted)
- Complex CAD models are inherently multipatch and often non-watertight

As a result, constructing analysis-suitable volumetric multipatch parametrizations requires substantial human intervention and remains costly and fragile

New family of embedded methods started to appear: FCM, IBRA, QueSO, ...

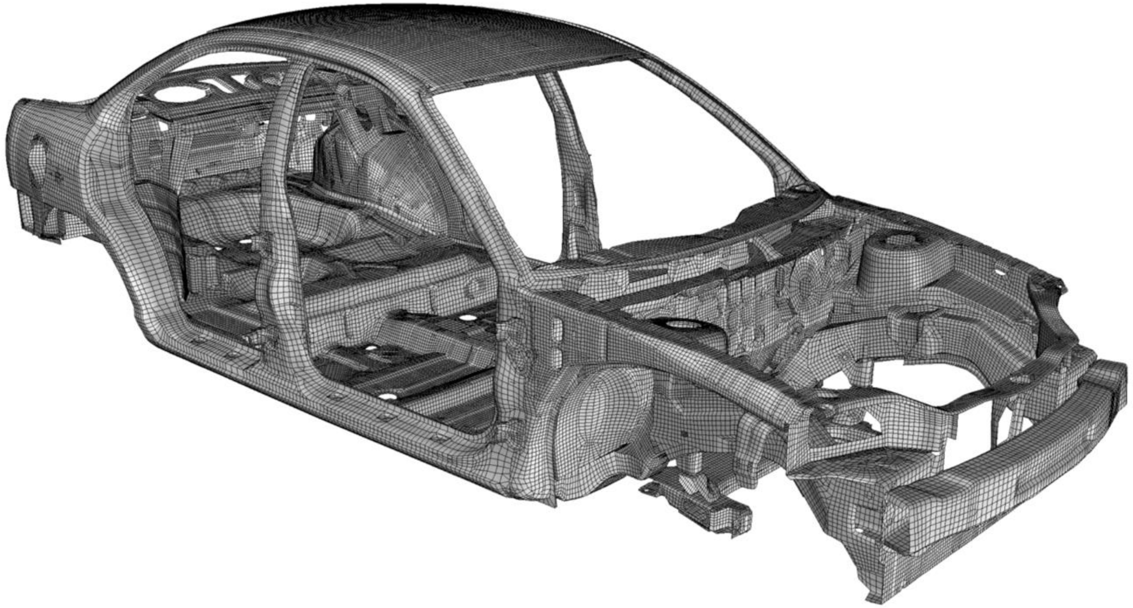

Parametrized multipatch model. Image taken from LS-DYNA [3]

[3] Implicit Roof Crush LS-DYNA, https://lsdyna.ansys.com/implicit-roofcrush, 2026.

Industrial CAD geometry makes analysis-suitable parameterizations the main bottleneck for standard IGA

- CAD are mainly defined by Boundary Representation (B-Rep) modelling (not body-fitted)
- Complex CAD models are inherently multipatch and often non-watertight

As a result, constructing analysis-suitable volumetric multipatch parametrizations requires substantial human intervention and remains costly and fragile

New family of embedded methods started to appear: FCM, IBRA, QueSO, ...

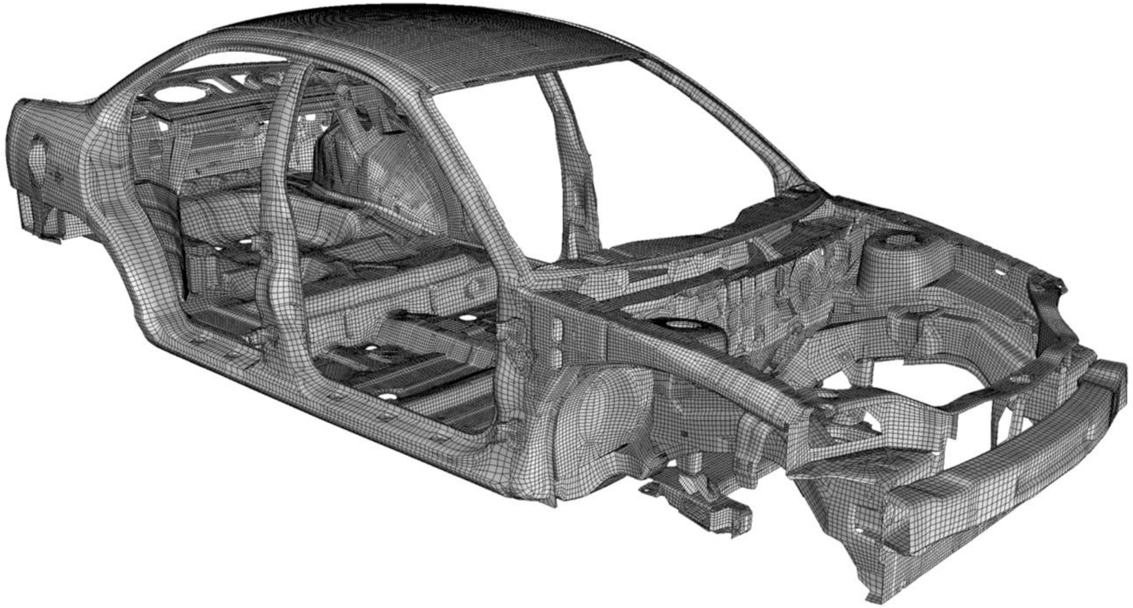

Parametrized multipatch model. Image taken from LS-DYNA [3]

[3] Implicit Roof Crush LS-DYNA, https://lsdyna.ansys.com/implicit-roofcrush, 2026.

From IGA to embedded IGA: a brief historical perspective

- To handle complex geometries, the field evolved toward **embedded IGA formulations**
- **Finite Cell Method (FCM)** high-order analysis can be performed on geometrically complex domains
- **Isogeometric B-Rep Analysis (IBRA)** pushed CAD-integrated analysis further by working directly with trimmed geometries
- **Quadrature for Embedded Solids (QueSO)** advanced CAD-integrated embedded IGA for **3D solid analysis**

From IGA to embedded IGA: a brief historical perspective

- To handle complex geometries, the field evolved toward **embedded IGA formulations**
- **Finite Cell Method (FCM)** high-order analysis can be performed on geometrically complex domains
- **Isogeometric B-Rep Analysis (IBRA)** pushed CAD-integrated analysis further by working directly with trimmed geometries
- **Quadrature for Embedded Solids (QueSO)** advanced CAD-integrated embedded IGA for **3D solid analysis**

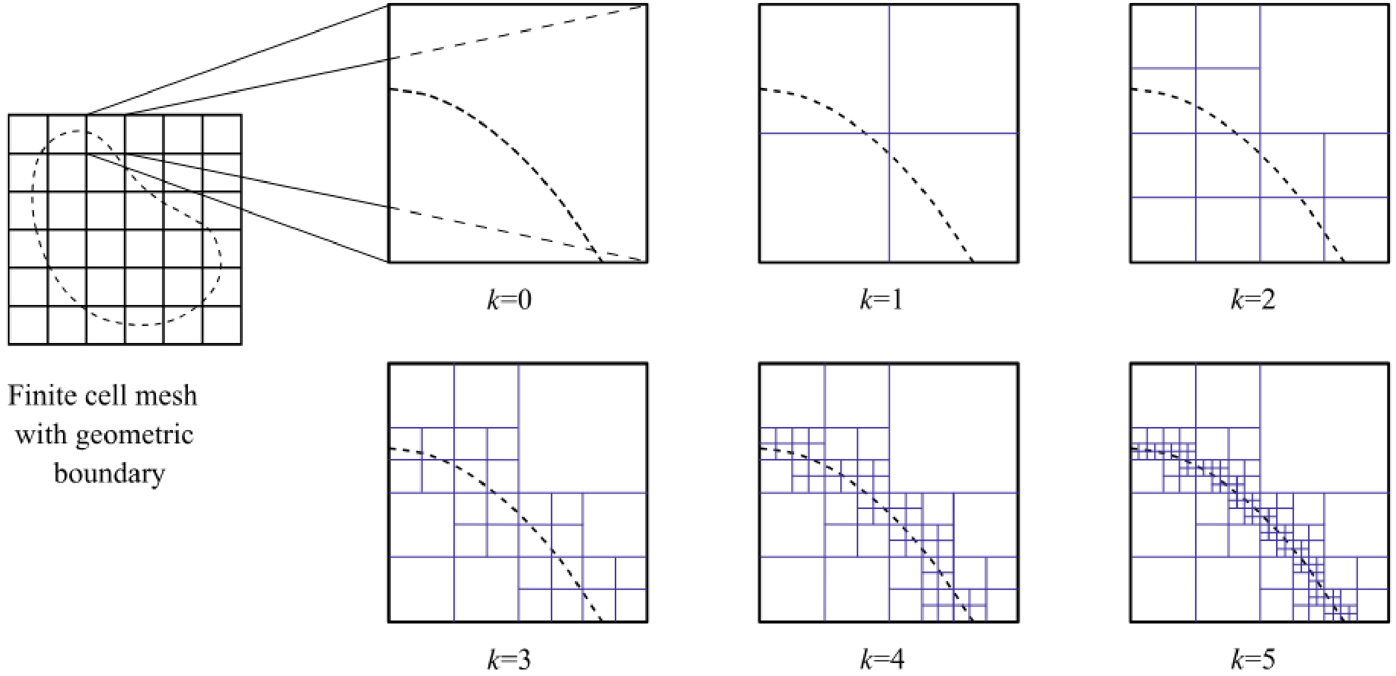

Finite Cell Method. Image taken from [4]

[4] Schillinger, Ruess, *The Finite Cell Method: A Review in the Context of Higher-Order Structural Analysis of CAD and Image-Based Geometric Models*, 2014.

From IGA to embedded IGA: a brief historical perspective

- To handle complex geometries, the field evolved toward **embedded IGA formulations**
- **Finite Cell Method (FCM)** high-order analysis can be performed on geometrically complex domains
- **Isogeometric B-Rep Analysis (IBRA)** pushed CAD-integrated analysis further by working directly with trimmed geometries
- **Quadrature for Embedded Solids (QueSO)** advanced CAD-integrated embedded IGA for **3D solid analysis**

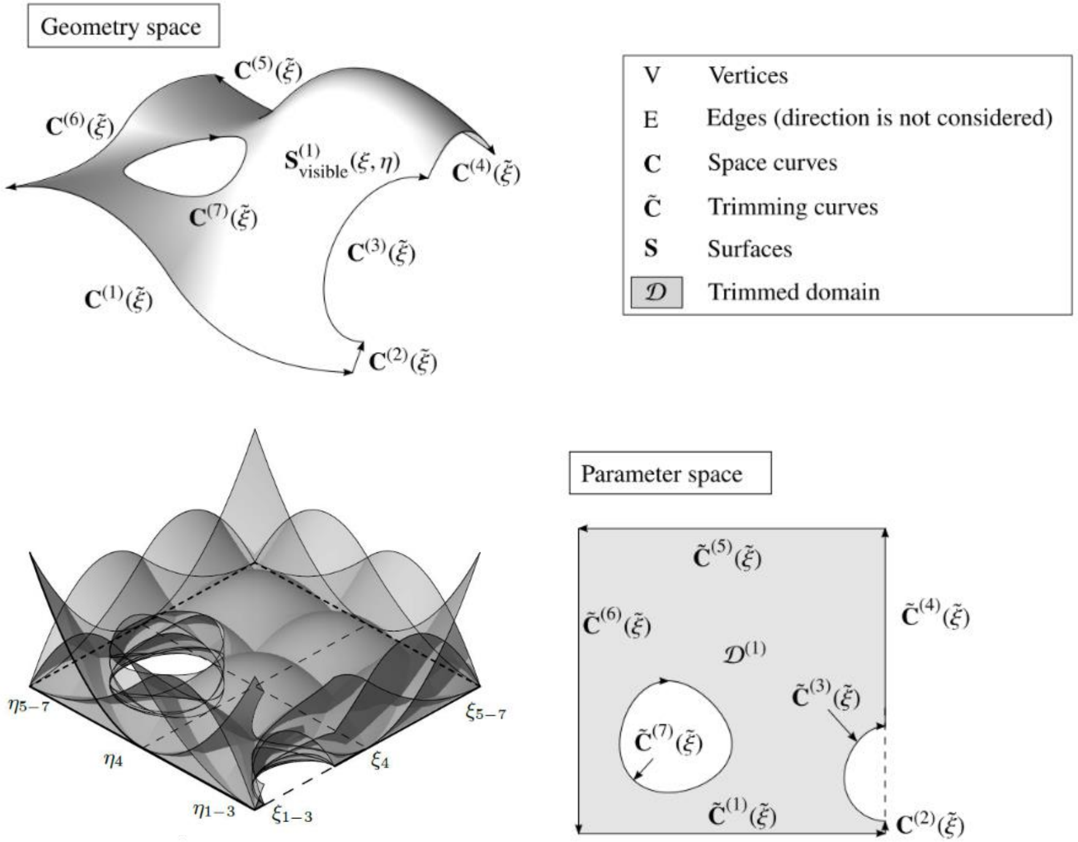

IBRA method. Image taken from [5]

[5] Philipp, Breitenberger, Wüchner, Bletzinger, *Membrane structures with the Isogeometric B-Rep Analysis (IBRA)*, 2015.

From IGA to embedded IGA: a brief historical perspective

- To handle complex geometries, the field evolved toward **embedded IGA formulations**
- **Finite Cell Method (FCM)** high-order analysis can be performed on geometrically complex domains
- **Isogeometric B-Rep Analysis (IBRA)** pushed CAD-integrated analysis further by working directly with trimmed geometries
- **Quadrature for Embedded Solids (QueSO)** advanced CAD-integrated embedded IGA for **3D solid analysis**

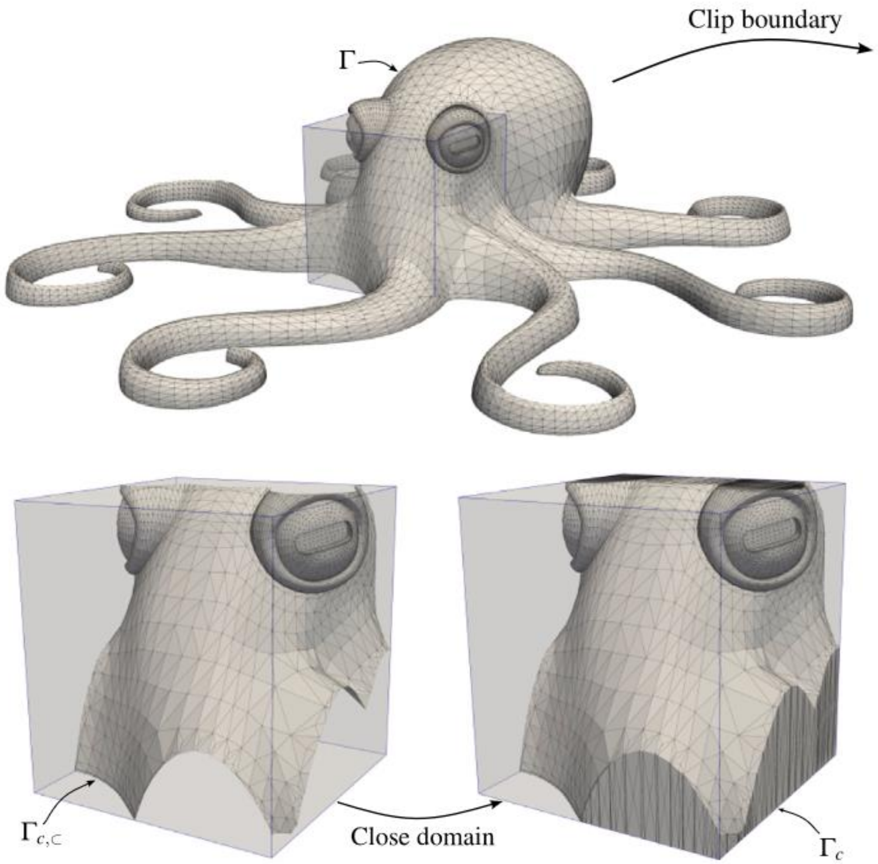

QueSO method. Image taken from [6]

[6] Meßmer, Kollmannsberger, Wüchner, Bletzinger, *Robust numerical integration of embedded solids described in boundary representation*, 2019.

From IGA to embedded IGA: a brief historical perspective

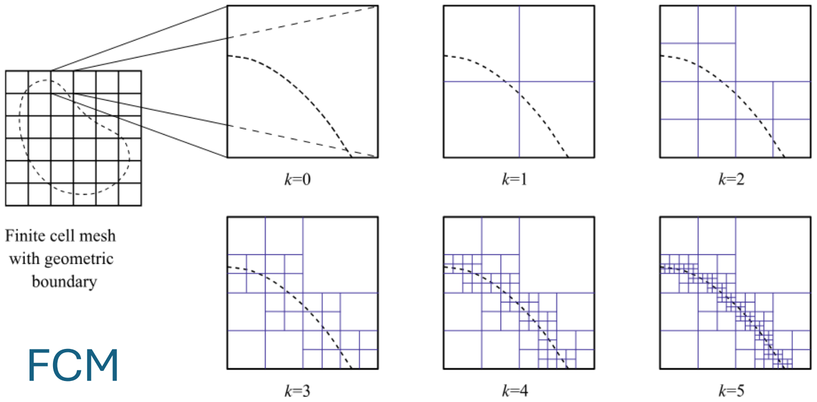

FCM

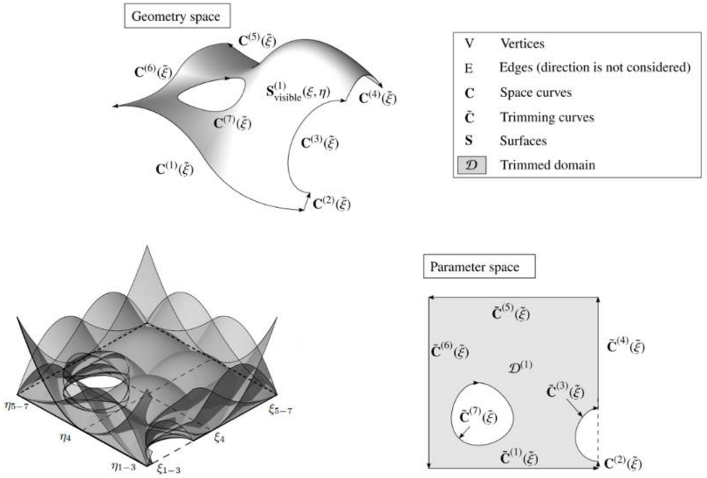

IBRA

However, these methods still rely on unfitted / trimmed integration, which may generate **small cut-cell instabilities and ill-conditioning**

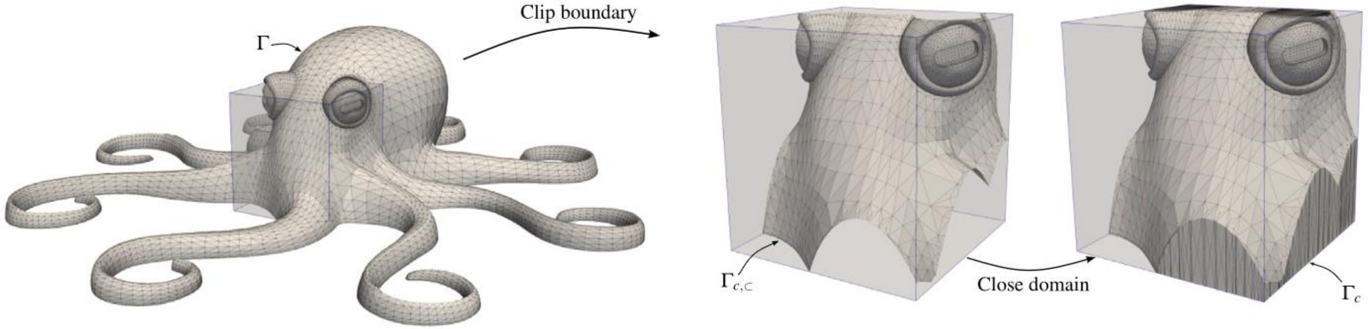

QueSO

The small cut-cell instability in CutFEM-like methods

Some active basis functions may have support only on a very small cut portion of the physical domain

Their contribution to the discrete system becomes extremely small, which leads to severe ill-conditioning

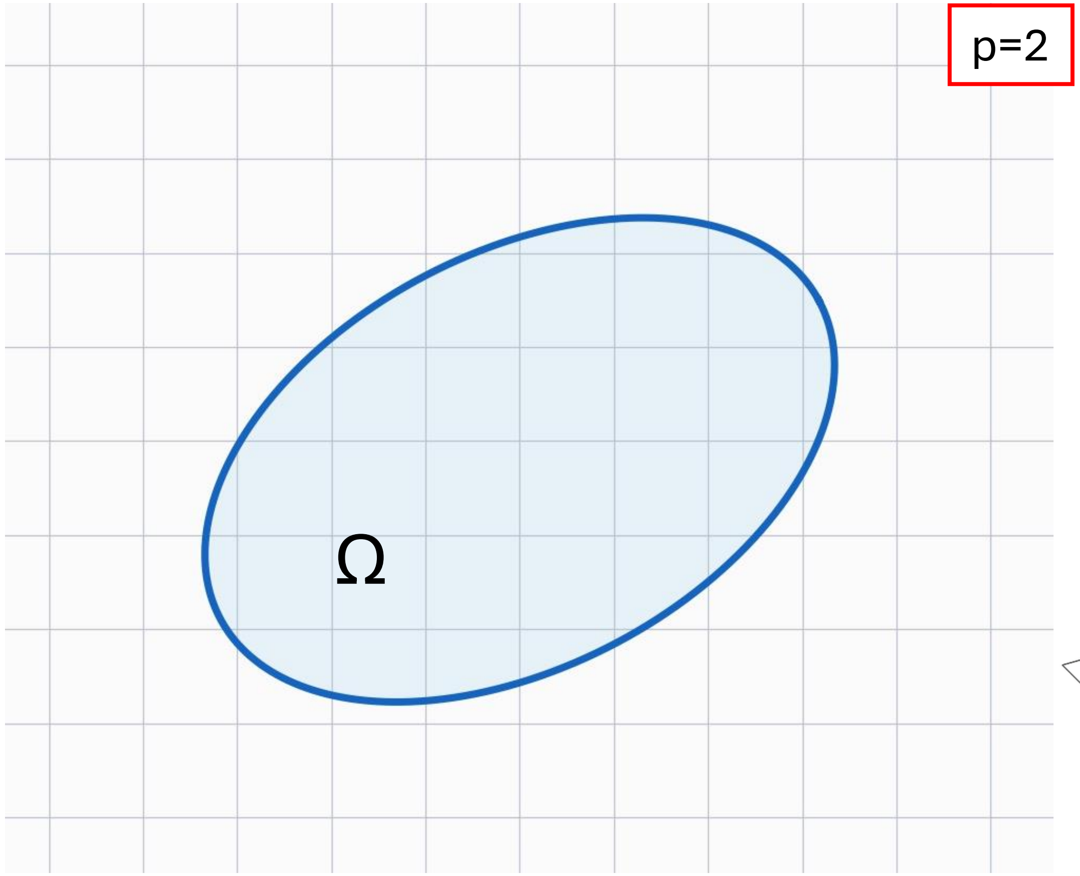

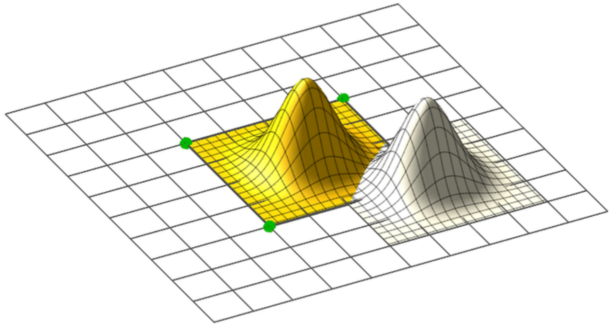

The small cut-cell instability in CutFEM-like methods

Some active basis functions may have support only on a very small cut portion of the physical domain

Their contribution to the discrete system becomes extremely small, which leads to severe ill-conditioning

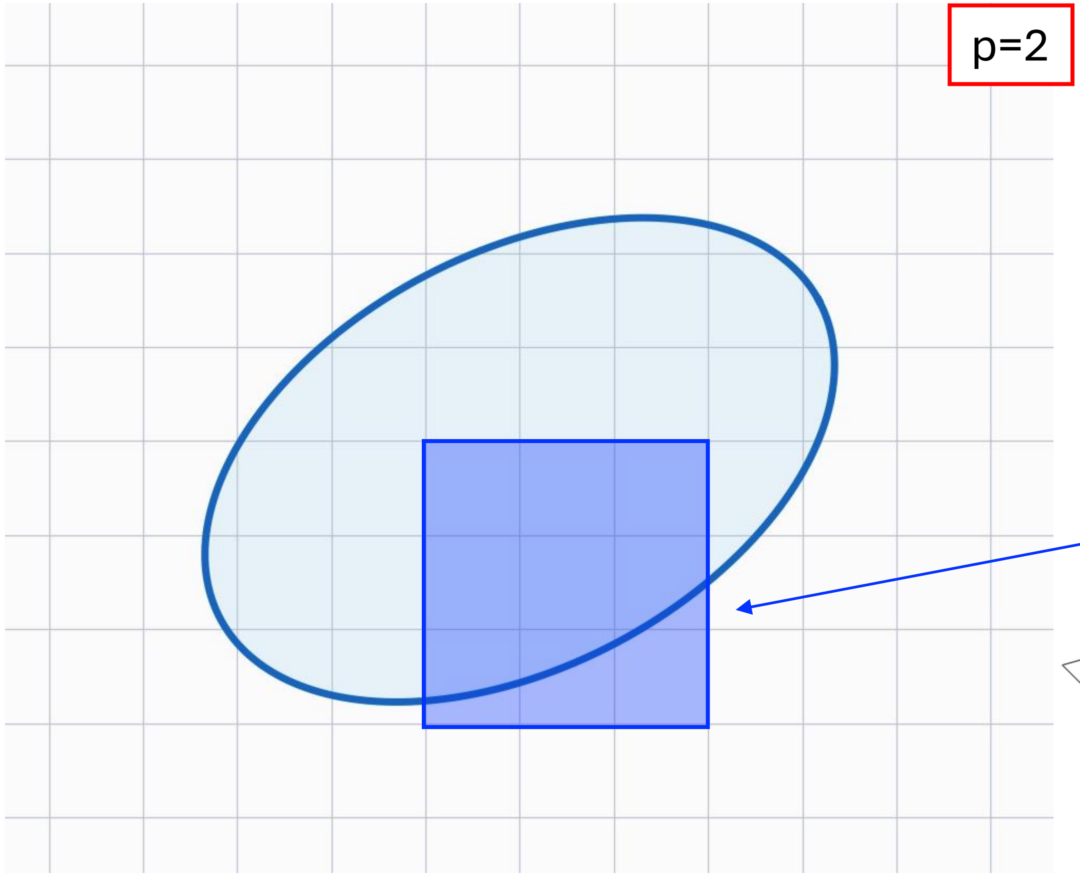

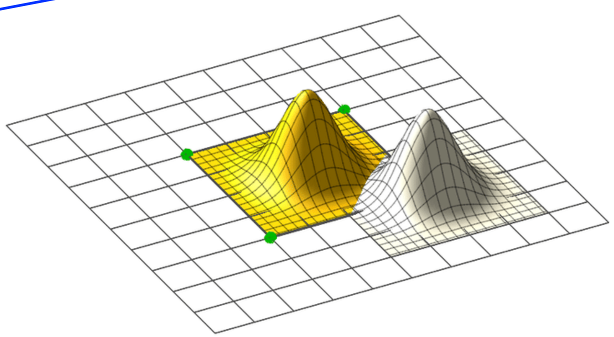

The small cut-cell instability in CutFEM-like methods

Some active basis functions may have support only on a very small cut portion of the physical domain

Their contribution to the discrete system becomes extremely small, which leads to severe ill-conditioning

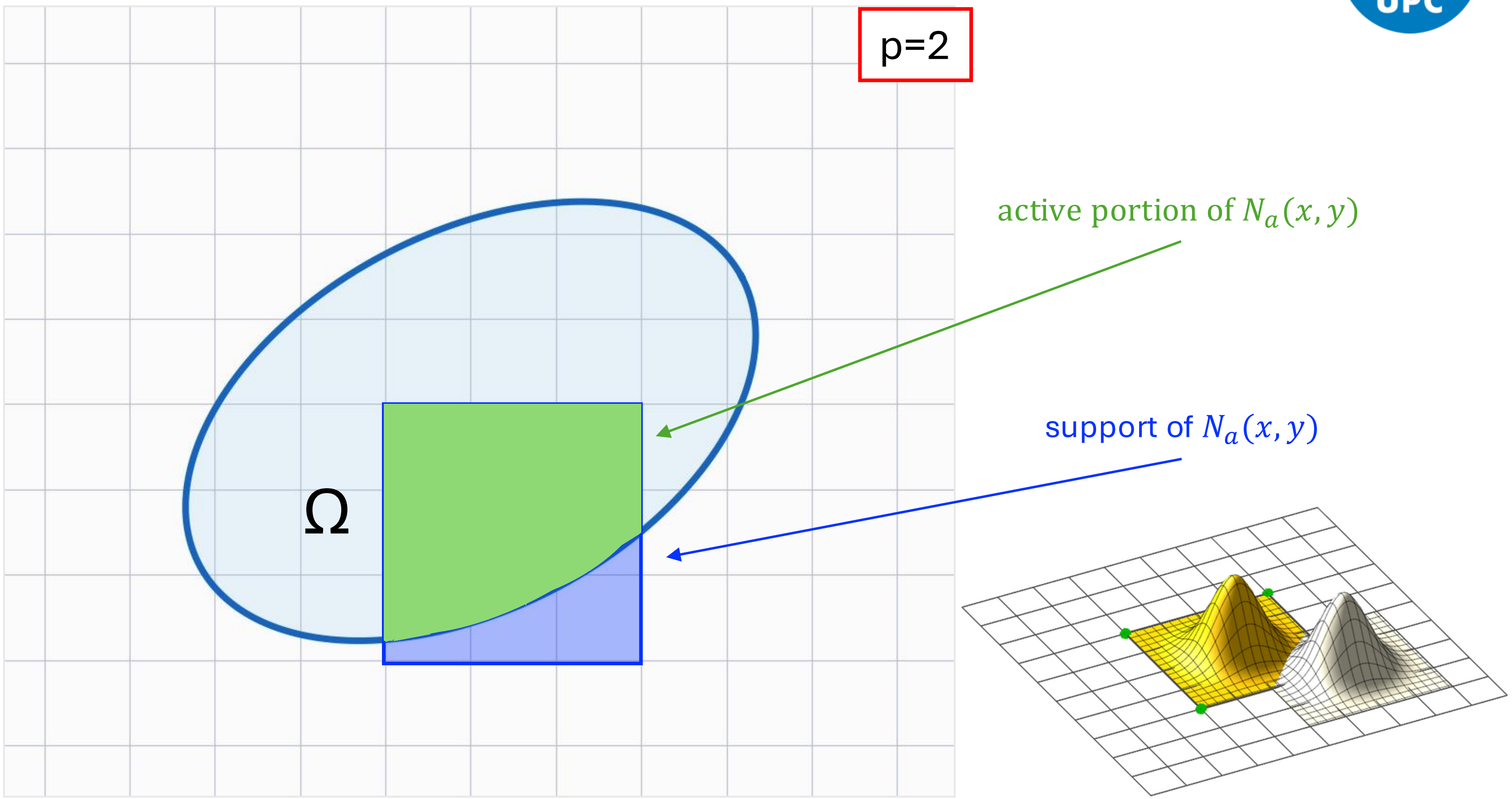

The small cut-cell instability in CutFEM-like methods

Some active basis functions may have support only on a very small cut portion of the physical domain

Their contribution to the discrete system becomes extremely small, which leads to severe ill-conditioning

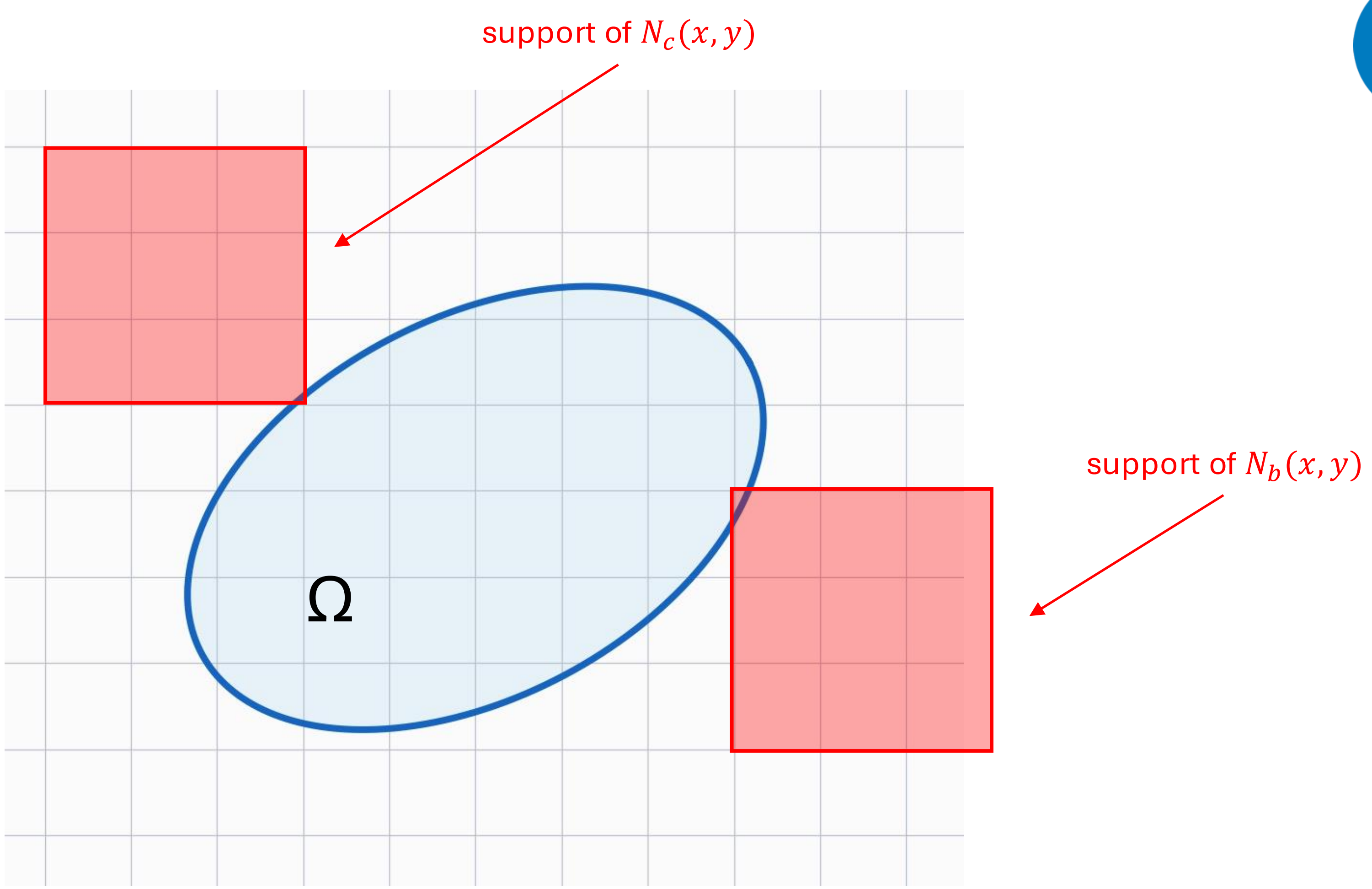

The small cut-cell instability in CutFEM-like methods

Some active basis functions may have support only on a very small cut portion of the physical domain

Their contribution to the discrete system becomes extremely small, which leads to severe ill-conditioning

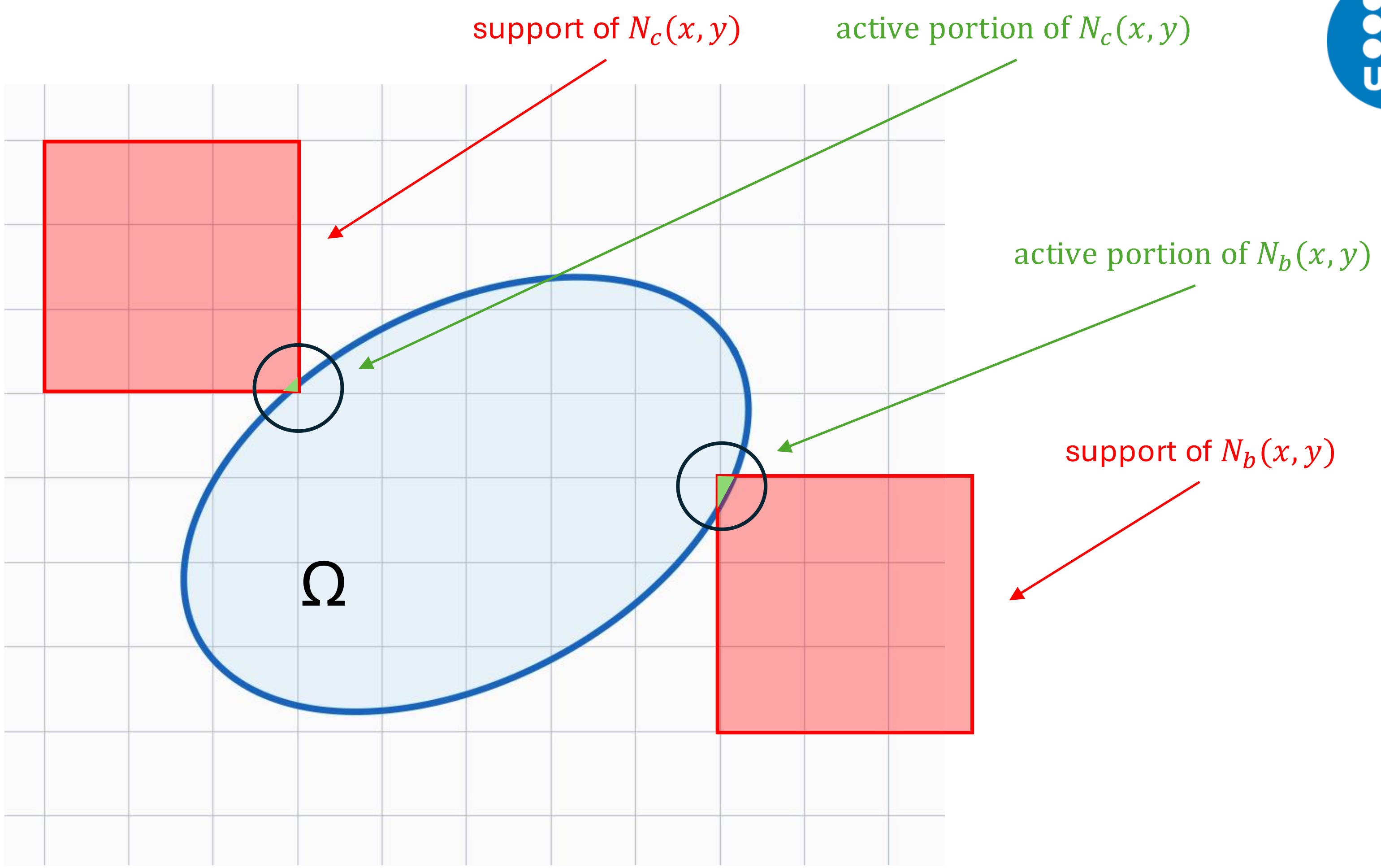

Small cut-cells drive ill-conditioning and solver degradation in embedded IGA

Trimming / unfitted integration can create arbitrarily small cut contributions

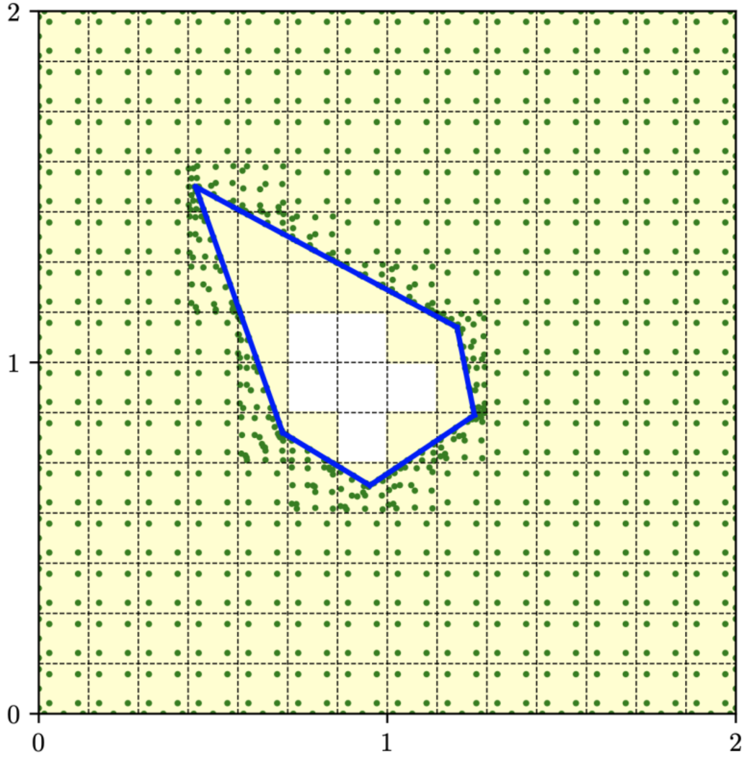

IBRA [5]

[5] Philipp, Breitenberger, Wüchner, Bletzinger, *Membrane structures with the Isogeometric B-Rep Analysis (IBRA)*, 2015.

Small cut-cells drive ill-conditioning and solver degradation in embedded IGA

Trimming / unfitted integration can create arbitrarily small cut contributions

As a result:

- The condition number grows unboundedly under refinement
- Iterative solvers and preconditioners become unreliable

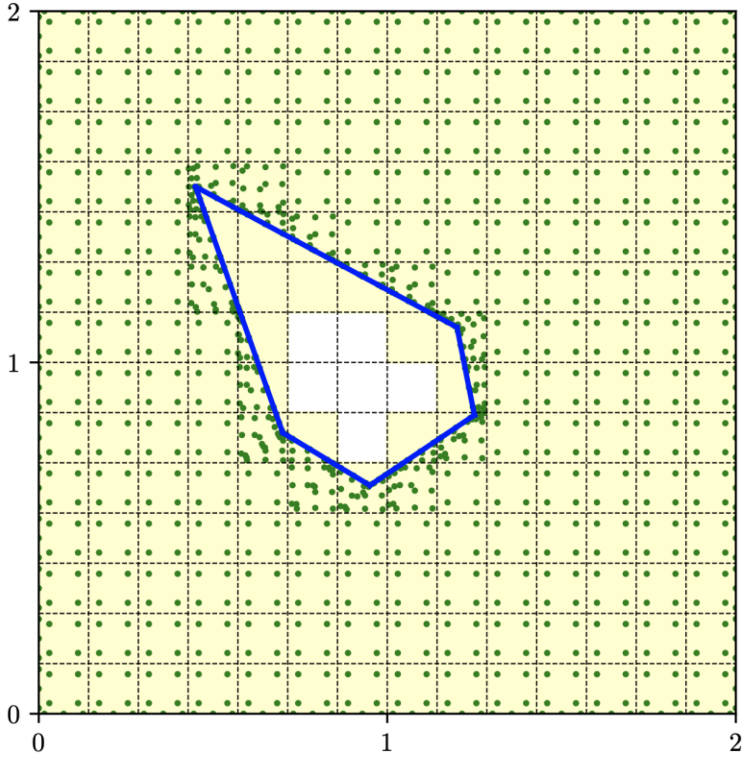

IBRA [5]

[5] Philipp, Breitenberger, Wüchner, Bletzinger, *Membrane structures with the Isogeometric B-Rep Analysis (IBRA)*, 2015.

Small cut-cells drive ill-conditioning and solver degradation in embedded IGA

Trimming / unfitted integration can create arbitrarily small cut contributions

As a result:

- The condition number grows unboundedly under refinement
- Iterative solvers and preconditioners become unreliable

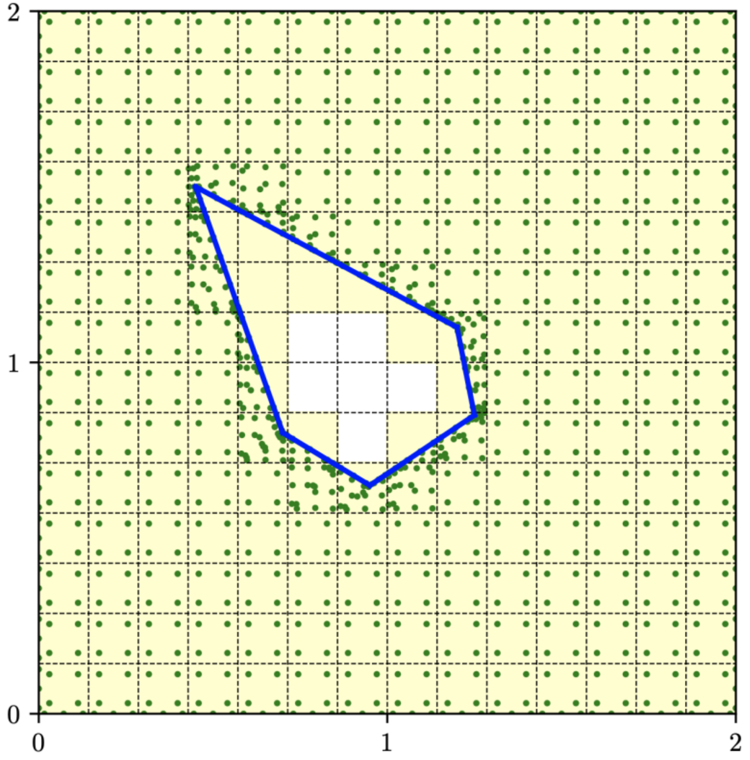

IBRA [5]

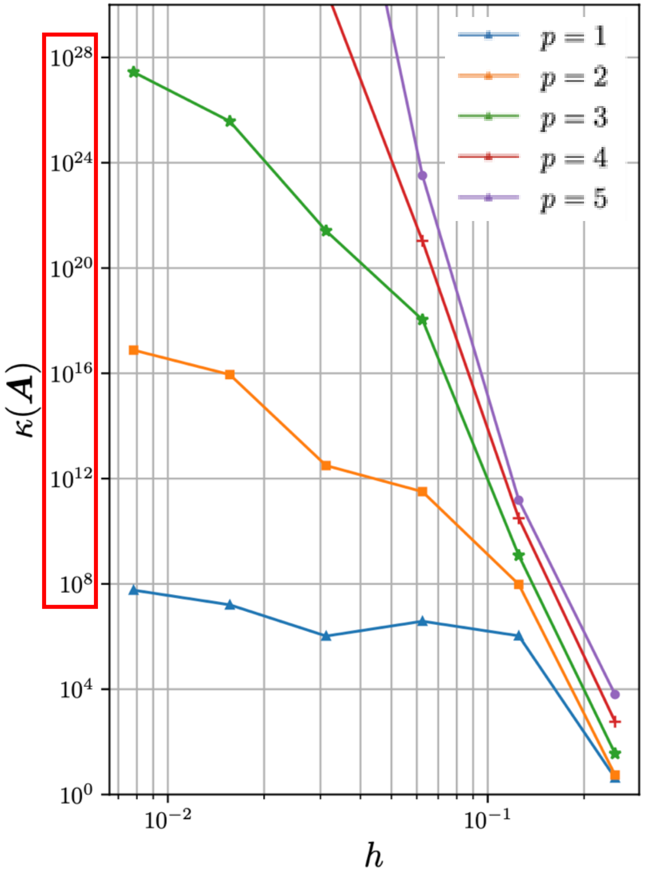

[5] Philipp, Breitenberger, Wüchner, Bletzinger, *Membrane structures with the Isogeometric B-Rep Analysis (IBRA)*, 2015.

The Shifted Boundary Method

The SBM [7] avoids cut-cell integration by imposing boundary conditions on a surrogate boundary

1. Replace the true boundary with a surrogate boundary
2. Project surrogate points onto the true boundary
3. Use a Taylor expansion to transfer the boundary conditions
4. Solve on a simple background mesh with no cut-cell quadrature

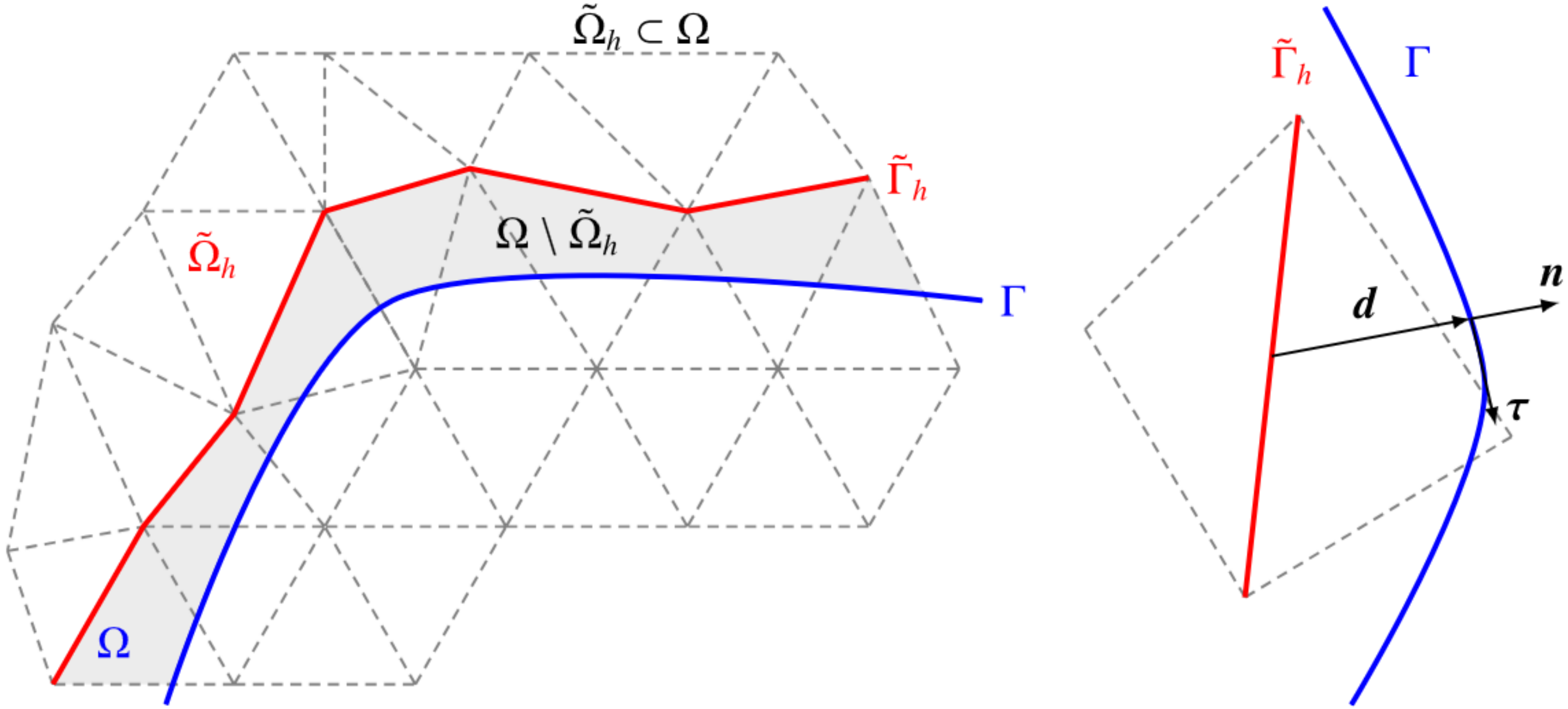

SBM. Image taken from [7]

[7] Main, Scovazzi. The shifted boundary method for embedded domain computations. Part i: Poisson and stokes problems, 2018.

High-order smooth spline bases make Taylor-based boundary shifting particularly natural in IGA

Spline bases provide smooth derivatives across elements

This makes higher-order SBM [8] natural and consistent

Order elevation improves accuracy without changing geometry handling

Goal: retain high-order rates while keeping robust conditioning

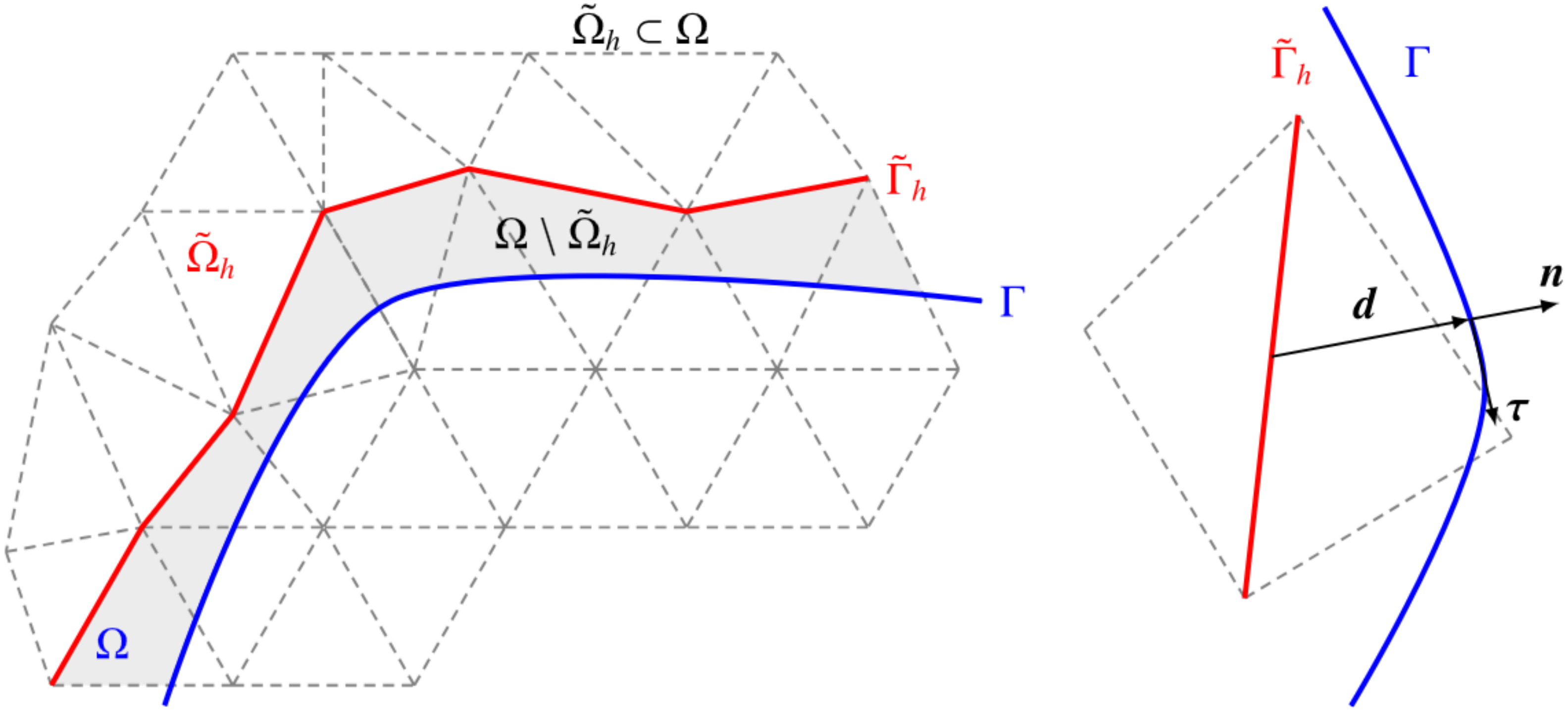

SBM. Image taken from [7]

[7] Main, Scovazzi. The shifted boundary method for embedded domain computations. Part i: Poisson and stokes problems, 2018.
[8] Atallah, Canuto, Scovazzi, *The high-order Shifted Boundary Method and its analysis*, 2022.

High-order smooth spline bases make Taylor-based boundary shifting particularly natural in IGA

Spline bases provide smooth derivatives across elements

This makes higher-order SBM [8] natural and consistent

Order elevation improves accuracy without changing geometry handling

Goal: retain high-order rates while keeping robust conditioning

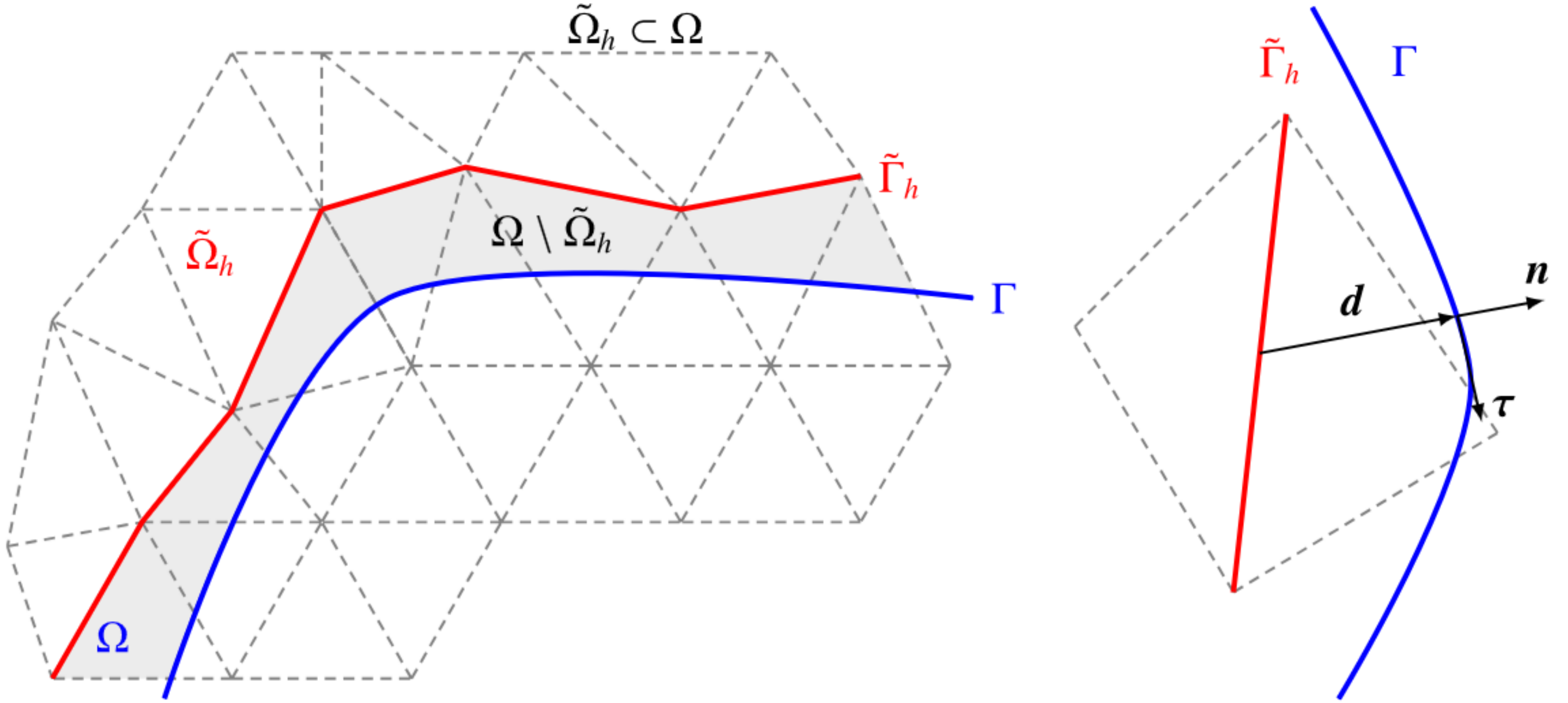

SBM. Image taken from [7]

[7] Main, Scovazzi. The shifted boundary method for embedded domain computations. Part i: Poisson and stokes problems, 2018.
[8] Atallah, Canuto, Scovazzi, *The high-order Shifted Boundary Method and its analysis*, 2022.

Publication I

Publication I:
Establishes SBM-IGA as a penalty-free, cut-cell-free method for Poisson problems in 2D and 3D.

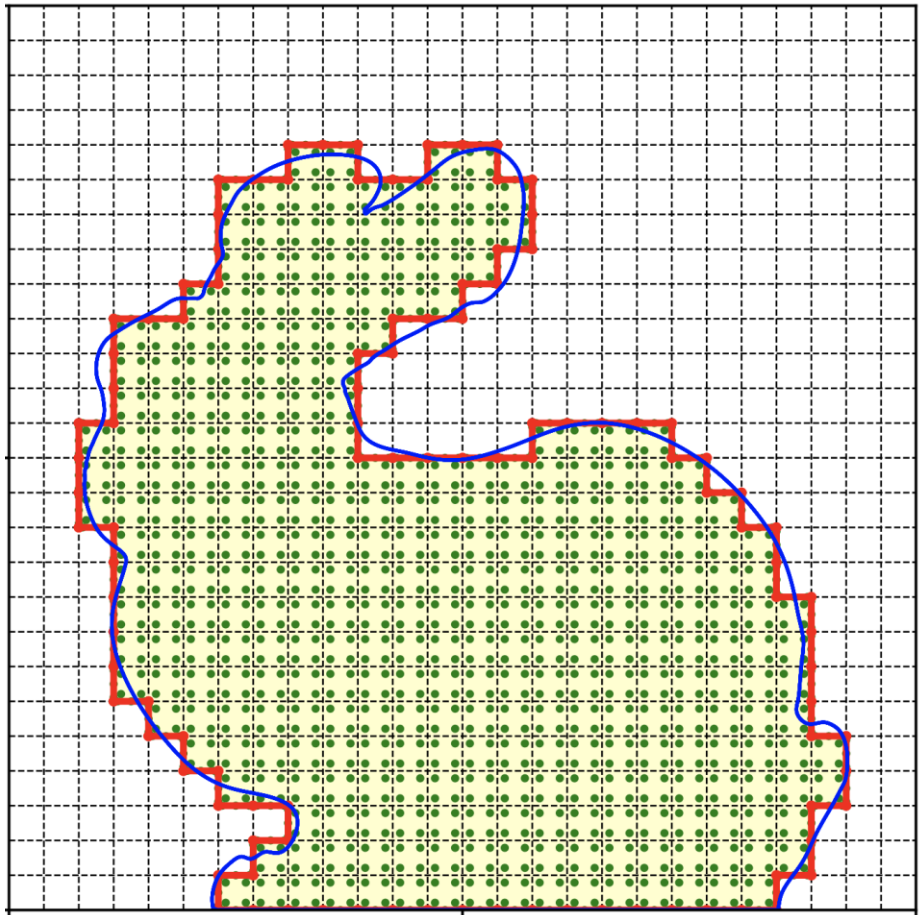

- Model problem: Poisson equation (2D and 3D)
- SBM boundary conditions: Dirichlet and Neumann type
- Boundary enforcement: penalty & penalty-free using SBM
- Validation with convergence studies and condition number analysis

Model problem: Poisson equation (2D and 3D)

$$\begin{aligned} -\Delta u &= f && \text{in } \Omega \\ u &= u_D && \text{on } \Gamma = \partial\Omega \end{aligned}$$

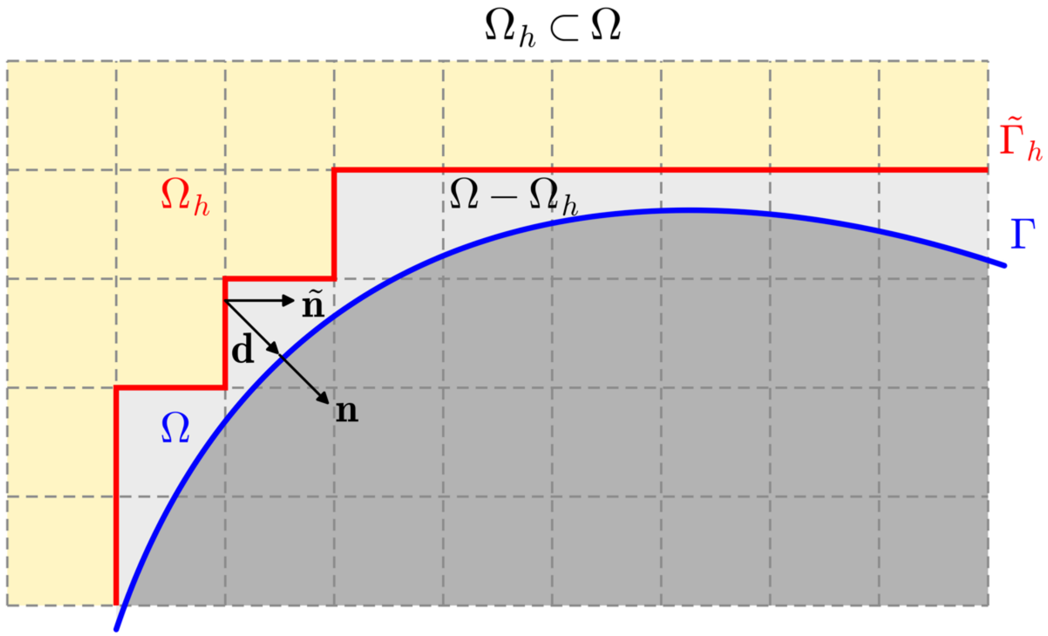

Model problem: Poisson equation (2D and 3D)

$$\begin{aligned} -\Delta u &= f \quad && \text{in } \Omega \\ u &= u_D \quad && \text{on } \Gamma = \partial\Omega \end{aligned}$$

True domain

True boundary

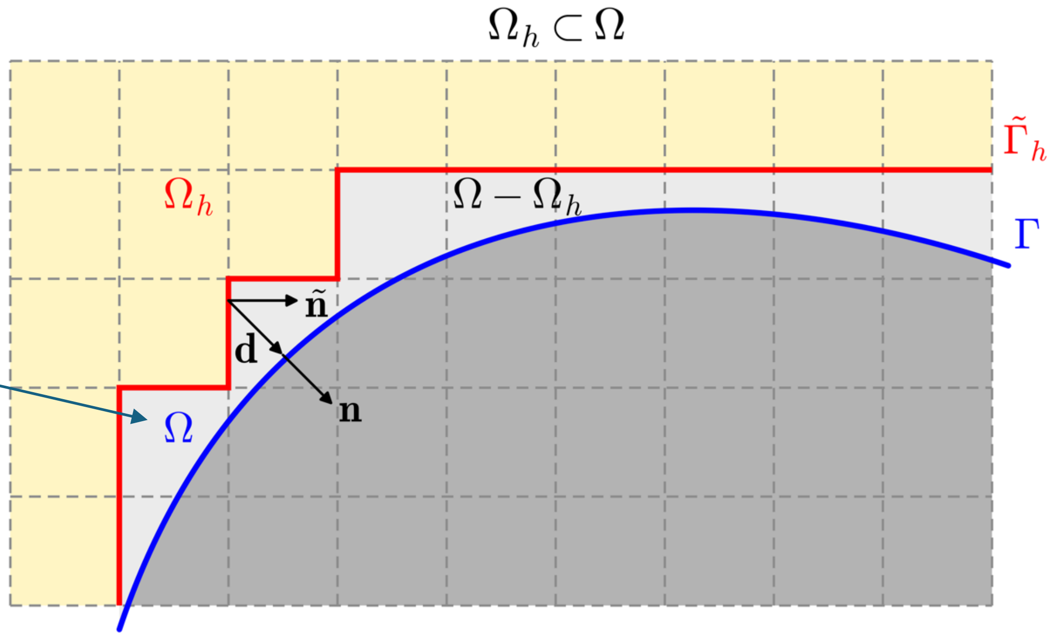

Model problem: Poisson equation (2D and 3D)

$$\begin{aligned} -\Delta u &= f \quad && \text{in } \Omega \\ u &= u_D \quad && \text{on } \Gamma = \partial\Omega \end{aligned}$$

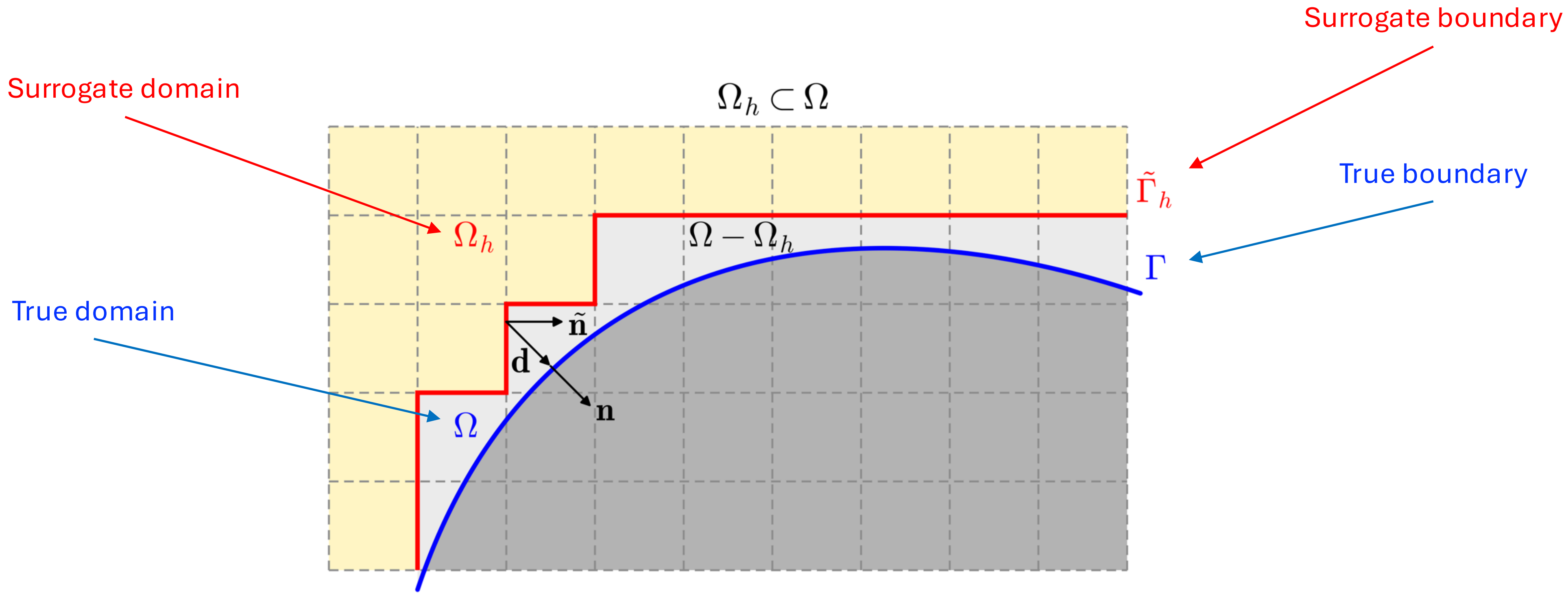

Model problem: Poisson equation (2D and 3D)

$$
\boxed{\begin{aligned} -\Delta u &= f && \text{in } \Omega \\ u &= u_D && \text{on } \Gamma = \partial\Omega \end{aligned}}
$$

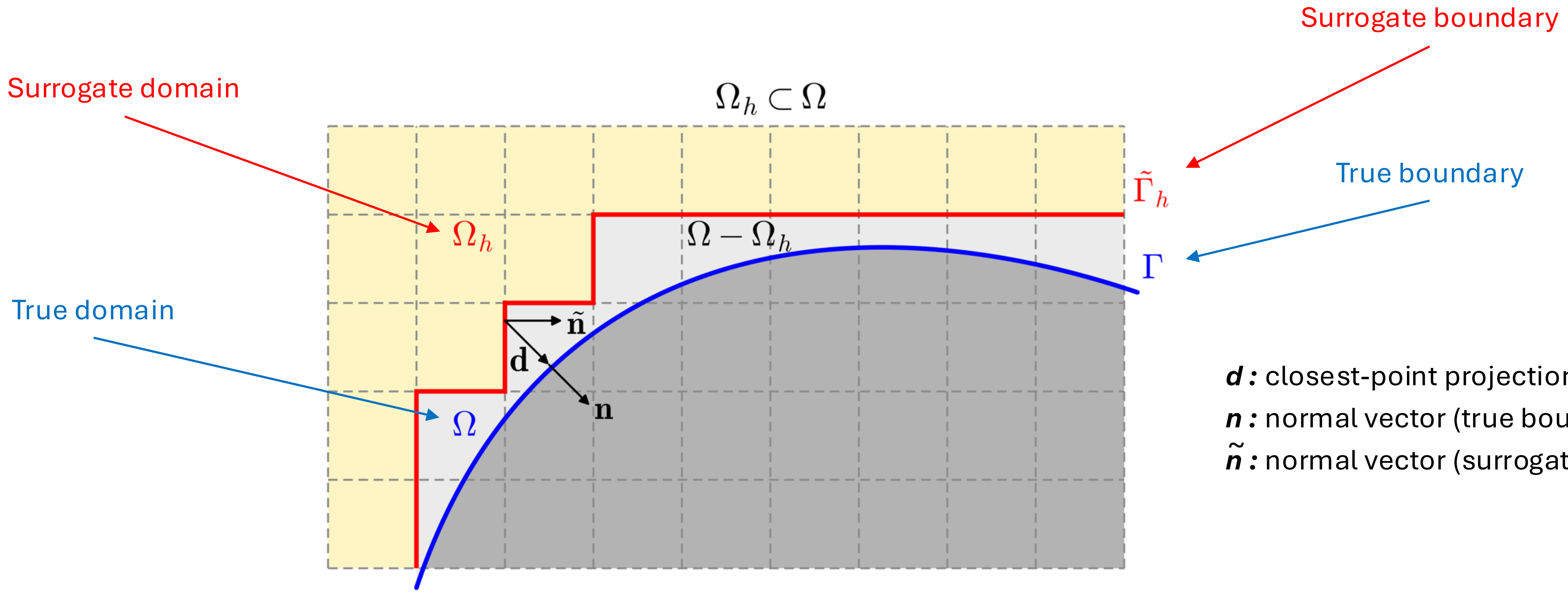

***d* :** closest-point projection

***n* :** normal vector (true boundary)

$\tilde{n}$: normal vector (surrogate boundary)

The Taylor expansion along the closest-point projection

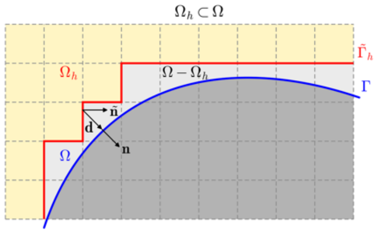

$$
\begin{aligned}
-\Delta u &= f && \text{in } \Omega \\
u &= u_D && \text{on } \Gamma = \partial\Omega
\end{aligned}
$$

Define the *i*-th order directional derivative along ***d***:

$$
\boxed{\mathrm{D}^i_{\boldsymbol{d}} u = \sum_{\boldsymbol{\alpha} \in \mathbb{N}^n, |\boldsymbol{\alpha}| = i} \frac{i!}{\boldsymbol{\alpha}!} \frac{\partial^i u}{\partial \boldsymbol{x}^{\boldsymbol{\alpha}}} \boldsymbol{d}^{\boldsymbol{\alpha}}}
$$

The Taylor expansion along the closest-point projection

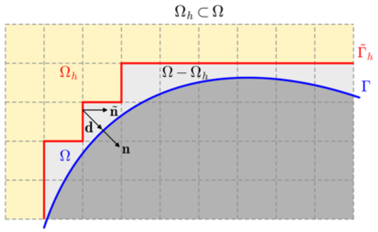

$$-\Delta u = f \qquad \text{in } \Omega$$

$$u = u_D \qquad \text{on } \Gamma = \partial\Omega$$

Define the i-th order directional derivative along $\boldsymbol{d}$:

$$\mathrm{D}^i_{\boldsymbol{d}} u = \sum_{\boldsymbol{\alpha}\in\mathbb{N}^n, |\boldsymbol{\alpha}|=i} \frac{i!}{\boldsymbol{\alpha}!} \frac{\partial^i u}{\partial \boldsymbol{x}^{\boldsymbol{\alpha}}} \boldsymbol{d}^{\boldsymbol{\alpha}}$$

The m-th order Taylor expansion of u between Γ and $\tilde{\Gamma}$

$$\boxed{u(\boldsymbol{x}) = u(\tilde{\boldsymbol{x}} + \boldsymbol{d}(\tilde{\boldsymbol{x}})) = u(\tilde{\boldsymbol{x}}) + \sum_{i=1}^{m} \frac{\mathrm{D}^i_{\boldsymbol{d}} u(\tilde{\boldsymbol{x}})}{i!} + (\mathrm{R}^m(u, \boldsymbol{d}))(\tilde{\boldsymbol{x}})}$$

The Taylor expansion along the closest-point projection

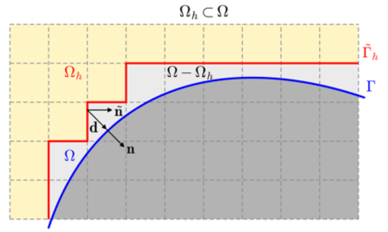

$$
\begin{aligned}
-\Delta u &= f && \text{in } \Omega \\
u &= u_D && \text{on } \Gamma = \partial\Omega
\end{aligned}
$$

Define the i-th order directional derivative along $\boldsymbol{d}$:

$$\mathrm{D}_{\boldsymbol{d}}^{i} u = \sum_{\boldsymbol{\alpha}\in\mathbb{N}^n, |\boldsymbol{\alpha}|=i} \frac{i!}{\boldsymbol{\alpha}!} \frac{\partial^i u}{\partial \boldsymbol{x}^{\boldsymbol{\alpha}}} \boldsymbol{d}^{\boldsymbol{\alpha}}$$

The m-th order Taylor expansion of u between Γ and $\tilde{\Gamma}$

$$u(\boldsymbol{x}) = u(\tilde{\boldsymbol{x}} + \boldsymbol{d}(\tilde{\boldsymbol{x}})) = u(\tilde{\boldsymbol{x}}) + \sum_{i=1}^{m} \frac{\mathrm{D}_{\boldsymbol{d}}^{i} u(\tilde{\boldsymbol{x}})}{i!} + (\mathrm{R}^m(u, \boldsymbol{d}))(\tilde{\boldsymbol{x}})$$

The boundary shift operator

$$\boxed{\mathrm{S}_{\boldsymbol{d}}^{m} u(\tilde{\boldsymbol{x}}) := u(\tilde{\boldsymbol{x}}) + \sum_{i=1}^{m} \frac{\mathrm{D}_{\boldsymbol{d}}^{i} u(\tilde{\boldsymbol{x}})}{i!}}$$

The Taylor expansion along the closest-point projection

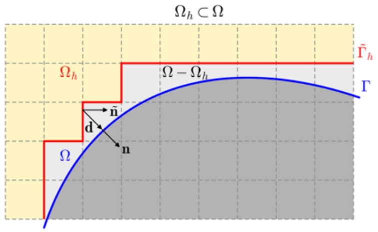

$$
\begin{aligned}
-\Delta u &= f \quad &&\text{in } \Omega \\
u &= u_D \quad &&\text{on } \Gamma = \partial\Omega
\end{aligned}
$$

Define the i-th order directional derivative along $\boldsymbol{d}$:

$$\mathrm{D}^i_{\boldsymbol{d}} u = \sum_{\boldsymbol{\alpha}\in\mathbb{N}^n, |\boldsymbol{\alpha}|=i} \frac{i!}{\boldsymbol{\alpha}!} \frac{\partial^i u}{\partial \boldsymbol{x}^{\boldsymbol{\alpha}}} \boldsymbol{d}^{\boldsymbol{\alpha}}$$

The m-th order Taylor expansion of u between Γ and $\tilde{\Gamma}$

$$u(\boldsymbol{x}) = u(\tilde{\boldsymbol{x}} + \boldsymbol{d}(\tilde{\boldsymbol{x}})) = u(\tilde{\boldsymbol{x}}) + \sum_{i=1}^{m} \frac{\mathrm{D}^i_{\boldsymbol{d}} u(\tilde{\boldsymbol{x}})}{i!} + (\mathrm{R}^m(u, \boldsymbol{d}))(\tilde{\boldsymbol{x}})$$

The boundary shift operator

$$\mathrm{S}^m_{\boldsymbol{d}} u(\tilde{\boldsymbol{x}}) := u(\tilde{\boldsymbol{x}}) + \sum_{i=1}^{m} \frac{\mathrm{D}^i_{\boldsymbol{d}} u(\tilde{\boldsymbol{x}})}{i!}$$

On the surrogate boundary we have

$$\boxed{\mathrm{S}^m_{\boldsymbol{d}} u - u_D + \mathrm{R}^m(u, \boldsymbol{d}) = 0 \quad \text{on } \tilde{\Gamma}_h}$$

The Taylor expansion along the closest-point projection

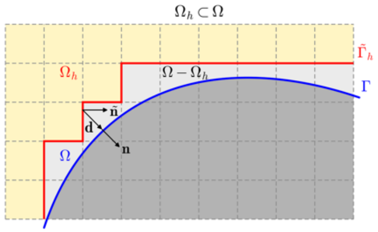

$$
\begin{aligned}
-\Delta u &= f && \text{in } \Omega \\
u &= u_D && \text{on } \Gamma = \partial\Omega
\end{aligned}
$$

Define the i-th order directional derivative along $\boldsymbol{d}$:

$$\mathrm{D}^i_{\boldsymbol{d}} u = \sum_{\boldsymbol{\alpha} \in \mathbb{N}^n, |\boldsymbol{\alpha}| = i} \frac{i!}{\boldsymbol{\alpha}!} \frac{\partial^i u}{\partial \boldsymbol{x}^{\boldsymbol{\alpha}}} \boldsymbol{d}^{\boldsymbol{\alpha}}$$

The m-th order Taylor expansion of u between Γ and $\tilde{\Gamma}$

$$u(\boldsymbol{x}) = u(\tilde{\boldsymbol{x}} + \boldsymbol{d}(\tilde{\boldsymbol{x}})) = u(\tilde{\boldsymbol{x}}) + \sum_{i=1}^{m} \frac{\mathrm{D}^i_{\boldsymbol{d}} u(\tilde{\boldsymbol{x}})}{i!} + (\mathrm{R}^m(u, \boldsymbol{d}))(\tilde{\boldsymbol{x}})$$

The boundary shift operator

$$\mathrm{S}^m_{\boldsymbol{d}} u(\tilde{\boldsymbol{x}}) := u(\tilde{\boldsymbol{x}}) + \sum_{i=1}^{m} \frac{\mathrm{D}^i_{\boldsymbol{d}} u(\tilde{\boldsymbol{x}})}{i!}$$

On the surrogate boundary we have

$$\mathrm{S}^m_{\boldsymbol{d}} u - u_D + \mathrm{R}^m(u, \boldsymbol{d}) = 0 \quad \text{on } \tilde{\Gamma}_h$$

The remainder satisfies

$$\boxed{|\mathrm{R}^m(u, \boldsymbol{d})| = O(\|\boldsymbol{d}\|^{m+1}) \text{ as } \|\boldsymbol{d}\| \to 0}$$

SBM weak formulations

$$-\Delta u = f \quad \text{in } \Omega$$
$$u = u_D \quad \text{on } \Gamma = \partial\Omega$$

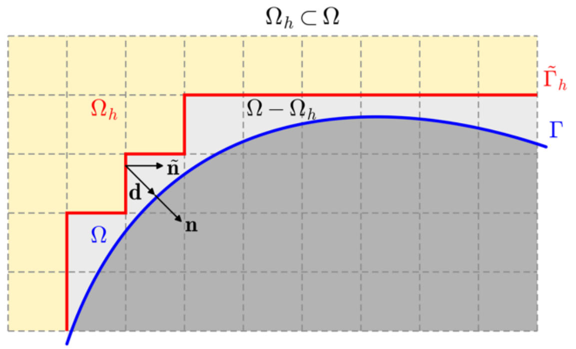

Nitsche ***penalty*** *weak formulation:*

$$a_h^m(u_h, v_h) = (\nabla u_h, \nabla v_h)_{\tilde{\Omega}_h} - \langle \nabla u_h \cdot \tilde{\boldsymbol{n}}, v_h \rangle_{\tilde{\Gamma}_h} - \langle S_{\boldsymbol{d}}^m u_h, \nabla v_h \cdot \tilde{\boldsymbol{n}} \rangle_{\tilde{\Gamma}_h} + \frac{\alpha}{h} \langle v_h, S_{\boldsymbol{d}}^m u_h \rangle_{\tilde{\Gamma}_h}$$
$$l_h(v_h) = (f, v_h)_{\tilde{\Omega}_h} - \langle u_D, \nabla v_h \cdot \tilde{\boldsymbol{n}} \rangle_{\tilde{\Gamma}_h} + \frac{\alpha}{h} \langle v_h, u_D \rangle_{\tilde{\Gamma}_h}$$

SBM weak formulations

$$-\Delta u = f \qquad \text{in } \Omega$$
$$u = u_D \qquad \text{on } \Gamma = \partial\Omega$$

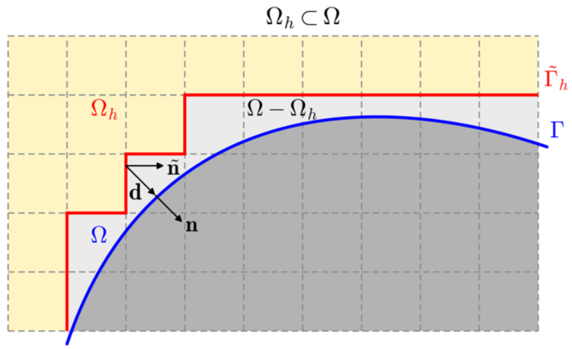

*Nitsche **penalty** weak formulation:*

$$a_h^m(u_h, v_h) = (\nabla u_h, \nabla v_h)_{\tilde{\Omega}_h} - \langle \nabla u_h \cdot \tilde{\boldsymbol{n}}, v_h \rangle_{\tilde{\Gamma}_h} - \langle \boxed{S_{\boldsymbol{d}}^m u_h}, \nabla v_h \cdot \tilde{\boldsymbol{n}} \rangle_{\tilde{\Gamma}_h} + \frac{\alpha}{h} \langle v_h, \boxed{S_{\boldsymbol{d}}^m u_h} \rangle_{\tilde{\Gamma}_h}$$
$$l_h(v_h) = (f, v_h)_{\tilde{\Omega}_h} - \langle \boxed{u_D}, \nabla v_h \cdot \tilde{\boldsymbol{n}} \rangle_{\tilde{\Gamma}_h} + \frac{\alpha}{h} \langle v_h, \boxed{u_D} \rangle_{\tilde{\Gamma}_h}$$

Dirichlet boundary values

boundary shift operator applied to the gradient

SBM weak formulations

$$-\Delta u = f \quad \text{in } \Omega$$
$$u = u_D \quad \text{on } \Gamma = \partial\Omega$$

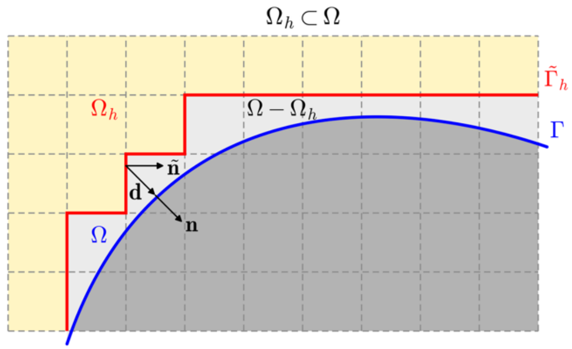

Nitsche penalty weak formulation:

$$a_h^m(u_h, v_h) = (\nabla u_h, \nabla v_h)_{\tilde{\Omega}_h} - \langle \nabla u_h \cdot \tilde{\boldsymbol{n}}, v_h \rangle_{\tilde{\Gamma}_h} - \langle \boxed{S_{\boldsymbol{d}}^m u_h}, \nabla v_h \cdot \tilde{\boldsymbol{n}} \rangle_{\tilde{\Gamma}_h} + \frac{\alpha}{h} \langle v_h, \boxed{S_{\boldsymbol{d}}^m u_h} \rangle_{\tilde{\Gamma}_h}$$
$$l_h(v_h) = (f, v_h)_{\tilde{\Omega}_h} - \langle \boxed{u_D}, \nabla v_h \cdot \tilde{\boldsymbol{n}} \rangle_{\tilde{\Gamma}_h} + \frac{\alpha}{h} \langle v_h, \boxed{u_D} \rangle_{\tilde{\Gamma}_h}$$

Nitsche ***penalty-free*** *weak formulation:*

$$a_h^m(u_h, v_h) = (\nabla u_h, \nabla v_h)_{\tilde{\Omega}_h} - \langle \nabla u_h \cdot \tilde{\boldsymbol{n}}, v_h \rangle_{\tilde{\Gamma}_h} + \langle \boxed{S_{\boldsymbol{d}}^m u_h}, \nabla v_h \cdot \tilde{\boldsymbol{n}} \rangle_{\tilde{\Gamma}_h}$$
$$l_h(v_h) = (f, v_h)_{\tilde{\Omega}_h} + \langle \boxed{u_D}, \nabla v_h \cdot \tilde{\boldsymbol{n}} \rangle_{\tilde{\Gamma}_h}$$

Dirichlet boundary conditions

- Higher-order Taylor expansions enable accurate boundary shifting

- Dirichlet BCs provide the clearest setting to observe high-order behavior

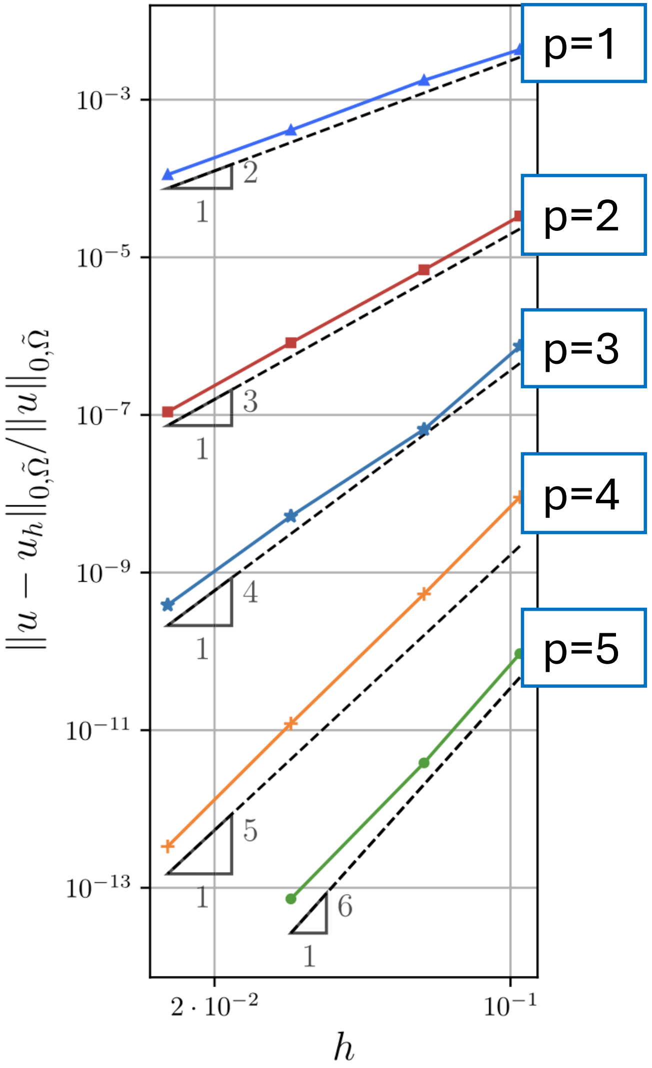

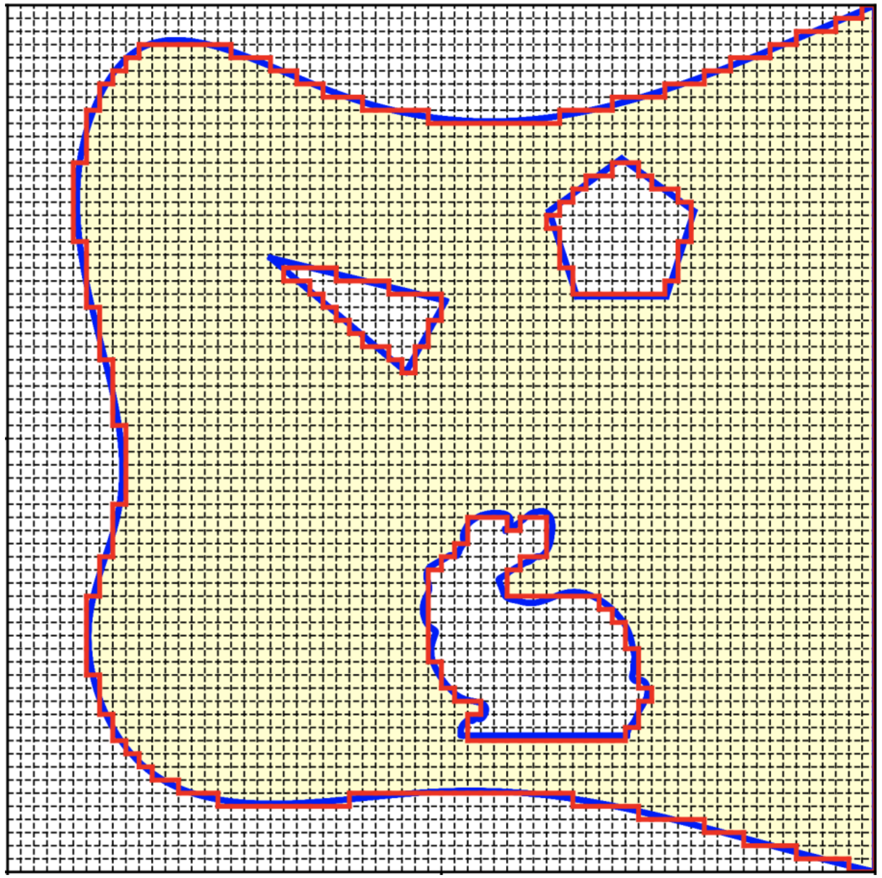

Neumann boundary conditions

- For Neumann BCs, SBM-IGA preserves optimal gradient accuracy but loses one order in the L^2-norm
- Shifted flux approximation ⇒ H^1-optimal , but L^2 rate drops from O(h^{p+1}) to O(h^p)
- Neumann conditions are more delicate, since shifting fluxes is harder than shifting values

Neumann boundary conditions

- For Neumann BCs, SBM-IGA preserves optimal gradient accuracy but loses one order in the L^2-norm
- Shifted flux approximation ⇒ H^1-optimal , but L^2 rate drops from O(h^{p+1}) to O(h^p)
- Neumann conditions are more delicate, since shifting fluxes is harder than shifting values

Neumann weak formulation:

$$\boxed{\begin{aligned} a_h^m(u_h, v_h) &= (\nabla u_h, \nabla v_h)_{\tilde{\Omega}_h} - \langle \nabla u_h \cdot \tilde{\boldsymbol{n}}, v_h \rangle_{\tilde{\Gamma}_h} + \langle (\mathrm{S}_{\boldsymbol{d}}^m \nabla u_h \cdot \boldsymbol{n}) \tilde{\boldsymbol{n}} \cdot \boldsymbol{n}, v_h \rangle_{\tilde{\Gamma}_h}, \\ l_h(v_h) &= (f, v_h)_{\tilde{\Omega}_h} + \langle t_N \tilde{\boldsymbol{n}} \cdot \boldsymbol{n}, v_h \rangle_{\tilde{\Gamma}_h}. \end{aligned}}$$

Neumann boundary conditions

- For Neumann BCs, SBM-IGA preserves optimal gradient accuracy but loses one order in the L^2-norm

- Shifted flux approximation $\Rightarrow$ H^1-optimal , but L^2 rate drops from O(h^{p+1}) to O(h^p)

- Neumann conditions are more delicate, since shifting fluxes is harder than shifting values

additional Nuemann boundary terms

Neumann weak formulation:

$$
\begin{aligned}
a_h^m(u_h, v_h) &= (\nabla u_h, \nabla v_h)_{\tilde{\Omega}_h} - \langle \nabla u_h \cdot \tilde{\boldsymbol{n}}, v_h \rangle_{\tilde{\Gamma}_h} + \boxed{\langle (\mathbf{S}_{\boldsymbol{d}}^m \nabla u_h \cdot \boldsymbol{n}) \tilde{\boldsymbol{n}} \cdot \boldsymbol{n}, v_h \rangle_{\tilde{\Gamma}_h}} \\
l_h(v_h) &= (f, v_h)_{\tilde{\Omega}_h} + \boxed{\langle t_N \tilde{\boldsymbol{n}} \cdot \boldsymbol{n}, v_h \rangle_{\tilde{\Gamma}_h}}
\end{aligned}
$$

Neumann boundary conditions

- For Neumann BCs, SBM-IGA preserves optimal gradient accuracy but loses one order in the L^2-norm

- Shifted flux approximation ⇒ H^1-optimal , but L^2 rate drops from O(h^{p+1}) to O(h^p)

- Neumann conditions are more delicate, since shifting fluxes is harder than shifting values

additional Nuemann boundary terms

boundary shift operator applied to the gradient

Neumann weak formulation:

$$a_h^m(u_h, v_h) = (\nabla u_h, \nabla v_h)_{\tilde{\Omega}_h} - \langle \nabla u_h \cdot \tilde{\boldsymbol{n}}, v_h \rangle_{\tilde{\Gamma}_h} + \boxed{\langle (\boxed{\mathbf{S}_{\boldsymbol{d}}^m \nabla u_h} \cdot \boldsymbol{n}) \tilde{\boldsymbol{n}} \cdot \boldsymbol{n}, v_h \rangle_{\tilde{\Gamma}_h}}$$

$$l_h(v_h) = (f, v_h)_{\tilde{\Omega}_h} + \boxed{\langle t_N \tilde{\boldsymbol{n}} \cdot \boldsymbol{n}, v_h \rangle_{\tilde{\Gamma}_h}}$$

Neumann boundary conditions

- For Neumann BCs, SBM-IGA preserves optimal gradient accuracy but loses one order in the L^2-norm

- Shifted flux approximation ⇒ H^1-optimal , but L^2 rate drops from O(h^{p+1}) to O(h^p)

- Neumann conditions are more delicate, since shifting fluxes is harder than shifting values

Point-wise error *localized* near the surrogate boundary

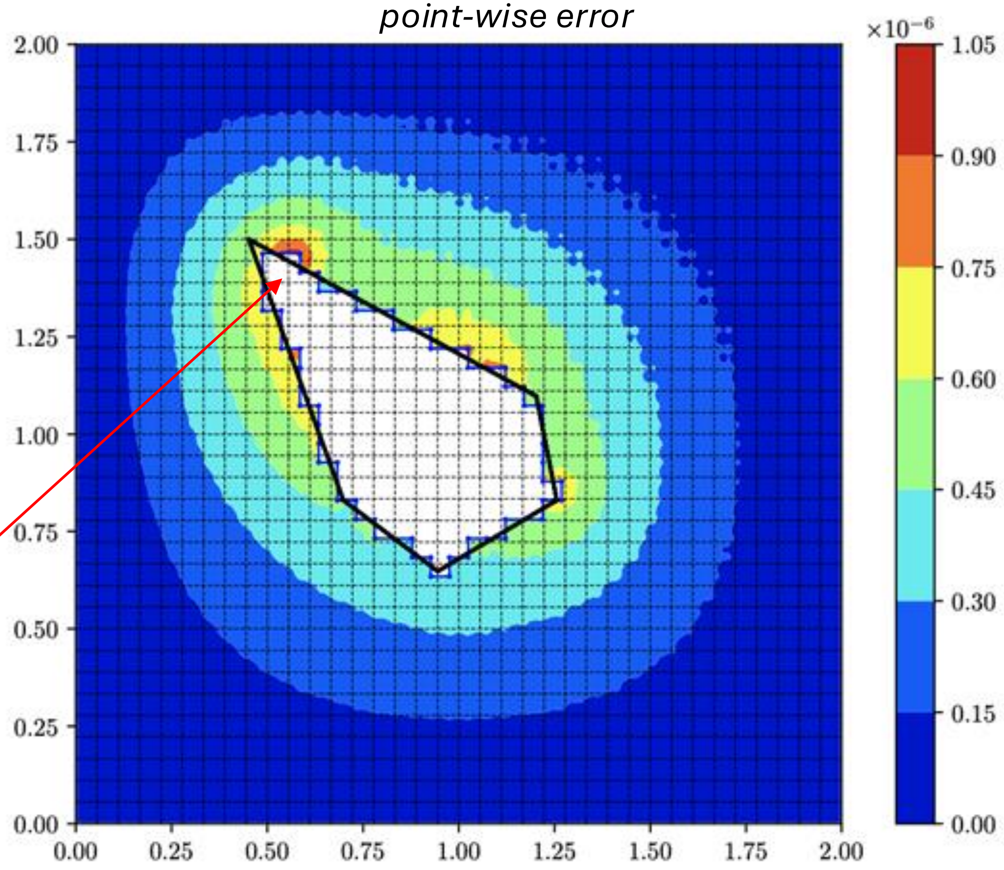

Neumann boundary conditions

- H^1 optimal behavior
- L^2 rate drops from O(h^{p+1}) to O(h^p)

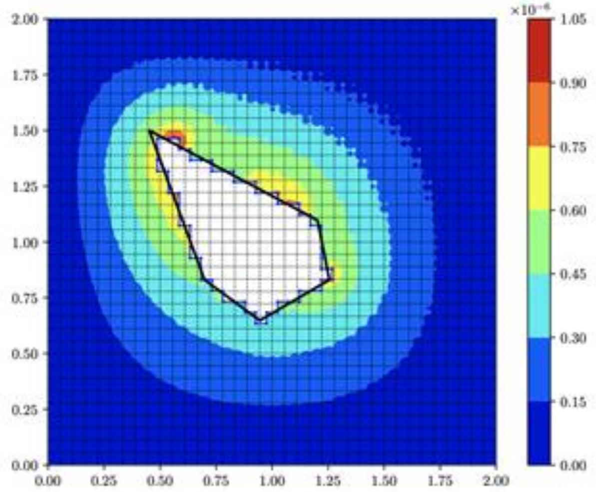

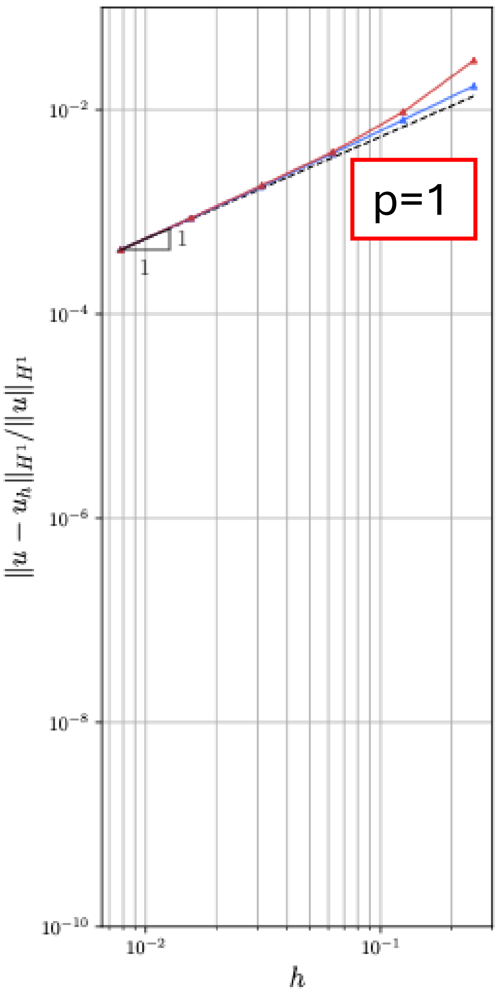

H^1- convergence

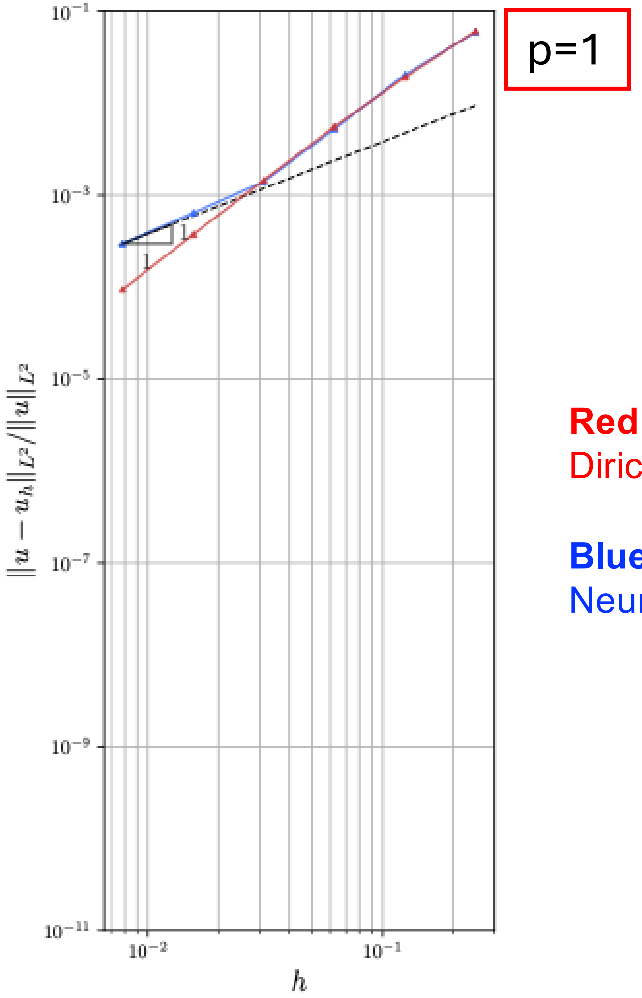

L^2- convergence

Red: Only SBM Dirichlet BCs

Blue: SBM Neumann BCs

Neumann boundary conditions

- H^1 optimal behavior
- L^2 rate drops from O(h^{p+1}) to O(h^p)

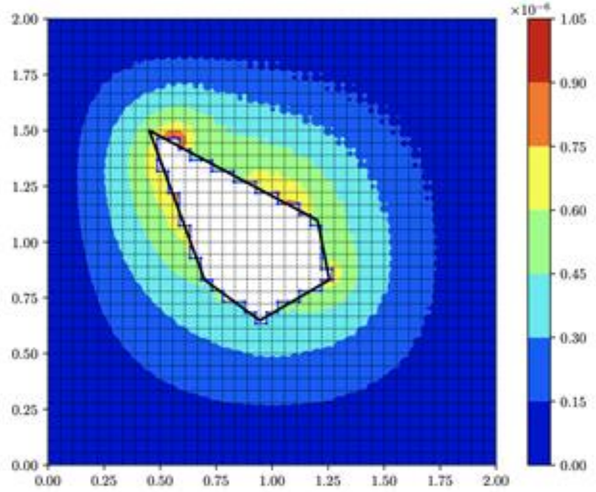

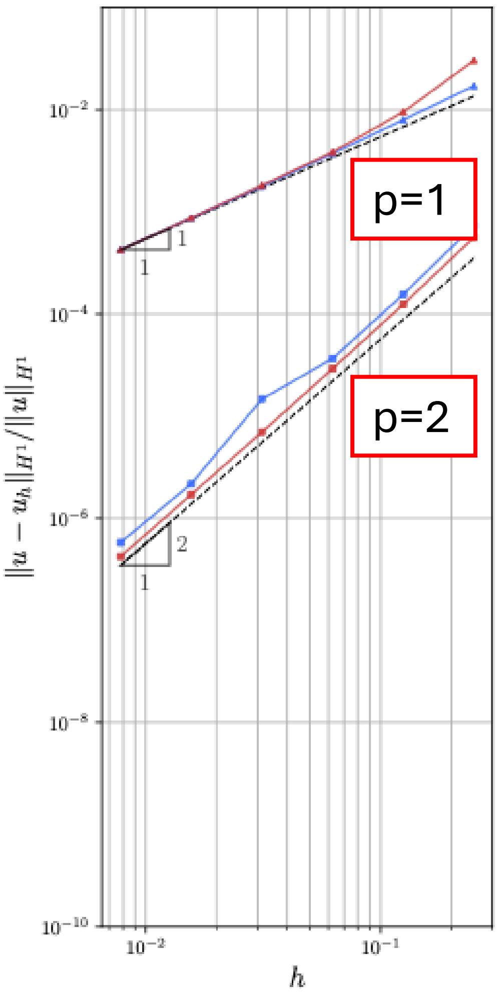

H^1- convergence

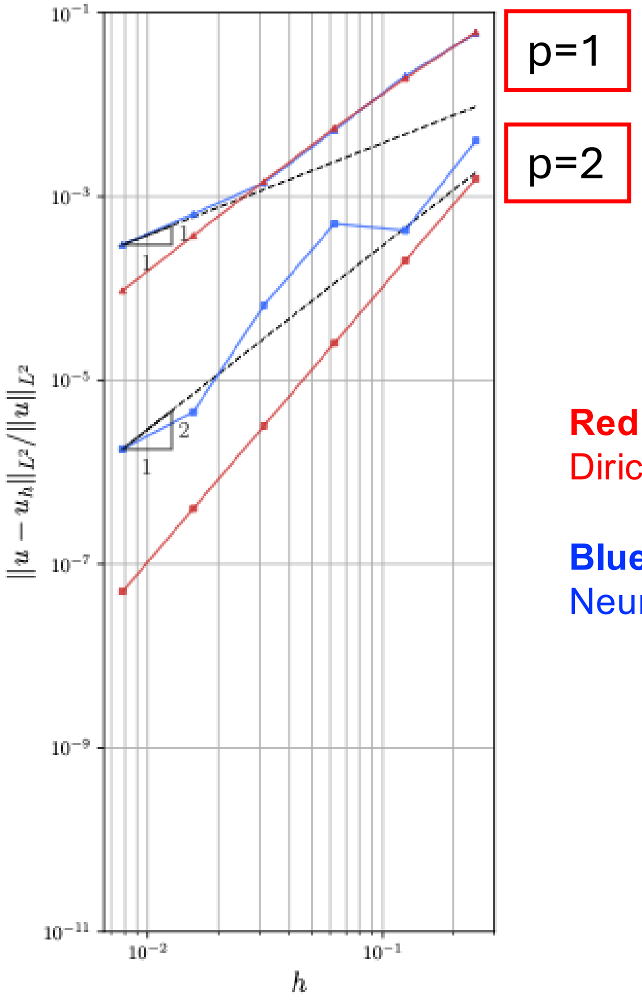

L^2- convergence

Red: Only SBM Dirichlet BCs

Blue: SBM Neumann BCs

Neumann boundary conditions

- H^1 optimal behavior
- L^2 rate drops from O(h^{p+1}) to O(h^p)

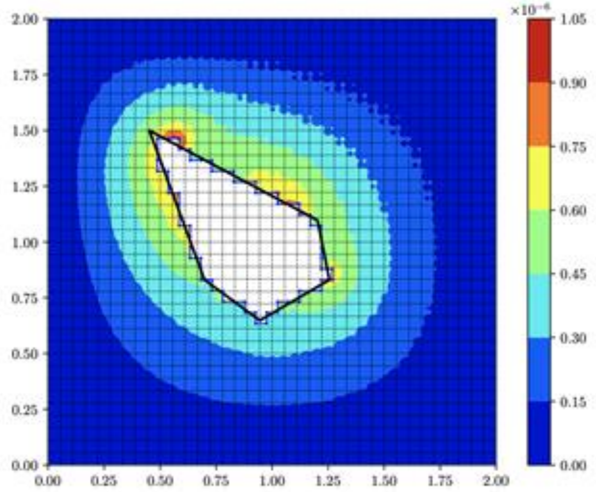

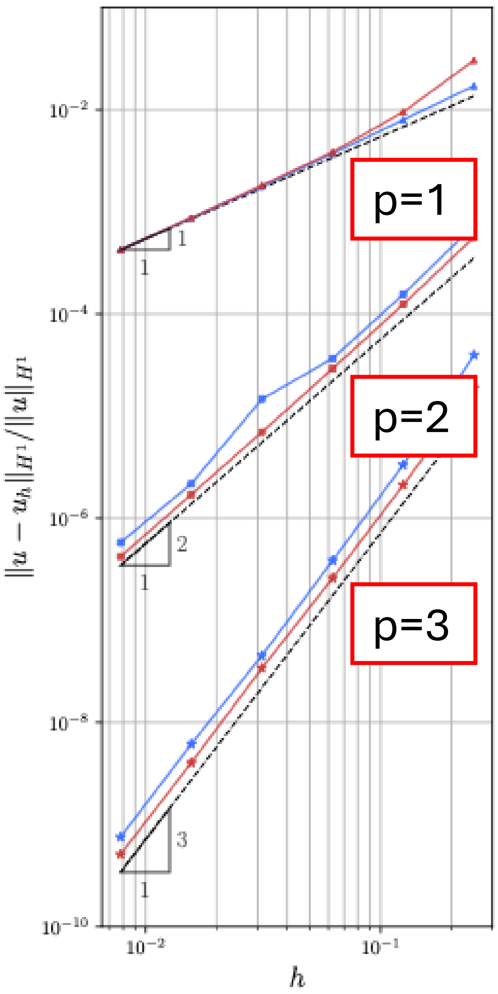

H^1- convergence

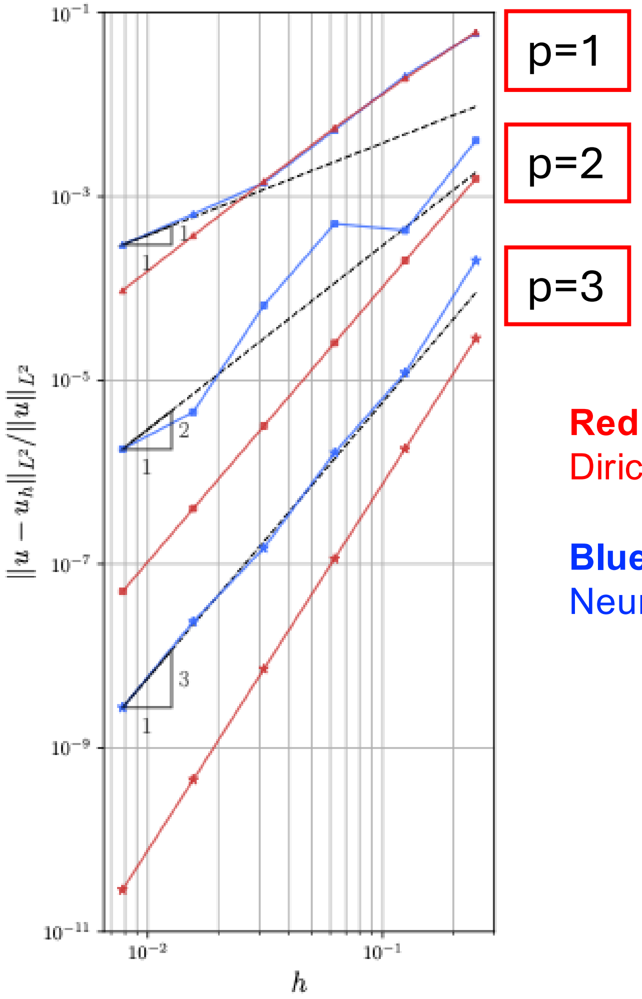

L^2- convergence

Red: Only SBM Dirichlet BCs

Blue: SBM Neumann BCs

SBM-IGA preserves favorable conditioning under refinement

- No cut-cell quadrature
- SBM-IGA avoids the small cut-cell instability
- SBM conditioning follows the expected h^{-2} trend
- Possible to use of iterative solvers

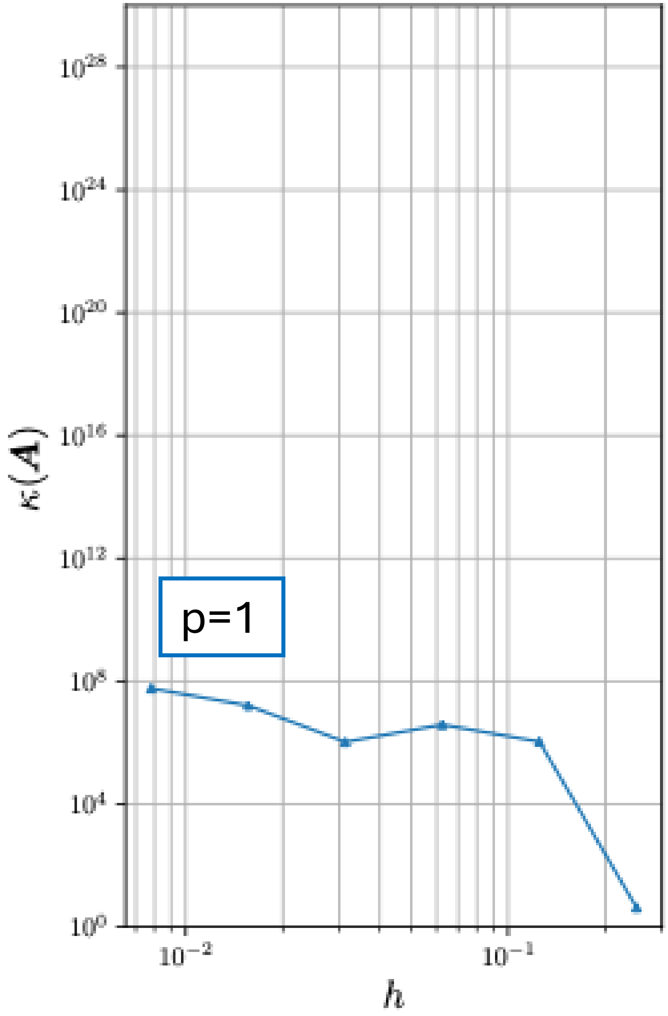

IBRA

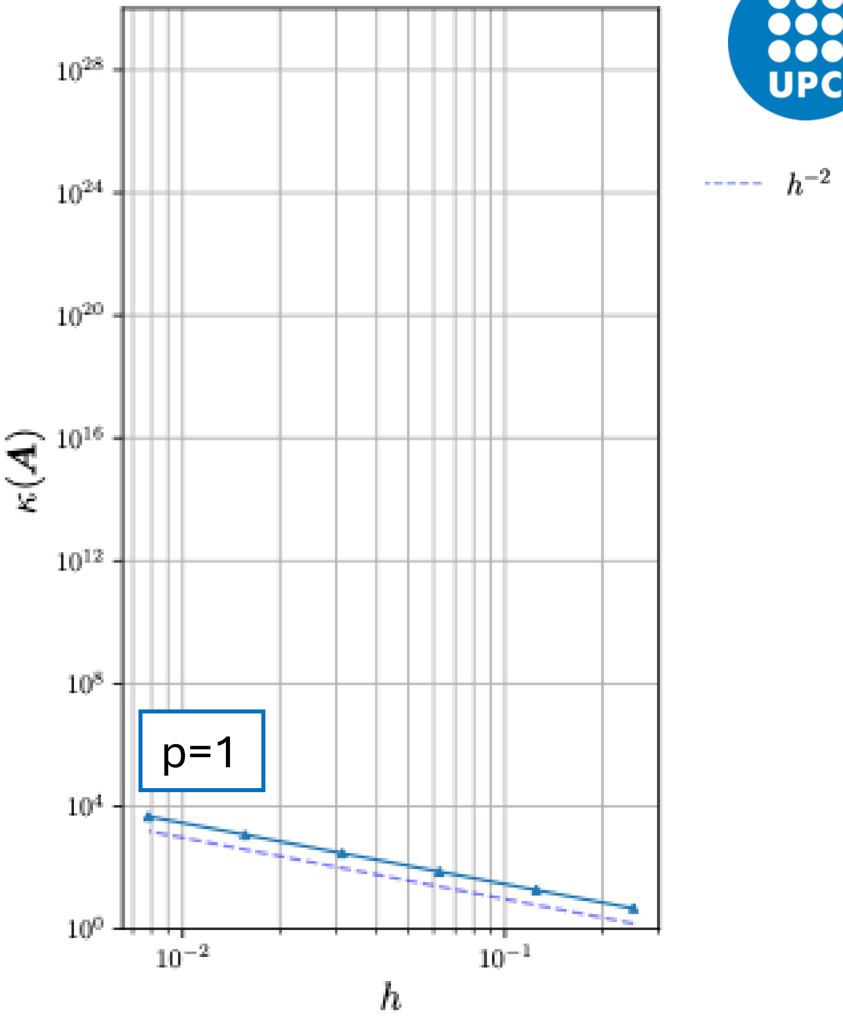

SBM

SBM-IGA preserves favorable conditioning under refinement

- No cut-cell quadrature
- SBM-IGA avoids the small cut-cell instability
- SBM conditioning follows the expected h^{-2} trend
- Possible to use of iterative solvers

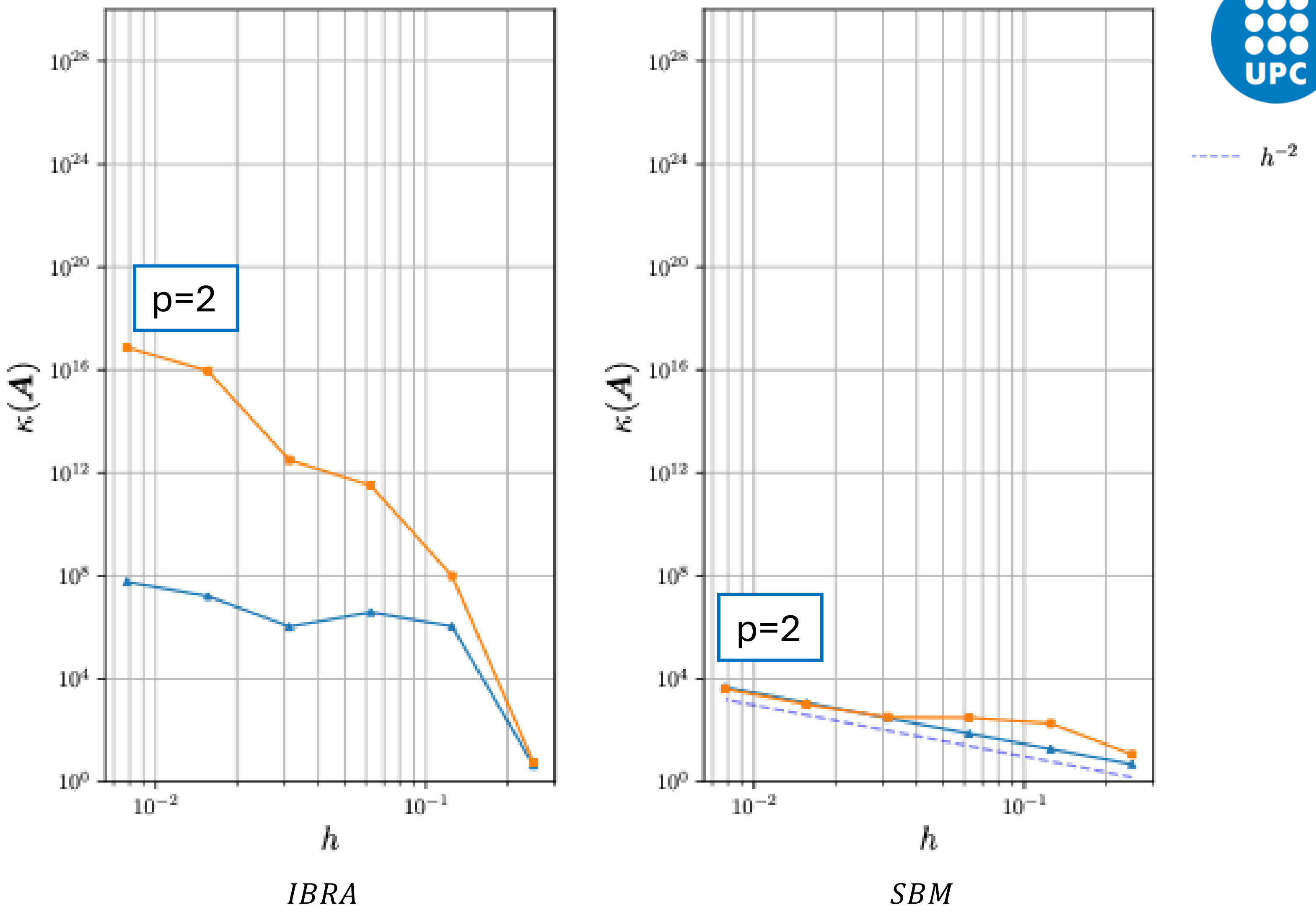

SBM-IGA preserves favorable conditioning under refinement

- No cut-cell quadrature
- SBM-IGA avoids the small cut-cell instability
- SBM conditioning follows the expected h^{-2} trend
- Possible to use of iterative solvers

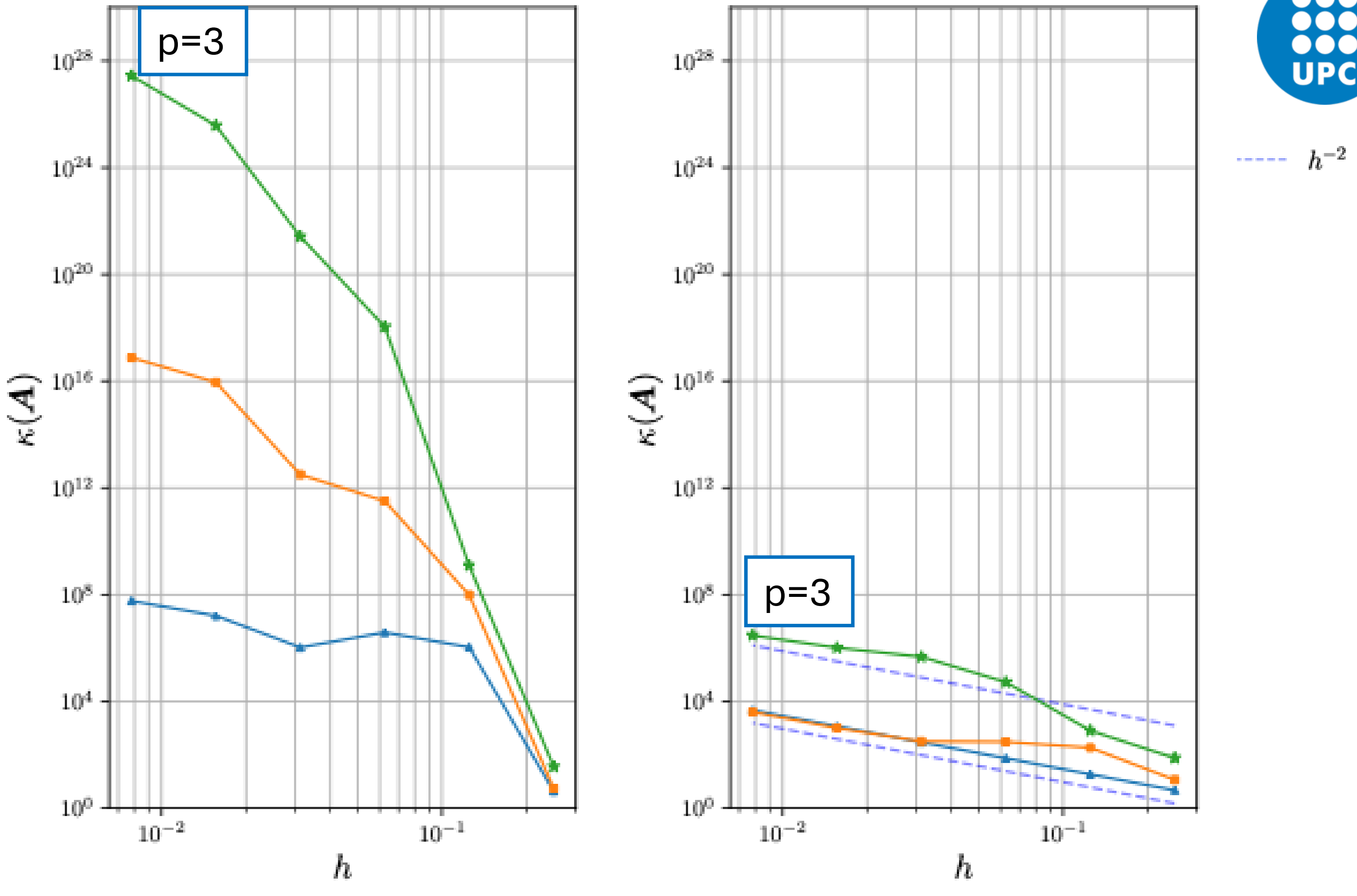

$IBRA$ SBM

SBM-IGA preserves favorable conditioning under refinement

- No cut-cell quadrature
- SBM-IGA avoids the small cut-cell instability
- SBM conditioning follows the expected h^{-2} trend
- Possible to use of iterative solvers

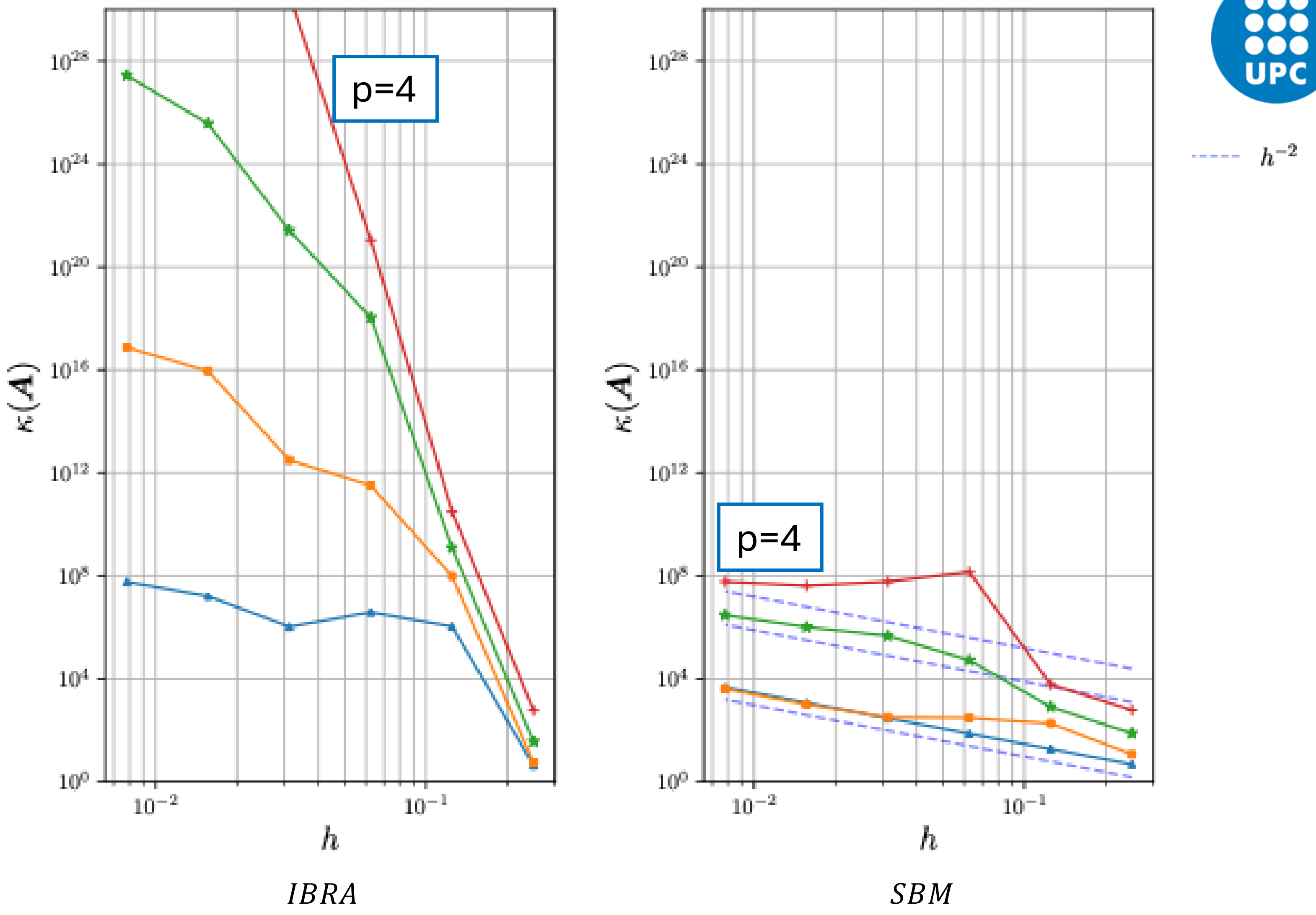

SBM-IGA preserves favorable conditioning under refinement

- No cut-cell quadrature
- SBM-IGA avoids the small cut-cell instability
- SBM conditioning follows the expected h^{-2} trend
- Possible to use of iterative solvers

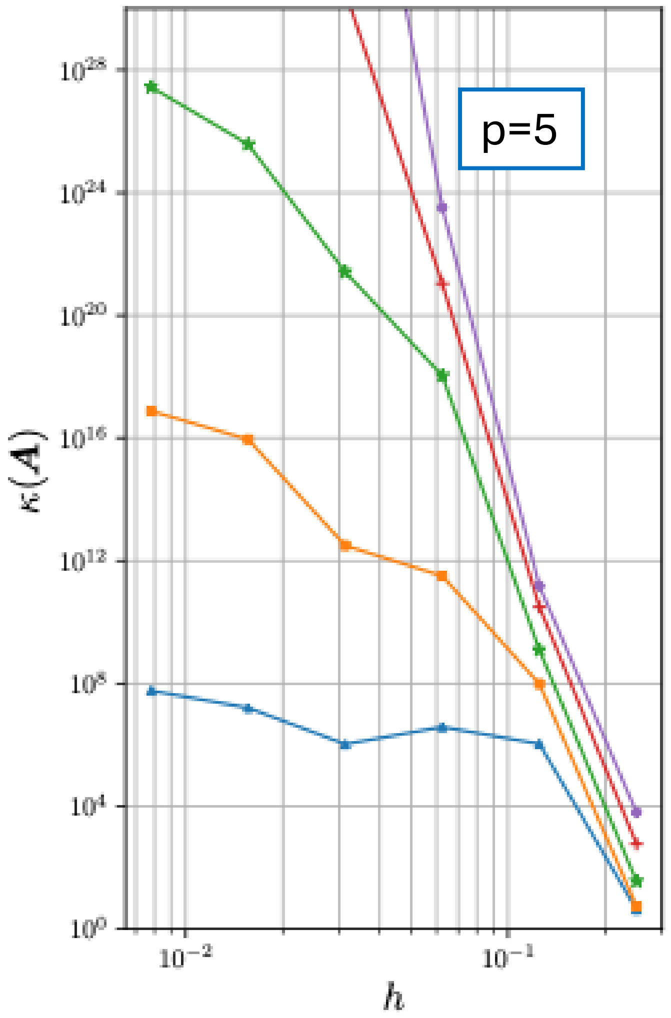

IBRA

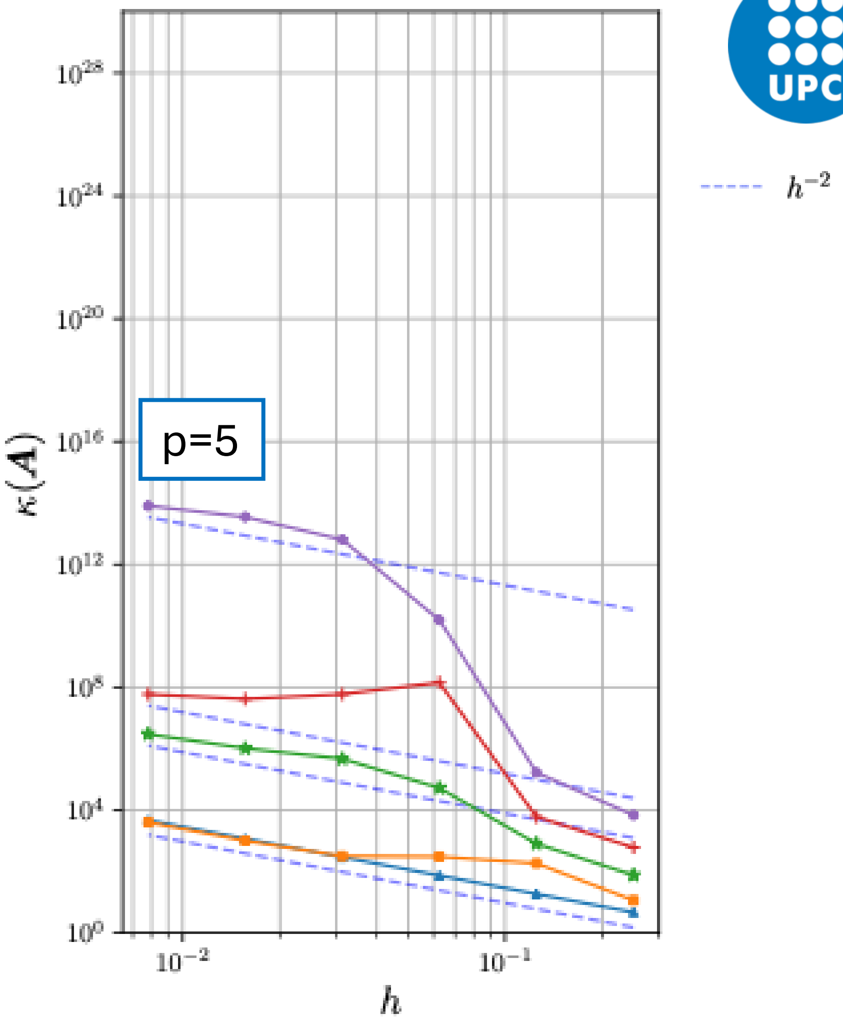

SBM

3D extension

SBM has a straightforward extension to robust three-dimensional implementation

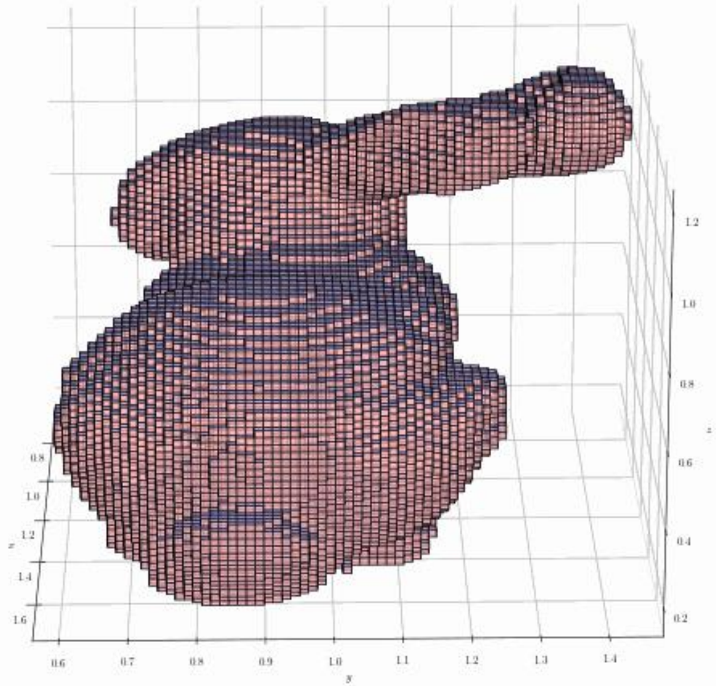

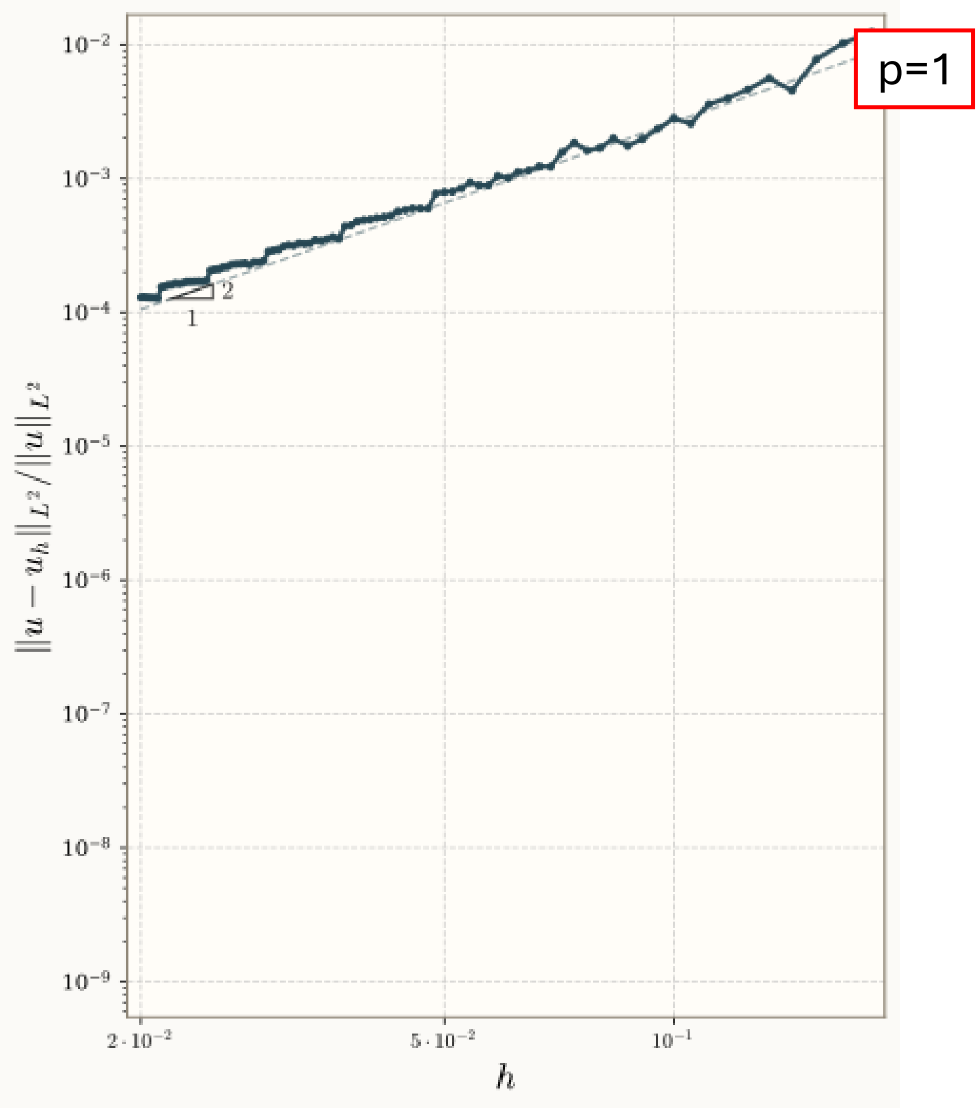

3D extension

SBM has a straightforward extension to robust three-dimensional implementation

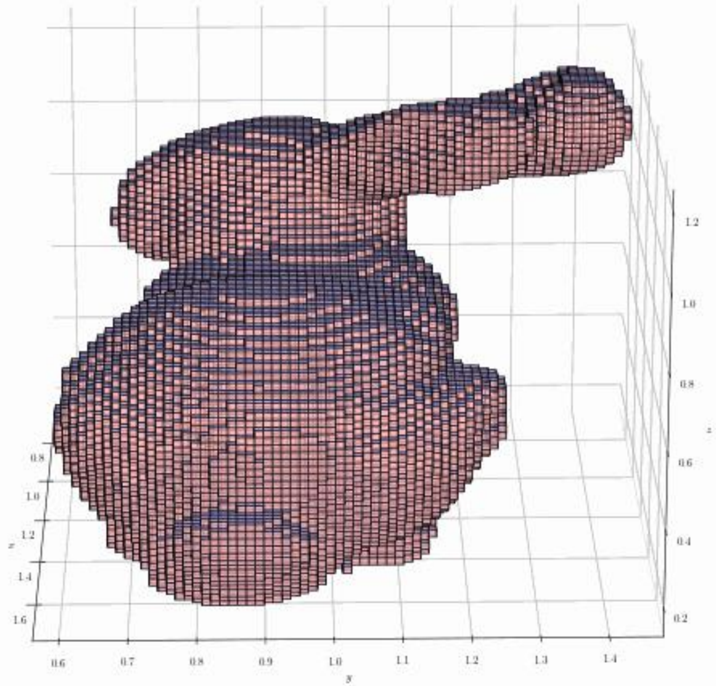

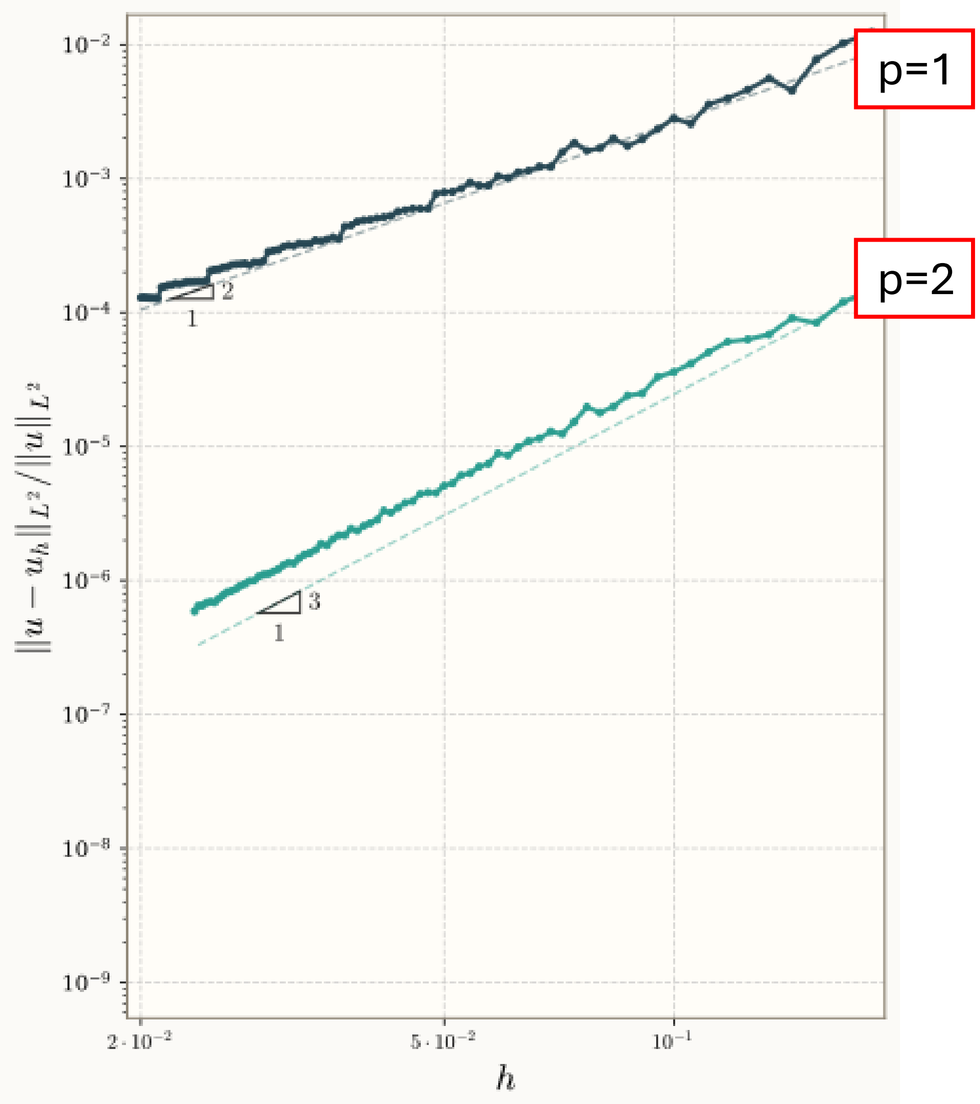

3D extension

SBM has a straightforward extension to robust three-dimensional implementation

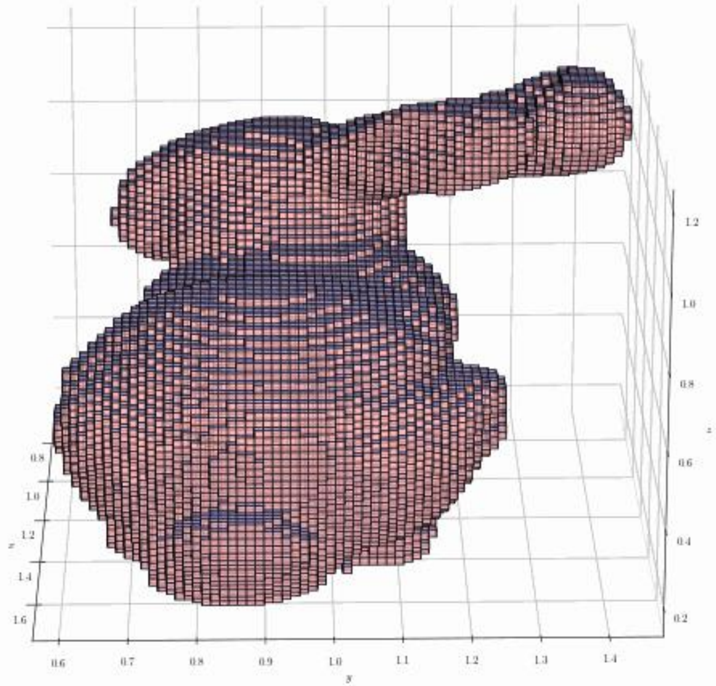

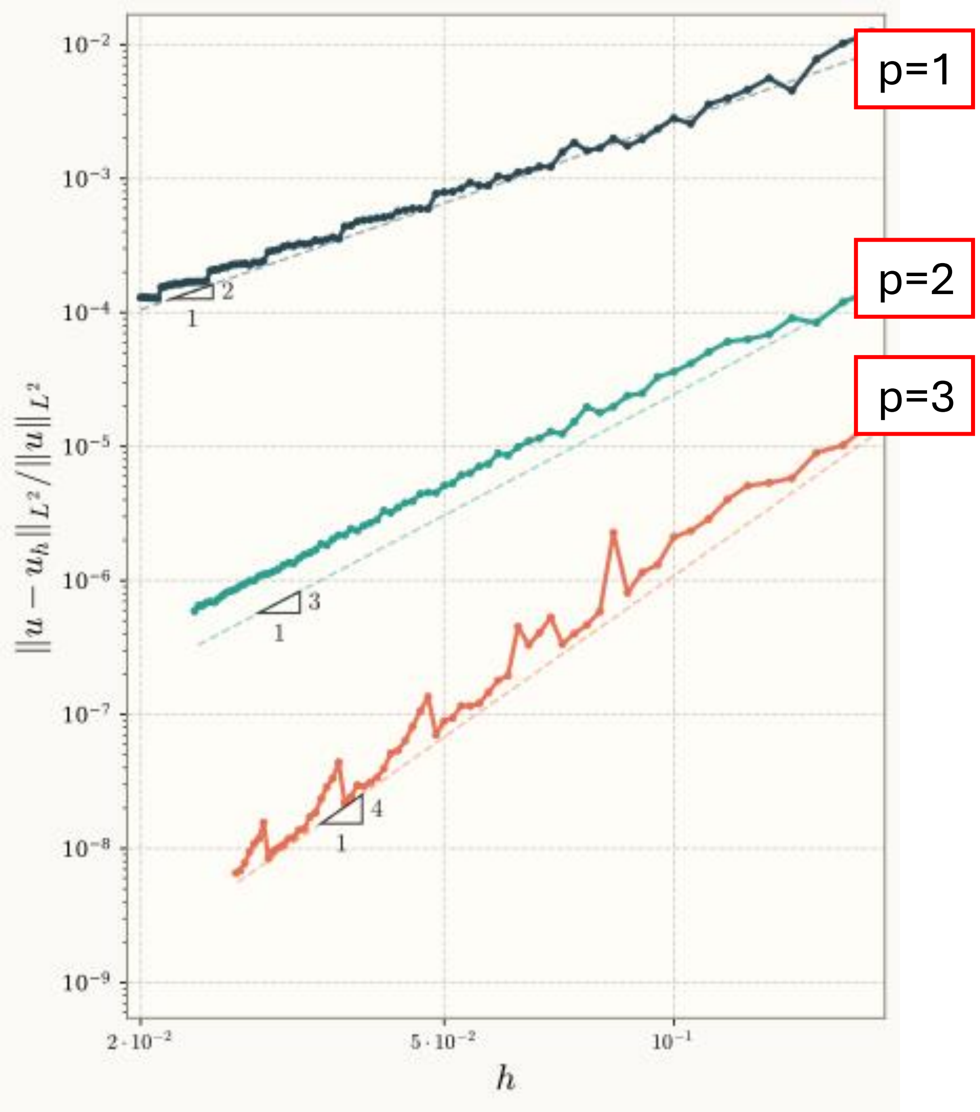

3D extension

SBM has a straightforward extension to robust three-dimensional implementation

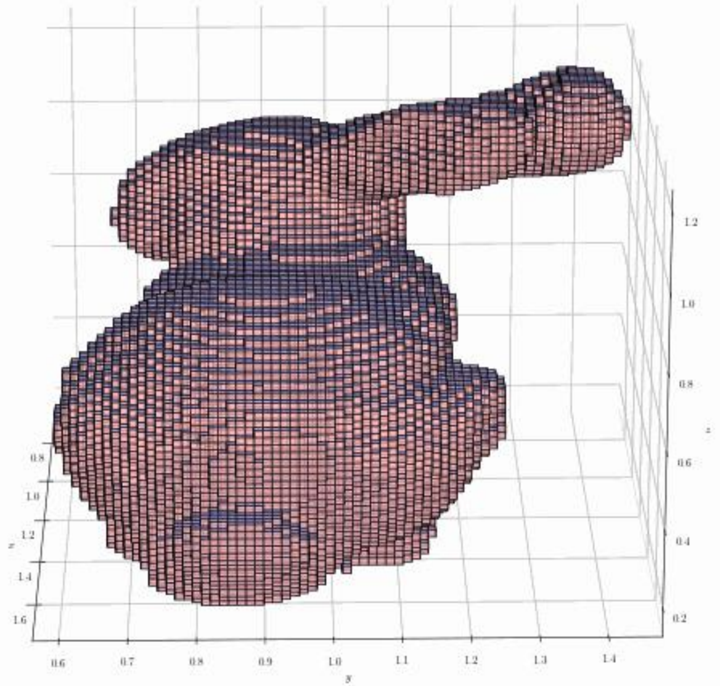

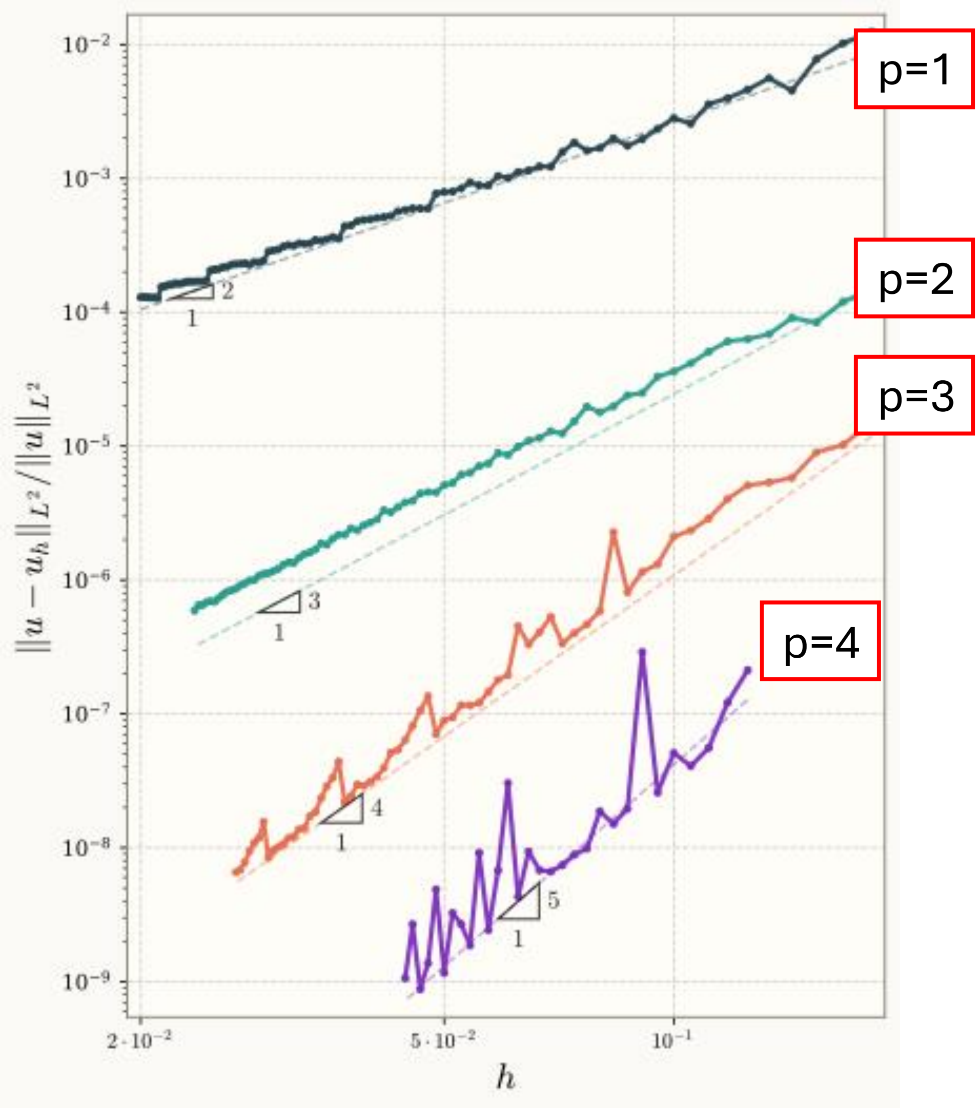

Publication Ⅱ

Publication II:
Extends SBM-IGA to incompressible Stokes flow and introduces VMS stabilization for equal-order velocity–pressure splines.

PDE: incompressible Stokes equations

Equal-order velocity/pressure discretization (IGA-friendly but inf–sup unstable)

Variational Multiscale (VMS) [9] stabilization ensures stability

SBM handles embedded boundaries without body-fitted meshing

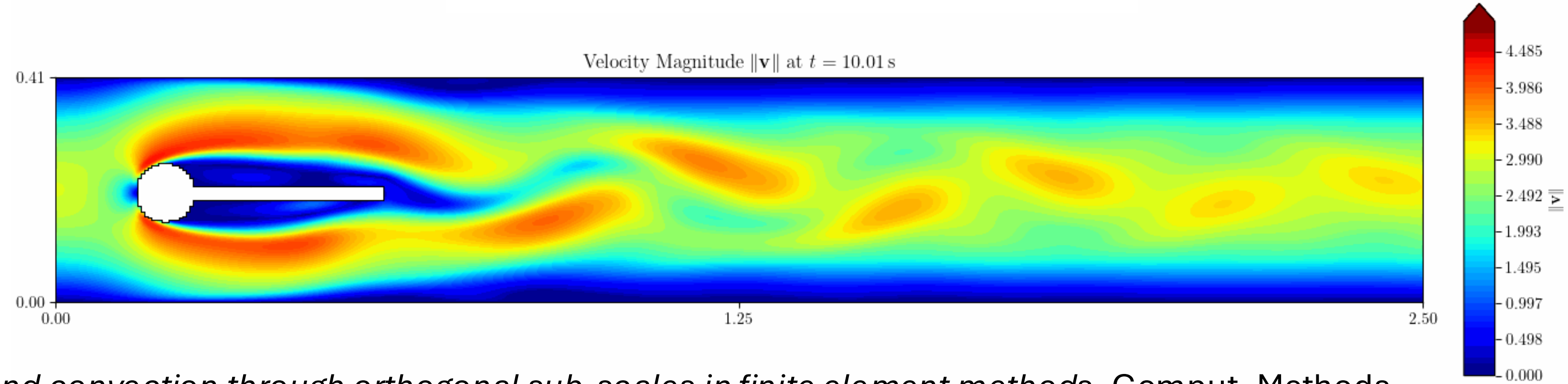

[9] Codina. *Stabilization of incompressibility and convection through orthogonal sub-scales in finite element methods*. Comput. Methods Appl. Mech. Eng., 2000.

Incompressible Stokes with VMS stabilization

PDE: incompressible Stokes fluid

$$-\nabla \cdot \boldsymbol{\tau}(\nabla^{s}\mathbf{u}) + \nabla p = \mathbf{f} \quad \text{in } \Omega$$
$$\nabla \cdot \mathbf{u} = 0 \quad \text{in } \Omega$$

Incompressible Stokes with VMS stabilization

PDE: incompressible Stokes fluid

$$-\nabla \cdot \boxed{\boldsymbol{\tau}(\nabla^s \mathbf{u})} + \nabla p = \mathbf{f} \quad \text{in } \Omega$$

$$\nabla \cdot \mathbf{u} = 0 \quad \text{in } \Omega$$

$$\boldsymbol{\tau}(\nabla^s \mathbf{u}) = 2\mu \nabla^s \mathbf{u}$$

The viscous stress tensor for a *Newtonian fluid*

Incompressible Stokes with VMS stabilization

PDE: incompressible Stokes fluid

$$-\nabla \cdot \boldsymbol{\tau}(\nabla^s \mathbf{u}) + \nabla p = \mathbf{f} \quad \text{in } \Omega$$

$$\nabla \cdot \mathbf{u} = 0 \quad \text{in } \Omega$$

Weak form

$$\int_\Omega \left(-\nabla \cdot \boldsymbol{\tau}(\nabla^s \mathbf{u}) + \nabla p - \mathbf{f}\right) \cdot \mathbf{v} = 0$$

$$\int_\Omega (\nabla \cdot \mathbf{u}) q = 0$$

Incompressible Stokes with VMS stabilization

PDE: incompressible Stokes fluid

$$-\nabla \cdot \boldsymbol{\tau}(\nabla^s \mathbf{u}) + \nabla p = \mathbf{f} \quad \text{in } \Omega$$

$$\nabla \cdot \mathbf{u} = 0 \quad \text{in } \Omega$$

Weak form

$$\int_\Omega \left(-\nabla \cdot \boldsymbol{\tau}(\nabla^s \mathbf{u}) + \nabla p - \mathbf{f}\right) \cdot \mathbf{v} = 0$$

$$\int_\Omega (\nabla \cdot \mathbf{u}) q = 0$$

Integrating by parts

$$\int_\Omega \nabla^s \mathbf{v} : \boldsymbol{\tau}(\nabla^s \mathbf{u}) - \int_\Omega p \nabla \cdot \mathbf{v} - \int_\Gamma (\boldsymbol{\tau}(\nabla^s \mathbf{u}) \cdot \mathbf{n}) \cdot \mathbf{v} + \int_\Gamma p(\mathbf{v} \cdot \mathbf{n}) = \int_\Omega \mathbf{f} \cdot \mathbf{v}$$

$$\int_\Omega q \nabla \cdot \mathbf{u} = 0$$

Incompressible Stokes with VMS stabilization

PDE: incompressible Stokes fluid

$$-\nabla \cdot \boldsymbol{\tau}(\nabla^s \mathbf{u}) + \nabla p = \mathbf{f} \quad \text{in } \Omega$$

$$\nabla \cdot \mathbf{u} = 0 \quad \text{in } \Omega$$

Weak form

$$\int_\Omega \left(-\nabla \cdot \boldsymbol{\tau}(\nabla^s \mathbf{u}) + \nabla p - \mathbf{f}\right) \cdot \mathbf{v} = 0$$

$$\int_\Omega (\nabla \cdot \mathbf{u}) q = 0$$

boundary terms

Integrating by parts

$$\int_\Omega \nabla^s \mathbf{v} : \boldsymbol{\tau}(\nabla^s \mathbf{u}) - \int_\Omega p \nabla \cdot \mathbf{v} - \boxed{\int_\Gamma (\boldsymbol{\tau}(\nabla^s \mathbf{u}) \cdot \mathbf{n}) \cdot \mathbf{v}} + \boxed{\int_\Gamma p(\mathbf{v} \cdot \mathbf{n})} = \int_\Omega \mathbf{f} \cdot \mathbf{v}$$

$$\int_\Omega q \nabla \cdot \mathbf{u} = 0$$

Incompressible Stokes with VMS stabilization

PDE: incompressible Stokes fluid

$$-\nabla\cdot\boldsymbol{\tau}(\nabla^s\mathbf{u})+\nabla p=\mathbf{f}\quad\text{in }\Omega$$
$$\nabla\cdot\mathbf{u}=0\quad\text{in }\Omega$$

Weak form

$$\int_\Omega\left(-\nabla\cdot\boldsymbol{\tau}(\nabla^s\mathbf{u})+\nabla p-\mathbf{f}\right)\cdot\mathbf{v}=0$$
$$\int_\Omega(\nabla\cdot\mathbf{u})q=0$$

boundary terms

Integrating by parts

$$\int_\Omega\nabla^s\mathbf{v}:\boldsymbol{\tau}(\nabla^s\mathbf{u})-\boxed{\int_\Omega p\,\nabla\cdot\mathbf{v}}-\boxed{\int_\Gamma(\boldsymbol{\tau}(\nabla^s\mathbf{u})\cdot\mathbf{n})\cdot\mathbf{v}}+\boxed{\int_\Gamma p(\mathbf{v}\cdot\mathbf{n})}=\int_\Omega\mathbf{f}\cdot\mathbf{v}$$
$$\boxed{\int_\Omega q\,\nabla\cdot\mathbf{u}}=0$$

symmetric coupling terms

Incompressible Stokes with VMS stabilization

PDE: incompressible Stokes fluid

$$-\nabla \cdot \boldsymbol{\tau}(\nabla^s \mathbf{u}) + \nabla p = \mathbf{f} \quad \text{in } \Omega$$
$$\nabla \cdot \mathbf{u} = 0 \quad \text{in } \Omega$$

Weak form

$$\int_\Omega \left(-\nabla \cdot \boldsymbol{\tau}(\nabla^s \mathbf{u}) + \nabla p - \mathbf{f}\right) \cdot \mathbf{v} = 0$$
$$\int_\Omega (\nabla \cdot \mathbf{u}) q = 0$$

Integrating by parts

boundary terms

forcing

$$\boxed{\int_\Omega \nabla^s \mathbf{v} : \boldsymbol{\tau}(\nabla^s \mathbf{u})} - \boxed{\int_\Omega p \nabla \cdot \mathbf{v}} - \boxed{\int_\Gamma (\boldsymbol{\tau}(\nabla^s \mathbf{u}) \cdot \mathbf{n}) \cdot \mathbf{v}} + \boxed{\int_\Gamma p(\mathbf{v} \cdot \mathbf{n})} = \boxed{\int_\Omega \mathbf{f} \cdot \mathbf{v}}$$
$$\boxed{\int_\Omega q \nabla \cdot \mathbf{u}} = 0$$

viscous term

symmetric coupling terms

Incompressible Stokes with VMS stabilization

$$\int_\Omega \nabla^s \mathbf{v} : \boldsymbol{\tau}(\nabla^s \mathbf{u}) - \int_\Omega p \nabla \cdot \mathbf{v} - \int_\Gamma (\boldsymbol{\tau}(\nabla^s \mathbf{u}) \cdot \mathbf{n}) \cdot \mathbf{v} + \int_\Gamma p(\mathbf{v} \cdot \mathbf{n}) = \int_\Omega \mathbf{f} \cdot \mathbf{v}$$

$$\int_\Omega q \nabla \cdot \mathbf{u} = 0$$

Incompressible Stokes with VMS stabilization

$$\int_\Omega \nabla^s \mathbf{v} : \boldsymbol{\tau}(\nabla^s \mathbf{u}) - \int_\Omega p \, \nabla \cdot \mathbf{v} - \int_\Gamma (\boldsymbol{\tau}(\nabla^s \mathbf{u}) \cdot \mathbf{n}) \cdot \mathbf{v} + \int_\Gamma p(\mathbf{v} \cdot \mathbf{n}) = \int_\Omega \mathbf{f} \cdot \mathbf{v}$$

$$\int_\Omega q \, \nabla \cdot \mathbf{u} = 0$$

Introducing the subscales

$$\mathbf{u} = \mathbf{u}_h + \mathbf{u}_s$$
$$p = p_h + p_s$$

Incompressible Stokes with VMS stabilization

$$\int_\Omega \nabla^s \mathbf{v} : \boldsymbol{\tau}(\nabla^s \mathbf{u}) - \int_\Omega p \, \nabla \cdot \mathbf{v} - \int_\Gamma (\boldsymbol{\tau}(\nabla^s \mathbf{u}) \cdot \mathbf{n}) \cdot \mathbf{v} + \int_\Gamma p(\mathbf{v} \cdot \mathbf{n}) = \int_\Omega \mathbf{f} \cdot \mathbf{v}$$

$$\int_\Omega q \, \nabla \cdot \mathbf{u} = 0$$

Introducing the subscales

$$\mathbf{u} = \mathbf{u}_h + \mathbf{u}_s$$
$$p = p_h + p_s$$

$$\mathbf{u}_s := \tau_m \mathcal{P}\left(\boxed{\mathbf{R}_m(\mathbf{u}_h, p_h)}\right)$$

$$p_s := \tau_c \mathcal{P}\left(\boxed{R_c(\mathbf{u}_h, p_h)}\right)$$

$$\int_\Omega \left(-\nabla \cdot \boldsymbol{\tau}(\nabla^s \mathbf{u}) + \nabla p - \mathbf{f}\right) \cdot \mathbf{v} = 0$$

$$\int_\Omega (\nabla \cdot \mathbf{u}) q = 0$$

Incompressible Stokes with VMS stabilization

$$\int_\Omega \nabla^s \mathbf{v} : \boldsymbol{\tau}(\nabla^s \mathbf{u}) - \int_\Omega p\, \nabla \cdot \mathbf{v} - \int_\Gamma (\boldsymbol{\tau}(\nabla^s \mathbf{u}) \cdot \mathbf{n}) \cdot \mathbf{v} + \int_\Gamma p(\mathbf{v} \cdot \mathbf{n}) = \int_\Omega \mathbf{f} \cdot \mathbf{v}$$

$$\int_\Omega q\, \nabla \cdot \mathbf{u} = 0$$

Introducing the subscales $\mathbf{u} = \mathbf{u}_h + \mathbf{u}_s$

$p = p_h + p_s$

Algebraic Sub-Grid Scale (ASGS)

$$\mathbf{u}_s := \tau_m \mathcal{P}(\mathbf{R}_m(\mathbf{u}_h, p_h)) \longrightarrow \mathbf{u}_s := \tau_m \mathbf{R}_m(\mathbf{u}_h, p_h)$$

$$p_s := \tau_c \mathcal{P}(R_c(\mathbf{u}_h, p_h)) \longrightarrow p_s := \tau_c R_c(\mathbf{u}_h, p_h)$$

Incompressible Stokes with VMS stabilization

$$\int_\Omega \nabla^s \mathbf{v} : \boldsymbol{\tau}(\nabla^s \mathbf{u}) - \int_\Omega p \, \nabla \cdot \mathbf{v} - \int_\Gamma (\boldsymbol{\tau}(\nabla^s \mathbf{u}) \cdot \mathbf{n}) \cdot \mathbf{v} + \int_\Gamma p(\mathbf{v} \cdot \mathbf{n}) = \int_\Omega \mathbf{f} \cdot \mathbf{v}$$

$$\int_\Omega q \, \nabla \cdot \mathbf{u} = 0$$

Introducing the subscales $\mathbf{u} = \mathbf{u}_h + \mathbf{u}_s$

$p = p_h + p_s$

Algebraic Sub-Grid Scale (ASGS)

$$\mathbf{u}_s := \tau_m \mathcal{P}(\mathbf{R}_m(\mathbf{u}_h, p_h)) \longrightarrow \mathbf{u}_s := \tau_m \mathbf{R}_m(\mathbf{u}_h, p_h)$$

$$p_s := \tau_c \mathcal{P}(R_c(\mathbf{u}_h, p_h)) \longrightarrow p_s := \tau_c R_c(\mathbf{u}_h, p_h)$$

Substituting:

$$\int_\Omega \nabla^s \mathbf{v} : \boldsymbol{\tau}(\nabla^s \mathbf{u}_h) - \int_\Omega (p_h + p_s) \, \nabla \cdot \mathbf{v} - \int_\Gamma (\boldsymbol{\tau}(\nabla^s \mathbf{u}_h) \cdot \mathbf{n}) \cdot \mathbf{v} + \int_\Gamma p(\mathbf{v} \cdot \mathbf{n}) = \int_\Omega \mathbf{f} \cdot \mathbf{v}$$

$$\int_\Omega q \, \nabla \cdot (\mathbf{u}_h + \mathbf{u}_s) = 0$$

Incompressible Stokes with VMS stabilization

$$\int_\Omega \nabla^s \mathbf{v} : \boldsymbol{\tau}(\nabla^s \mathbf{u}) - \int_\Omega p\,\nabla\cdot\mathbf{v} - \int_\Gamma (\boldsymbol{\tau}(\nabla^s\mathbf{u})\cdot\mathbf{n})\cdot\mathbf{v} + \int_\Gamma p(\mathbf{v}\cdot\mathbf{n}) = \int_\Omega \mathbf{f}\cdot\mathbf{v}$$

$$\int_\Omega q\,\nabla\cdot\mathbf{u} = 0$$

Introducing the subscales
$$\mathbf{u} = \mathbf{u}_h + \mathbf{u}_s$$
$$p = p_h + p_s$$

Algebraic Sub-Grid Scale (ASGS)

$$\mathbf{u}_s := \tau_m \mathcal{P}(\mathbf{R}_m(\mathbf{u}_h, p_h)) \longrightarrow \mathbf{u}_s := \tau_m \mathbf{R}_m(\mathbf{u}_h, p_h)$$

$$p_s := \tau_c \mathcal{P}(R_c(\mathbf{u}_h, p_h)) \longrightarrow p_s := \tau_c R_c(\mathbf{u}_h, p_h)$$

Substituting:

$$\int_\Omega \nabla^s \mathbf{v} : \boldsymbol{\tau}(\boxed{\nabla^s \mathbf{u}_h}) - \int_\Omega (\boxed{p_h + p_s})\,\nabla\cdot\mathbf{v} - \int_\Gamma (\boldsymbol{\tau}(\nabla^s\mathbf{u}_h)\cdot\mathbf{n})\cdot\mathbf{v} + \int_\Gamma p(\mathbf{v}\cdot\mathbf{n}) = \int_\Omega \mathbf{f}\cdot\mathbf{v}$$

$$\int_\Omega q\,\nabla\cdot(\boxed{\mathbf{u}_h + \mathbf{u}_s}) = 0$$

subscale not needed

subscale is needed

Incompressible Stokes with VMS stabilization

$$\int_\Omega \nabla^s \mathbf{v} : \boldsymbol{\tau}(\nabla^s \mathbf{u}_h) - \int_\Omega (p_h + p_s)\, \nabla \cdot \mathbf{v} - \int_\Gamma (\boldsymbol{\tau}(\nabla^s \mathbf{u}_h) \cdot \mathbf{n}) \cdot \mathbf{v} + \int_\Gamma p(\mathbf{v} \cdot \mathbf{n}) = \int_\Omega \mathbf{f} \cdot \mathbf{v}$$

$$\int_\Omega q\, \nabla \cdot (\mathbf{u}_h + \mathbf{u}_s) = 0$$

Incompressible Stokes with VMS stabilization

$$\int_\Omega \nabla^s \mathbf{v} : \boldsymbol{\tau}(\nabla^s \mathbf{u}_h) - \int_\Omega (p_h + \boxed{p_s}) \nabla \cdot \mathbf{v} - \int_\Gamma (\boldsymbol{\tau}(\nabla^s \mathbf{u}_h) \cdot \mathbf{n}) \cdot \mathbf{v} + \int_\Gamma p(\mathbf{v} \cdot \mathbf{n}) = \int_\Omega \mathbf{f} \cdot \mathbf{v}$$

$$\int_\Omega q \, \nabla \cdot (\mathbf{u}_h + \boxed{\mathbf{u}_s}) = 0$$

Incompressible Stokes with VMS stabilization

$$\int_\Omega \nabla^s \mathbf{v} : \boldsymbol{\tau}(\nabla^s \mathbf{u}_h) - \int_\Omega (p_h + \boxed{p_s})\, \nabla \cdot \mathbf{v} - \int_\Gamma (\boldsymbol{\tau}(\nabla^s \mathbf{u}_h) \cdot \mathbf{n}) \cdot \mathbf{v} + \int_\Gamma p(\mathbf{v} \cdot \mathbf{n}) = \int_\Omega \mathbf{f} \cdot \mathbf{v}$$

$$\int_\Omega q\, \nabla \cdot (\mathbf{u}_h + \boxed{\mathbf{u}_s}) = 0$$

Only one term needs additional care with respect to low order FEM

$$\int_\Omega q\, \nabla \cdot \mathbf{u}_s = - \int_\Omega \nabla q \cdot \mathbf{u}_s + \underbrace{\cancel{\int_\Gamma q\, \mathbf{u}_s \cdot \mathbf{n}}}_{= 0 \text{ on } \Gamma}$$

Incompressible Stokes with VMS stabilization

$$\int_\Omega \nabla^s \mathbf{v} : \boldsymbol{\tau}(\nabla^s \mathbf{u}_h) - \int_\Omega (p_h + \boxed{p_s}) \nabla \cdot \mathbf{v} - \int_\Gamma (\boldsymbol{\tau}(\nabla^s \mathbf{u}_h) \cdot \mathbf{n}) \cdot \mathbf{v} + \int_\Gamma p(\mathbf{v} \cdot \mathbf{n}) = \int_\Omega \mathbf{f} \cdot \mathbf{v}$$

$$\int_\Omega q \nabla \cdot (\mathbf{u}_h + \boxed{\mathbf{u}_s}) = 0$$

= 0 on Γ

Only one term needs additional care with respect to low order FEM

$$\int_\Omega q \nabla \cdot \mathbf{u}_s = -\int_\Omega \nabla q \cdot \mathbf{u}_s + \cancel{\int_\Gamma q \mathbf{u}_s \cdot \mathbf{n}}$$

$$-\tau_m \underline{\int_\Omega \nabla q \cdot \mathbf{f}} - \boxed{\tau_m \int_\Omega \nabla q \cdot (\nabla \cdot \boldsymbol{\tau}(\nabla^s \mathbf{u}_h))} + \tau_m \underline{\int_\Omega \nabla q \cdot \nabla p}$$

Incompressible Stokes with VMS stabilization

Only one term needs additional care with respect to low order FEM

$$-\underline{\tau_m \int_\Omega \nabla q \cdot \mathbf{f}} - \boxed{\tau_m \int_\Omega \nabla q \cdot (\nabla \cdot \boldsymbol{\tau}(\nabla^s \mathbf{u}_h))} + \underline{\tau_m \int_\Omega \nabla q \cdot \nabla p}$$

Incompressible Stokes with VMS stabilization

Only one term needs additional care with respect to low order FEM

$$-\tau_m \int_\Omega \nabla q \cdot \mathbf{f} - \boxed{\tau_m \int_\Omega \nabla q \cdot (\nabla \cdot \boldsymbol{\tau}(\nabla^s \mathbf{u}_h))} + \tau_m \int_\Omega \nabla q \cdot \nabla p$$

- For *p=1* this term vanishes
- For *p>1* it is essential to preserve optimal convergence

$$\begin{bmatrix} N_1(\xi_1,\eta_1) & N_2(\xi_1,\eta_1) & \cdots & N_{n_{cp}}(\xi_1,\eta_1) \\ N_1(\xi_2,\eta_2) & N_2(\xi_2,\eta_2) & \cdots & N_{n_{cp}}(\xi_2,\eta_2) \\ \vdots & \vdots & \ddots & \vdots \\ N_1(\xi_{n_{cp}},\eta_{n_{cp}}) & N_2(\xi_{n_{cp}},\eta_{n_{cp}}) & \cdots & N_{n_{cp}}(\xi_{n_{cp}},\eta_{n_{cp}}) \end{bmatrix} \begin{bmatrix} c_{1,xx} \\ c_{2,xx} \\ \vdots \\ c_{n_{cp},xx} \end{bmatrix} = \begin{bmatrix} \tau_{xx}(\xi_1,\eta_1) \\ \tau_{xx}(\xi_2,\eta_2) \\ \vdots \\ \tau_{xx}(\xi_{n_{cp}},\eta_{n_{cp}}) \end{bmatrix}$$

A local reconstruction of the stress tensor is done using the B-Spline discretization

$$\nabla \cdot \boldsymbol{\tau} \approx \begin{bmatrix} \sum_{i=1}^{n_{cp}} \left(c_{i,xx} \frac{\partial N_i}{\partial x} + c_{i,xy} \frac{\partial N_i}{\partial y} \right) \\ \sum_{i=1}^{n_{cp}} \left(c_{i,xy} \frac{\partial N_i}{\partial x} + c_{i,yy} \frac{\partial N_i}{\partial y} \right) \end{bmatrix}$$

In smooth Newtonian regimes, VMS-stabilized SBM-IGA achieves the expected high-order accuracy

Consider a smooth solution

$$\mathbf{u} = \begin{bmatrix} \cosh(x)\sinh(y) \\ -\sinh(x)\cosh(y) \end{bmatrix}$$

$$p = \sin(x)\cos(y)$$

In smooth Newtonian regimes, VMS-stabilized SBM-IGA achieves the expected high-order accuracy

Consider a smooth solution

$$\mathbf{u} = \begin{bmatrix} \cosh(x)\sinh(y) \\ -\sinh(x)\cosh(y) \end{bmatrix}$$

$$p = \sin(x)\cos(y)$$

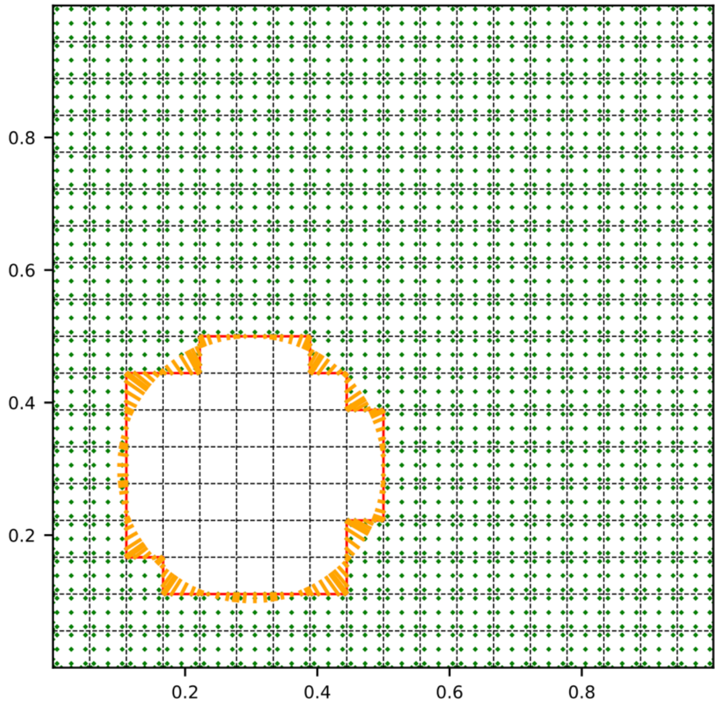

Problem geometry

In smooth Newtonian regimes, VMS-stabilized SBM-IGA achieves the expected high-order accuracy

Consider a smooth solution

$$\mathbf{u} = \begin{bmatrix} \cosh(x)\sinh(y) \\ -\sinh(x)\cosh(y) \end{bmatrix}$$

$$p = \sin(x)\cos(y)$$

The forcing turns out to be

$$\mathbf{f}(x, y) = \begin{bmatrix} -2\mu\cosh(x)\sinh(y) + \cos(x)\cos(y) \\ 2\mu\sinh(x)\cosh(y) - \sin(x)\sin(y) \end{bmatrix}$$

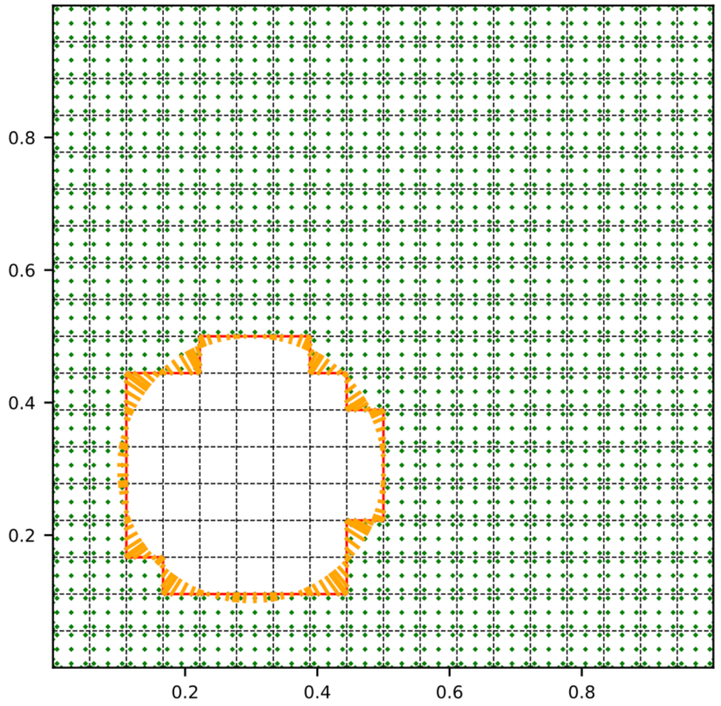

Problem geometry

In smooth Newtonian regimes, VMS-stabilized SBM-IGA achieves the expected high-order accuracy

Convergence study using a manufactured solution

- SBM treatment is high-order accurate
- IGA achieves high-order convergence

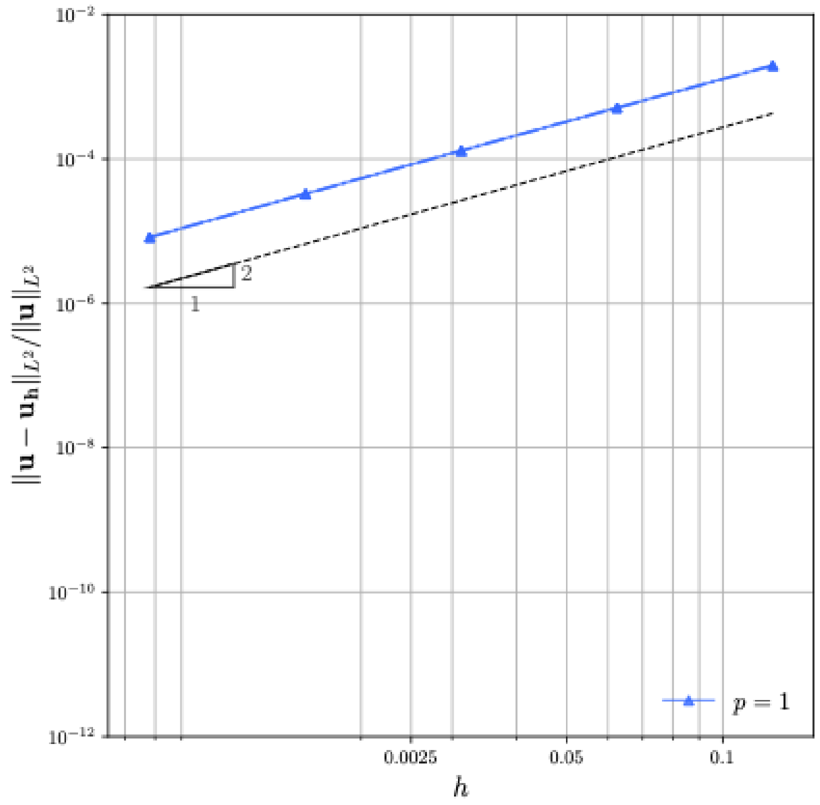

Velocity

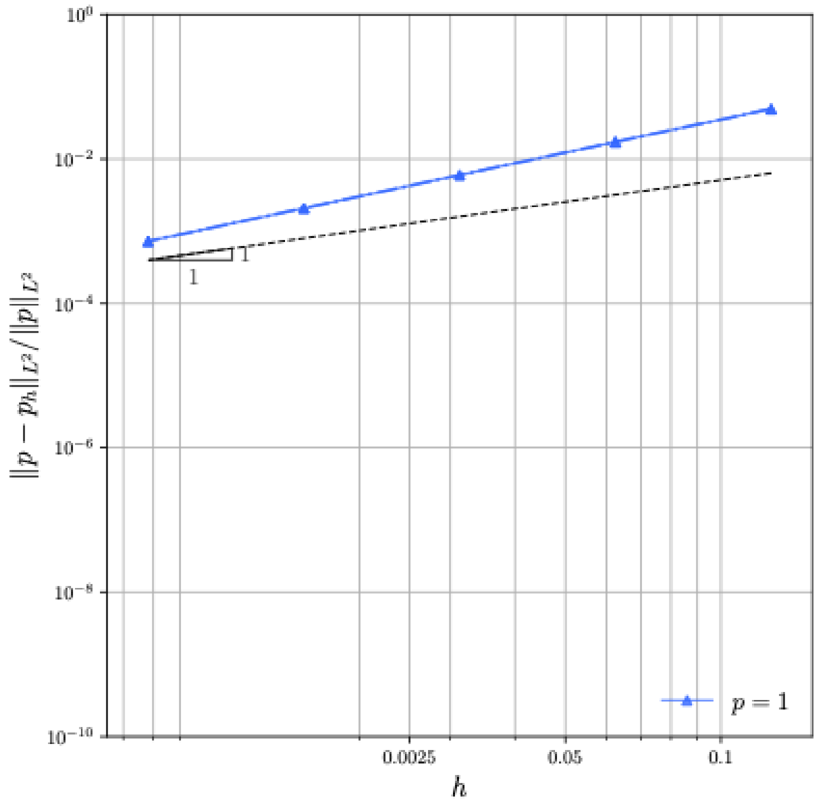

Pressure

In smooth Newtonian regimes, VMS-stabilized SBM-IGA achieves the expected high-order accuracy

Convergence study using a manufactured solution

- SBM treatment is high-order accurate
- IGA achieves high-order convergence

without stress reconstruction
(dashed lines)

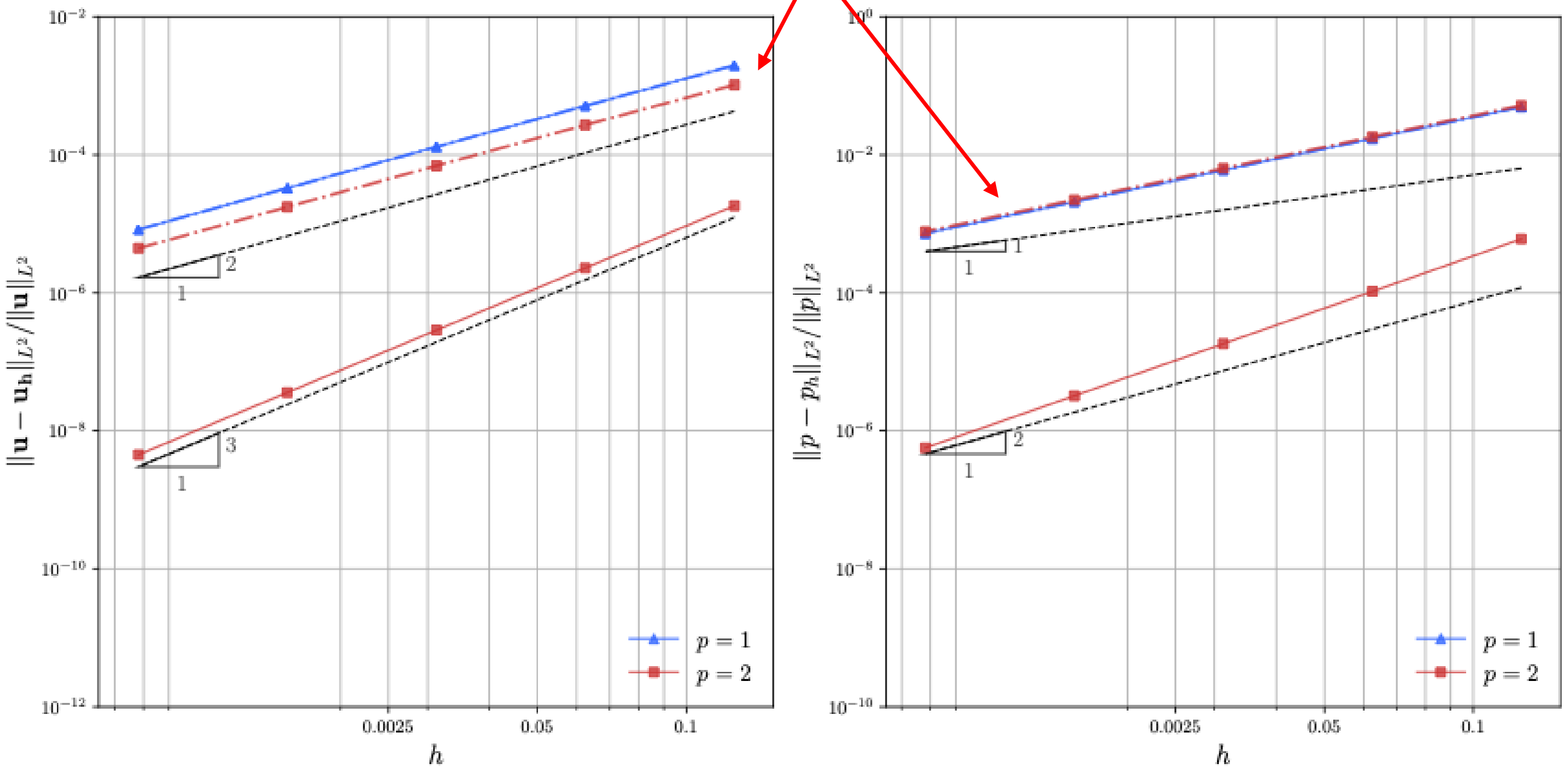

Velocity

Pressure

In smooth Newtonian regimes, VMS-stabilized SBM-IGA achieves the expected high-order accuracy

Convergence study using a manufactured solution

- SBM treatment is high-order accurate
- IGA achieves high-order convergence

without stress reconstruction
(dashed lines)

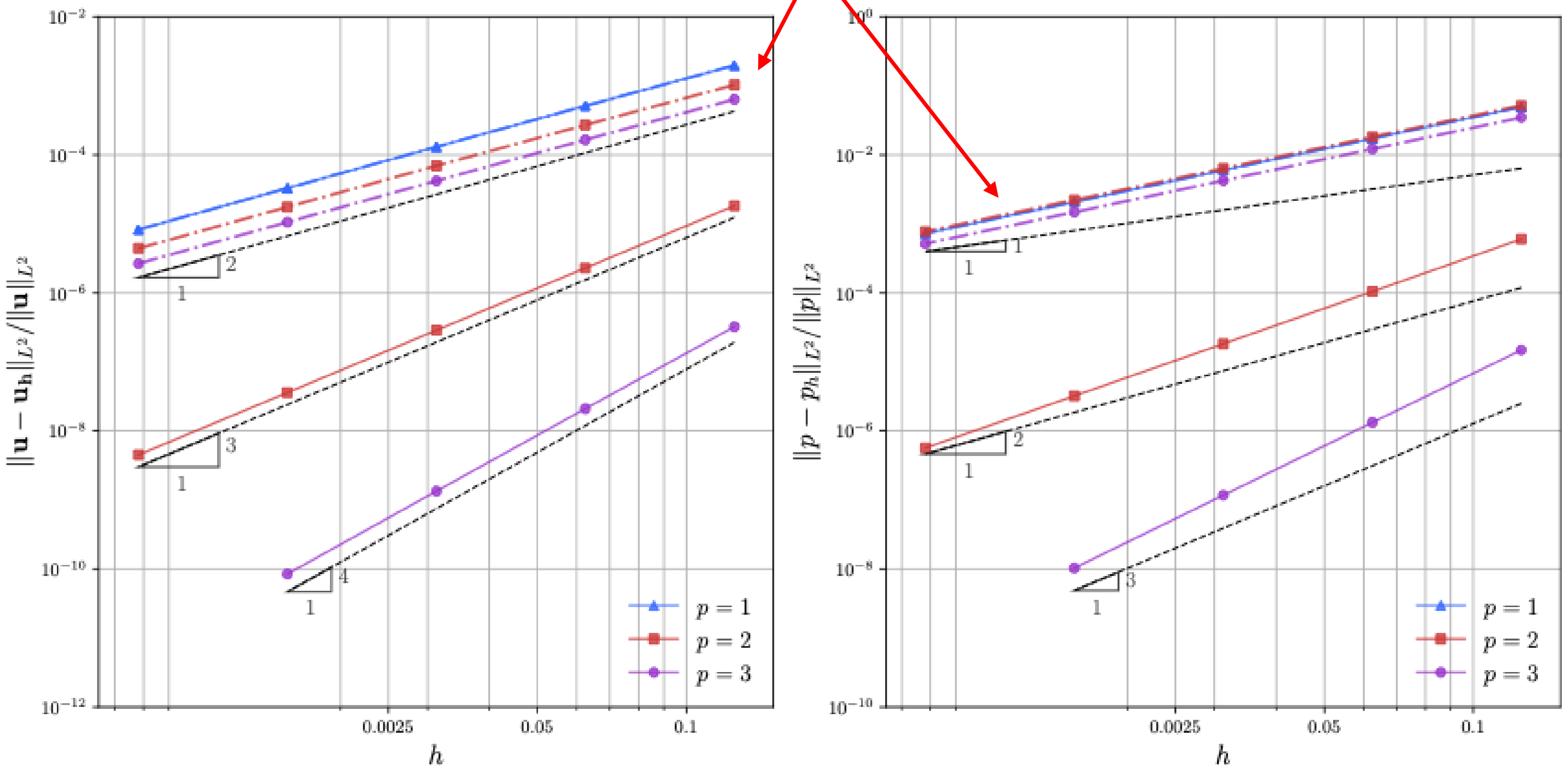

Velocity

Pressure

Viscoplastic Bingham flow introduces yield surfaces that reduce solution regularity

Non-Newtonian fluids:

- Stress–strain relation is nonlinear
- Change of material properties
- Sharp transitions

Viscoplastic Bingham flow introduces yield surfaces that reduce solution regularity

Non-Newtonian fluids:

- Stress–strain relation is nonlinear
- Change of material properties
- Sharp transitions

Bingham Model:
$$\tau = \begin{cases} \tau_y & \text{for } |\boldsymbol{\tau}| \leq \tau_y \\ \tau_y + \mu\dot{\gamma} & \text{for } |\boldsymbol{\tau}| > \tau_y \end{cases}$$

Viscoplastic Bingham flow introduces yield surfaces that reduce solution regularity

Non-Newtonian fluids:

- Stress–strain relation is nonlinear
- Change of material properties
- Sharp transitions

Bingham Model: $$\tau = \begin{cases} \tau_y & \text{for } |\boldsymbol{\tau}| \leq \tau_y \\ \tau_y + \mu\dot{\gamma} & \text{for } |\boldsymbol{\tau}| > \tau_y \end{cases}$$

Regularized Bingham [10]: $$\tau = \tau_y\left(1 - e^{-m\dot{\gamma}}\right) + \mu\dot{\gamma}$$

[10] Mitsoulis and Huilgol. Entry flows of bingham plastics in expansions. Journal of non-newtonian fluid mechanics, 2004.

Viscoplastic Bingham flow introduces yield surfaces that reduce solution regularity

Non-Newtonian fluids:

- Stress–strain relation is nonlinear
- Change of material properties
- Sharp transitions

Bingham Model: $$\tau = \begin{cases} \tau_y & \text{for } |\boldsymbol{\tau}| \le \tau_y \\ \tau_y + \mu\dot{\gamma} & \text{for } |\boldsymbol{\tau}| > \tau_y \end{cases}$$

Regularized Bingham [10]: $$\tau = \tau_y\left(1 - e^{-m\dot{\gamma}}\right) + \mu\dot{\gamma}$$

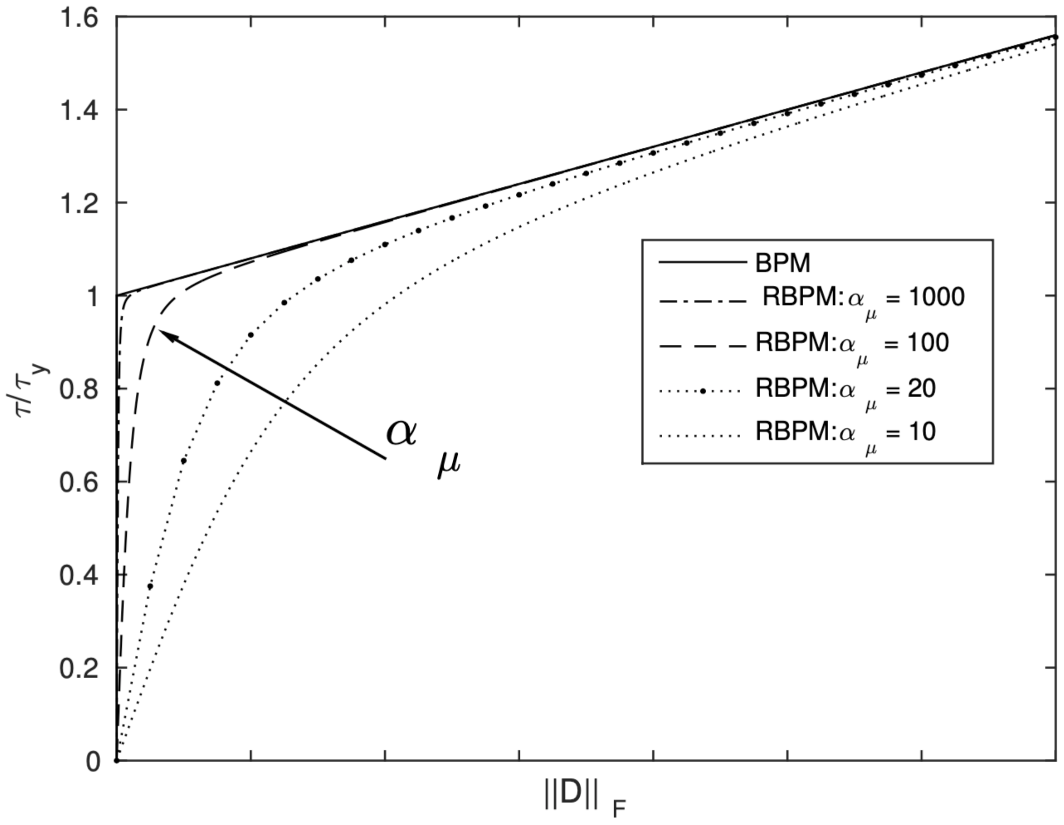

Regularized Bingham model. Image taken from [11]

[10] Mitsoulis and Huilgol. Entry flows of bingham plastics in expansions. Journal of non-newtonian fluid mechanics, 2004.
[11] Krimi, et al. Multiphase Smoothed Particle Hydrodynamics approach for modeling Soil-Water interactions. Advances in Water Resources, 2018.

In Poiseuille Bingham flow convergence is limited

Consider a simple Poiseuille flow of Bingham fluid

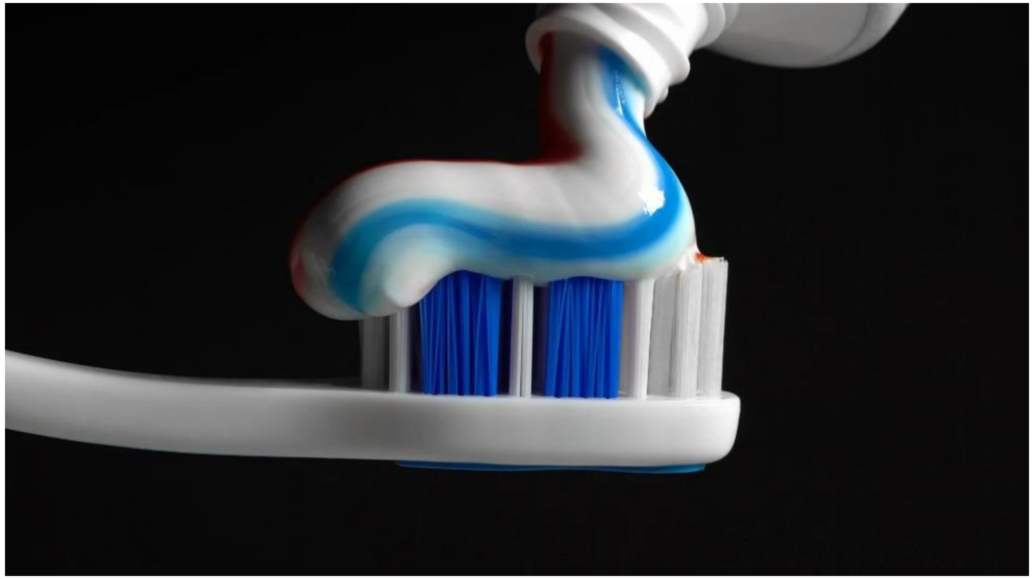

In Poiseuille Bingham flow convergence is limited

Consider a simple Poiseuille flow of Bingham fluid

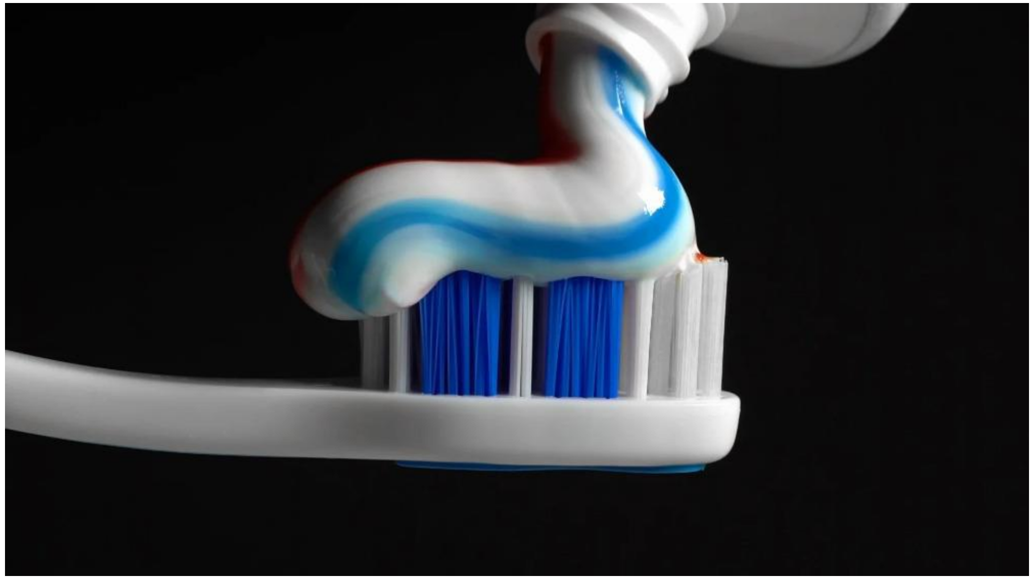

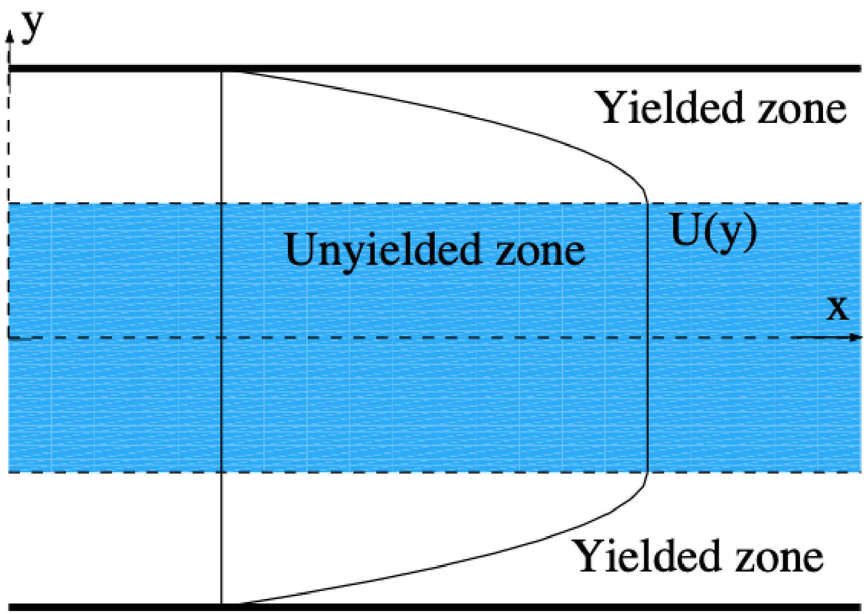

Bingham Poiseuille flow. Image taken from [12]

[12] Nouar et al. Stability of plane Poiseuille flow and energy growth in the case of a Bingham fluid. Mechanics of 21° Century, 2004.

In Poiseuille Bingham flow convergence is limited

Consider a simple Poiseuille flow of Bingham fluid

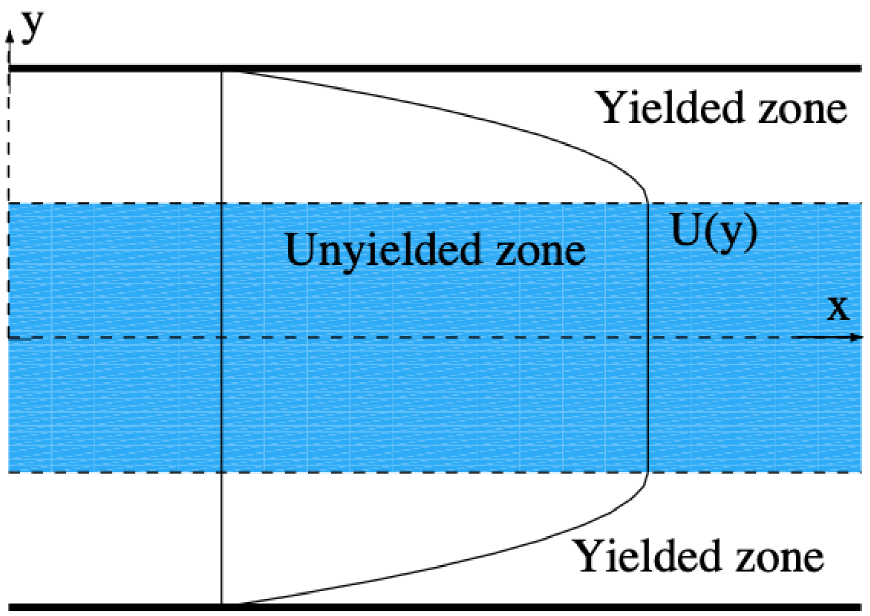

Bingham Poiseuille flow. Image taken from [12]

[12] Nouar et al. Stability of plane Poiseuille flow and energy growth in the case of a Bingham fluid. Mechanics of 21° Century, 2004.

In Poiseuille Bingham flow convergence is limited

Consider a simple Poiseuille flow of Bingham fluid

The analytical solution is available:

$$u_x(y) = \begin{cases} \frac{1}{2\mu}\left(-\frac{\Delta p}{L}\right)\left((h_1 + \frac{H}{2})^2 - (h_1 - y)^2\right) & \text{if } -\frac{H}{2} \leq y < h_1 \\ \frac{1}{2\mu}\left(-\frac{\Delta p}{L}\right) h_1^2 & \text{if } h_1 \leq y < h_2 \\ \frac{1}{2\mu}\left(-\frac{\Delta p}{L}\right)\left((\frac{H}{2} - h_2)^2 - (y - h_2)^2\right) & \text{if } h_2 \leq y \leq \frac{H}{2} \end{cases}$$

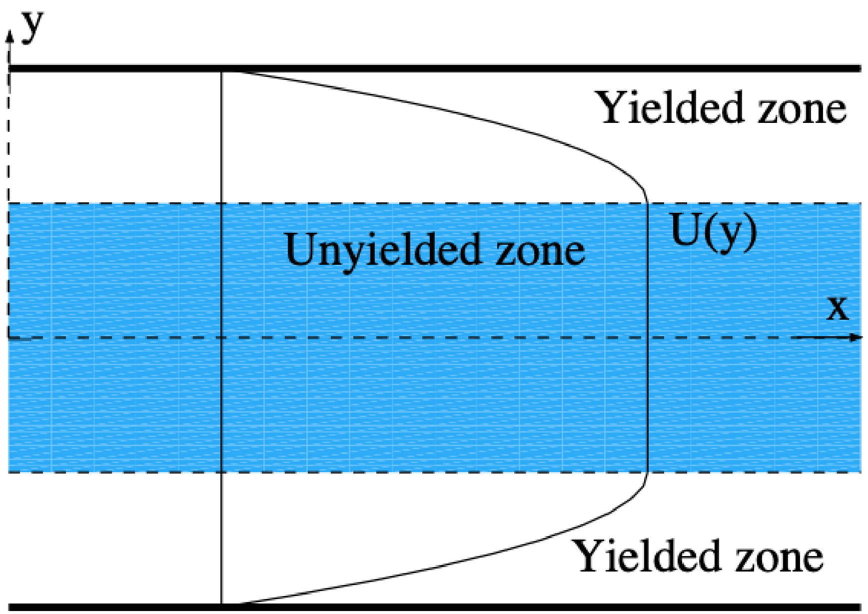

Bingham Poiseuille flow. Image taken from [12]

[12] Nouar et al. Stability of plane Poiseuille flow and energy growth in the case of a Bingham fluid. Mechanics of 21° Century, 2004.

In Poiseuille Bingham flow convergence is limited

Consider a simple Poiseuille flow of Bingham fluid

The analytical solution is available:

$$u_x(y) = \begin{cases} \frac{1}{2\mu}\left(-\frac{\Delta p}{L}\right)\left((h_1 + \frac{H}{2})^2 - (h_1 - y)^2\right) & \text{if } -\frac{H}{2} \leq y < h_1 \\ \frac{1}{2\mu}\left(-\frac{\Delta p}{L}\right) h_1^2 & \text{if } h_1 \leq y < h_2 \\ \frac{1}{2\mu}\left(-\frac{\Delta p}{L}\right)\left((\frac{H}{2} - h_2)^2 - (y - h_2)^2\right) & \text{if } h_2 \leq y \leq \frac{H}{2} \end{cases}$$

The horizontal component is a simple **piecewise quadratic solution** and it is globally C^1

$$h_1 = -\tau_y\left(-\frac{\Delta p}{L}\right)^{-1}$$

$$h_2 = \tau_y\left(-\frac{\Delta p}{L}\right)^{-1}$$

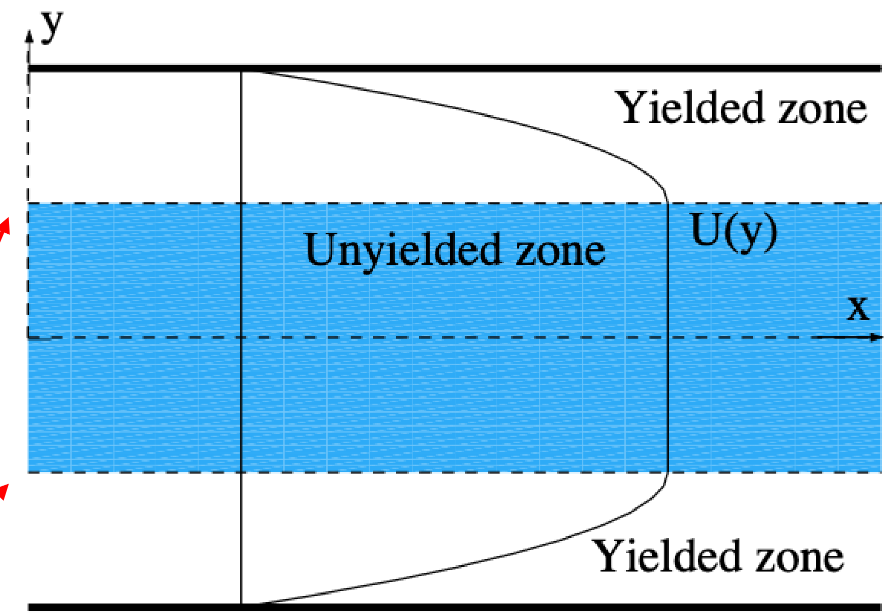

Bingham Poiseuille flow. Image taken from [12]

[12] Nouar et al. Stability of plane Poiseuille flow and energy growth in the case of a Bingham fluid. Mechanics of 21° Century, 2004.

In Poiseuille Bingham flow convergence is limited

$$u_x(y) = \begin{cases} \frac{1}{2\mu}\left(-\frac{\Delta p}{L}\right)\left((h_1 + \frac{H}{2})^2 - (h_1 - y)^2\right) & \text{if } -\frac{H}{2} \leq y < h_1 \\ \frac{1}{2\mu}\left(-\frac{\Delta p}{L}\right) h_1^2 & \text{if } h_1 \leq y < h_2 \\ \frac{1}{2\mu}\left(-\frac{\Delta p}{L}\right)\left((\frac{H}{2} - h_2)^2 - (y - h_2)^2\right) & \text{if } h_2 \leq y \leq \frac{H}{2} \end{cases}$$

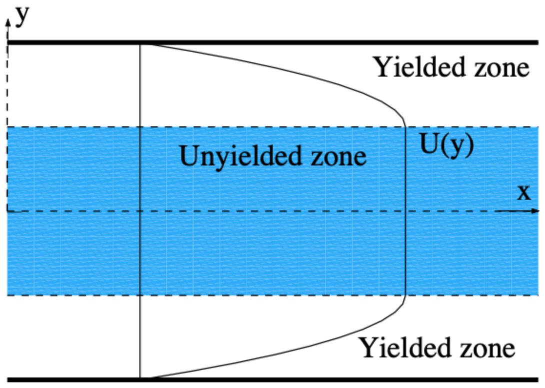

Increasing p beyond 2 does not improve convergence

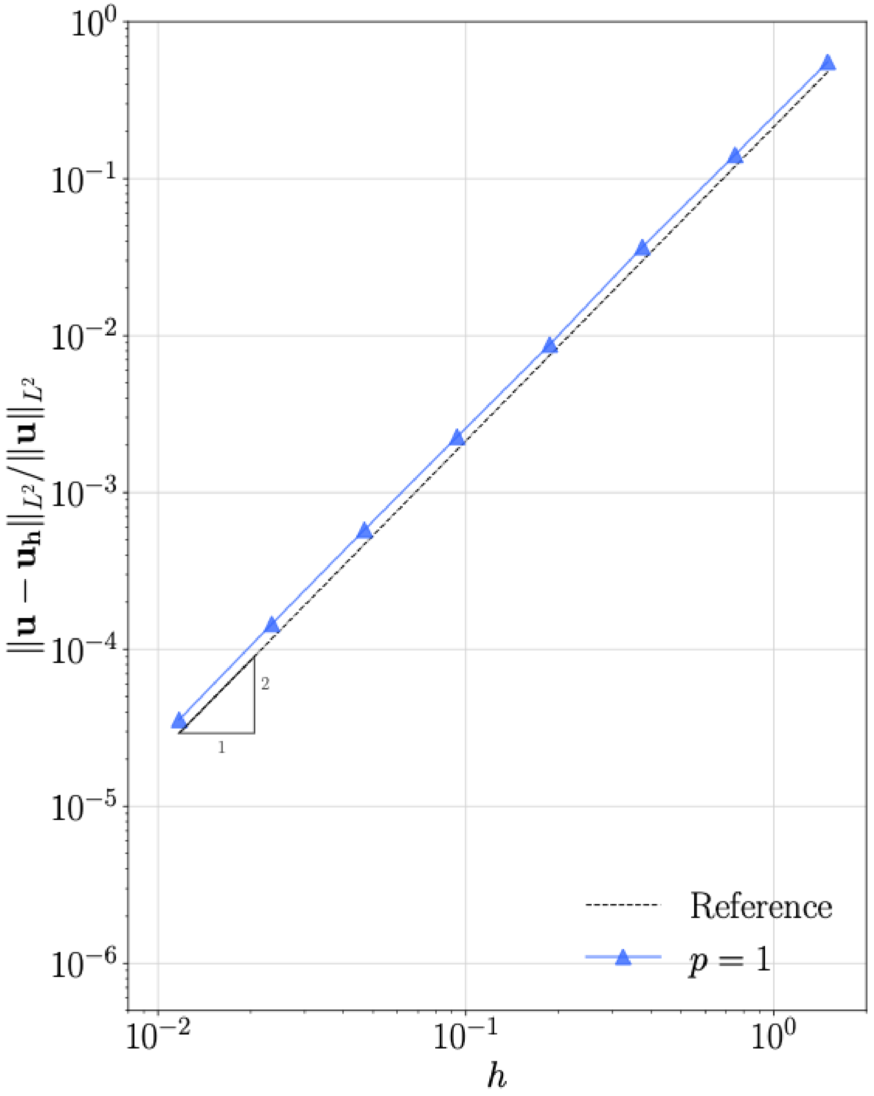

In Poiseuille Bingham flow convergence is limited

$$u_x(y) = \begin{cases} \frac{1}{2\mu}\left(-\frac{\Delta p}{L}\right)\left((h_1 + \frac{H}{2})^2 - (h_1 - y)^2\right) & \text{if } -\frac{H}{2} \le y < h_1 \\ \frac{1}{2\mu}\left(-\frac{\Delta p}{L}\right)h_1^2 & \text{if } h_1 \le y < h_2 \\ \frac{1}{2\mu}\left(-\frac{\Delta p}{L}\right)\left((\frac{H}{2} - h_2)^2 - (y - h_2)^2\right) & \text{if } h_2 \le y \le \frac{H}{2} \end{cases}$$

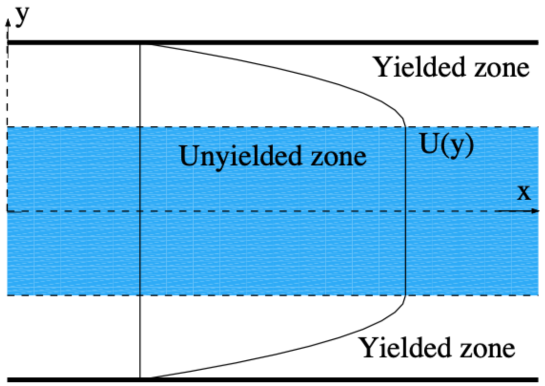

Increasing p beyond 2 does not improve convergence

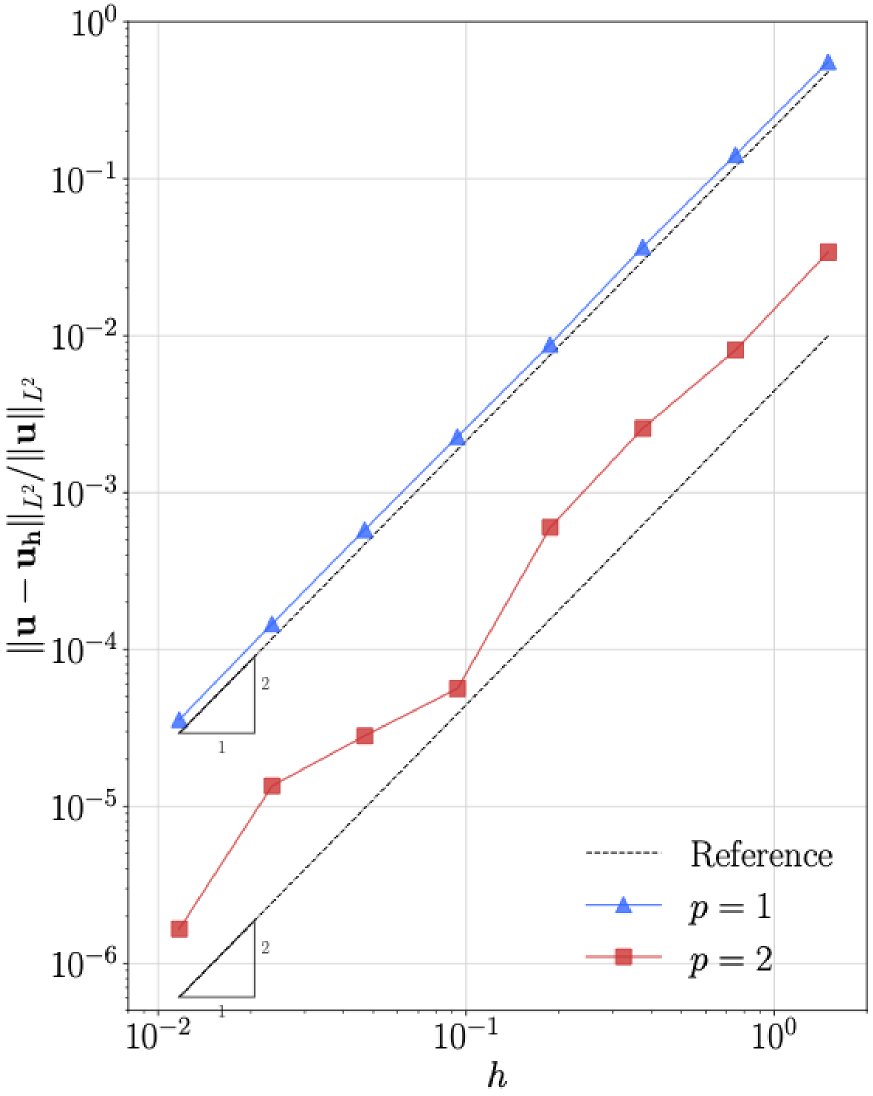

In Poiseuille Bingham flow convergence is limited

$$u_x(y) = \begin{cases} \frac{1}{2\mu}\left(-\frac{\Delta p}{L}\right)\left((h_1 + \frac{H}{2})^2 - (h_1 - y)^2\right) & \text{if } -\frac{H}{2} \leq y < h_1 \\ \frac{1}{2\mu}\left(-\frac{\Delta p}{L}\right) h_1^2 & \text{if } h_1 \leq y < h_2 \\ \frac{1}{2\mu}\left(-\frac{\Delta p}{L}\right)\left((\frac{H}{2} - h_2)^2 - (y - h_2)^2\right) & \text{if } h_2 \leq y \leq \frac{H}{2} \end{cases}$$

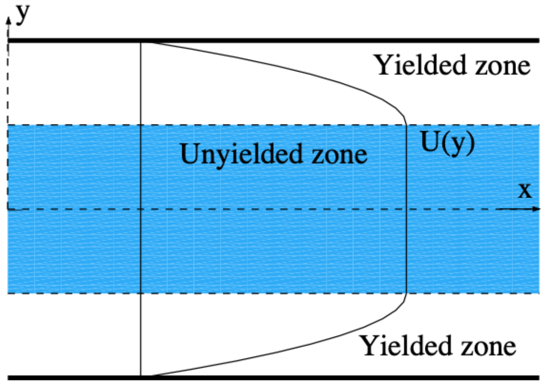

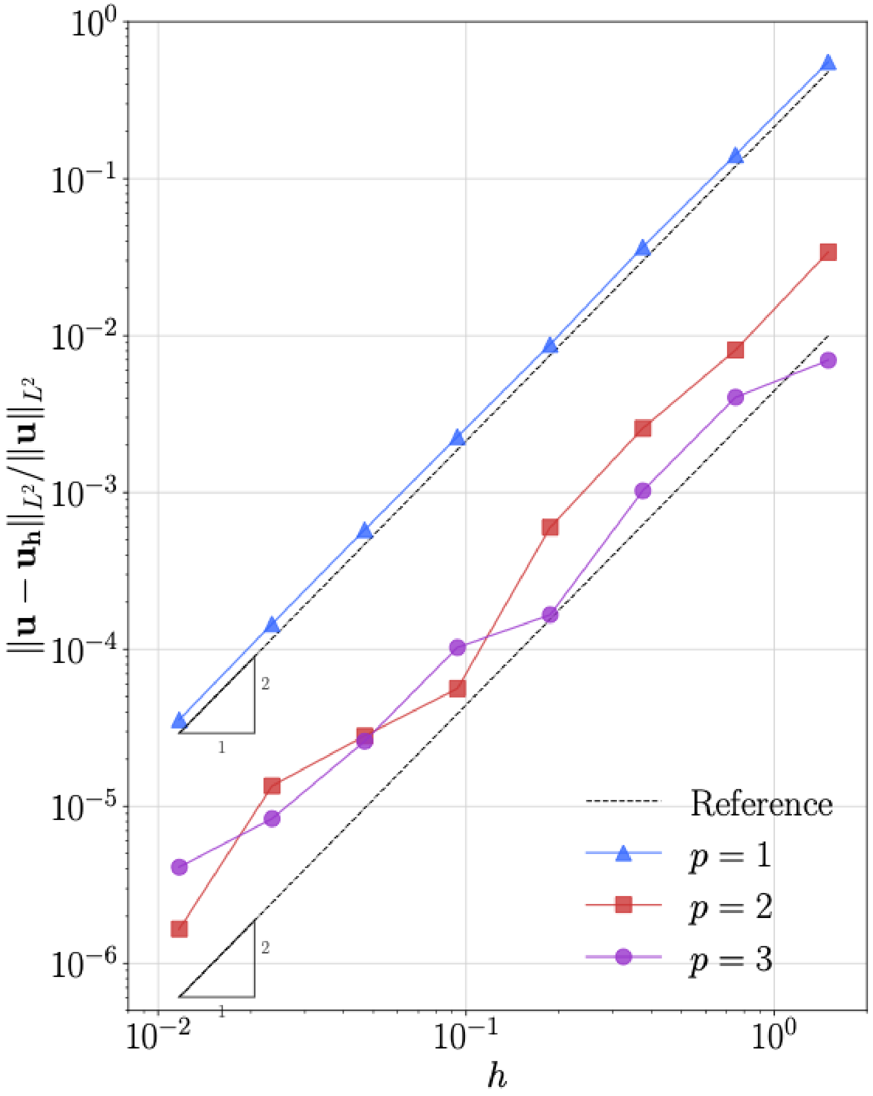

Increasing p beyond 2 does not improve convergence

In Poiseuille Bingham flow convergence is limited

$$u_x(y) = \begin{cases} \frac{1}{2\mu}\left(-\frac{\Delta p}{L}\right)\left((h_1 + \frac{H}{2})^2 - (h_1 - y)^2\right) & \text{if } -\frac{H}{2} \leq y < h_1 \\ \frac{1}{2\mu}\left(-\frac{\Delta p}{L}\right) h_1^2 & \text{if } h_1 \leq y < h_2 \\ \frac{1}{2\mu}\left(-\frac{\Delta p}{L}\right)\left((\frac{H}{2} - h_2)^2 - (y - h_2)^2\right) & \text{if } h_2 \leq y \leq \frac{H}{2} \end{cases}$$

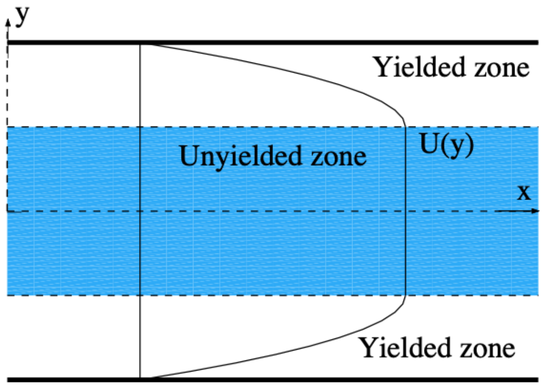

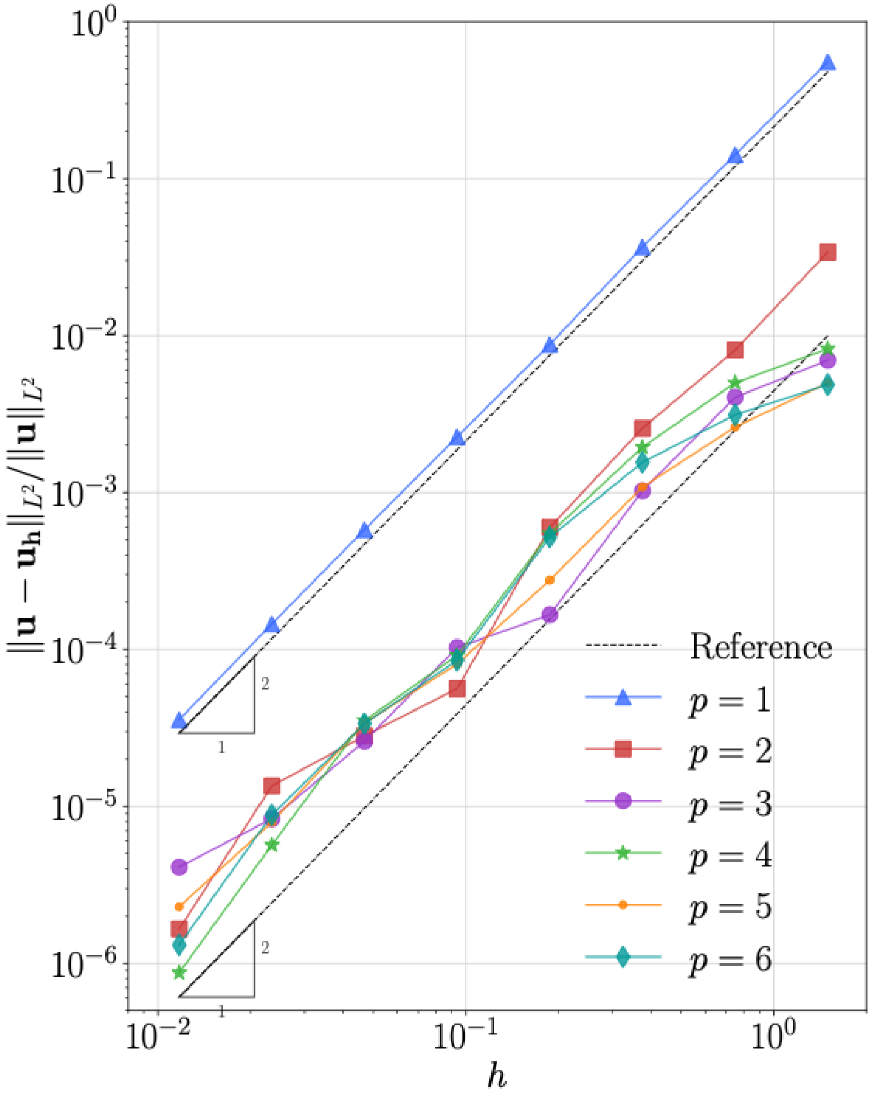

Increasing p beyond 2 does not improve convergence

In Poiseuille Bingham flow convergence is limited

The error in the L^2-norm for a given finite element (or isogeometric approximation) is governed by the regularity of the exact solution [13]

$$\|u - u_h\|_{L^2} \leq C h^{p+1} \sum_{i=0}^{p+1} \|D^i u\|_{L^2}$$

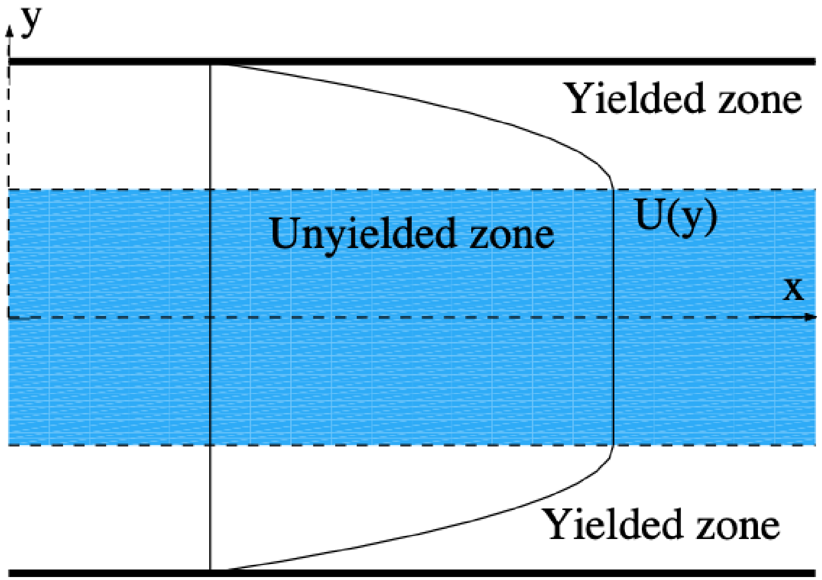

$$u_x(y) = \begin{cases} \frac{1}{2\mu}\left(-\frac{\Delta p}{L}\right)\left((h_1 + \frac{H}{2})^2 - (h_1 - y)^2\right) & \text{if } -\frac{H}{2} \leq y < h_1 \\ \frac{1}{2\mu}\left(-\frac{\Delta p}{L}\right) h_1^2 & \text{if } h_1 \leq y < h_2 \\ \frac{1}{2\mu}\left(-\frac{\Delta p}{L}\right)\left((\frac{H}{2} - h_2)^2 - (y - h_2)^2\right) & \text{if } h_2 \leq y \leq \frac{H}{2} \end{cases}$$

[13] Bazilevs, Beirao da Veiga, Cottrell, Hughes, Sangalli. Isogeometric analysis: approximation, stability and error estimates for h-refined meshes. Math. Models Methods Appl. Sci., 2006.

In Poiseuille Bingham flow convergence is limited

The error in the L^2-norm for a given finite element (or isogeometric approximation) is governed by the regularity of the exact solution [13]

$$\|u - u_h\|_{L^2} \leq C h^{p+1} \sum_{i=0}^{p+1} \|D^i u\|_{L^2}$$

For instance, we can ensure quadratic convergence

$$\|u - u_h\|_{L^2} \leq C h^2 (\|u\|_{L^2} + \|Du\|_{L^2} + \|D^2 u\|_{L^2})$$

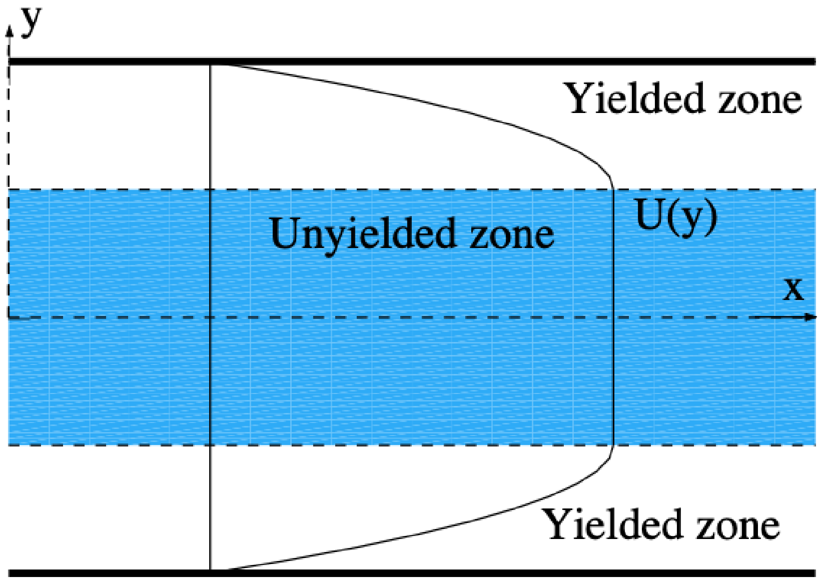

$$u_x(y) = \begin{cases} \frac{1}{2\mu}\left(-\frac{\Delta p}{L}\right)\left((h_1 + \frac{H}{2})^2 - (h_1 - y)^2\right) & \text{if } -\frac{H}{2} \leq y < h_1 \\ \frac{1}{2\mu}\left(-\frac{\Delta p}{L}\right) h_1^2 & \text{if } h_1 \leq y < h_2 \\ \frac{1}{2\mu}\left(-\frac{\Delta p}{L}\right)\left((\frac{H}{2} - h_2)^2 - (y - h_2)^2\right) & \text{if } h_2 \leq y \leq \frac{H}{2} \end{cases}$$

[13] Bazilevs, Beirao da Veiga, Cottrell, Hughes, Sangalli. Isogeometric analysis: approximation, stability and error estimates for h-refined meshes. Math. Models Methods Appl. Sci., 2006.

In Poiseuille Bingham flow convergence is limited

The error in the L^2-norm for a given finite element (or isogeometric approximation) is governed by the regularity of the exact solution [13]

$$\|u - u_h\|_{L^2} \leq C h^{p+1} \sum_{i=0}^{p+1} \|D^i u\|_{L^2}$$

For instance, we can ensure quadratic convergence

$$\|u - u_h\|_{L^2} \leq C h^2 (\|u\|_{L^2} + \|Du\|_{L^2} + \|D^2 u\|_{L^2})$$

But we can't have cubic because $\|D^3 u\|_{L^2}$ is unbounded

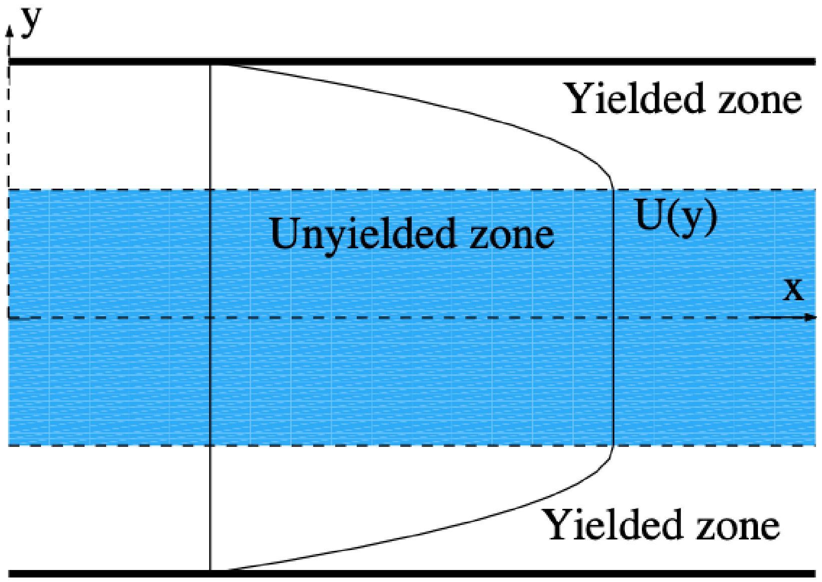

$$u_x(y) = \begin{cases} \frac{1}{2\mu}\left(-\frac{\Delta p}{L}\right)\left((h_1 + \frac{H}{2})^2 - (h_1 - y)^2\right) & \text{if } -\frac{H}{2} \leq y < h_1 \\ \frac{1}{2\mu}\left(-\frac{\Delta p}{L}\right) h_1^2 & \text{if } h_1 \leq y < h_2 \\ \frac{1}{2\mu}\left(-\frac{\Delta p}{L}\right)\left((\frac{H}{2} - h_2)^2 - (y - h_2)^2\right) & \text{if } h_2 \leq y \leq \frac{H}{2} \end{cases}$$

[13] Bazilevs, Beirao da Veiga, Cottrell, Hughes, Sangalli. Isogeometric analysis: approximation, stability and error estimates for h-refined meshes. Math. Models Methods Appl. Sci., 2006.

Bingham benchmark: sudden expansion of Bingham flow

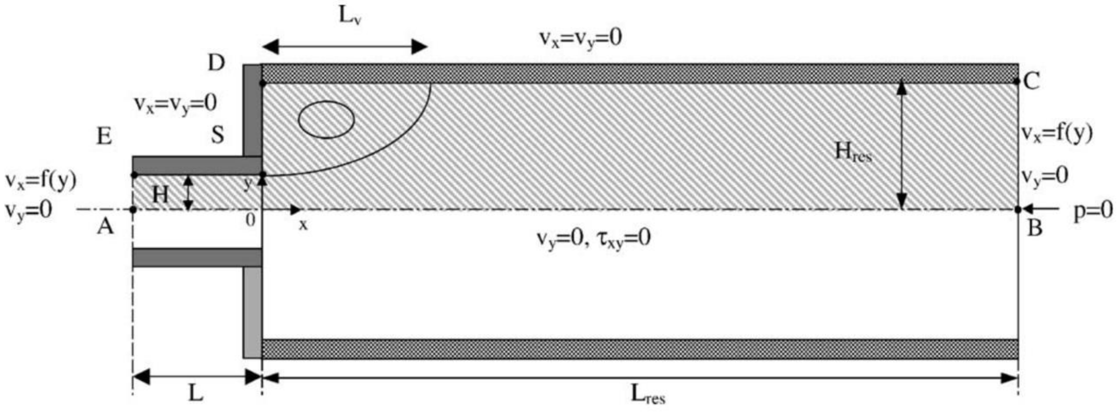

Problem geometry

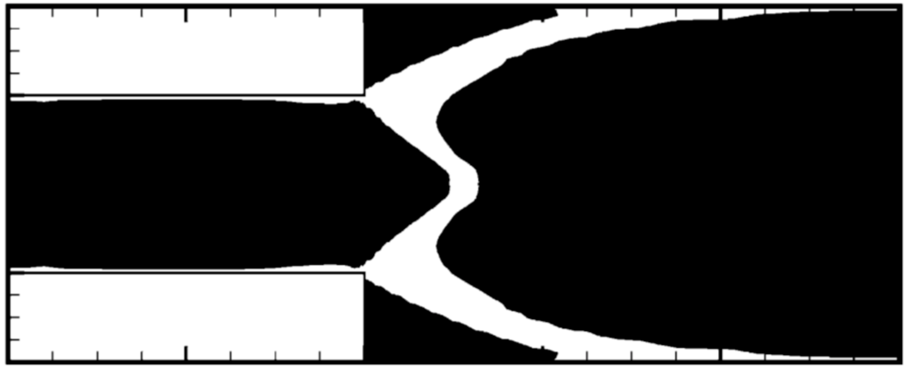

Reference solution: *Mitsoulis results* [10]

Consider the well-known benchmark sudden expansion of Bingham fluid

The yielded (white) and unyielded (dark) regions are in general very difficult to capture

[10] Mitsoulis and Huilgol. Entry flows of bingham plastics in expansions. Journal of non-newtonian fluid mechanics, 2004.

Bingham benchmark: sudden expansion of Bingham flow

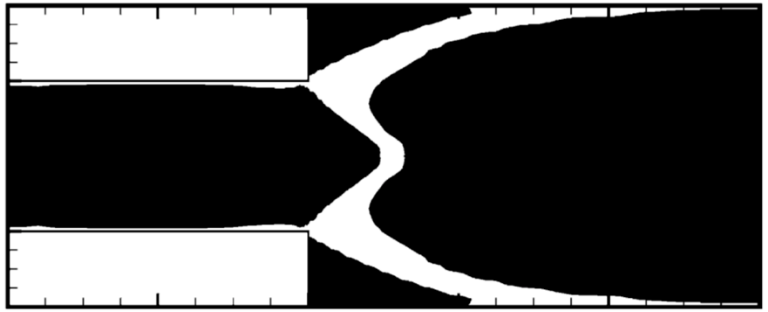

Reference solution: *Mitsoulis results*

p=1

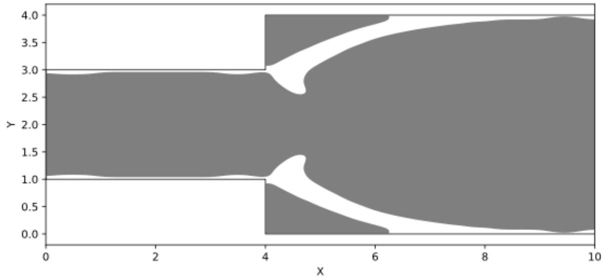

Coarse

Refined

Bingham benchmark: sudden expansion of Bingham flow

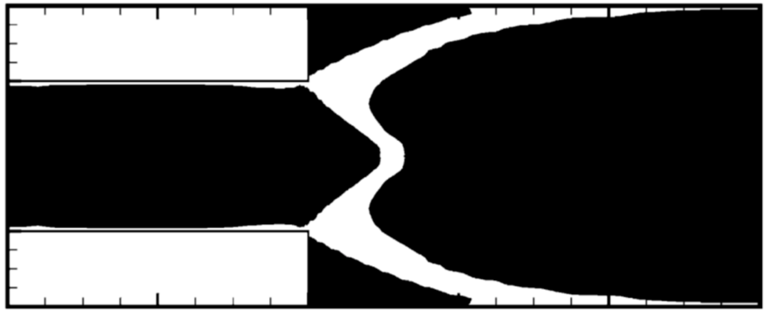

Reference solution: *Mitsoulis results*

p=1

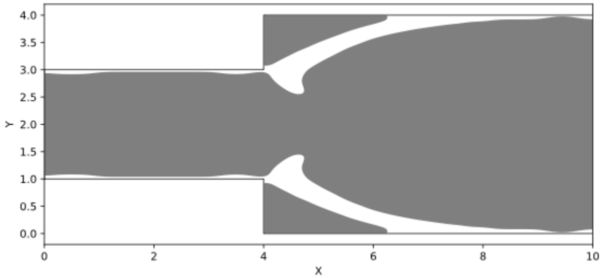

Coarse

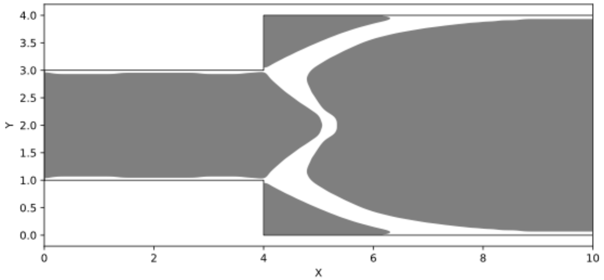

Refined

Bingham benchmark: sudden expansion of Bingham flow

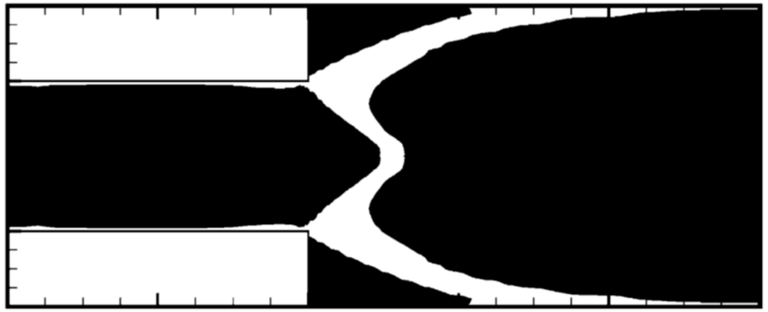

Reference solution: *Mitsoulis results*

p=1

p=2

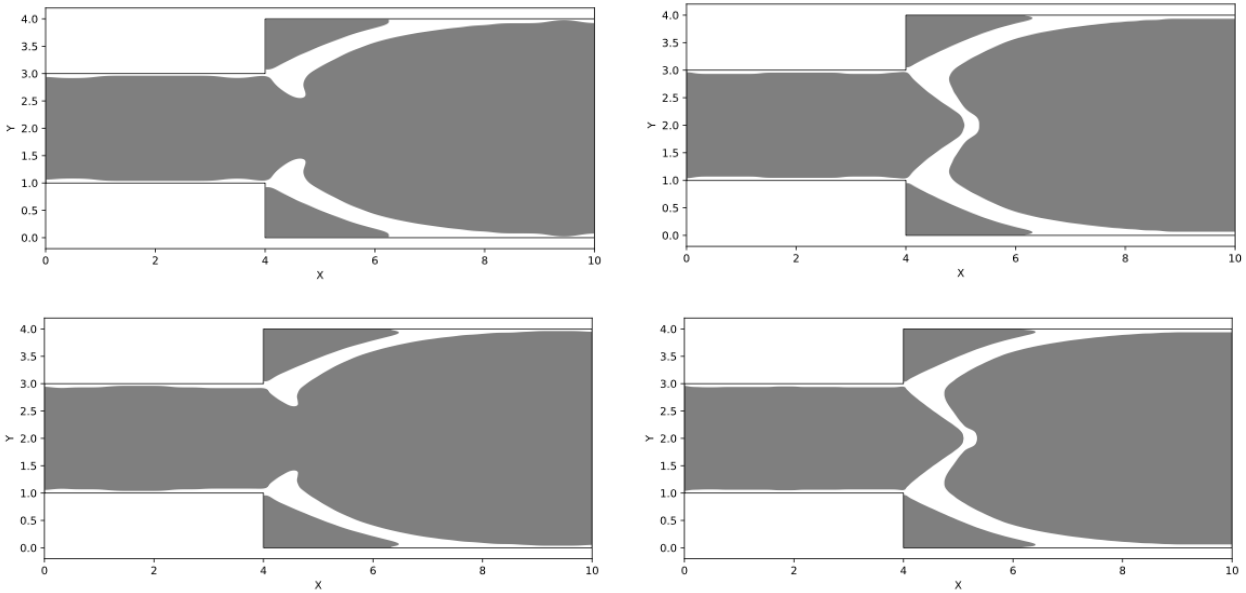

Coarse *Refined*

Bingham benchmark: sudden expansion of Bingham flow

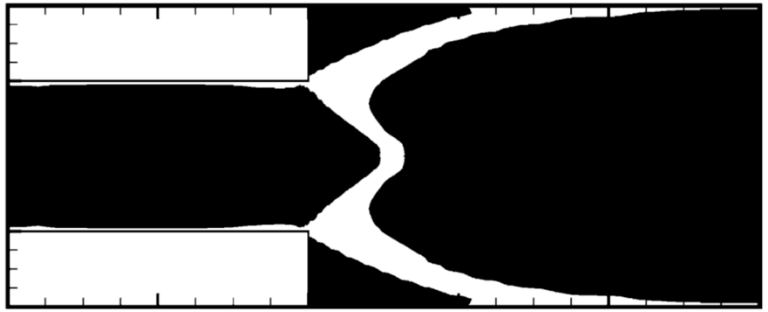

Reference solution: *Mitsoulis results*

p=1

p=2

p=3

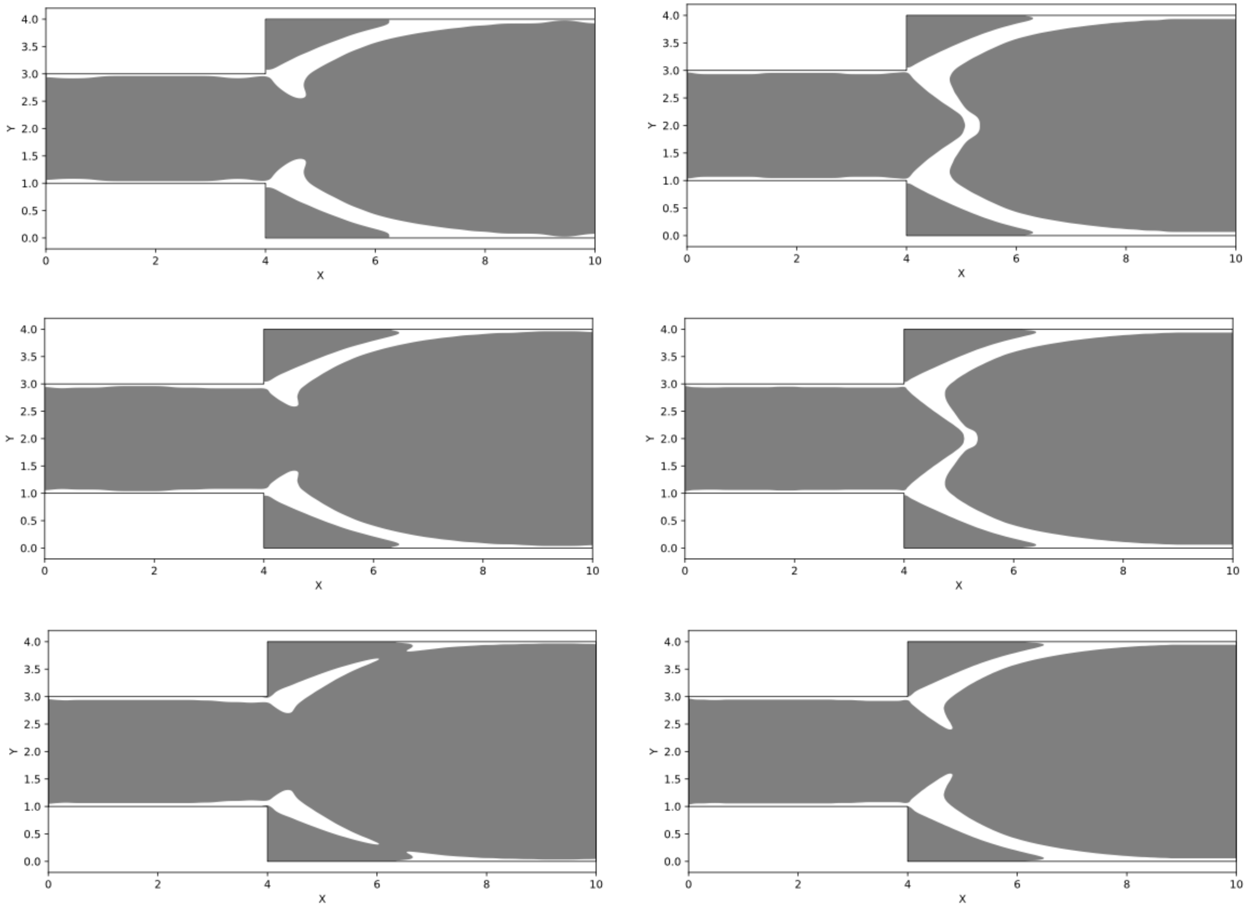

Coarse *Refined*

Bingham benchmark: sudden expansion of Bingham flow

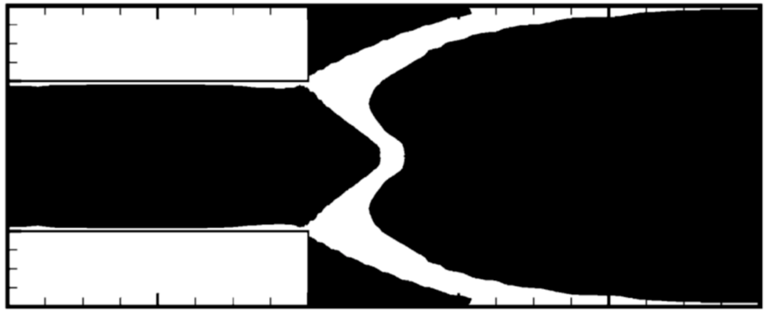

Reference solution: *Mitsoulis results*

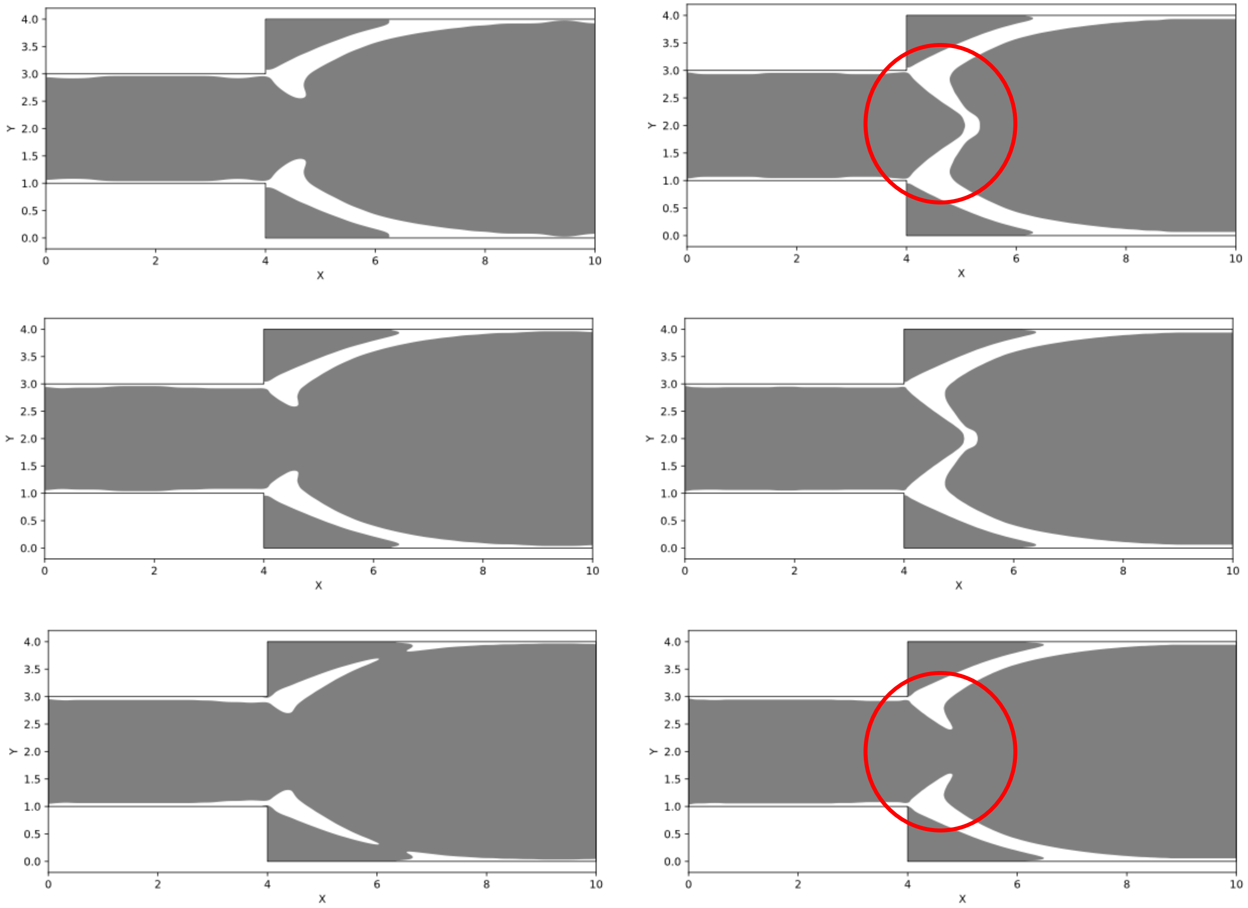

p=1

p=2

p=3

Coarse

Refined

Conclusions of Publication II

- Use high-order discretizations when the solution is sufficiently smooth
- Local stress-divergence reconstruction is essential for *p>1*
- IGA basis functions (large support, high continuity) are less suitable for non-Newtonian flows
- Non-smooth physics calls for local h-refinement to capture localized features

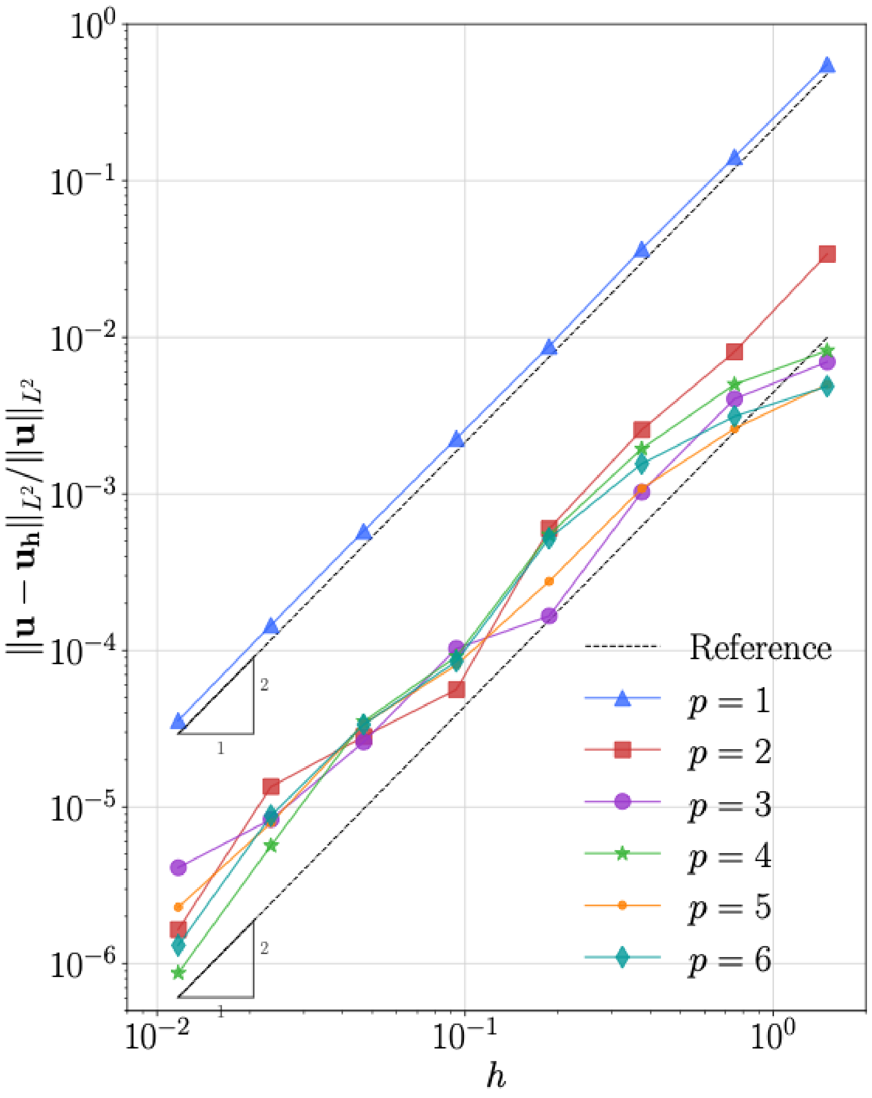

Conclusions of Publication II

- Use high-order discretizations when the solution is sufficiently smooth
- Local stress-divergence reconstruction is essential for *p>1*
- IGA basis functions (large support, high continuity) are less suitable for non-Newtonian flows
- Non-smooth physics calls for local h-refinement to capture localized features

Motivate the need of a flexible multipatch refinement strategy

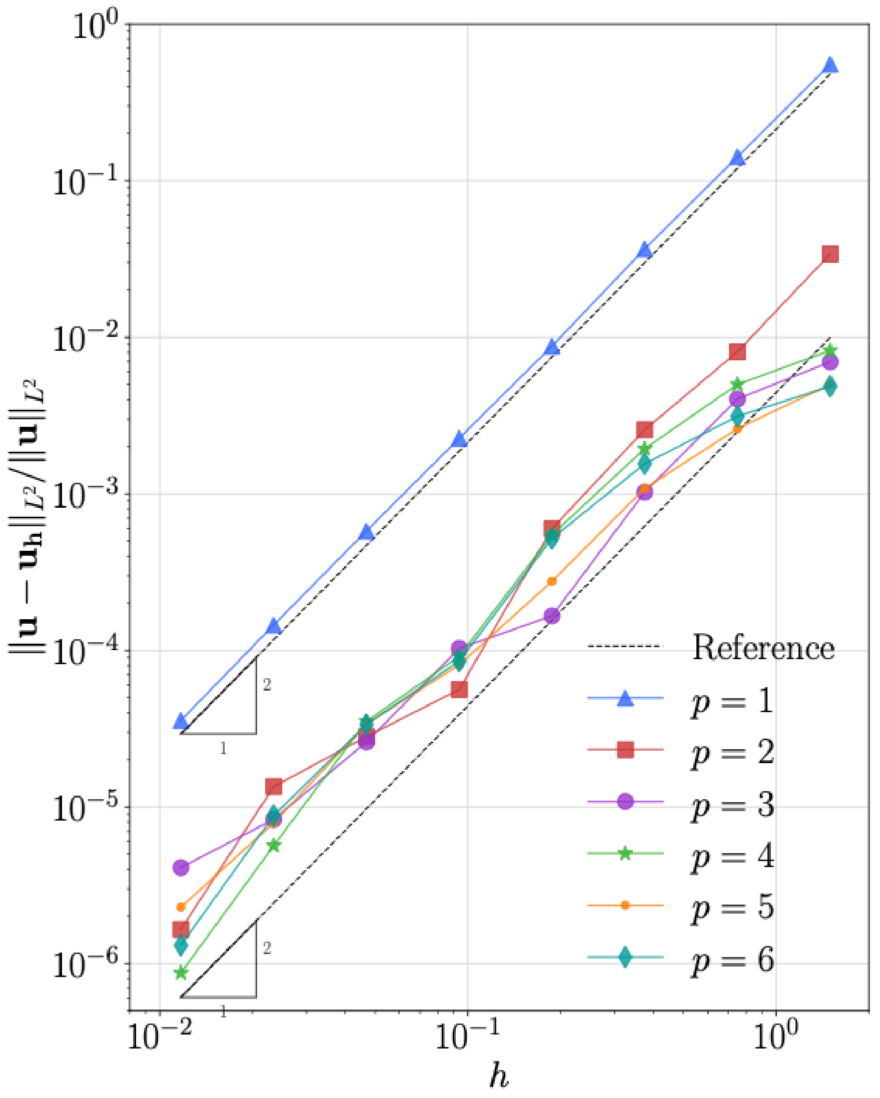

Publication Ⅲ

Publication III:
Isogeometric multipatch coupling with arbitrary refinement using the Gap–Shifted Boundary Method

- Industrial CAD geometries are typically given as **trimmed *NURBS multipatch*** models

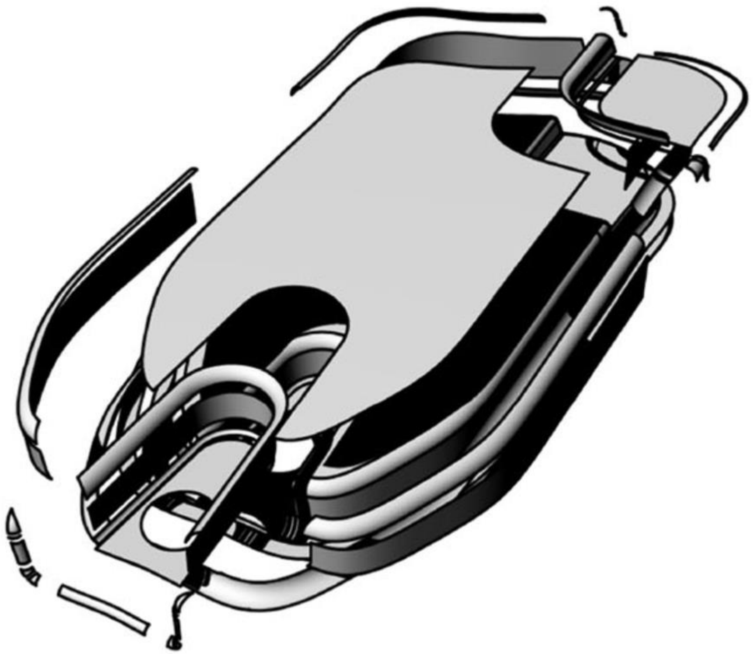

Multipatch model. Image taken from [2]

[2] Realization of CAD-integrated shell simulation based on isogeometric B-Rep analysis. T. Teschemacher , A. M. Bauer , T. Oberbichler, M. Breitenberger, R. Rossi, R. Wüchner and K.-U. Bletzinger, 2018.

Publication III:
Isogeometric multipatch coupling with arbitrary refinement using the Gap–Shifted Boundary Method

- Industrial CAD geometries are typically given as **trimmed *NURBS multipatch*** models

- **Trimming-based coupling** techniques are a natural choice, but require cut-cell integration ⇒ severe conditioning

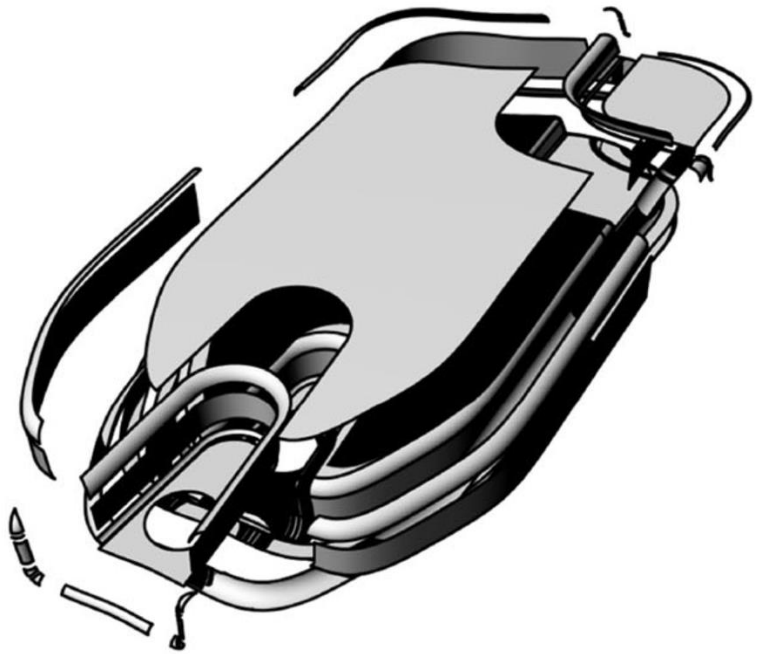

Multipatch model. Image taken from [2]

[2] Realization of CAD-integrated shell simulation based on isogeometric B-Rep analysis. T. Teschemacher , A. M. Bauer , T. Oberbichler, M. Breitenberger, R. Rossi, R. Wüchner and K.-U. Bletzinger, 2018.

Publication III:
Isogeometric multipatch coupling with arbitrary refinement using the Gap–Shifted Boundary Method

- Industrial CAD geometries are typically given as **trimmed *NURBS multipatch*** models

- **Trimming-based coupling** techniques are a natural choice, but require cut-cell integration ⇒ severe conditioning

Idea: achieve robust high-order coupling under arbitrary interface mismatch using the SBM

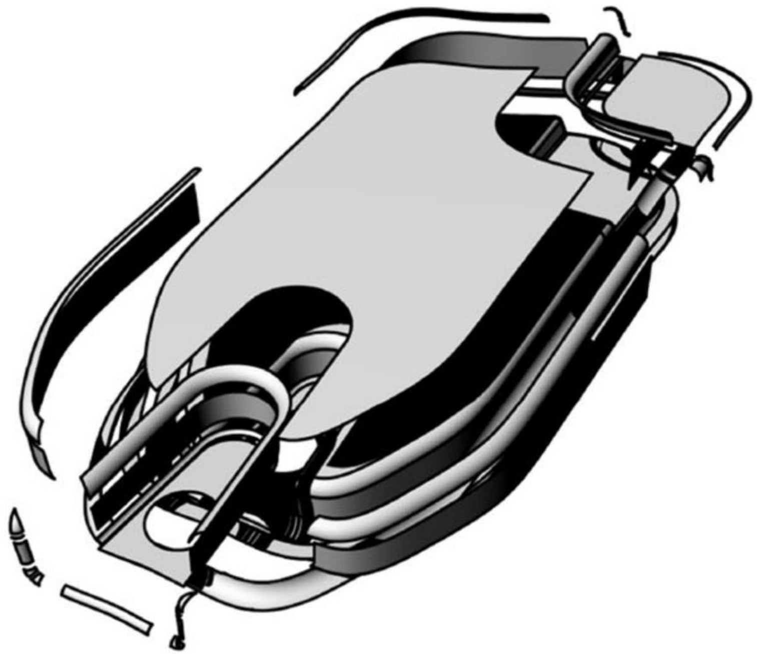

Multipatch model. Image taken from [2]

[2] Realization of CAD-integrated shell simulation based on isogeometric B-Rep analysis. T. Teschemacher , A. M. Bauer , T. Oberbichler, M. Breitenberger, R. Rossi, R. Wüchner and K.-U. Bletzinger, 2018.

Additional motivations

- Local features often require additional resolution only in restricted regions ⇒ Change of material properties or Neumann BCs

- Classical local refinement strategies such as THB-splines [14] are very effective, but they rely on a more structured refinement framework

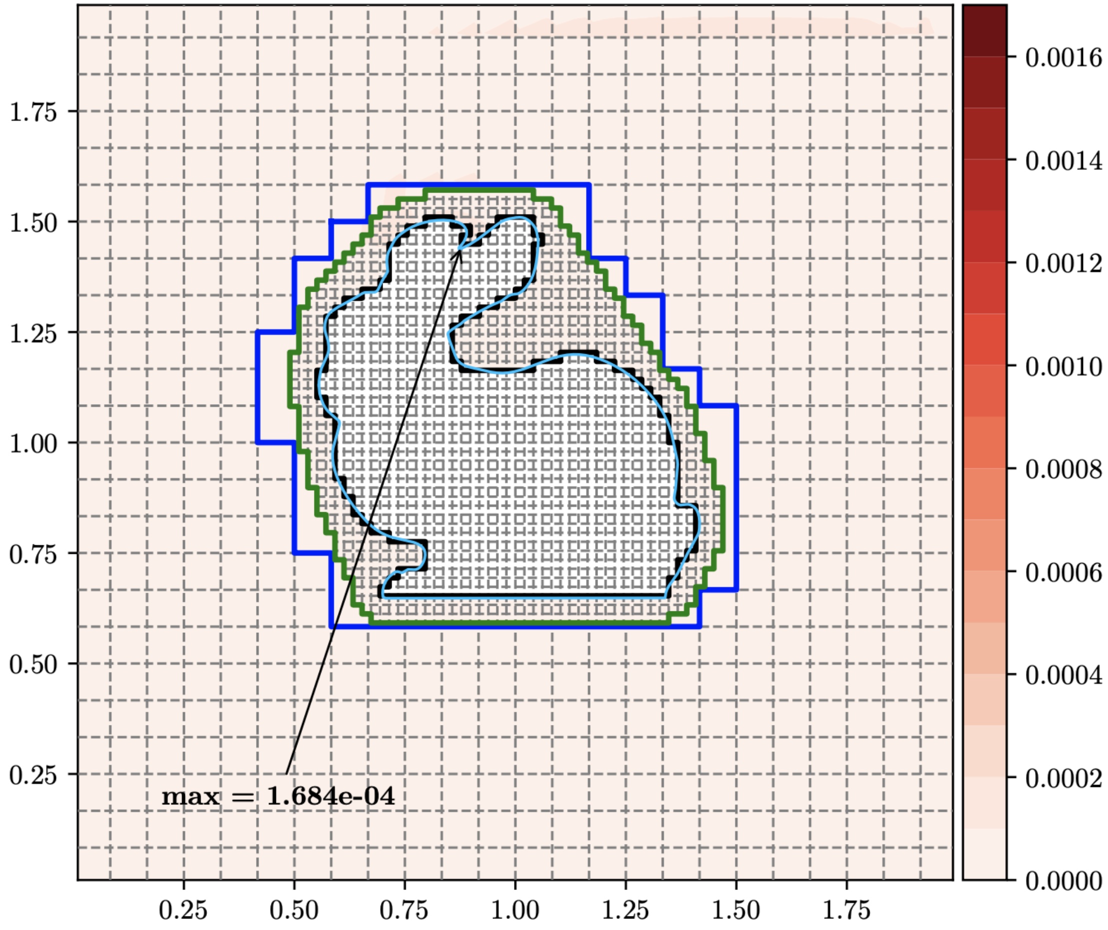

(c) Multipatch *h*-refinement

[14] Giannelli, Jüttler, Speleers. *THB-splines: The truncated basis for hierarchical splines*. Computer Aided Geometric Design, 2012.

Additional motivations

- Local features often require additional resolution only in restricted regions ⇒ Change of material properties or Neumann BCs

- Classical local refinement strategies such as THB-splines [14] are very effective, but they rely on a more structured refinement framework

Embedded local patches could provide a flexible way to refine only where needed

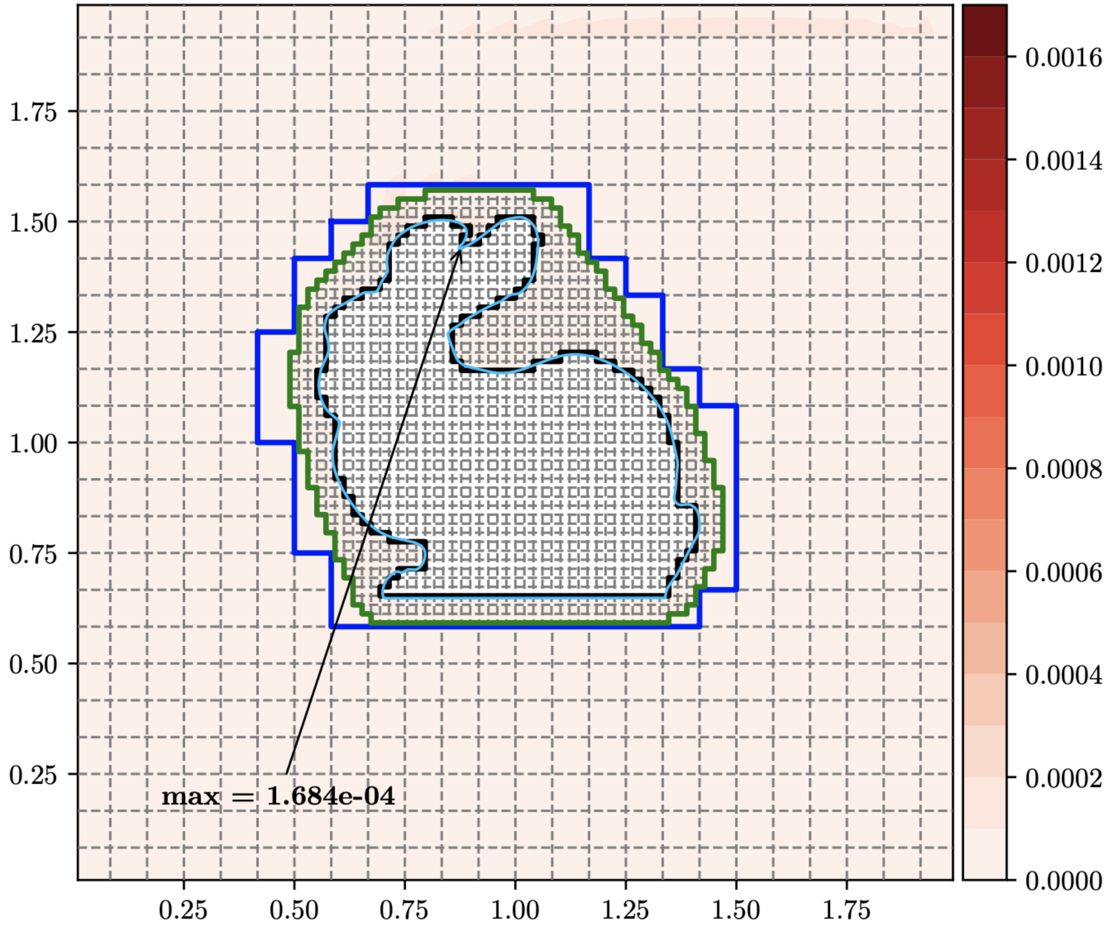

(c) Multipatch *h*-refinement

[14] Giannelli, Jüttler, Speleers. *THB-splines: The truncated basis for hierarchical splines*. Computer Aided Geometric Design, 2012.

Gap-SBM explicitly reconstructs the gap between the surrogate and true boundaries

- The Gap-SBM [15] starts from the SBM idea: a surrogate boundary $\tilde{\Gamma}$ is built using the background mesh

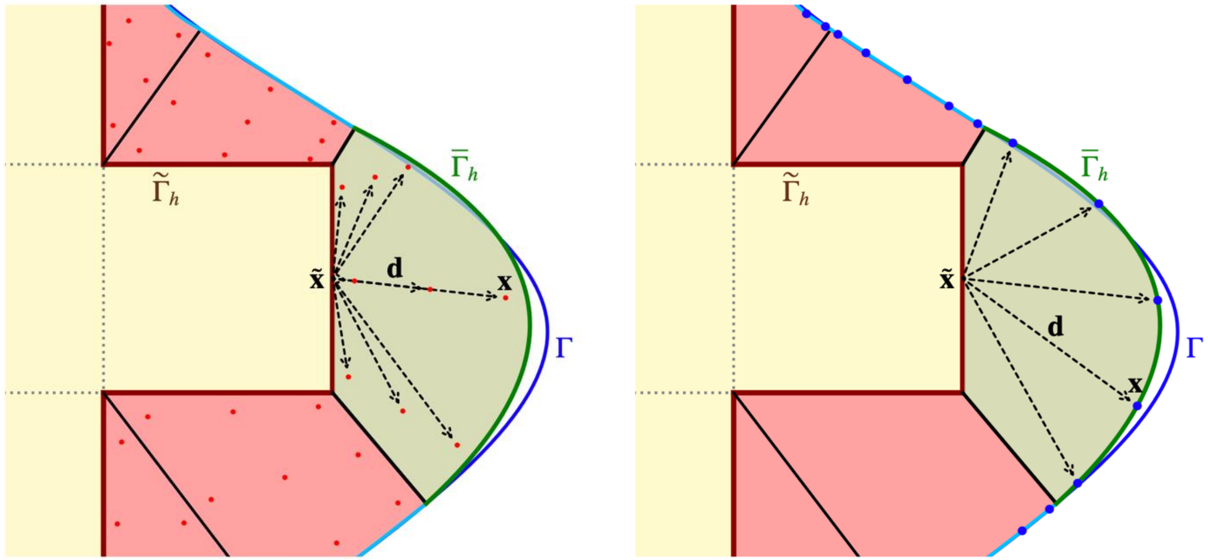

[15] Collins, Li, Lozinski, Scovazzi. *Gap-SBM: A new conceptualization of the shifted boundary method with optimal convergence for the Neumann and Dirichlet problems*. Computer Methods in Applied Mechanics and Engineering, 2026.

Gap-SBM explicitly reconstructs the gap between the surrogate and true boundaries

- The Gap-SBM [15] starts from the SBM idea: a surrogate boundary $\tilde{\Gamma}$ is built using the background mesh
- Instead of neglecting the region between the surrogate and true boundaries, Gap-SBM explicitly accounts for this geometric gap

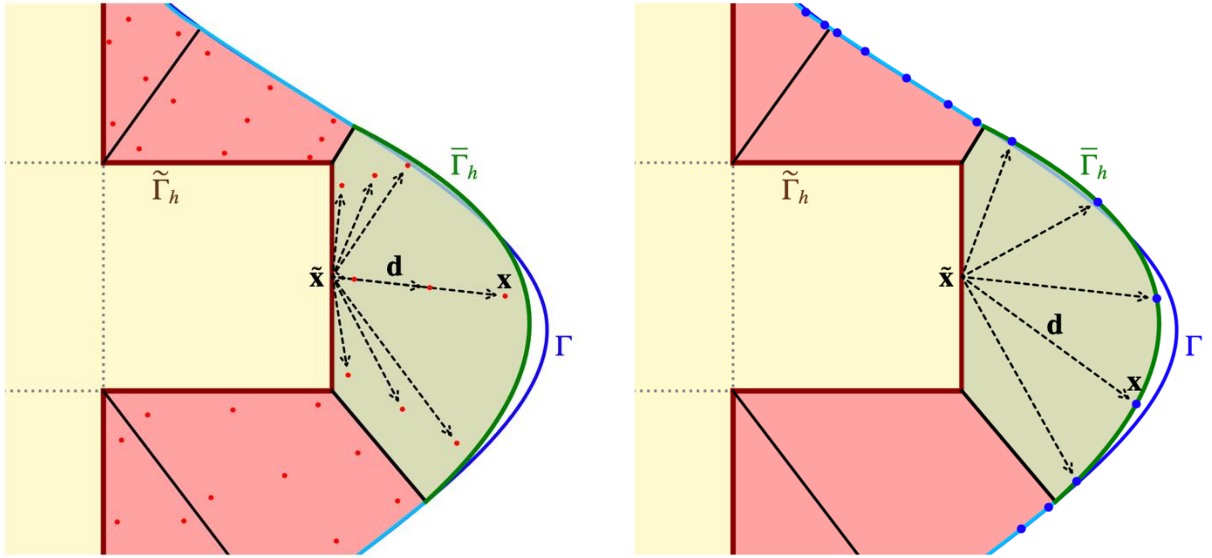

[15] Collins, Li, Lozinski, Scovazzi. *Gap-SBM: A new conceptualization of the shifted boundary method with optimal convergence for the Neumann and Dirichlet problems*. Computer Methods in Applied Mechanics and Engineering, 2026.

Gap-SBM explicitly reconstructs the gap between the surrogate and true boundaries

- The Gap-SBM [15] starts from the SBM idea: a surrogate boundary $\tilde{\Gamma}$ is built using the background mesh

- Instead of neglecting the region between the surrogate and true boundaries, Gap-SBM explicitly accounts for this geometric gap

- The gap is discretized into curvilinear gap elements [16], and active basis functions are extended into it by high-order Taylor expansions

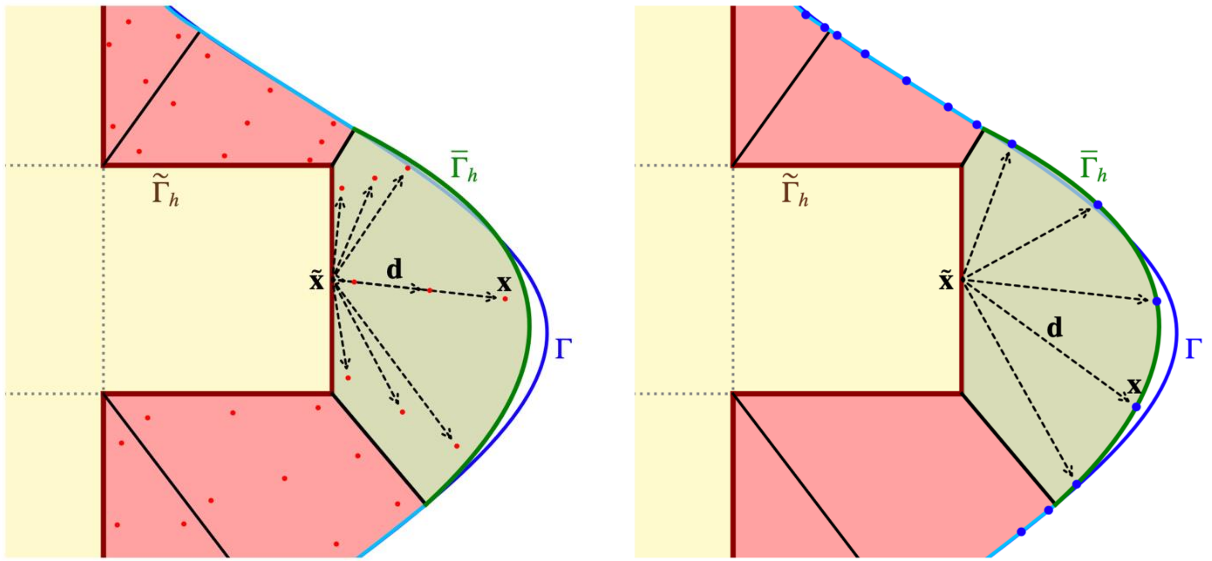

[15] Collins, Li, Lozinski, Scovazzi. *Gap-SBM: A new conceptualization of the shifted boundary method with optimal convergence for the Neumann and Dirichlet problems*. Computer Methods in Applied Mechanics and Engineering, 2026.
[16] Gorgi, Antonelli, Cornejo, Scovazzi, Rossi. *The Isogeometric Gap-Shifted Boundary Method*. Preprint, 2026.

Gap-SBM explicitly reconstructs the gap between the surrogate and true boundaries

- The Gap-SBM [15] starts from the SBM idea: a surrogate boundary $\tilde{\Gamma}$ is built using the background mesh

- Instead of neglecting the region between the surrogate and true boundaries, Gap-SBM explicitly accounts for this geometric gap

- The gap is discretized into curvilinear gap elements [16], and active basis functions are extended into it by high-order Taylor expansions

- This retains the **favorable conditioning** of the SBM, while recovering high accuracy for **Neumann boundary conditions**

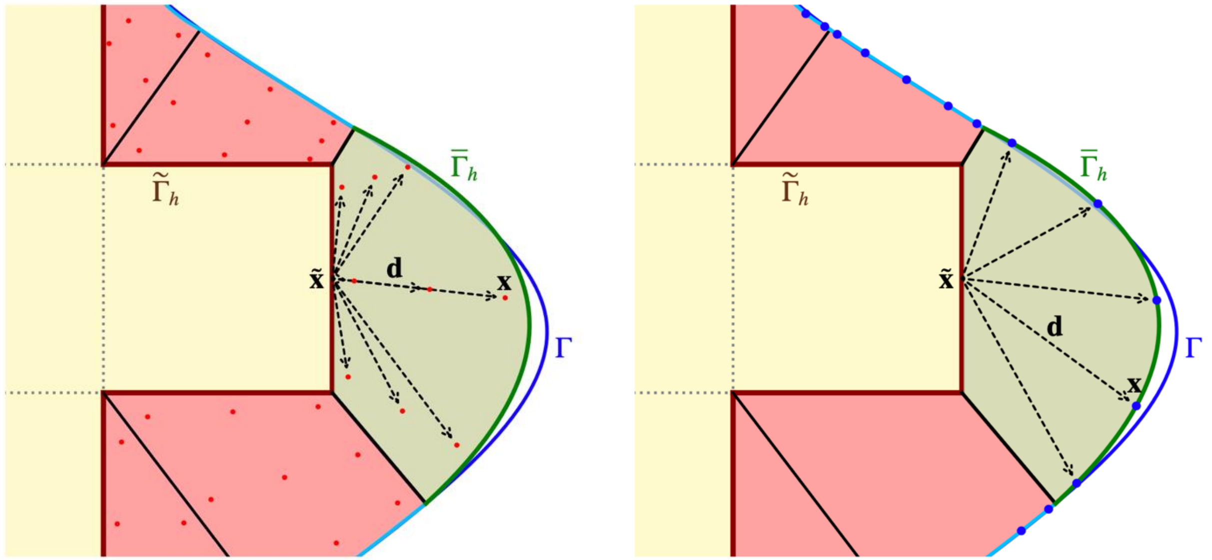

[15] Collins, Li, Lozinski, Scovazzi. *Gap-SBM: A new conceptualization of the shifted boundary method with optimal convergence for the Neumann and Dirichlet problems*. Computer Methods in Applied Mechanics and Engineering, 2026.
[16] Gorgi, Antonelli, Cornejo, Scovazzi, Rossi. *The Isogeometric Gap-Shifted Boundary Method*. Preprint, 2026.

Gap–SBM couples nonconforming patches by integrating over the gap region

- **One patch defines the “true” interface; the other needs a surrogate interface**
- The mismatch becomes a thin gap region that is integrated explicitly
- Basis functions are extended into the gap via Taylor expansions; therefore, no additional DOFs are introduced, and all contributions are projected onto the existing bases
- Coupling is enforced with a penalty-free skew-symmetric Nitsche formulation

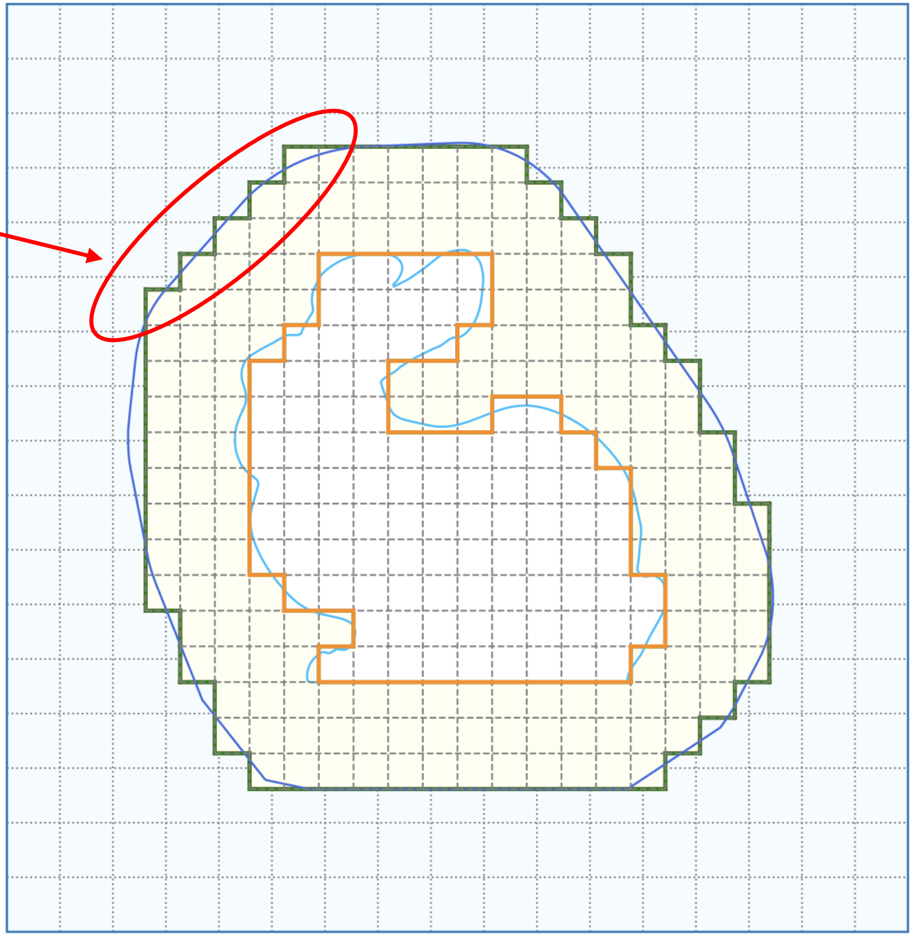

Gap–SBM couples nonconforming patches by integrating over the gap region

- One patch defines the “true” interface; the other needs a surrogate interface
- **The mismatch becomes a thin gap region that is integrated explicitly**
- Basis functions are extended into the gap via Taylor expansions; therefore, no additional DOFs are introduced, and all contributions are projected onto the existing bases
- Coupling is enforced with a penalty-free skew-symmetric Nitsche formulation

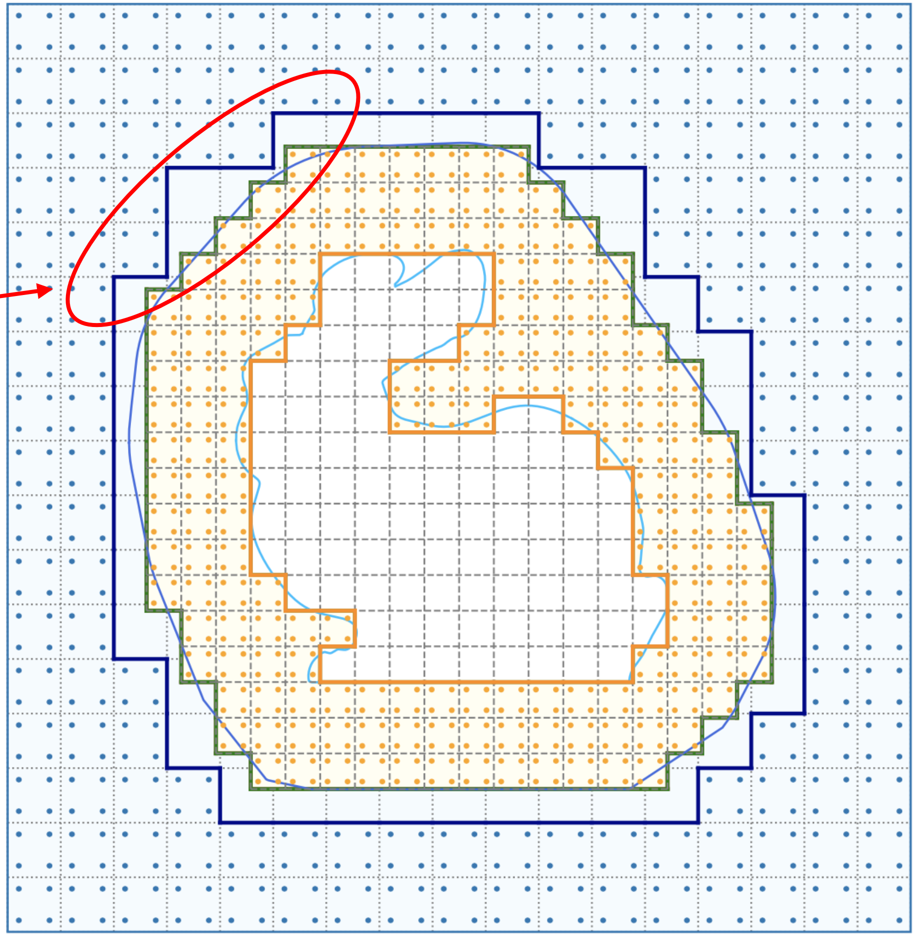

Gap–SBM couples nonconforming patches by integrating over the gap region

- One patch defines the “true” interface; the other needs a surrogate interface
- The mismatch becomes a thin gap region that is integrated explicitly
- **Basis functions are extended into the gap via Taylor expansions; therefore, no additional DOFs are introduced, and all contributions are projected onto the existing bases**
- Coupling is enforced with a penalty-free skew-symmetric Nitsche formulation

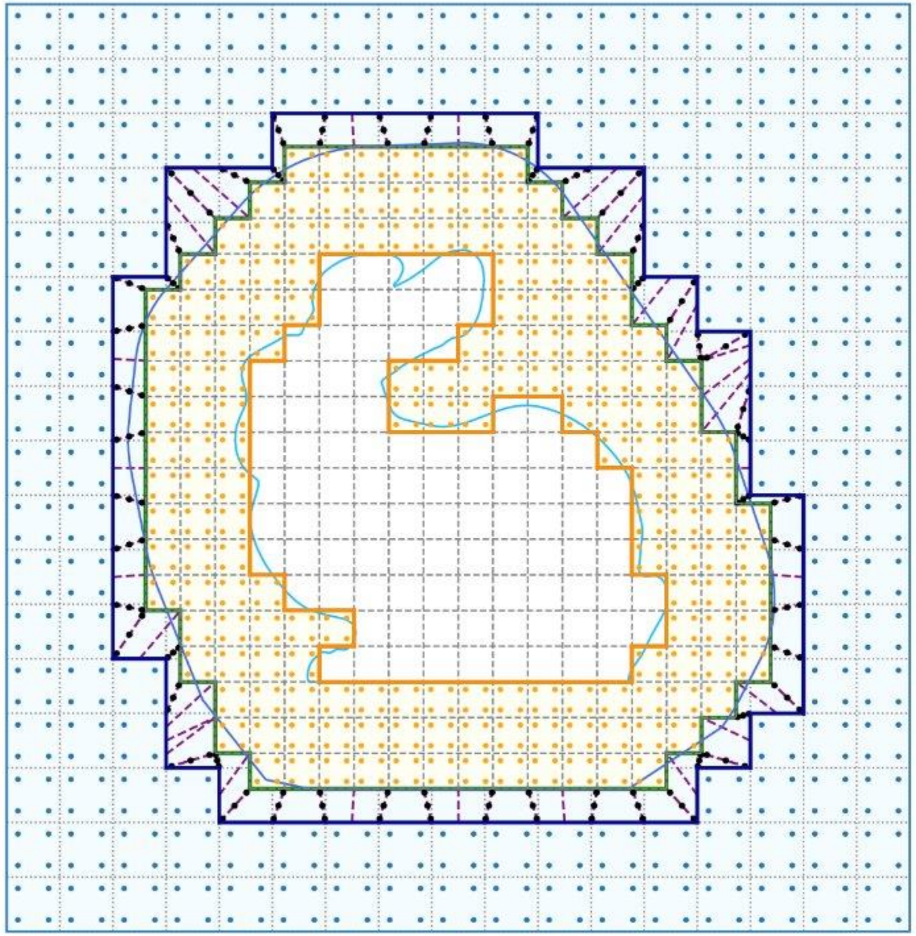

Gap–SBM couples nonconforming patches by integrating over the gap region

- One patch defines the “true” interface; the other needs a surrogate interface
- The mismatch becomes a thin gap region that is integrated explicitly
- Basis functions are extended into the gap via Taylor expansions; therefore, no additional DOFs are introduced, and all contributions are projected onto the existing bases
- **Coupling is enforced with a penalty-free skew-symmetric Nitsche formulation**

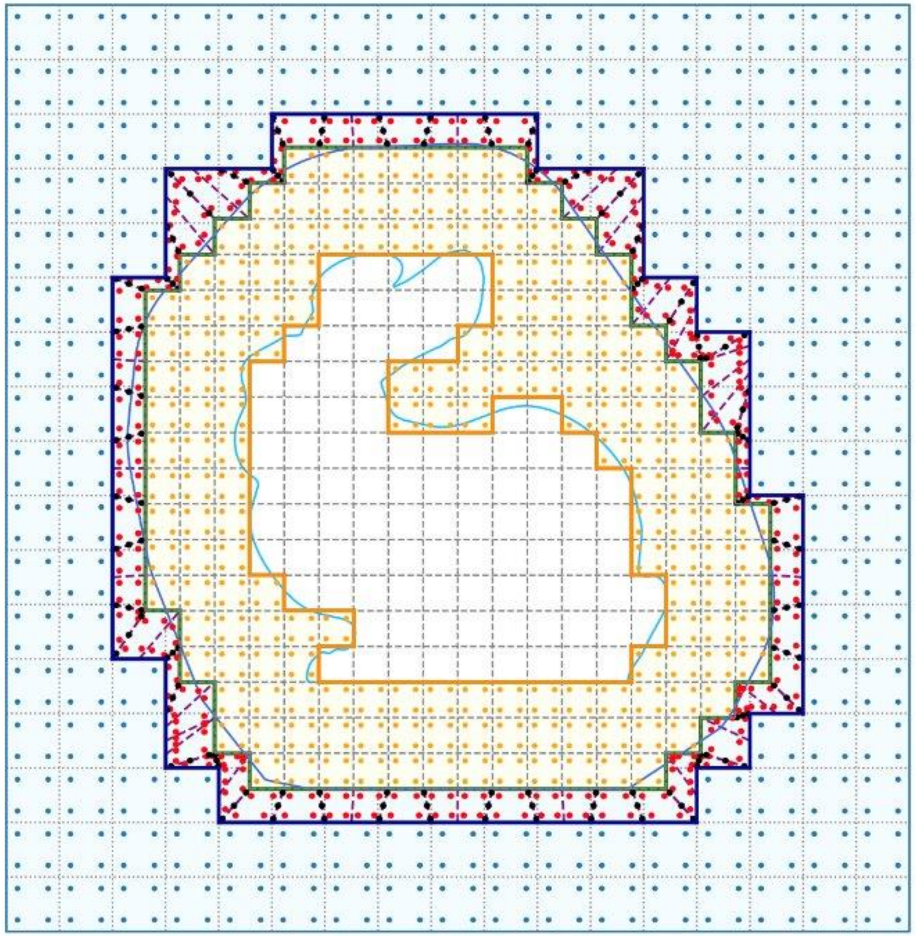

Continuity can be enforced with a penalty-free Nitsche formulation

Consider the Discontinuous Galerkin notation of jump and average:

$$[[w]] := w^A - w^B \qquad \{\!\{w\}\!\} := \frac{1}{2}(w^A + w^B)$$

$$[[\partial_{\boldsymbol{n}} w]] := \partial_{\boldsymbol{n}^A} w^A - \partial_{\boldsymbol{n}^B} w^B \qquad \{\!\{\partial_{\boldsymbol{n}} w\}\!\} := \frac{1}{2}(\partial_{\boldsymbol{n}^A} w^A + \partial_{\boldsymbol{n}^B} w^B)$$

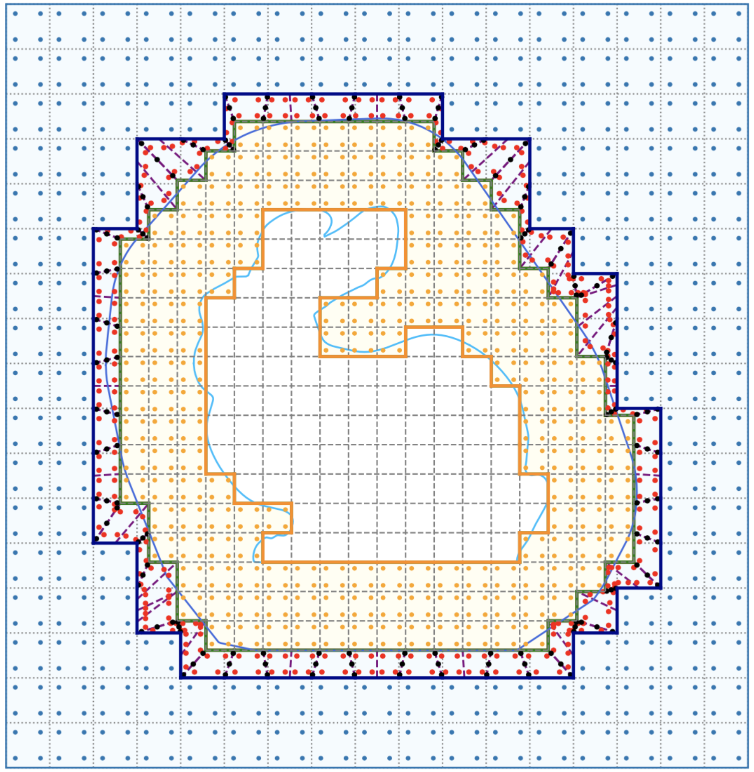

Continuity can be enforced with a penalty-free Nitsche formulation

Consider the Discontinuous Galerkin notation of jump and average:

$$[[w]] := w^A - w^B \qquad \{\!\{w\}\!\} := \frac{1}{2}(w^A + w^B)$$

$$[[\partial_{\boldsymbol{n}} w]] := \partial_{\boldsymbol{n}^A} w^A - \partial_{\boldsymbol{n}^B} w^B \qquad \{\!\{\partial_{\boldsymbol{n}} w\}\!\} := \frac{1}{2}(\partial_{\boldsymbol{n}^A} w^A + \partial_{\boldsymbol{n}^B} w^B)$$

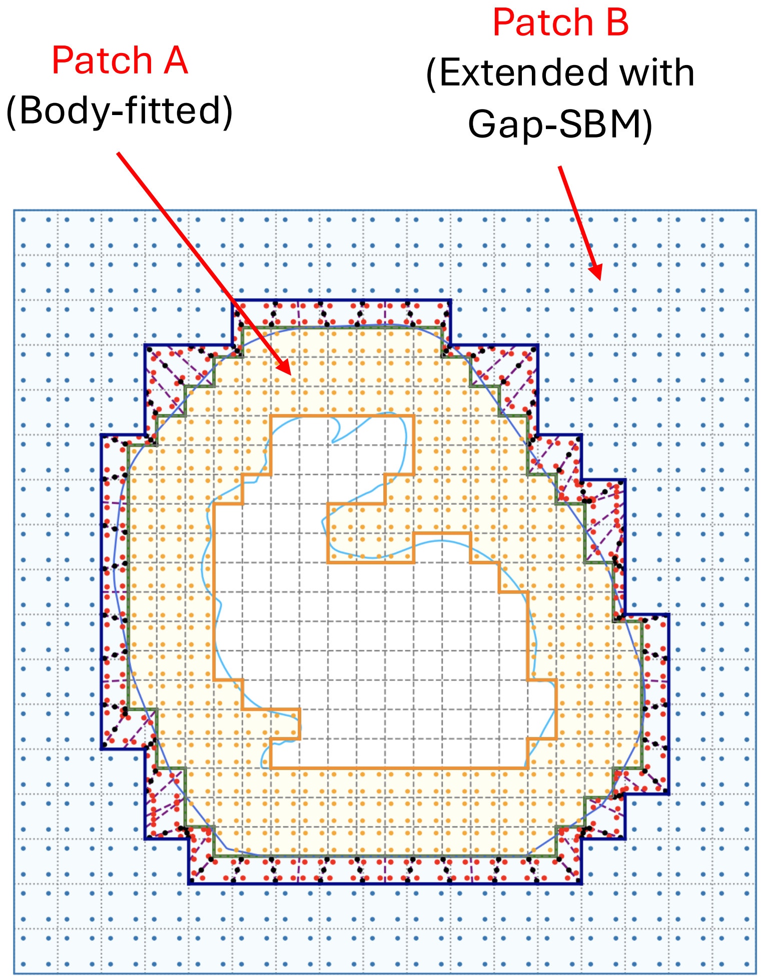

Continuity can be enforced with a penalty-free Nitsche formulation

Consider the Discontinuous Galerkin notation of jump and average:

$$[[w]] := w^A - w^B \qquad \{\{w\}\} := \frac{1}{2}(w^A + w^B)$$

$$[[\partial_{\boldsymbol{n}} w]] := \partial_{\boldsymbol{n}^A} w^A - \partial_{\boldsymbol{n}^B} w^B \qquad \{\{\partial_{\boldsymbol{n}} w\}\} := \frac{1}{2}(\partial_{\boldsymbol{n}^A} w^A + \partial_{\boldsymbol{n}^B} w^B)$$

The Nitsche coupling terms are then defined as

$$a^{\mathrm{sym}}_{\Gamma_{AB}}(u, v) = -\langle \{\{\partial_{\boldsymbol{n}} u\}\}, [[v]] \rangle_{\Gamma_{AB}} - \langle [[u]], \{\{\partial_{\boldsymbol{n}} v\}\} \rangle_{\Gamma_{AB}} + \left\langle \frac{\alpha}{h} [[u]], [[v]] \right\rangle_{\Gamma_{AB}}$$

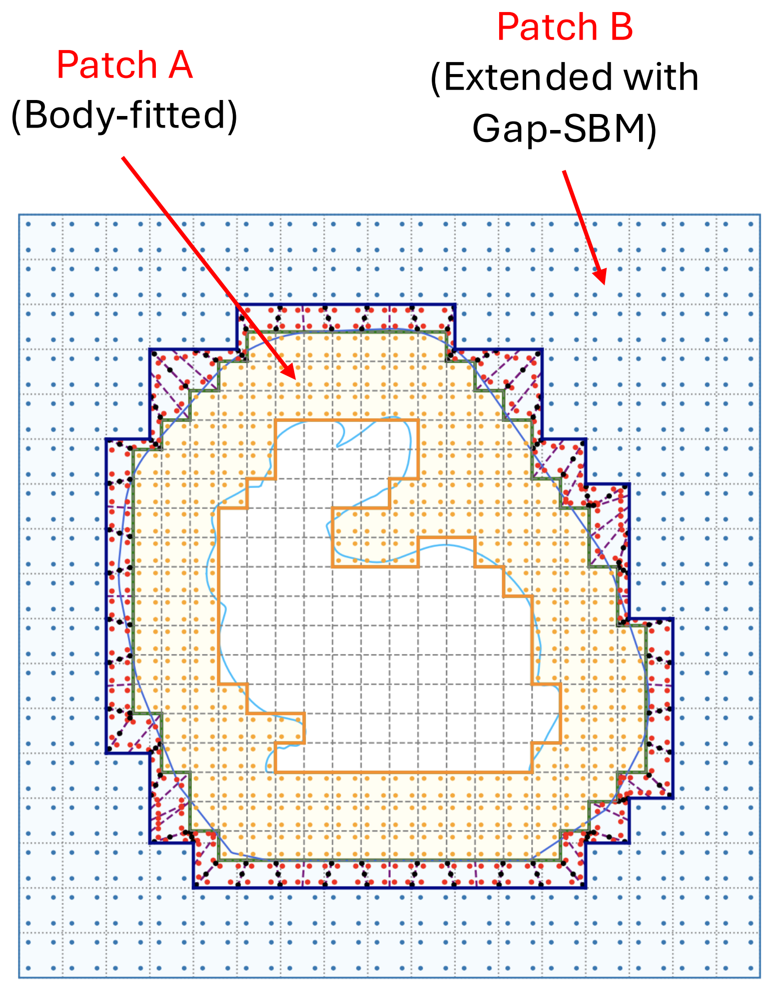

Continuity can be enforced with a penalty-free Nitsche formulation

Consider the Discontinuous Galerkin notation of jump and average:

$$[[w]] := w^A - w^B \qquad \{\{w\}\} := \frac{1}{2}(w^A + w^B)$$

$$[[\partial_{\boldsymbol{n}} w]] := \partial_{\boldsymbol{n}^A} w^A - \partial_{\boldsymbol{n}^B} w^B \qquad \{\{\partial_{\boldsymbol{n}} w\}\} := \frac{1}{2}(\partial_{\boldsymbol{n}^A} w^A + \partial_{\boldsymbol{n}^B} w^B)$$

The Nitsche coupling terms are then defined as

$$a^{\mathrm{sym}}_{\Gamma_{AB}}(u, v) = \boxed{-\langle \{\{\partial_{\boldsymbol{n}} u\}\}, [[v]] \rangle_{\Gamma_{AB}}} - \langle [[u]], \{\{\partial_{\boldsymbol{n}} v\}\} \rangle_{\Gamma_{AB}} + \left\langle \frac{\alpha}{h} [[u]], [[v]] \right\rangle_{\Gamma_{AB}}$$

flux continuity

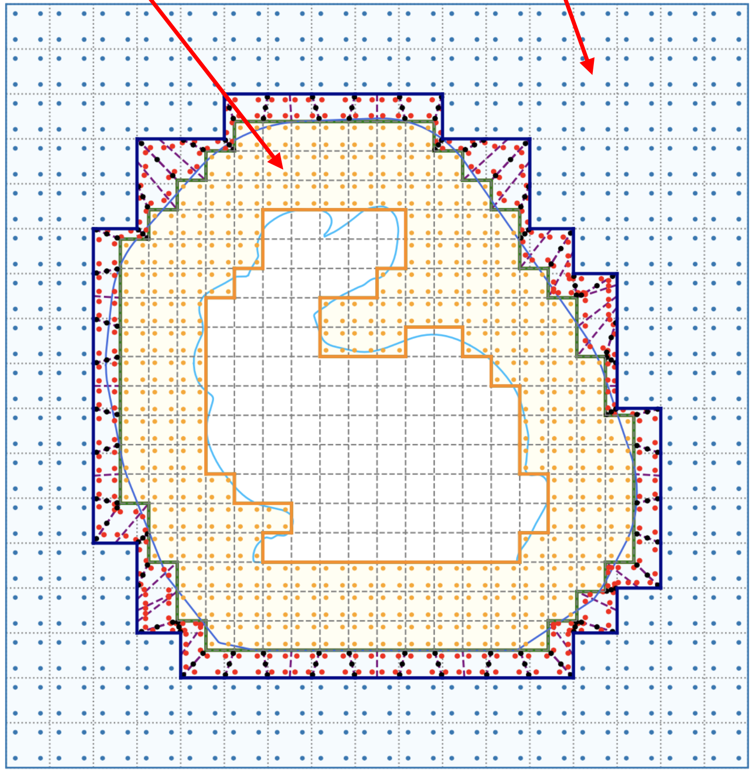

Continuity can be enforced with a penalty-free Nitsche formulation

Consider the Discontinuous Galerkin notation of jump and average:

$$[[w]] := w^A - w^B \qquad \{\!\{w\}\!\} := \tfrac{1}{2}(w^A + w^B)$$

$$[[\partial_n w]] := \partial_{n^A} w^A - \partial_{n^B} w^B \qquad \{\!\{\partial_n w\}\!\} := \tfrac{1}{2}(\partial_{n^A} w^A + \partial_{n^B} w^B)$$

The Nitsche coupling terms are then defined as

$$a^{\text{sym}}_{\Gamma_{AB}}(u,v) = \underbrace{\boxed{-\langle \{\!\{\partial_n u\}\!\}, [[v]] \rangle_{\Gamma_{AB}}}}_{\text{flux continuity}} \underbrace{\boxed{-\langle [[u]], \{\!\{\partial_n v\}\!\} \rangle_{\Gamma_{AB}}}}_{\text{Nitsche term}} + \left\langle \frac{\alpha}{h} [[u]], [[v]] \right\rangle_{\Gamma_{AB}}$$

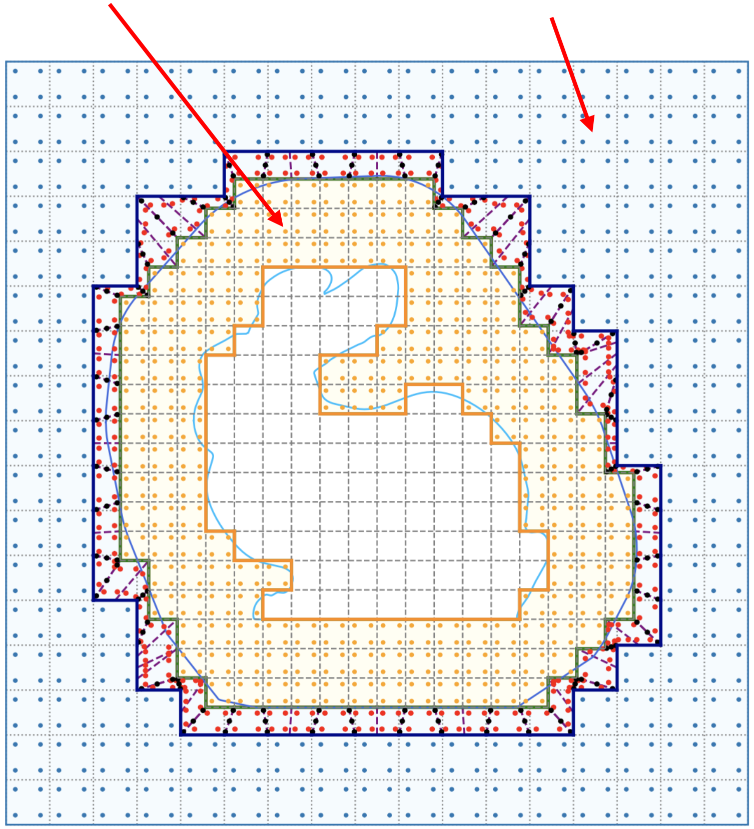

Continuity can be enforced with a penalty-free Nitsche formulation

Consider the Discontinuous Galerkin notation of jump and average:

$$[[w]] := w^A - w^B \qquad \{\!\{w\}\!\} := \frac{1}{2}(w^A + w^B)$$

$$[[\partial_n w]] := \partial_{n^A} w^A - \partial_{n^B} w^B \qquad \{\!\{\partial_n w\}\!\} := \frac{1}{2}(\partial_{n^A} w^A + \partial_{n^B} w^B)$$

The Nitsche coupling terms are then defined as

$$a^{\mathrm{sym}}_{\Gamma_{AB}}(u,v) = \underbrace{\boxed{-\langle \{\!\{\partial_n u\}\!\}, [[v]]\rangle_{\Gamma_{AB}}}}_{\text{flux continuity}} \underbrace{\boxed{-\langle [[u]], \{\!\{\partial_n v\}\!\}\rangle_{\Gamma_{AB}}}}_{\text{Nitsche term}} + \underbrace{\boxed{\left\langle \frac{\alpha}{h}[[u]], [[v]]\right\rangle_{\Gamma_{AB}}}}_{\text{penalty term}}$$

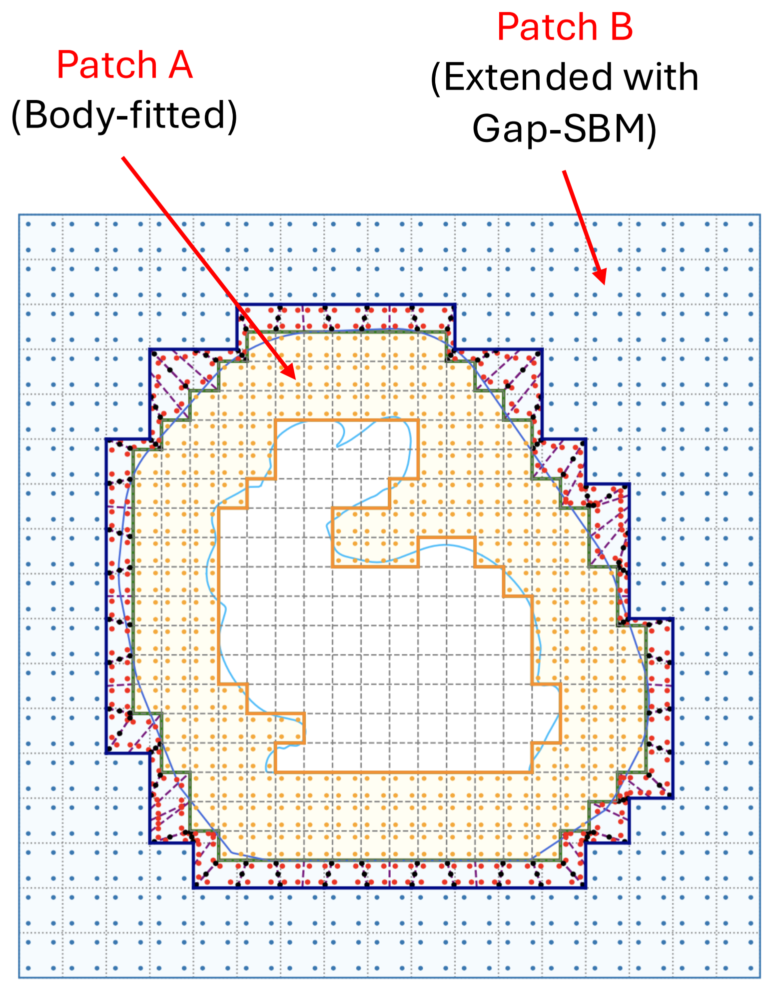

Continuity can be enforced with a penalty-free Nitsche formulation

Consider the Discontinuous Galerkin notation of jump and average:

$$[[w]] := w^A - w^B \qquad \{\{w\}\} := \frac{1}{2}(w^A + w^B)$$

$$[[\partial_{\boldsymbol{n}} w]] := \partial_{\boldsymbol{n}^A} w^A - \partial_{\boldsymbol{n}^B} w^B \qquad \{\{\partial_{\boldsymbol{n}} w\}\} := \frac{1}{2}(\partial_{\boldsymbol{n}^A} w^A + \partial_{\boldsymbol{n}^B} w^B)$$

The Nitsche coupling terms are then defined as

$$a^{\text{sym}}_{\Gamma_{AB}}(u, v) = -\langle \{\{\partial_{\boldsymbol{n}} u\}\}, [[v]] \rangle_{\Gamma_{AB}} - \langle [[u]], \{\{\partial_{\boldsymbol{n}} v\}\} \rangle_{\Gamma_{AB}} + \left\langle \frac{\alpha}{h} [[u]], [[v]] \right\rangle_{\Gamma_{AB}}$$

$$\boxed{a^{\text{pf}}_{\Gamma_{AB}}(u, v)} = -\langle \{\{\partial_{\boldsymbol{n}} u\}\}, [[v]] \rangle_{\Gamma_{AB}} + \langle \{\{\partial_{\boldsymbol{n}} v\}\}, [[u]] \rangle_{\Gamma_{AB}}$$

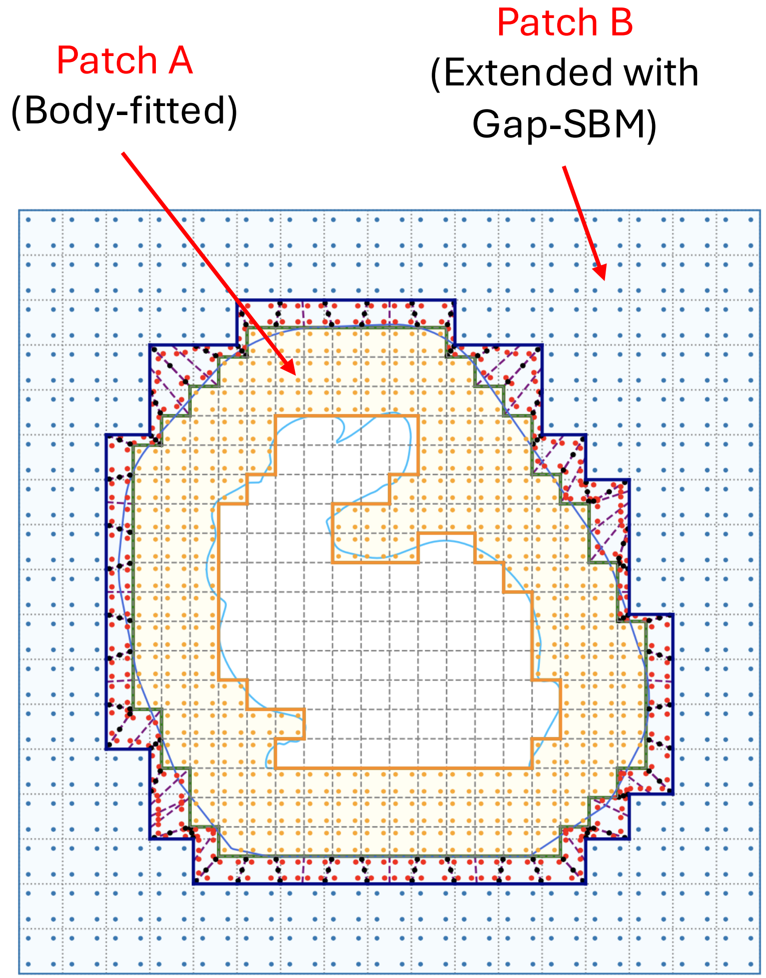

Continuity can be enforced with a penalty-free Nitsche formulation

Consider the Discontinuous Galerkin notation of jump and average:

$$[[w]] := w^A - w^B \qquad \{\!\{w\}\!\} := \tfrac{1}{2}(w^A + w^B)$$

$$[[\partial_n w]] := \partial_{n^A} w^A - \partial_{n^B} w^B \qquad \{\!\{\partial_n w\}\!\} := \tfrac{1}{2}(\partial_{n^A} w^A + \partial_{n^B} w^B)$$

The Nitsche coupling terms are then defined as

$$a^{\mathrm{sym}}_{\Gamma_{AB}}(u,v) = -\langle \{\!\{\partial_n u\}\!\}, [[v]] \rangle_{\Gamma_{AB}} - \langle [[u]], \{\!\{\partial_n v\}\!\} \rangle_{\Gamma_{AB}} + \left\langle \frac{\alpha}{h} [[u]], [[v]] \right\rangle_{\Gamma_{AB}}$$

$$\boxed{a^{\mathrm{pf}}_{\Gamma_{AB}}(u,v)} = \underbrace{\boxed{-\langle \{\!\{\partial_n u\}\!\}, [[v]] \rangle_{\Gamma_{AB}}}}_{\text{flux continuity}} + \underbrace{\boxed{\langle \{\!\{\partial_n v\}\!\}, [[u]] \rangle_{\Gamma_{AB}}}}_{\text{Nitsche term}}$$

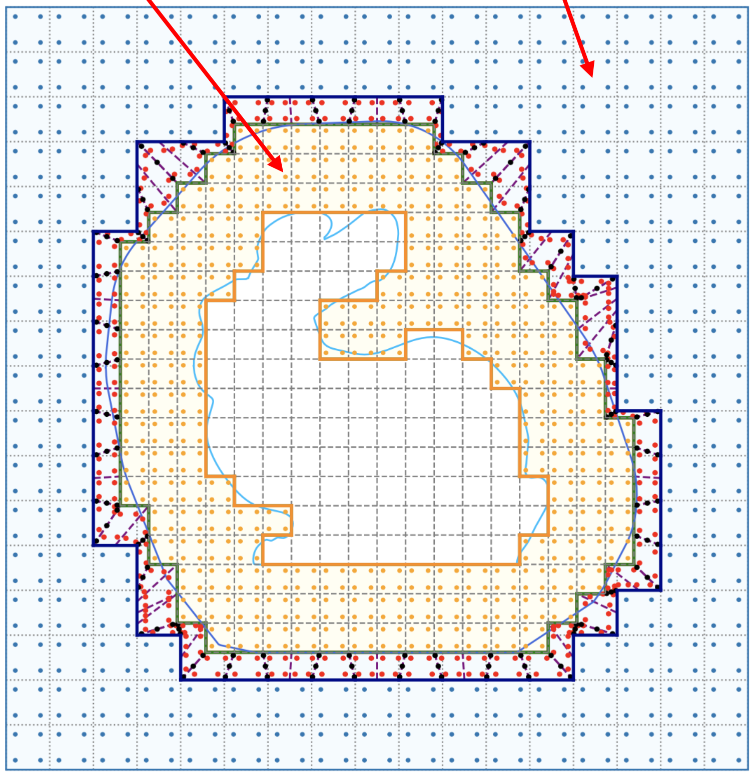

No additional DOFs are introduced contributions project to already existing DOFs

Consider the **extended** Discontinuous Galerkin notation of jump and average:

$$[[v]] = v^{A} - v^{B,\text{ext}} \qquad [[u]] = u^{A} - u^{B,\text{ext}}$$

$$\{\{\partial_{\boldsymbol{n}} v\}\} = \frac{1}{2}\left(\partial_{\tilde{\boldsymbol{n}}^{A}} v^{A} + \partial_{\boldsymbol{n}^{B}} v^{B,\text{ext}}\right) \qquad \{\{\partial_{\boldsymbol{n}} u\}\} = \frac{1}{2}\left(\partial_{\tilde{\boldsymbol{n}}^{A}} u^{A} + \partial_{\boldsymbol{n}^{B}} u^{B,\text{ext}}\right)$$

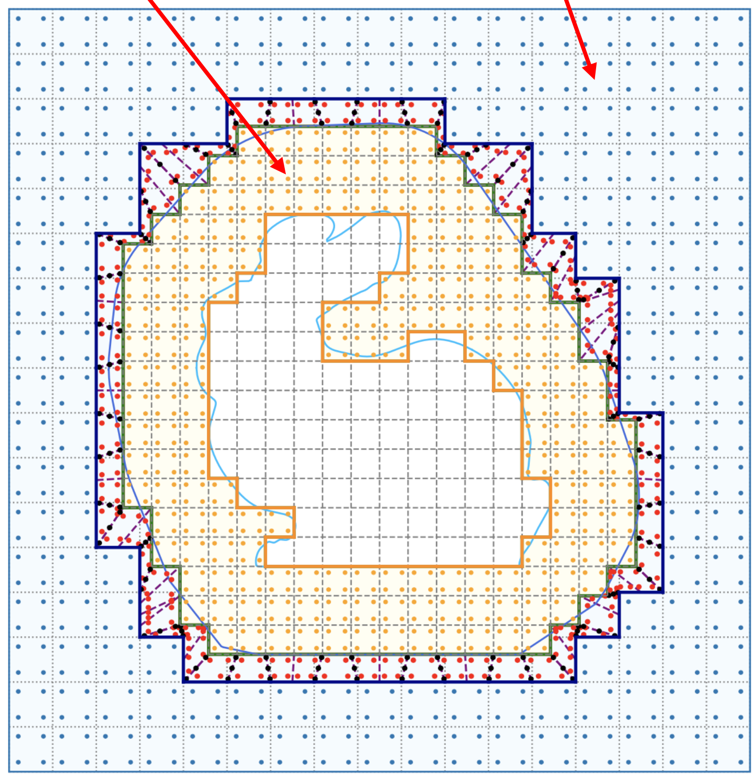

No additional DOFs are introduced contributions project to already existing DOFs

Consider the **extended** Discontinuous Galerkin notation of jump and average:

$$[[v]] = v^A - \boxed{v^{B,\mathrm{ext}}} \qquad [[u]] = u^A - \boxed{u^{B,\mathrm{ext}}}$$

$$\{\{\partial_{\boldsymbol{n}} v\}\} = \frac{1}{2}\left(\partial_{\tilde{\boldsymbol{n}}^A} v^A + \partial_{\boldsymbol{n}^B} \boxed{v^{B,\mathrm{ext}}}\right) \qquad \{\{\partial_{\boldsymbol{n}} u\}\} = \frac{1}{2}\left(\partial_{\tilde{\boldsymbol{n}}^A} u^A + \partial_{\boldsymbol{n}^B} \boxed{u^{B,\mathrm{ext}}}\right)$$

Patch A
(Body-fitted)

Patch B
(Extended with
Gap-SBM)

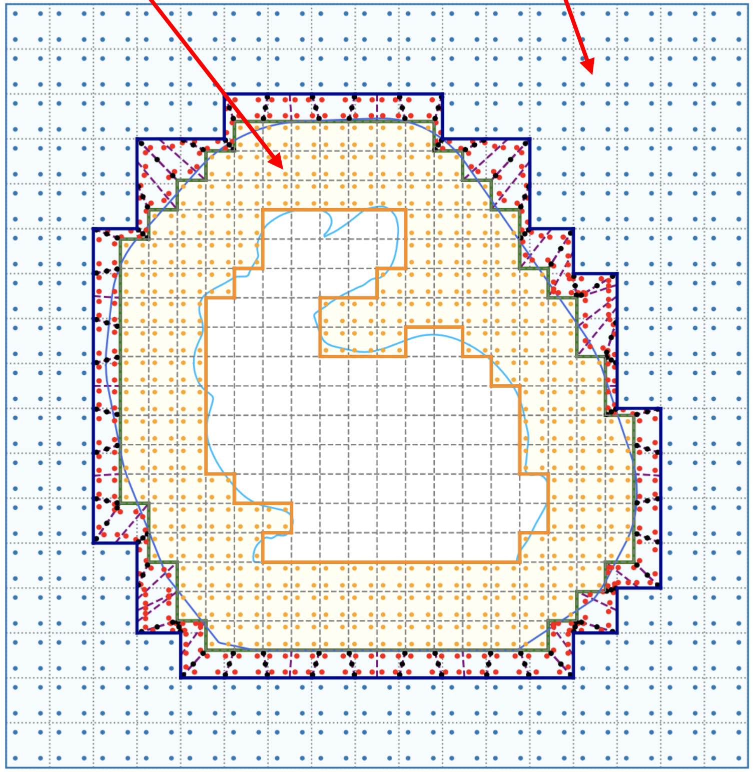

No additional DOFs are introduced contributions project to already existing DOFs

Consider the **extended** Discontinuous Galerkin notation of jump and average:

$$[[v]] = v^A - \boxed{v^{B,\text{ext}}} \qquad [[u]] = u^A - \boxed{u^{B,\text{ext}}}$$

$$\{\{\partial_{\boldsymbol{n}} v\}\} = \frac{1}{2}\left(\partial_{\tilde{\boldsymbol{n}}^A} v^A + \partial_{\boldsymbol{n}^B} \boxed{v^{B,\text{ext}}}\right) \qquad \{\{\partial_{\boldsymbol{n}} u\}\} = \frac{1}{2}\left(\partial_{\tilde{\boldsymbol{n}}^A} u^A + \partial_{\boldsymbol{n}^B} \boxed{u^{B,\text{ext}}}\right)$$

Extended basis functions definition using the closest point projection on the surrogate boundary

$$u^{\text{ext}}(\boldsymbol{x}) = \sum_i u_i \boxed{\widetilde{\mathbb{S}}_{\boldsymbol{d}}^m(N_i(\tilde{\boldsymbol{x}}))}$$

Taylor shift operator

Patch A
(Body-fitted)

Patch B
(Extended with
Gap-SBM)

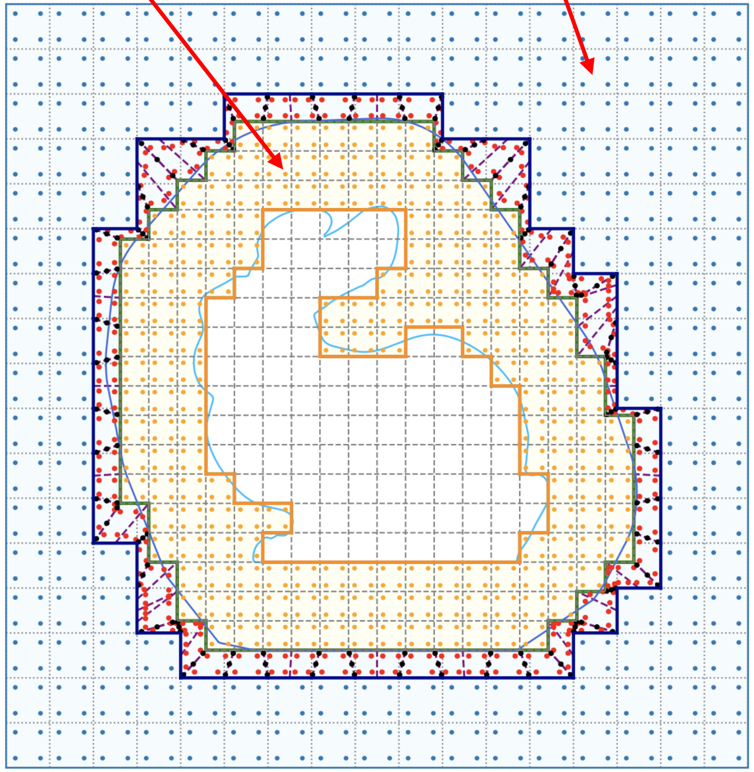

No additional DOFs are introduced contributions project to already existing DOFs

Consider the **extended** Discontinuous Galerkin notation of jump and average:

$$[[v]] = v^A - v^{B,\text{ext}} \qquad [[u]] = u^A - u^{B,\text{ext}}$$

$$\{\!\{\partial_{\boldsymbol{n}} v\}\!\} = \frac{1}{2}\left(\partial_{\tilde{\boldsymbol{n}}^A} v^A + \partial_{\boldsymbol{n}^B} v^{B,\text{ext}}\right) \qquad \{\!\{\partial_{\boldsymbol{n}} u\}\!\} = \frac{1}{2}\left(\partial_{\tilde{\boldsymbol{n}}^A} u^A + \partial_{\boldsymbol{n}^B} u^{B,\text{ext}}\right)$$

Gap volumes terms and Nitsche **extended** coupling terms (penalty-free):

$$(\nabla u^{B,\text{ext}}, \nabla v^{B,\text{ext}})_{\Omega^B} - \langle \{\!\{\partial_{\boldsymbol{n}} u\}\!\}, [[v]] \rangle_{\Gamma_{AB}} + \langle [[u]], \{\!\{\partial_{\boldsymbol{n}} v\}\!\} \rangle_{\Gamma_{AB}} = (f, v^{B,\text{ext}})_{\Omega^B}$$

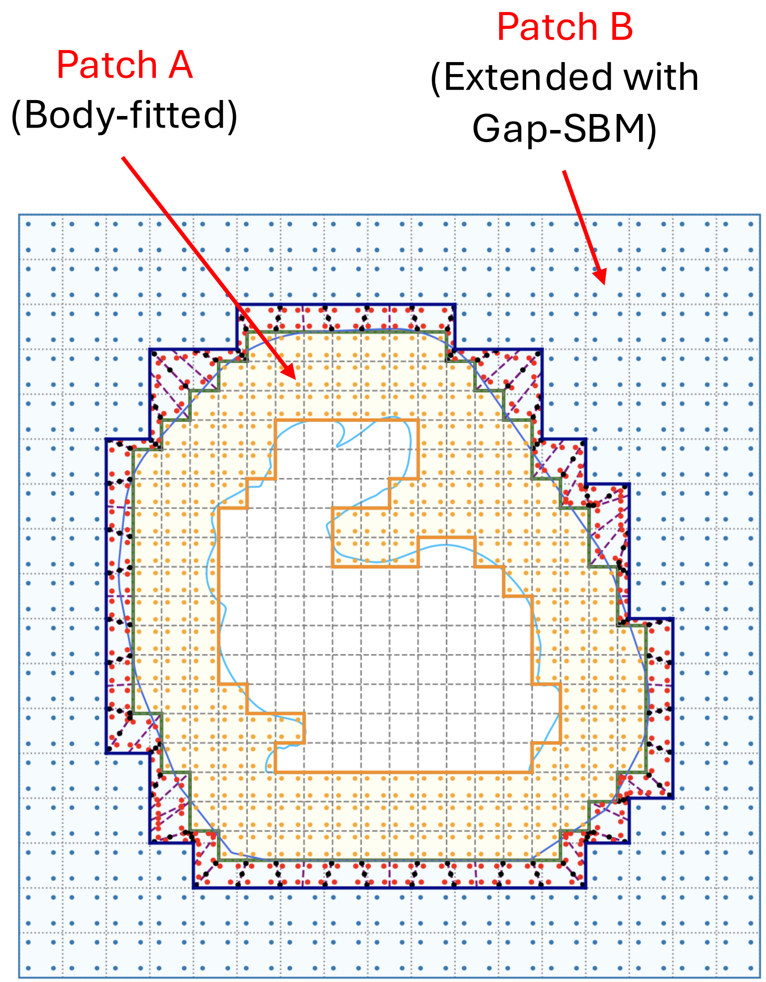

No additional DOFs are introduced contributions project to already existing DOFs

Consider the **extended** Discontinuous Galerkin notation of jump and average:

$$[[v]] = v^A - v^{B,\text{ext}} \qquad [[u]] = u^A - u^{B,\text{ext}}$$

$$\{\{\partial_{\boldsymbol{n}} v\}\} = \frac{1}{2}\left(\partial_{\tilde{\boldsymbol{n}}^A} v^A + \partial_{\boldsymbol{n}^B} v^{B,\text{ext}}\right) \qquad \{\{\partial_{\boldsymbol{n}} u\}\} = \frac{1}{2}\left(\partial_{\tilde{\boldsymbol{n}}^A} u^A + \partial_{\boldsymbol{n}^B} u^{B,\text{ext}}\right)$$

$\boxed{\text{Gap volumes terms}}$ and Nitsche **extended** coupling terms (penalty-free):

$$\left(\boxed{\nabla u^{B,\text{ext}}}, \boxed{\nabla v^{B,\text{ext}}}\right)_{\Omega^B} - \langle \{\{\partial_{\boldsymbol{n}} u\}\}, [[v]] \rangle_{\Gamma_{AB}} + \langle [[u]], \{\{\partial_{\boldsymbol{n}} v\}\} \rangle_{\Gamma_{AB}} = \left(f, \boxed{v^{B,\text{ext}}}\right)_{\Omega^B}$$

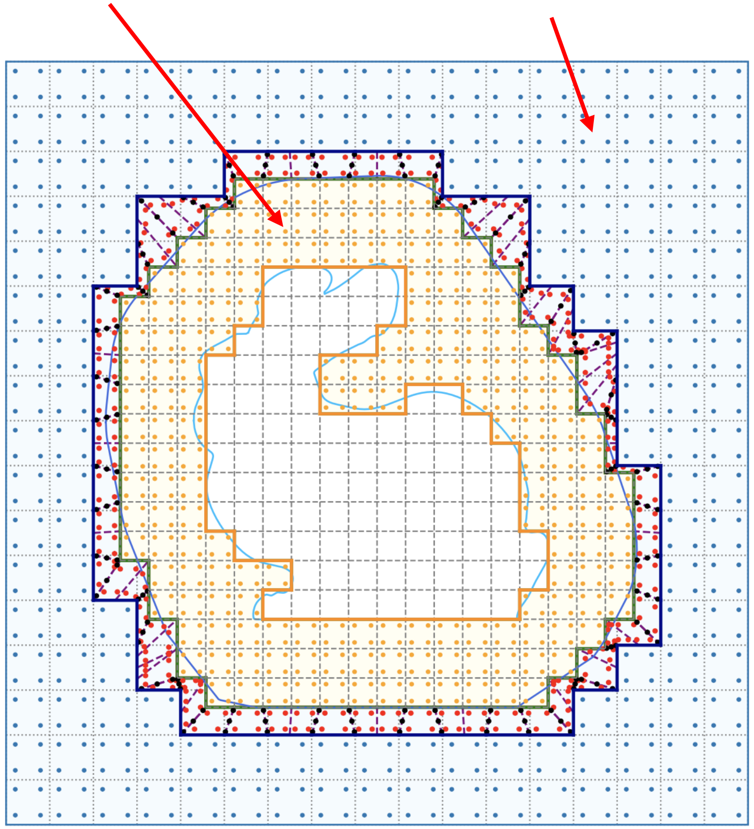

No additional DOFs are introduced contributions project to already existing DOFs

Consider the **extended** Discontinuous Galerkin notation of jump and average:

$$[[v]] = v^A - v^{B,\text{ext}} \qquad [[u]] = u^A - u^{B,\text{ext}}$$

$$\{\{\partial_{\boldsymbol{n}} v\}\} = \frac{1}{2}\left(\partial_{\tilde{\boldsymbol{n}}^A} v^A + \partial_{\boldsymbol{n}^B} v^{B,\text{ext}}\right) \qquad \{\{\partial_{\boldsymbol{n}} u\}\} = \frac{1}{2}\left(\partial_{\tilde{\boldsymbol{n}}^A} u^A + \partial_{\boldsymbol{n}^B} u^{B,\text{ext}}\right)$$

Gap volumes terms and Nitsche **extended** coupling terms (penalty-free):

$$(\nabla u^{B,\text{ext}}, \nabla v^{B,\text{ext}})_{\Omega^B} \boxed{- \langle \{\{\partial_{\boldsymbol{n}} u\}\}, [[v]] \rangle_{\Gamma_{AB}} + \langle [[u]], \{\{\partial_{\boldsymbol{n}} v\}\} \rangle_{\Gamma_{AB}}} = (f, v^{B,\text{ext}})_{\Omega^B}$$

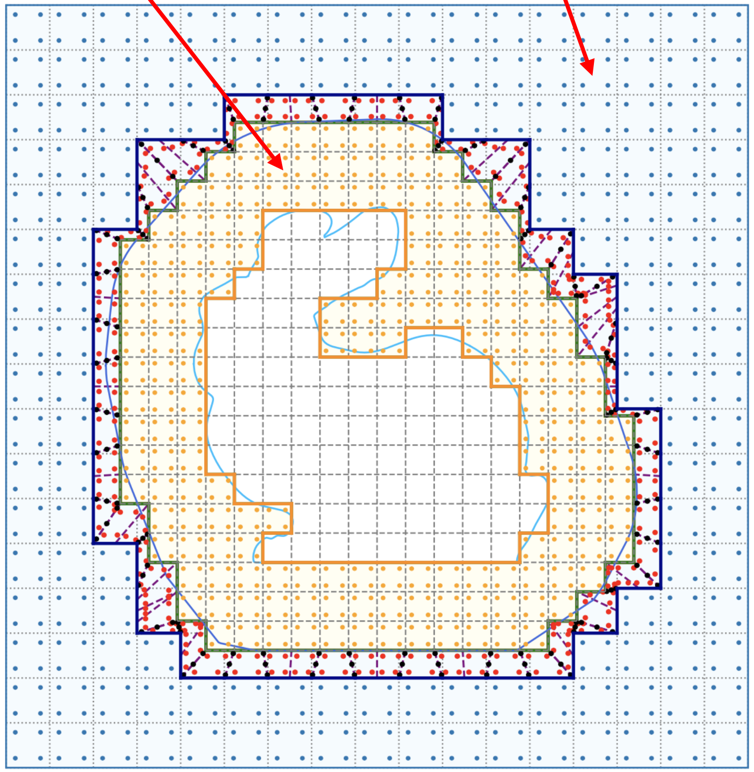

Gap–SBM couples nonconforming patches: Results

Single patch *vs* **two-patches "body-fitted"** *vs* **two-patches Gap-SBM**

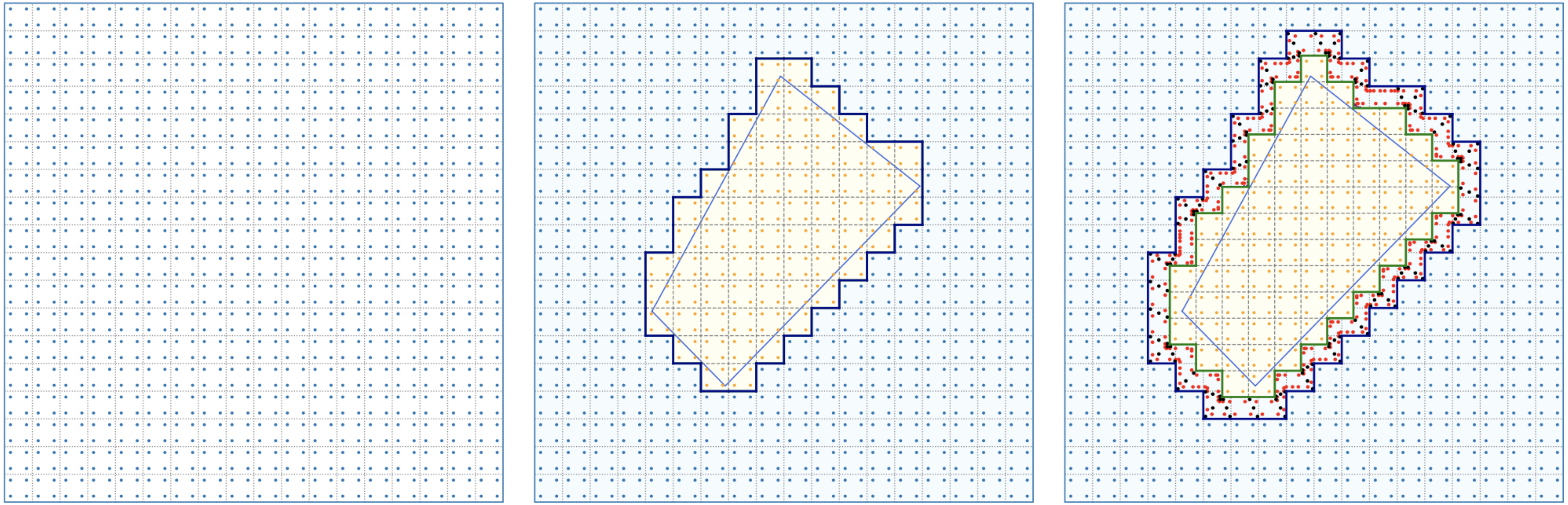

single patch *multipatch body-fitted* *multipatch Gap-SBM*

Gap–SBM couples nonconforming patches: Results

Single patch vs two-patches:

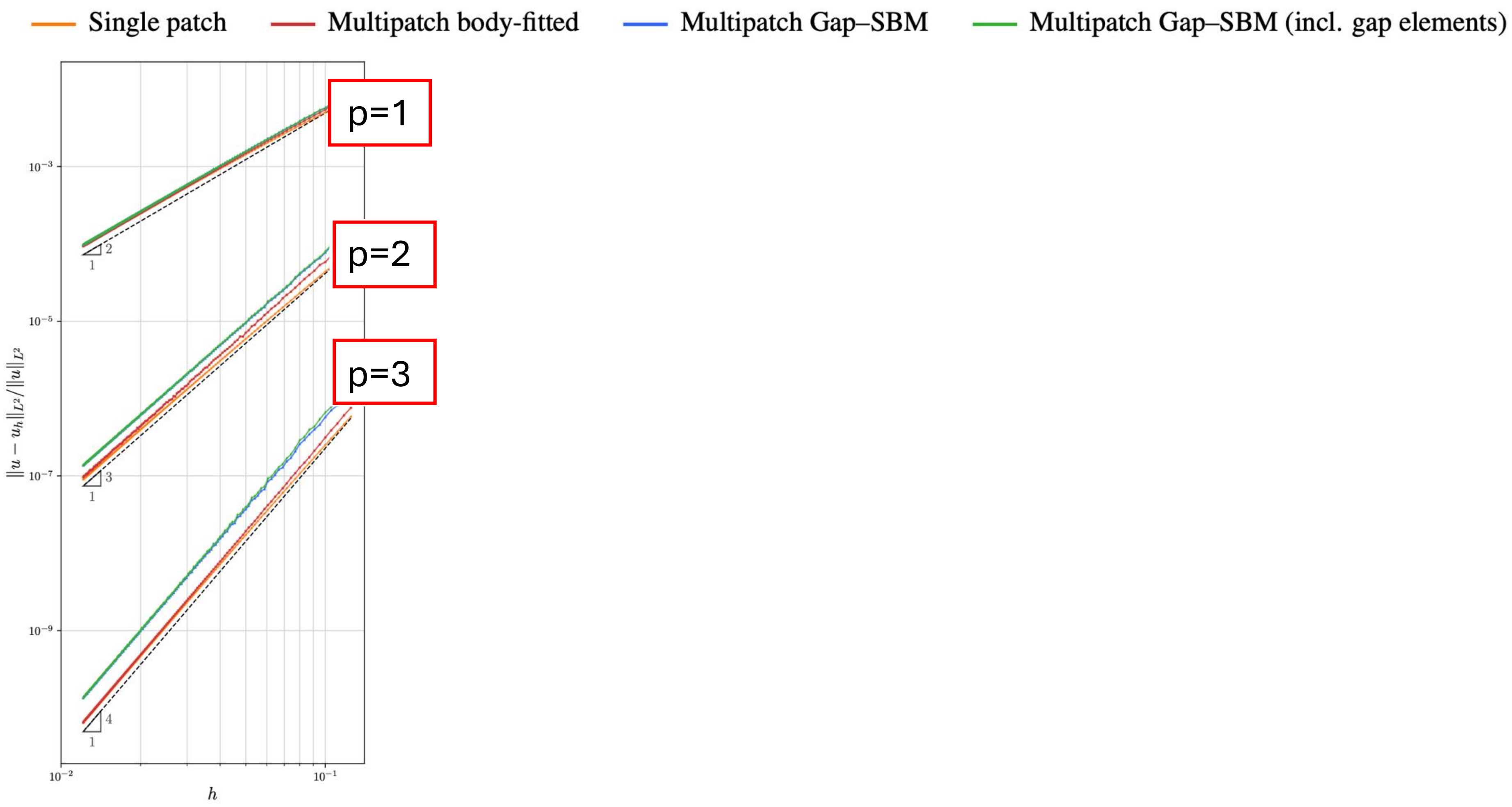

L^2 error vs h

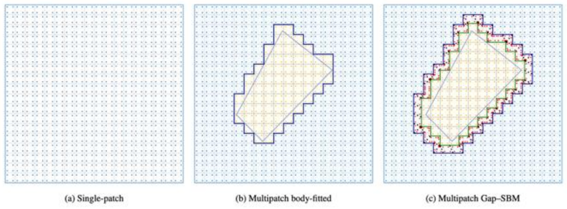

Gap–SBM couples nonconforming patches: Results

Single patch vs two-patches:

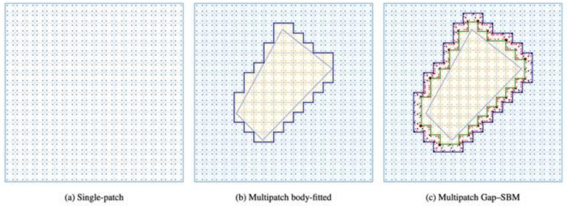

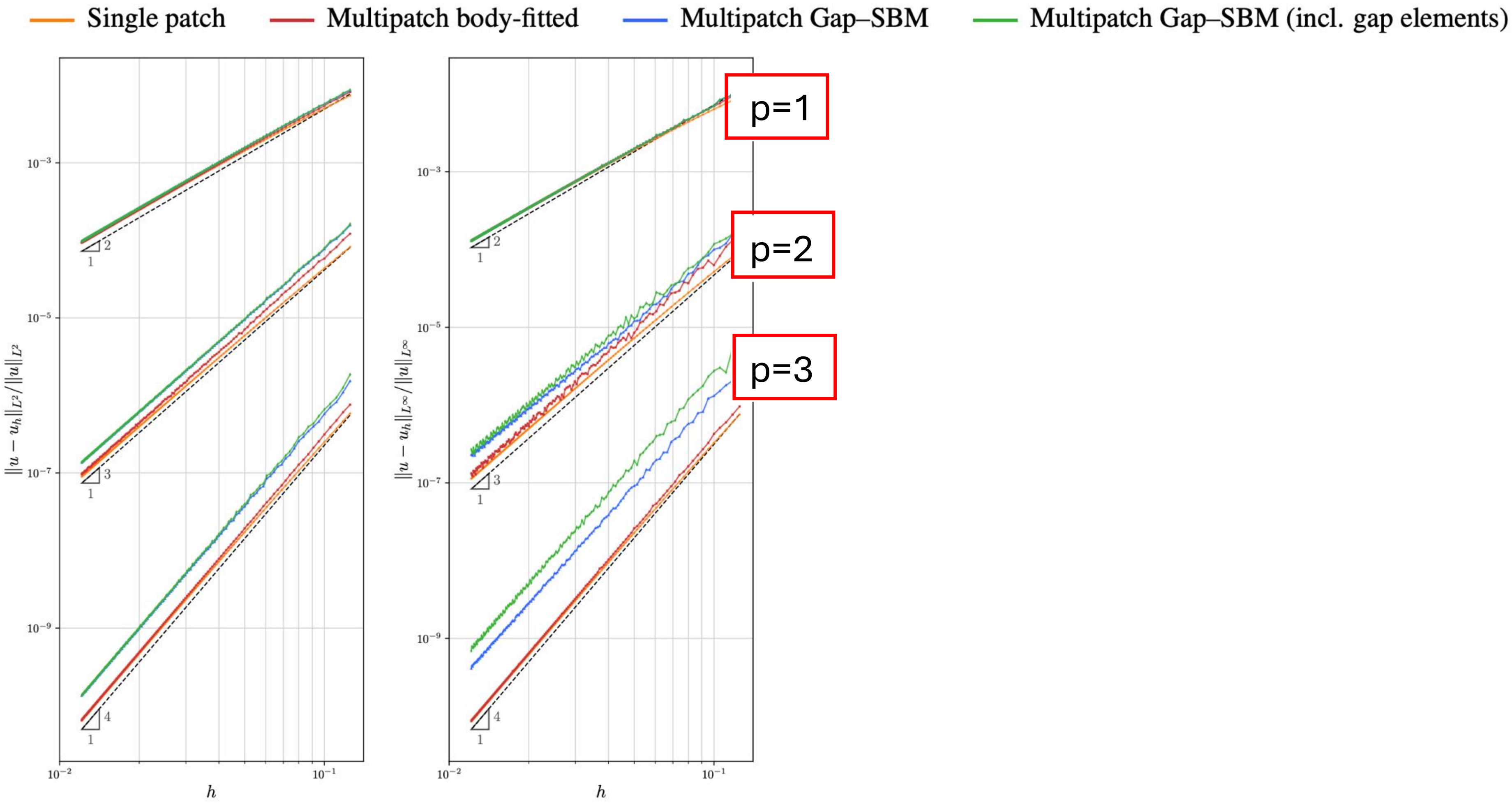

L^2 error vs h $\quad$ H^1 error vs h

Gap–SBM couples nonconforming patches: Results

Single patch vs two-patches:

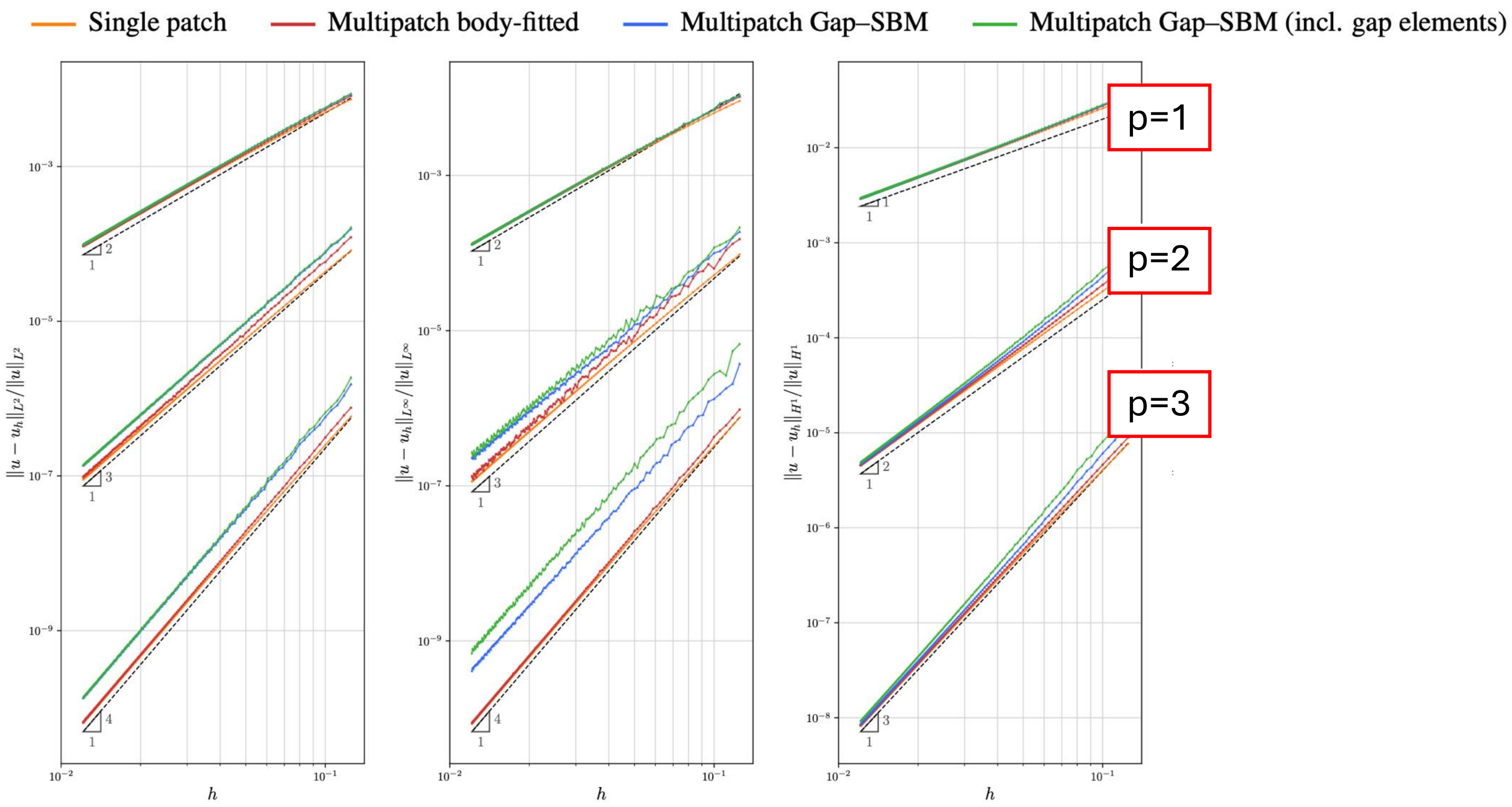

L^2 error vs h H^1 error vs h L^∞ error vs h

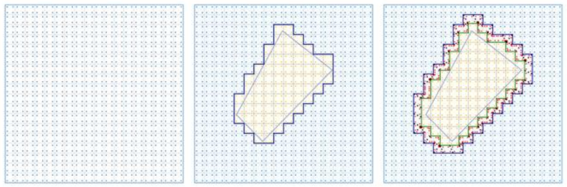

(a) Single-patch (b) Multipatch body-fitted (c) Multipatch Gap–SBM

Gap–SBM couples nonconforming patches: Results

Single patch vs two-patches:

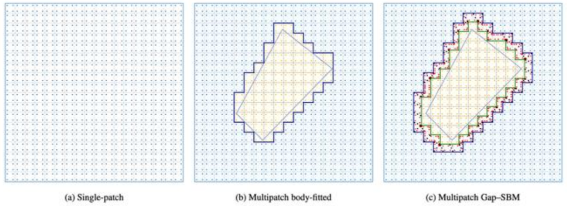

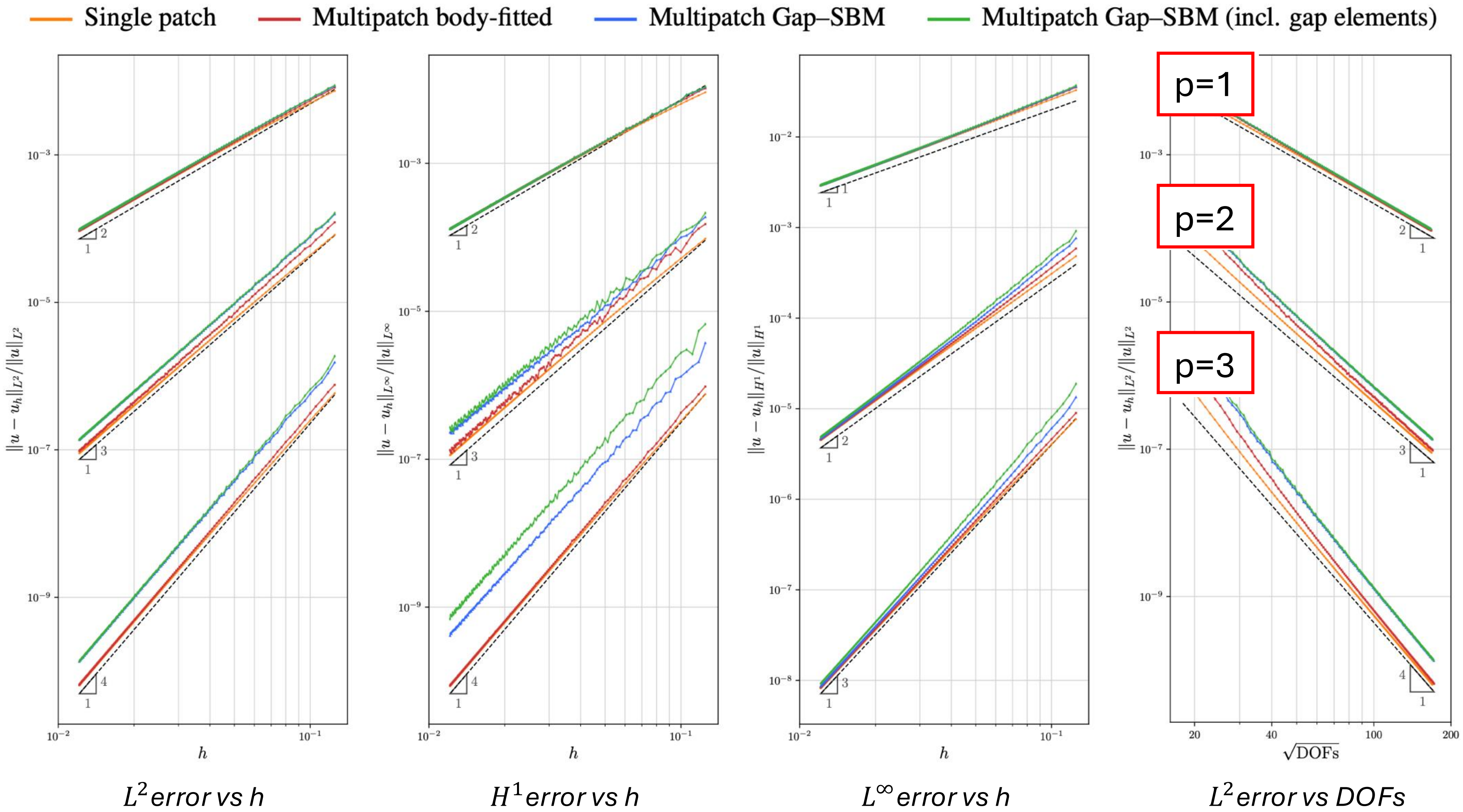

Multipatch Gap-SBM for local refinement

Consider a problem with an embedded boundary where ***Neumann*** BCs must be imposed

Using the classical SBM, the error is always concentrated near the surrogate boundary due to the extension of the gradient term

point-wise error

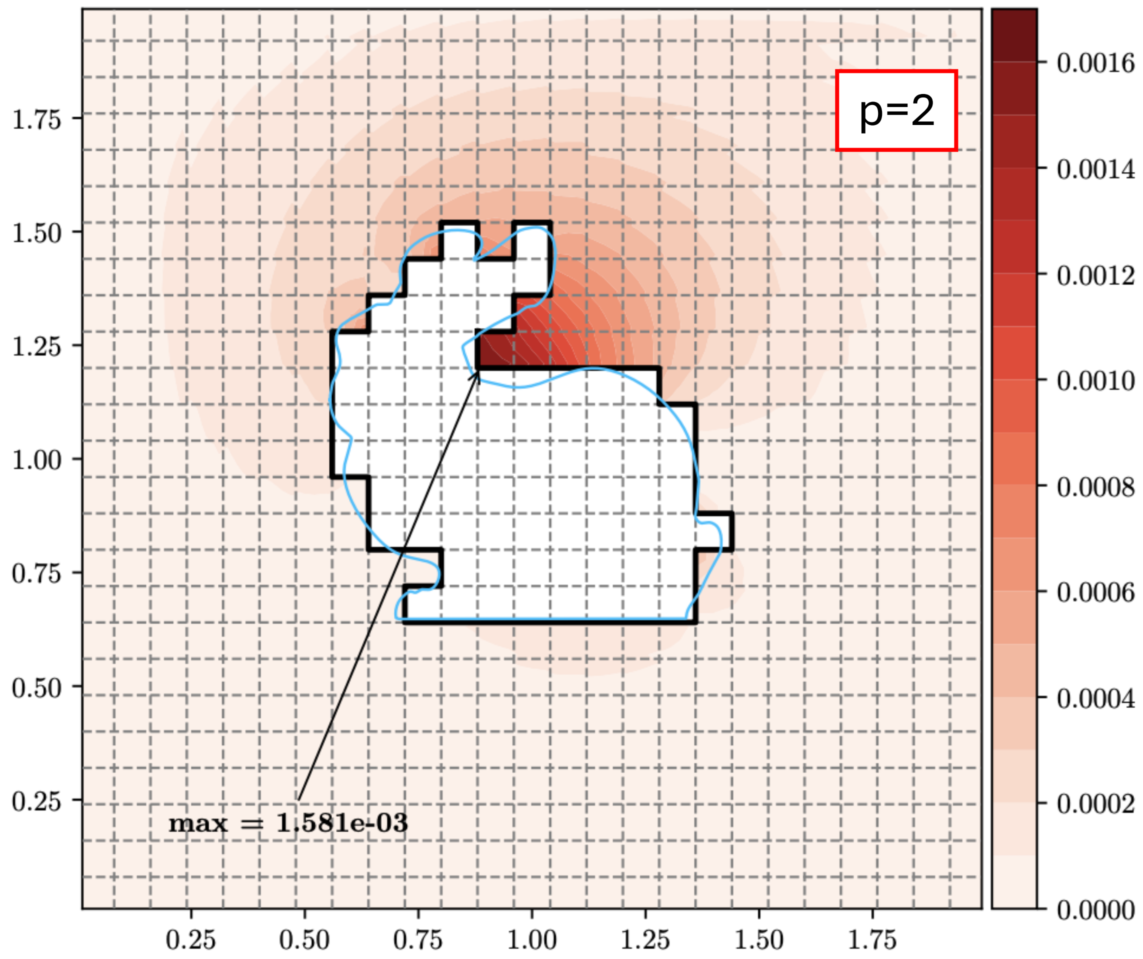

Multipatch Gap-SBM for local refinement

Consider a problem with an embedded boundary where ***Neumann*** BCs must be imposed

Using the classical SBM, the error is always concentrated near the surrogate boundary due to the extension of the gradient term

What if we add an artificial patch and apply *p*- or *h*-refinement?

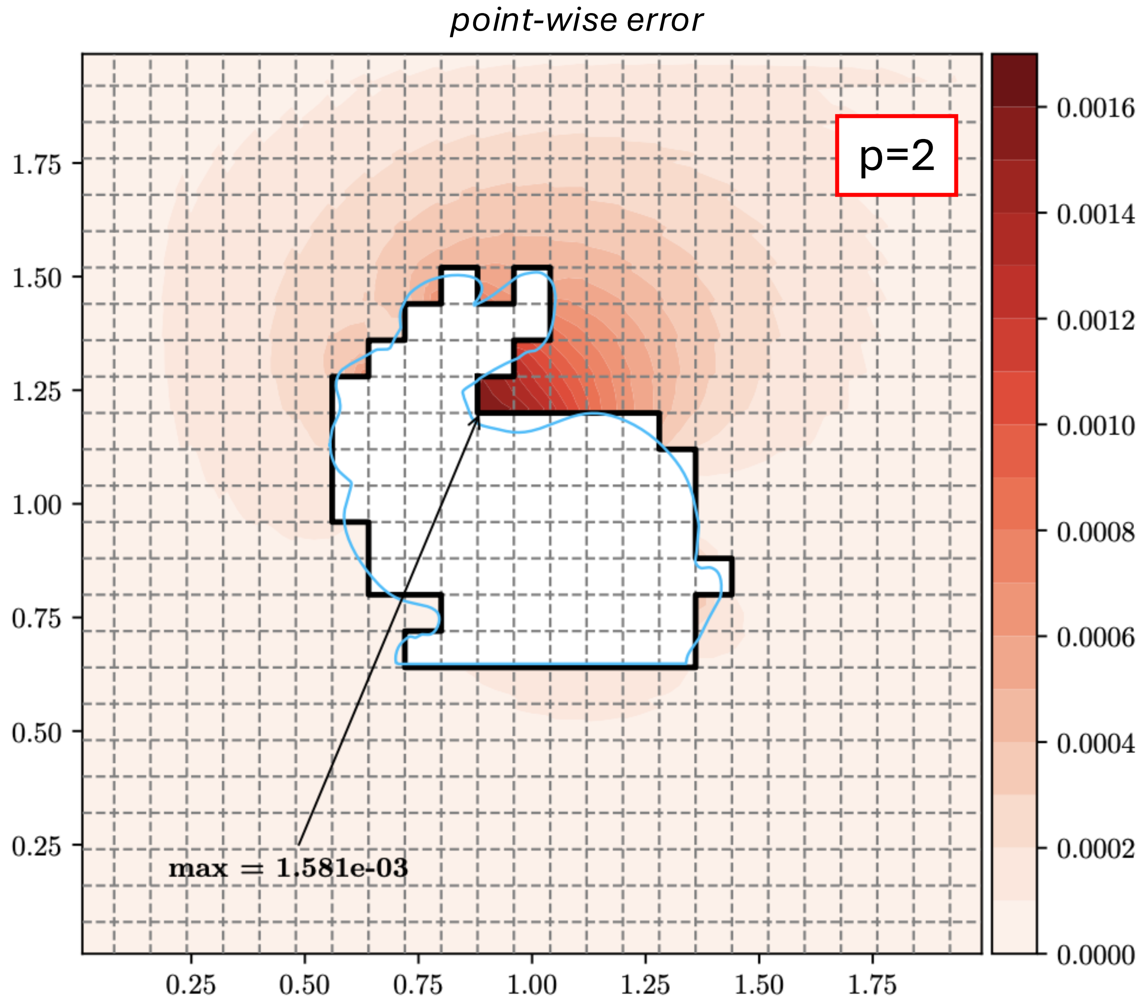

Multipatch Gap-SBM for local refinement

Same polynomial degree and similar mesh size

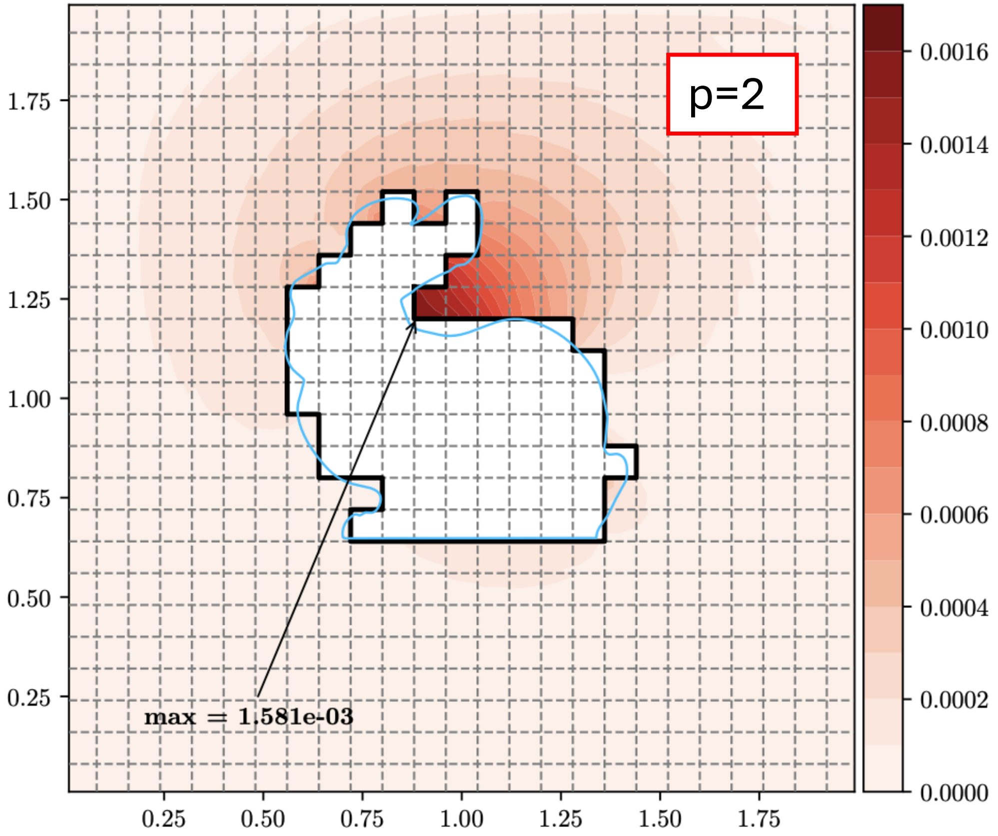

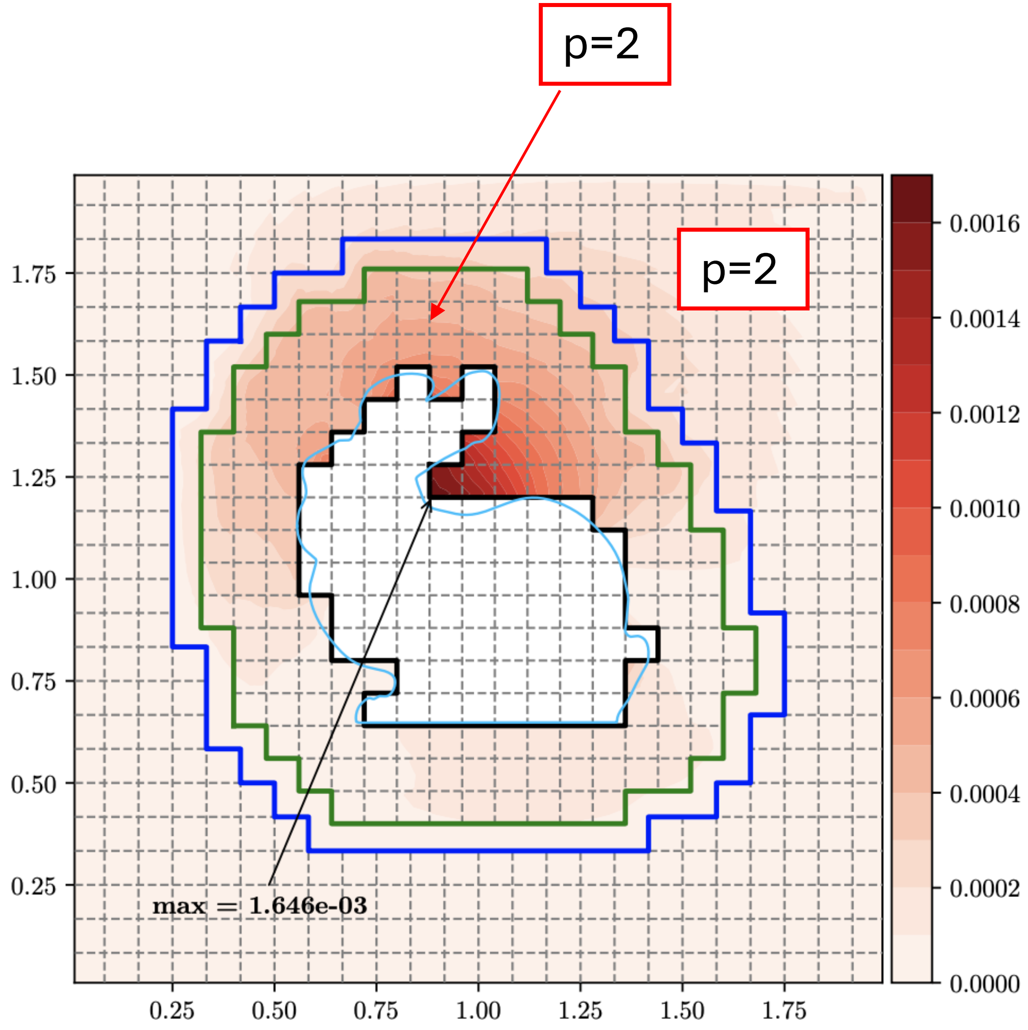

Multipatch Gap-SBM for local refinement

Same polynomial degree and local **h-refinement**

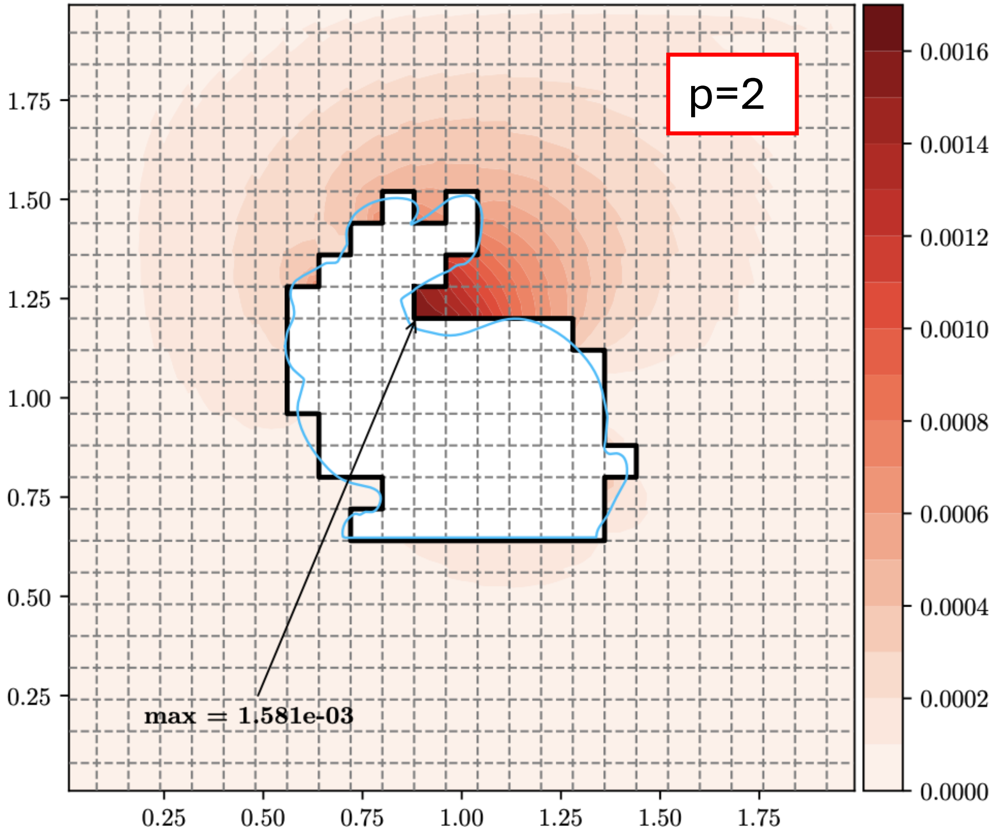

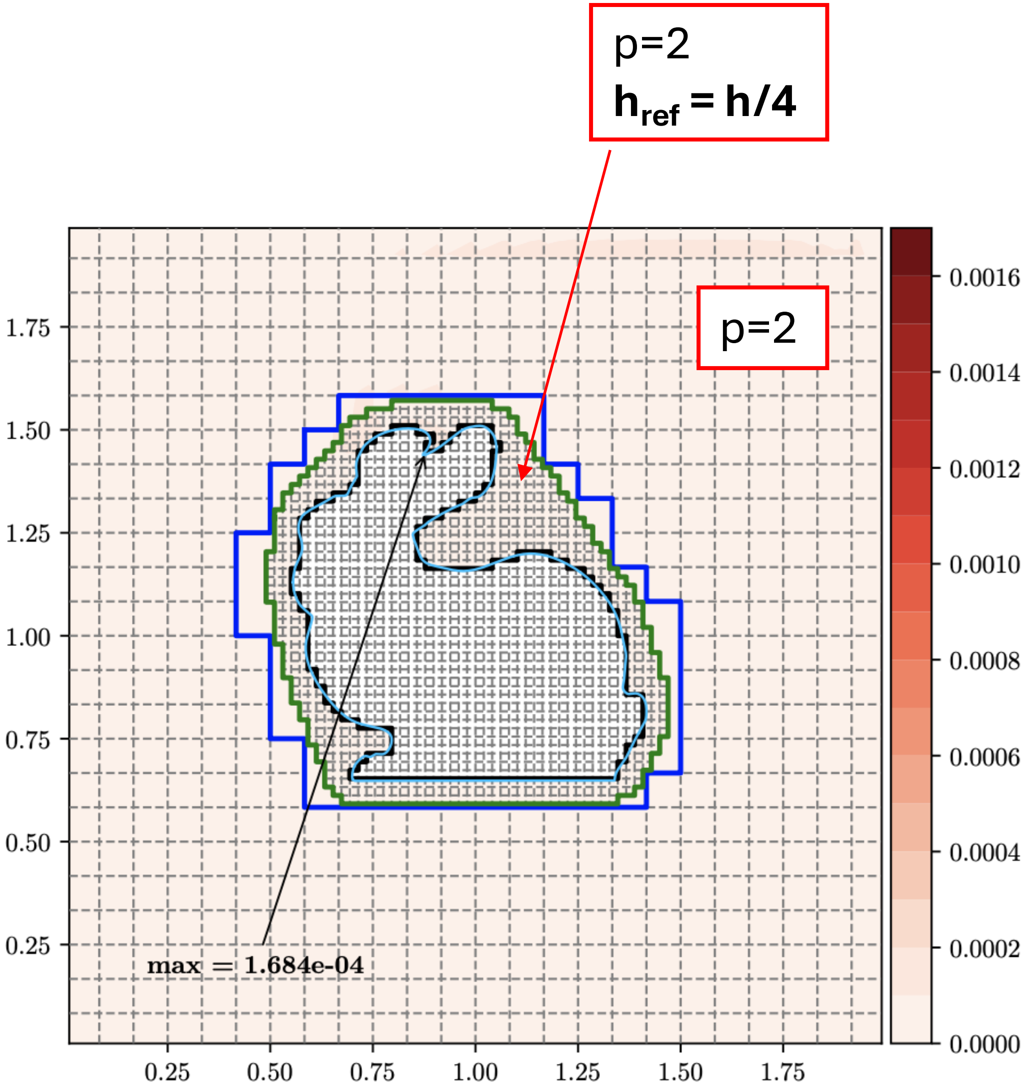

Multipatch Gap-SBM for local refinement

Local **p-refinement** and similar mesh size

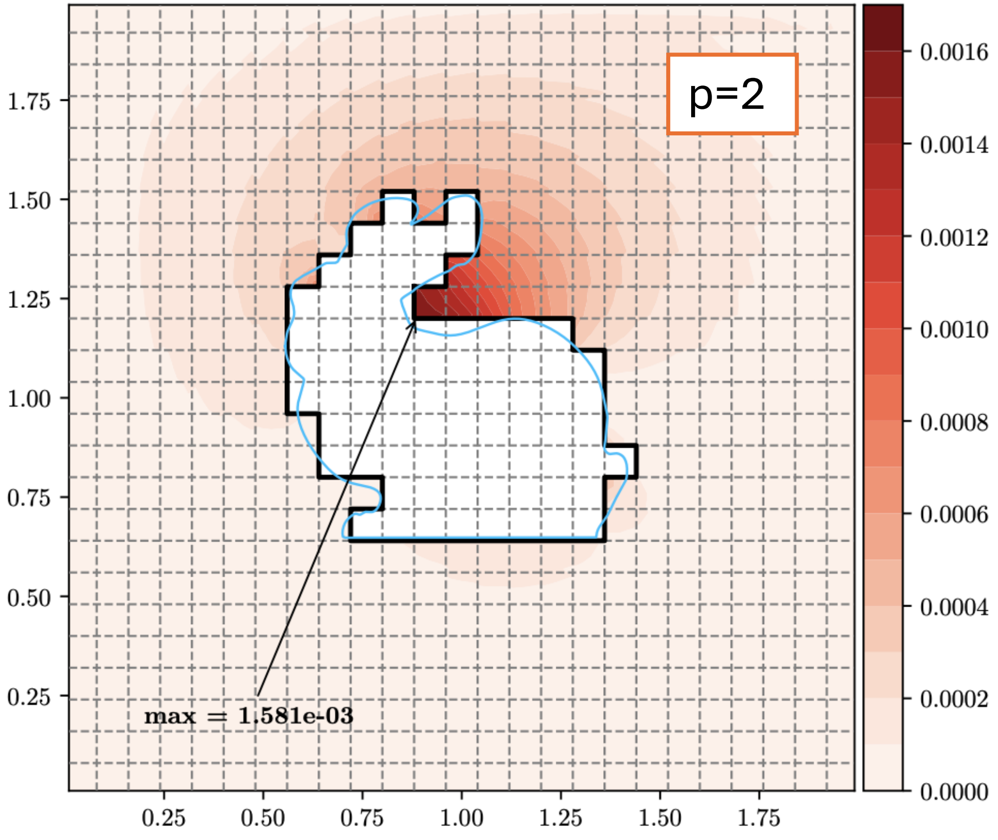

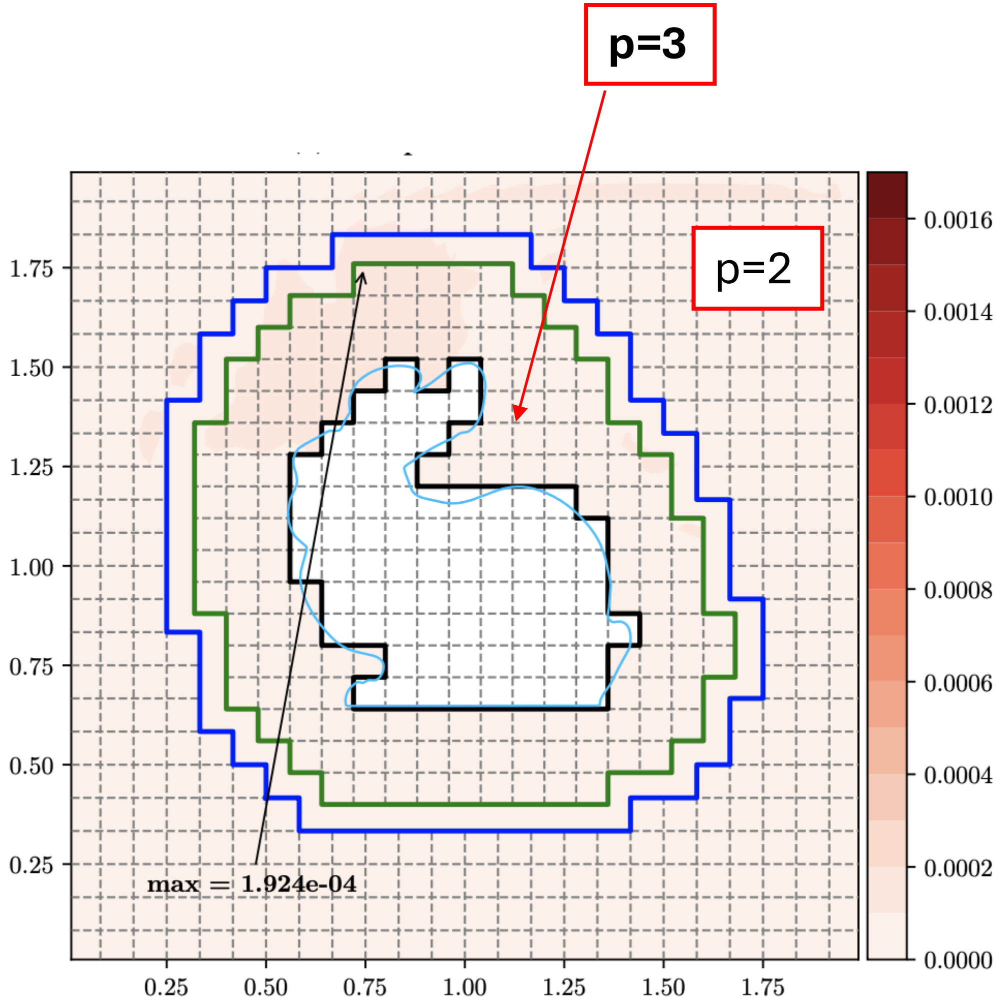

Multipatch Gap-SBM and condition number

Consider the previous example:

single patch vs **multipatch Gap-SBM** with similar mesh size

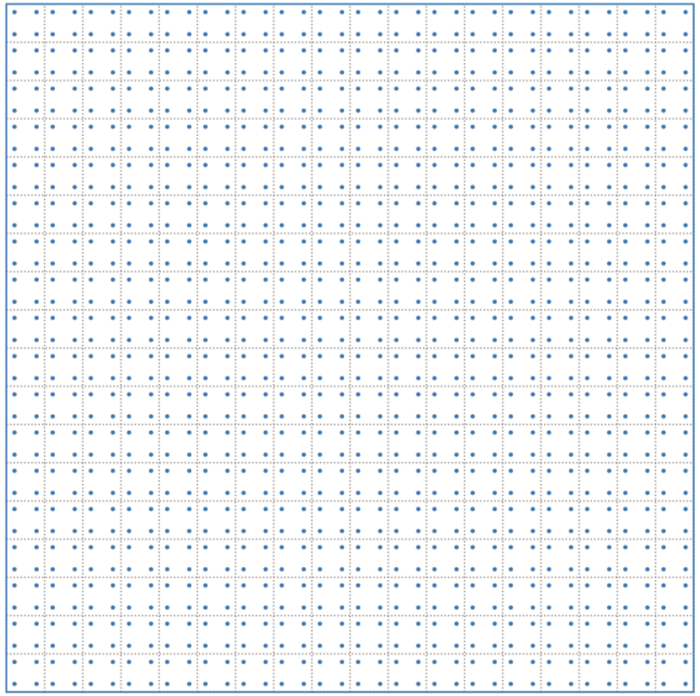

single patch

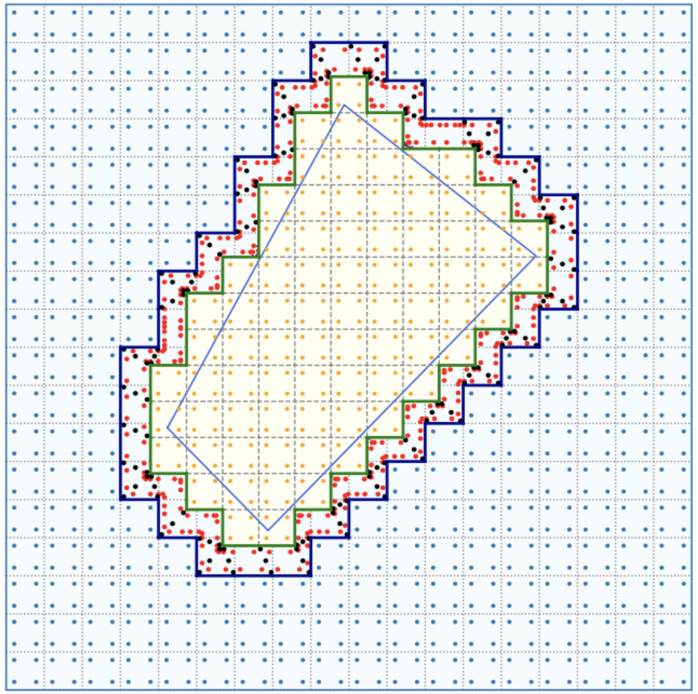

multipatch Gap-SBM

Multipatch Gap-SBM and condition number

The condition number grows asymptotically with the expected h^{-2} rate

single patch
p=1,2 and 3

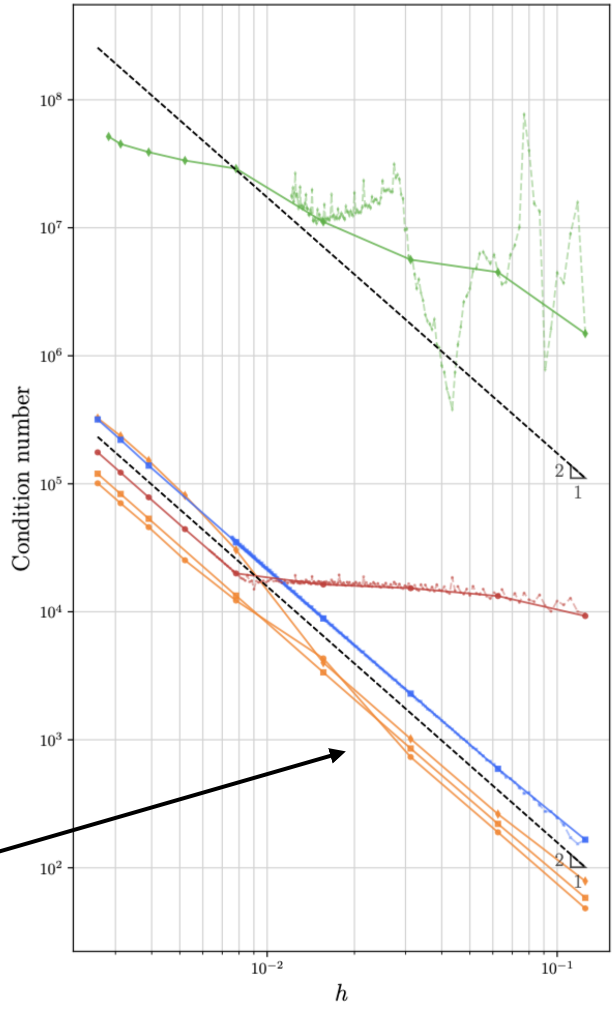

condition number vs h

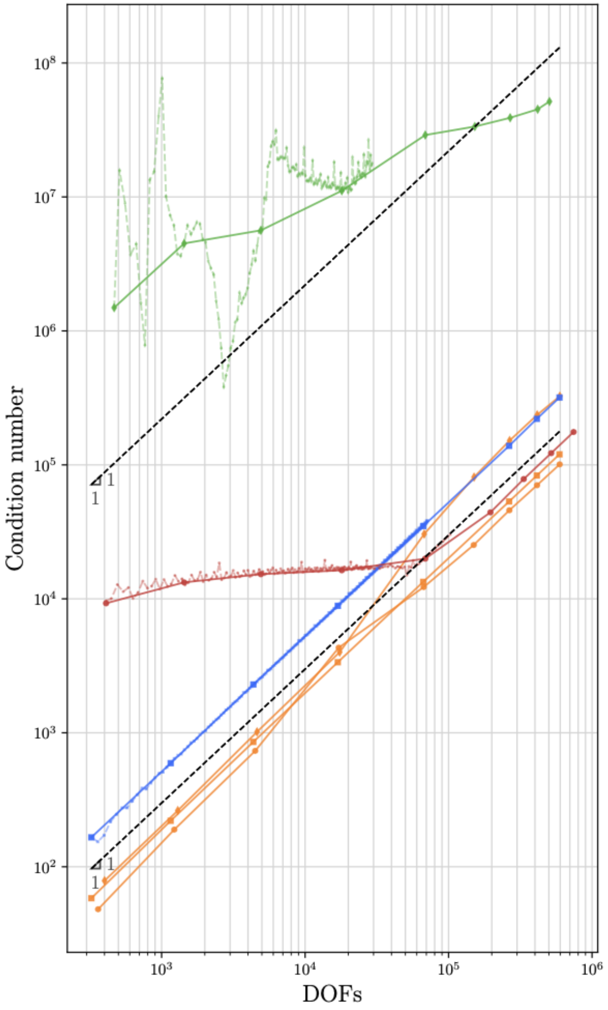

condition number vs DOFs

Multipatch Gap-SBM and condition number

The condition number grows asymptotically with the expected h^{-2} rate

Gap-SBM p=1

single patch
p=1,2 and 3

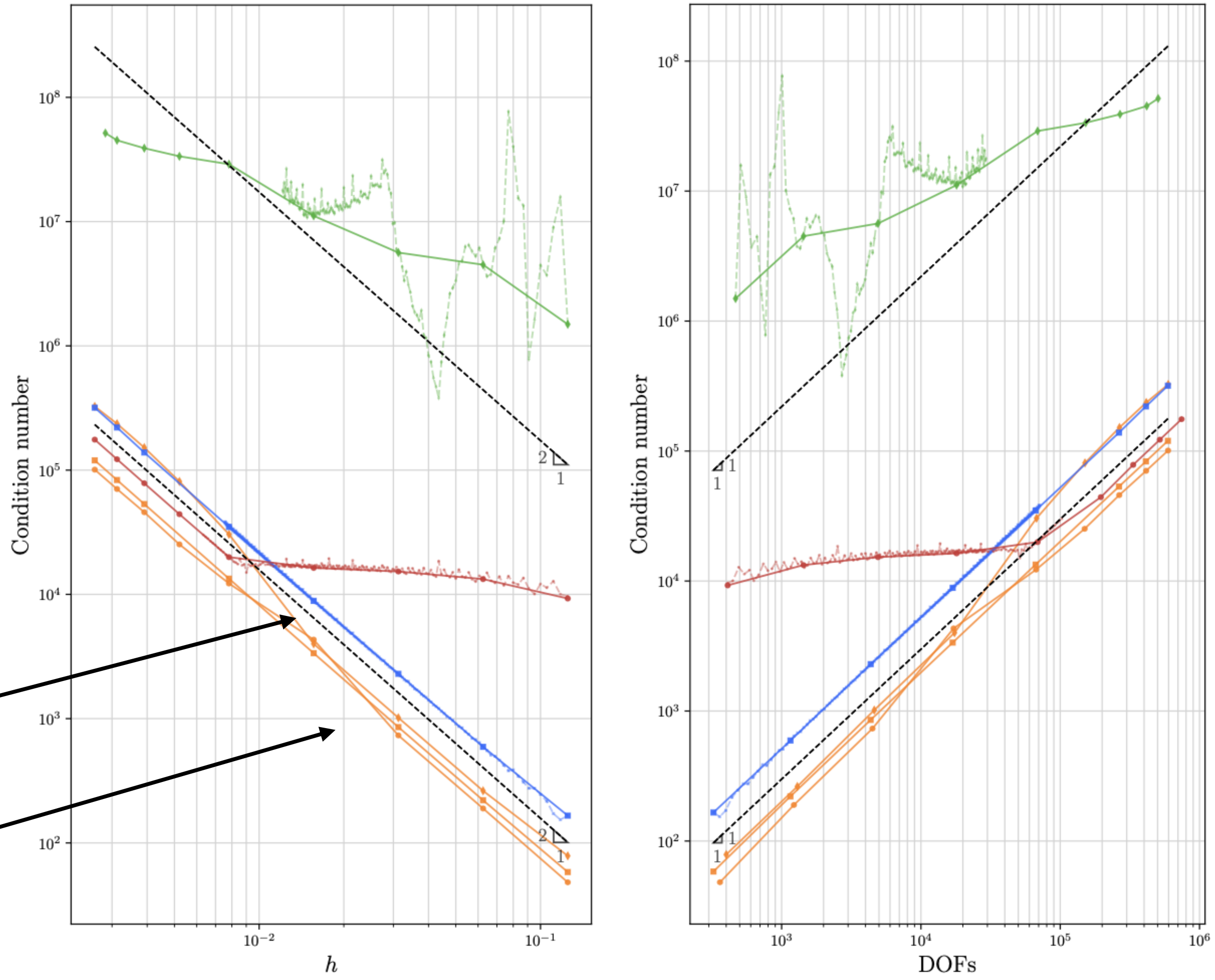

condition number vs h *condition number vs DOFs*

Multipatch Gap-SBM and condition number

The condition number grows asymptotically with the expected h^{-2} rate

Gap-SBM p=2

Gap-SBM p=1

single patch
p=1,2 and 3

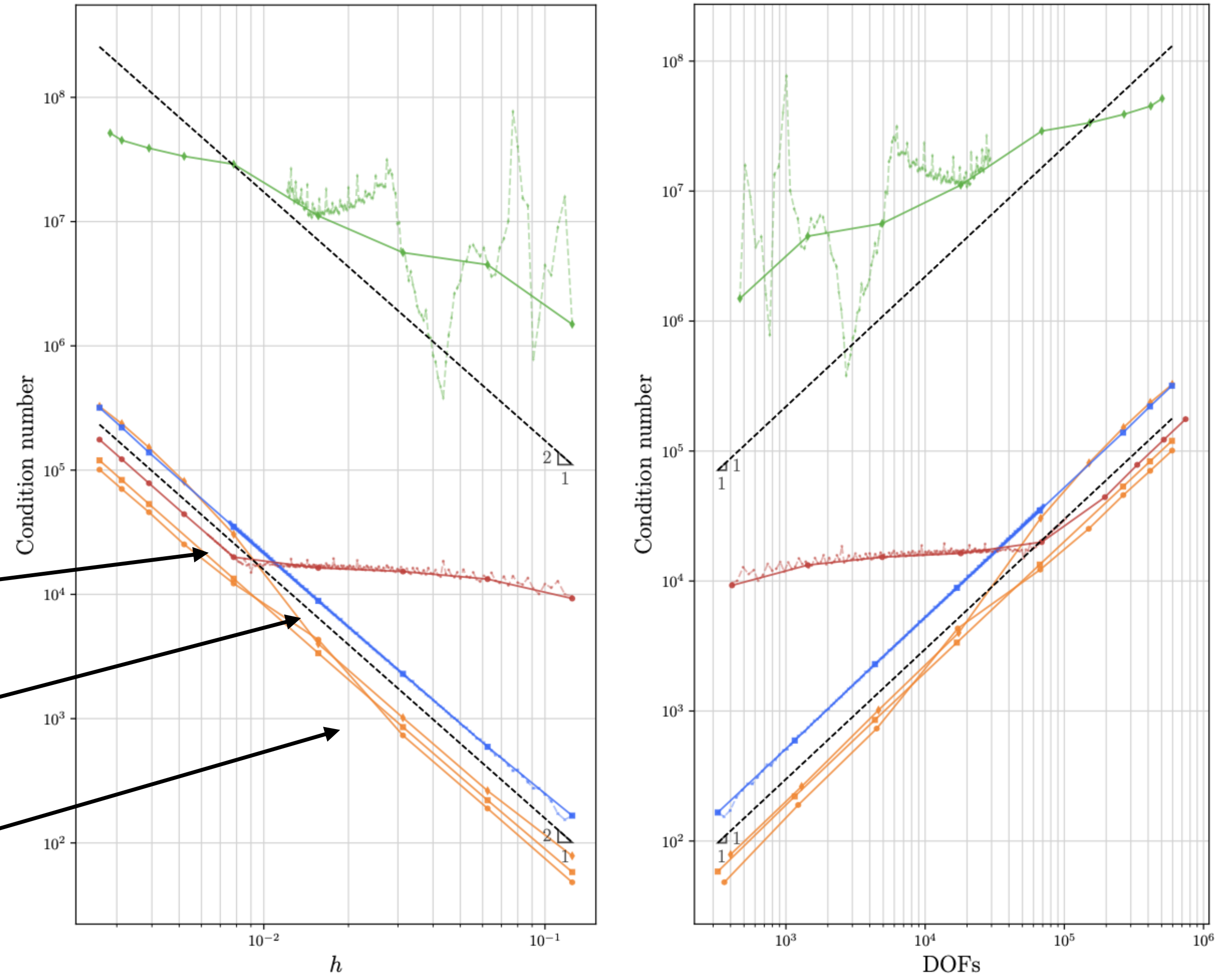

condition number vs h *condition number vs DOFs*

Multipatch Gap-SBM and condition number

The condition number grows asymptotically with the expected h^{-2} rate

Gap-SBM p=3

Gap-SBM p=2

Gap-SBM p=1

single patch
p=1,2 and 3

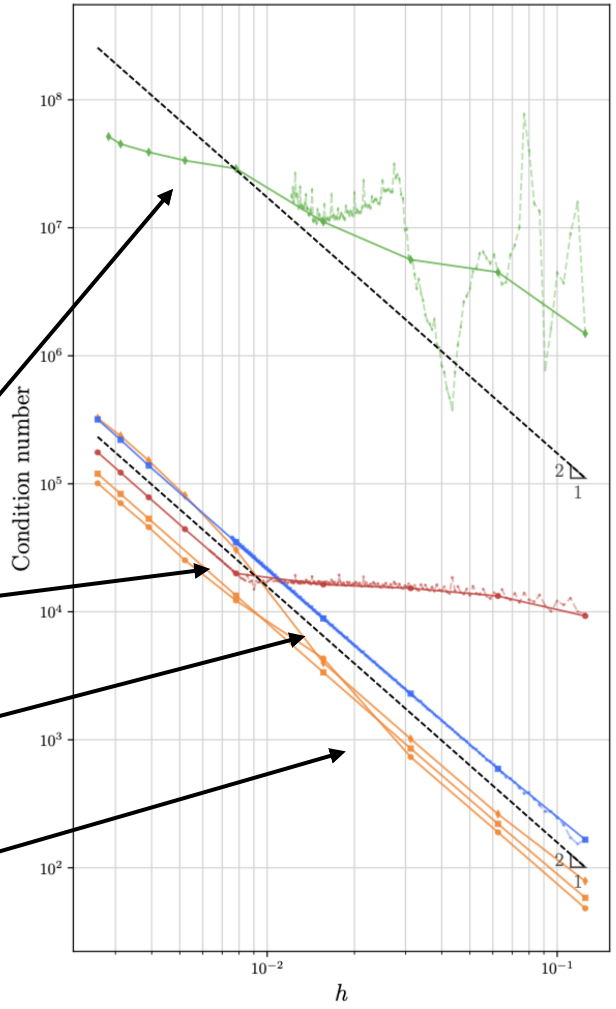

condition number vs h

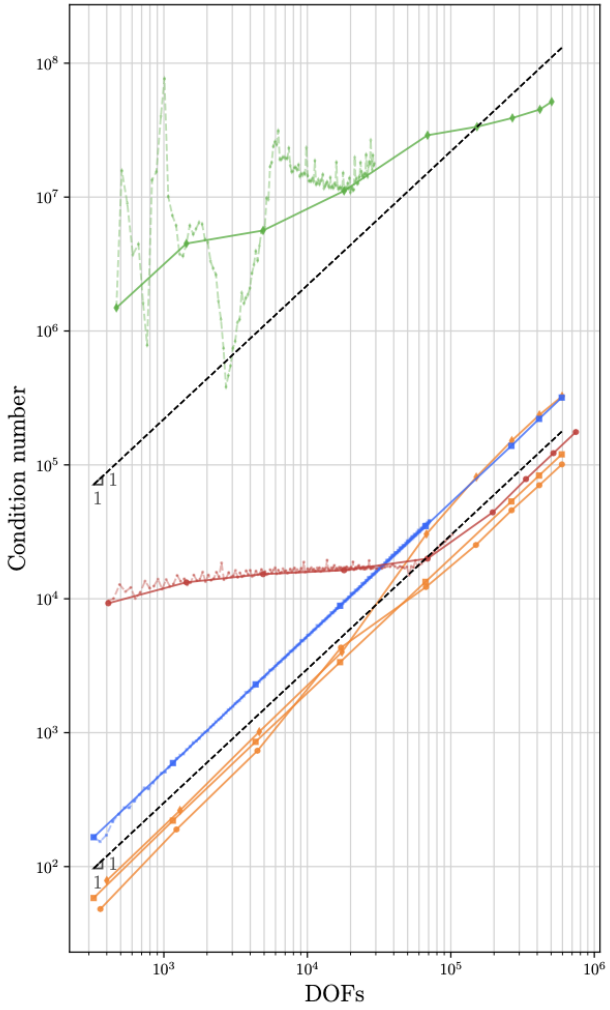

condition number vs DOFs

Conclusions of Publication III

- Penalty-free coupling for nonconforming multipatch discretizations
- Optimal convergence under arbitrary refinement and parametrization mismatch
- No additional DOFs: gap contributions transferred to active basis functions
- Local refinement through multipatch
- Favorable conditioning preserved

This makes Gap-SBM a promising route for flexible CAD-integrated multipatch analysis

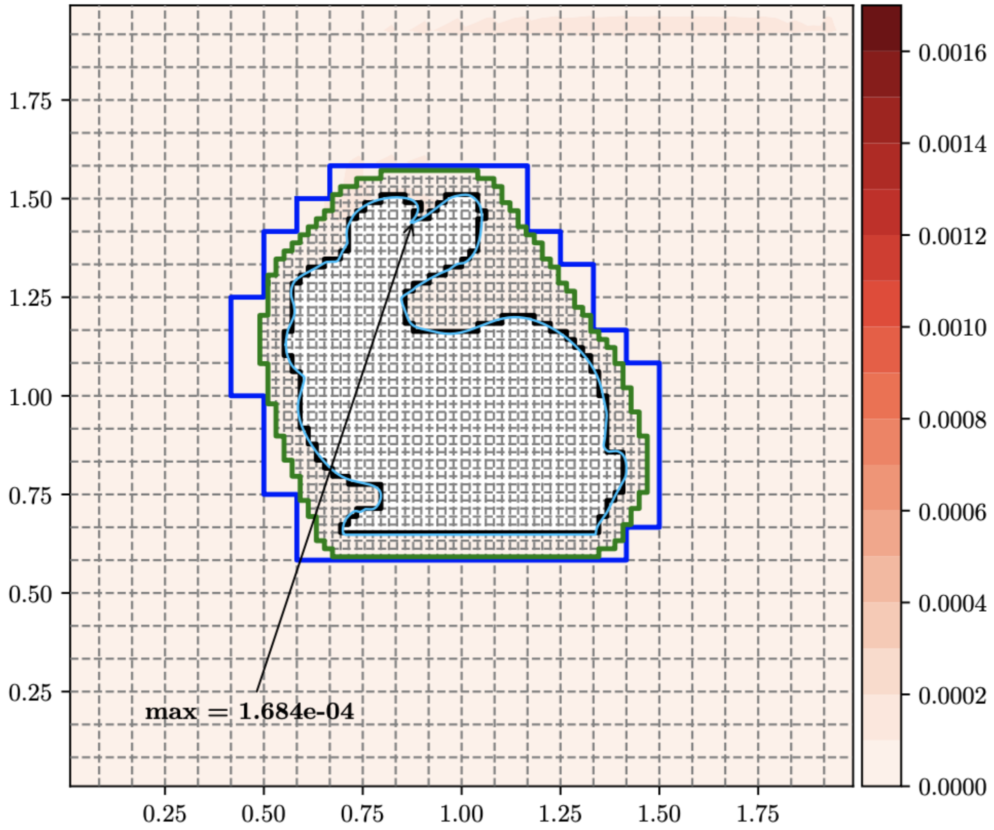

Additional developments and applications

Turek CFD benchmark

- Framework: **transient Navier–Stokes** with SBM-IGA (2D and 3D)

- Implemented in the open-source software *Kratos Multiphysics*

Turek CFD benchmark

- Framework: **transient Navier–Stokes** with SBM-IGA (2D and 3D)
- Implemented in the open-source software *Kratos Multiphysics*
- Validated on the Turek CFD benchmark [17]

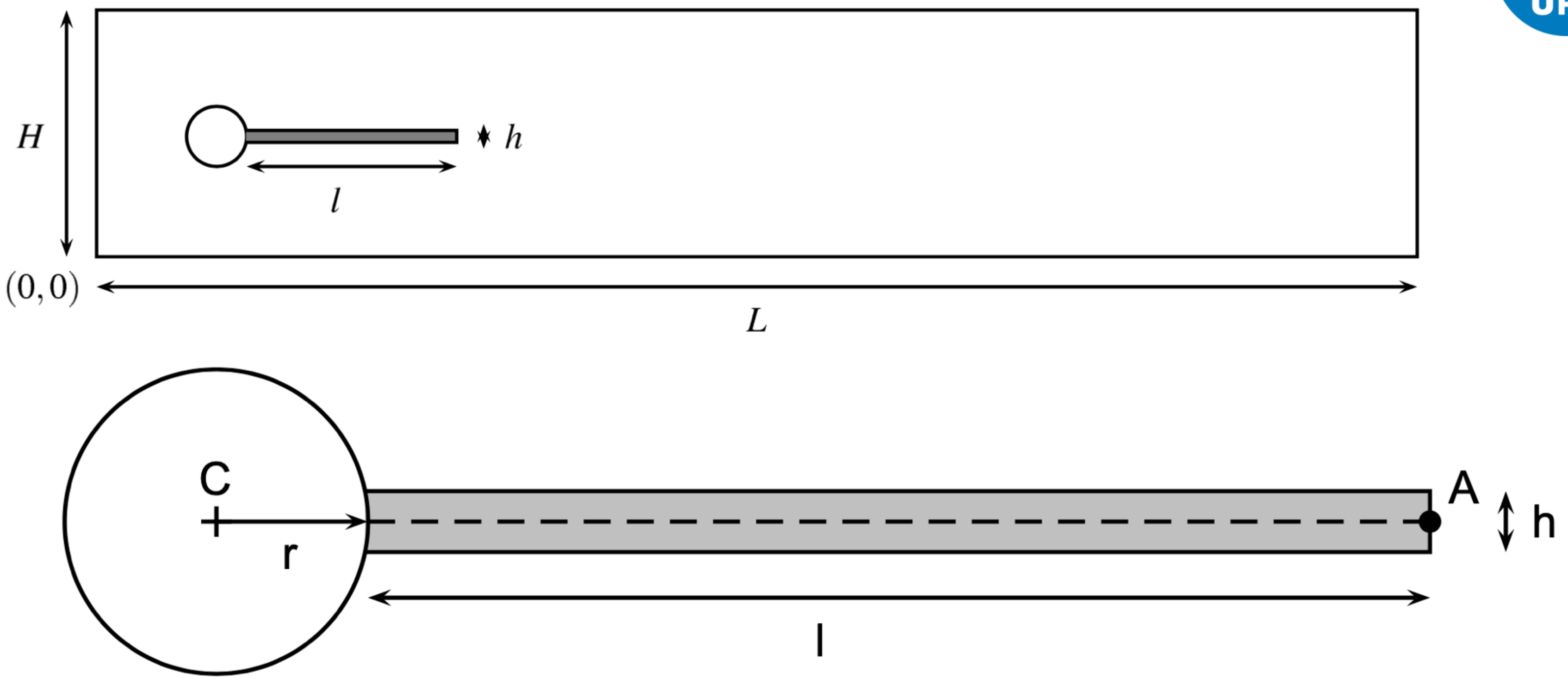

Turek problem geometry. Image taken from [17]

[17] Turek, Hron, Razzaq, Wobker, Schäfer. *Numerical Benchmarking of Fluid-Structure Interaction: A comparison of different discretization and solution approaches*. In *Fluid Structure Interaction II*, 2010.

Turek CFD benchmark

- Framework: **transient Navier–Stokes** with SBM-IGA (2D and 3D)
- Implemented in the open-source software *Kratos Multiphysics*
- Validated on the Turek CFD benchmark [17]

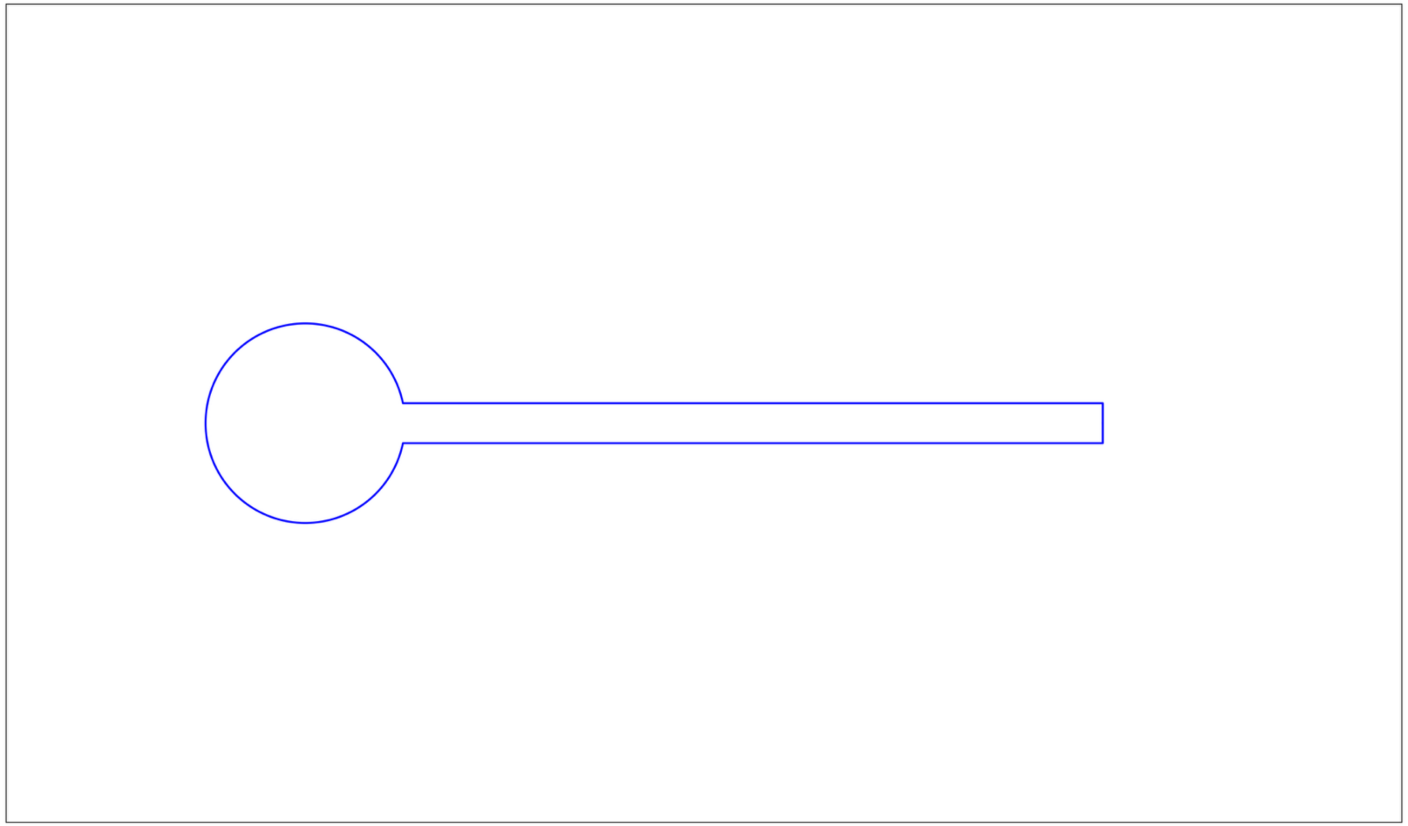

[16] Turek, Hron, Razzaq, Wobker, Schäfer. *Numerical Benchmarking of Fluid-Structure Interaction: A comparison of different discretization and solution approaches*. In *Fluid Structure Interaction II*, 2010.

Turek CFD benchmark

- Framework: **transient Navier–Stokes** with SBM-IGA (2D and 3D)
- Implemented in the open-source software *Kratos Multiphysics*
- Validated on the Turek CFD benchmark [17]

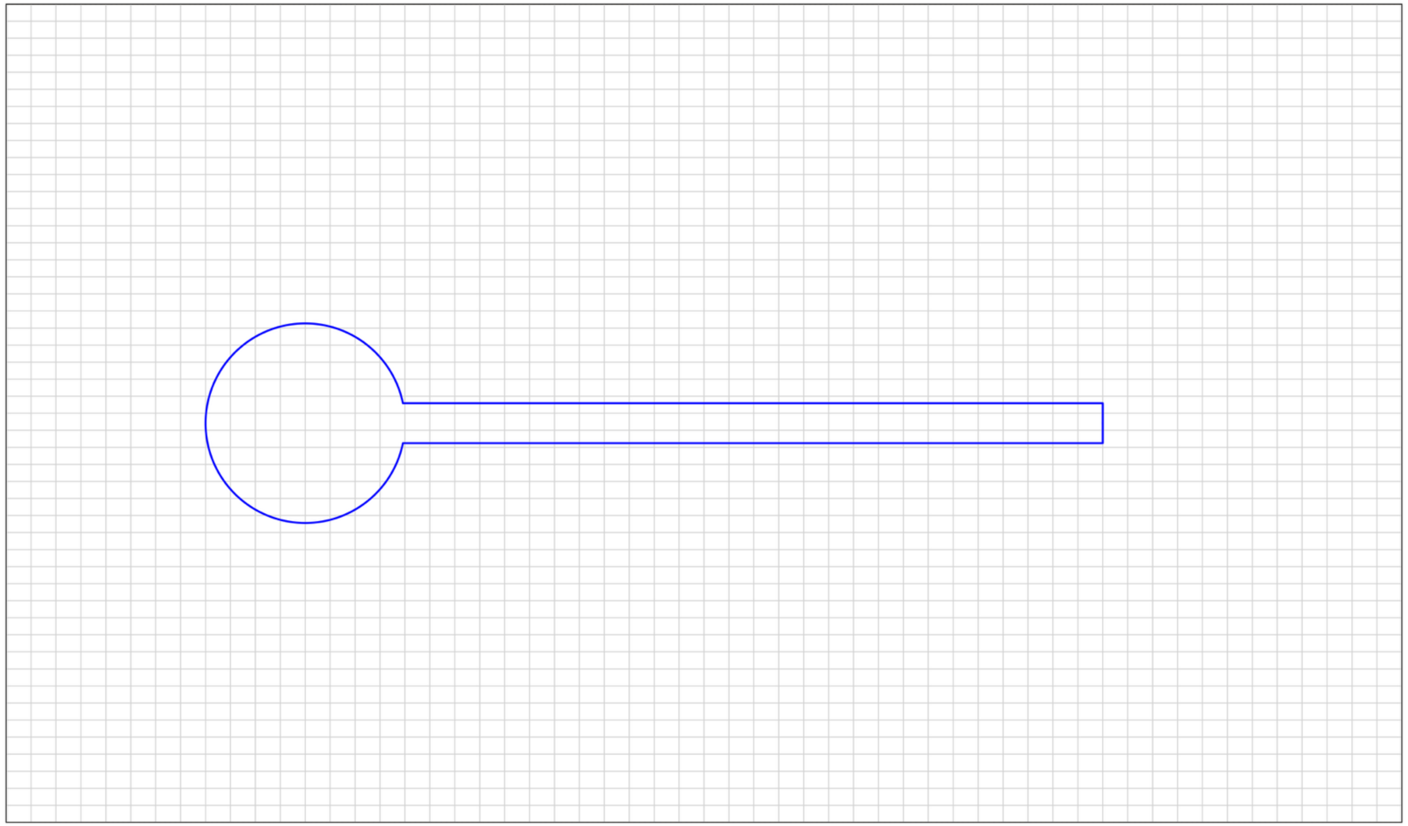

[16] Turek, Hron, Razzaq, Wobker, Schäfer. *Numerical Benchmarking of Fluid-Structure Interaction: A comparison of different discretization and solution approaches*. In *Fluid Structure Interaction II*, 2010.

Turek CFD benchmark

- Framework: **transient Navier–Stokes** with SBM-IGA (2D and 3D)

- Implemented in the open-source software *Kratos Multiphysics*

- Validated on the Turek CFD benchmark [17]

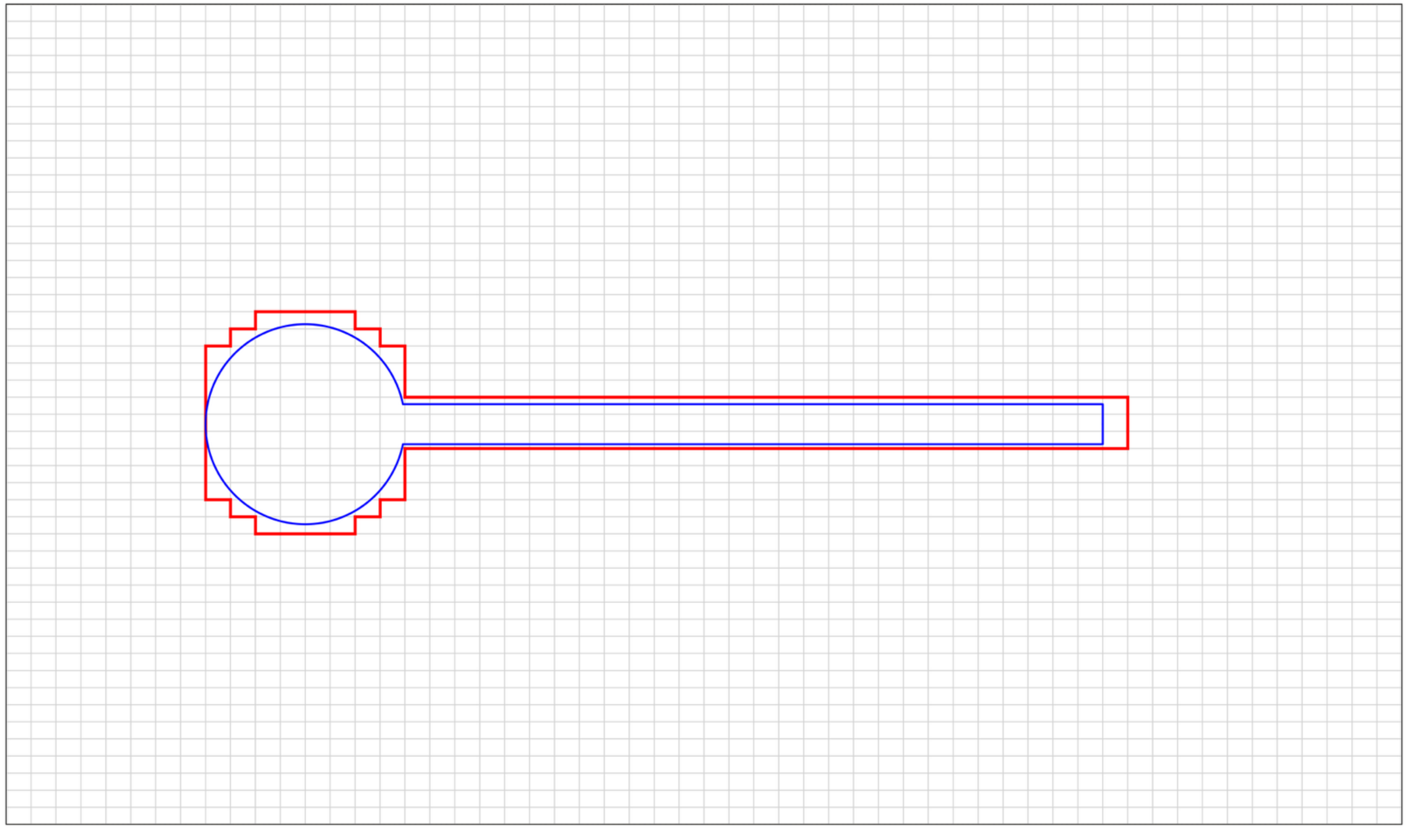

[16] Turek, Hron, Razzaq, Wobker, Schäfer. *Numerical Benchmarking of Fluid-Structure Interaction: A comparison of different discretization and solution approaches*. In *Fluid Structure Interaction II*, 2010.

SBM-IGA vs Body-fitted FEM

FEM body-fitted
h = 0.001, p=1

Velocity

Pressure

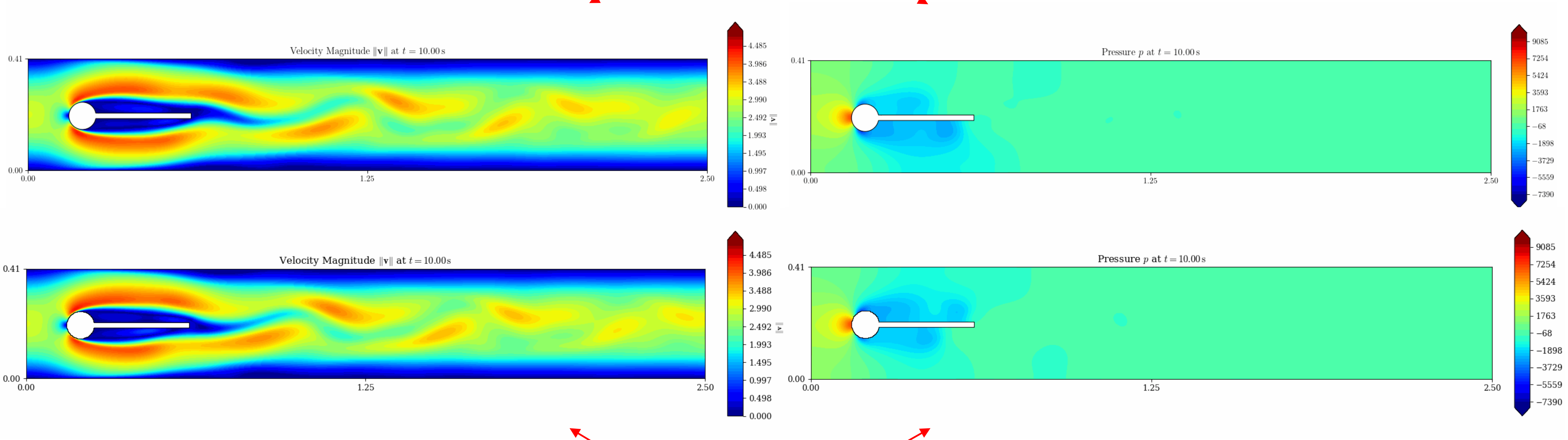

SBM-IGA
h = 0.001, p=1

SBM-IGA vs Body-fitted FEM

Drag and lift comparison of the Turek benchmark for *t=[9,9.6]*

Nek5000
Turek and Hron
→ reference body-fitted

Mesh5, p = 1; Mesh3, p = 1
Mesh2, p = 2; Mesh2, p = 3
Mesh4, p = 2; Mesh2, p = 3

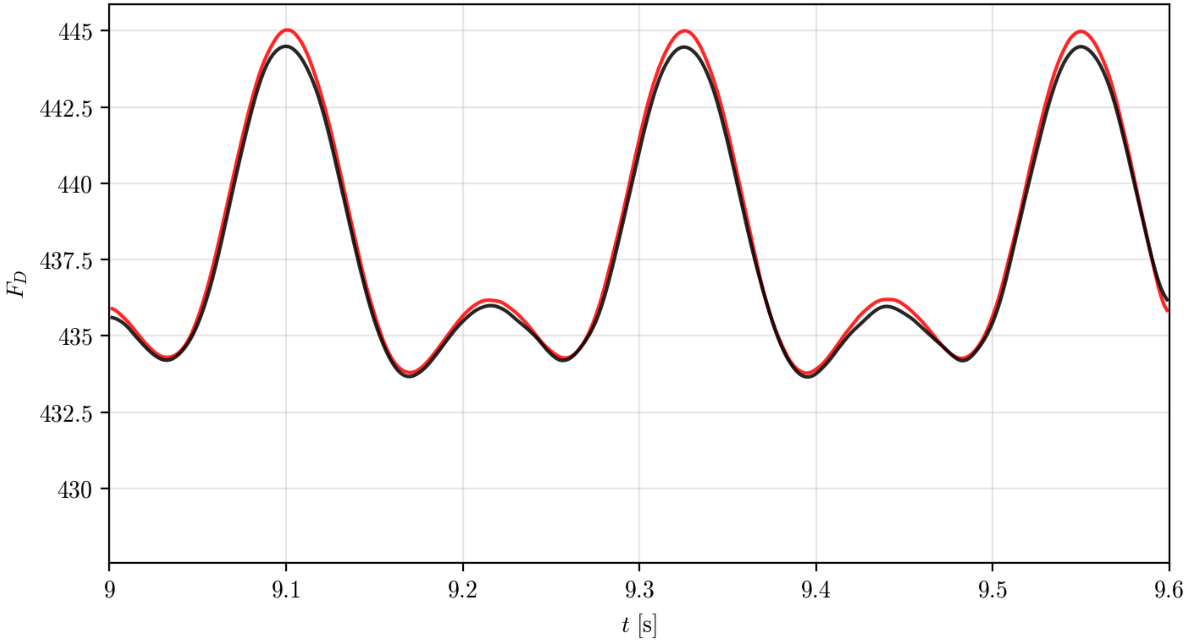

Drag

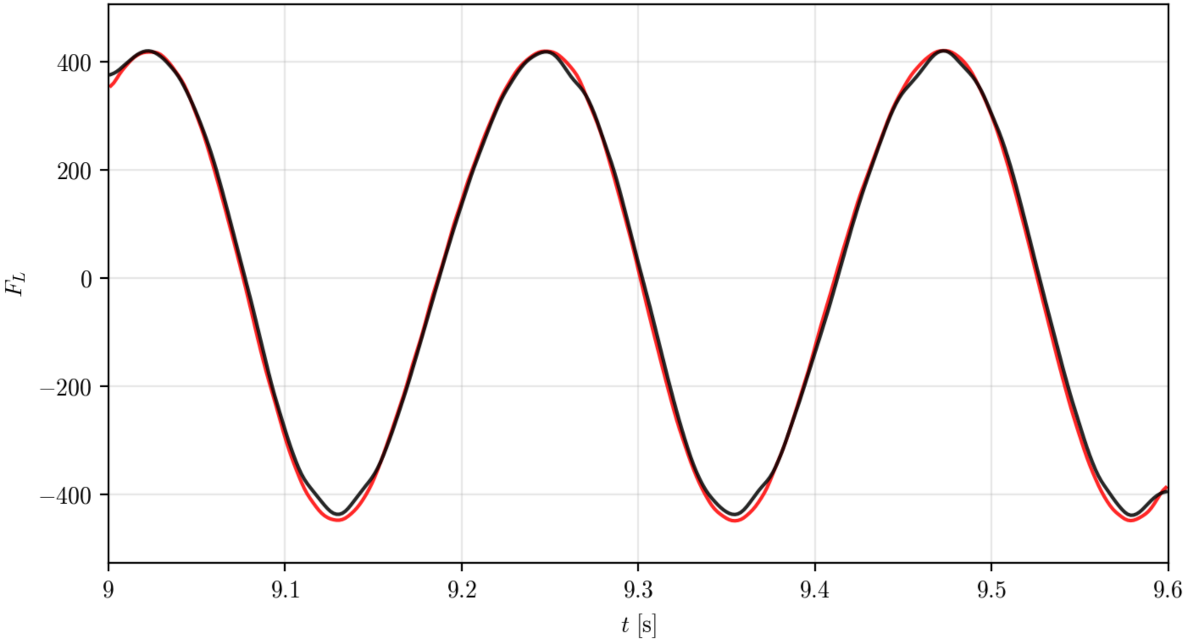

Lift

SBM-IGA vs Body-fitted FEM

Drag and lift comparison of the Turek benchmark for *t=[9,9.6]*

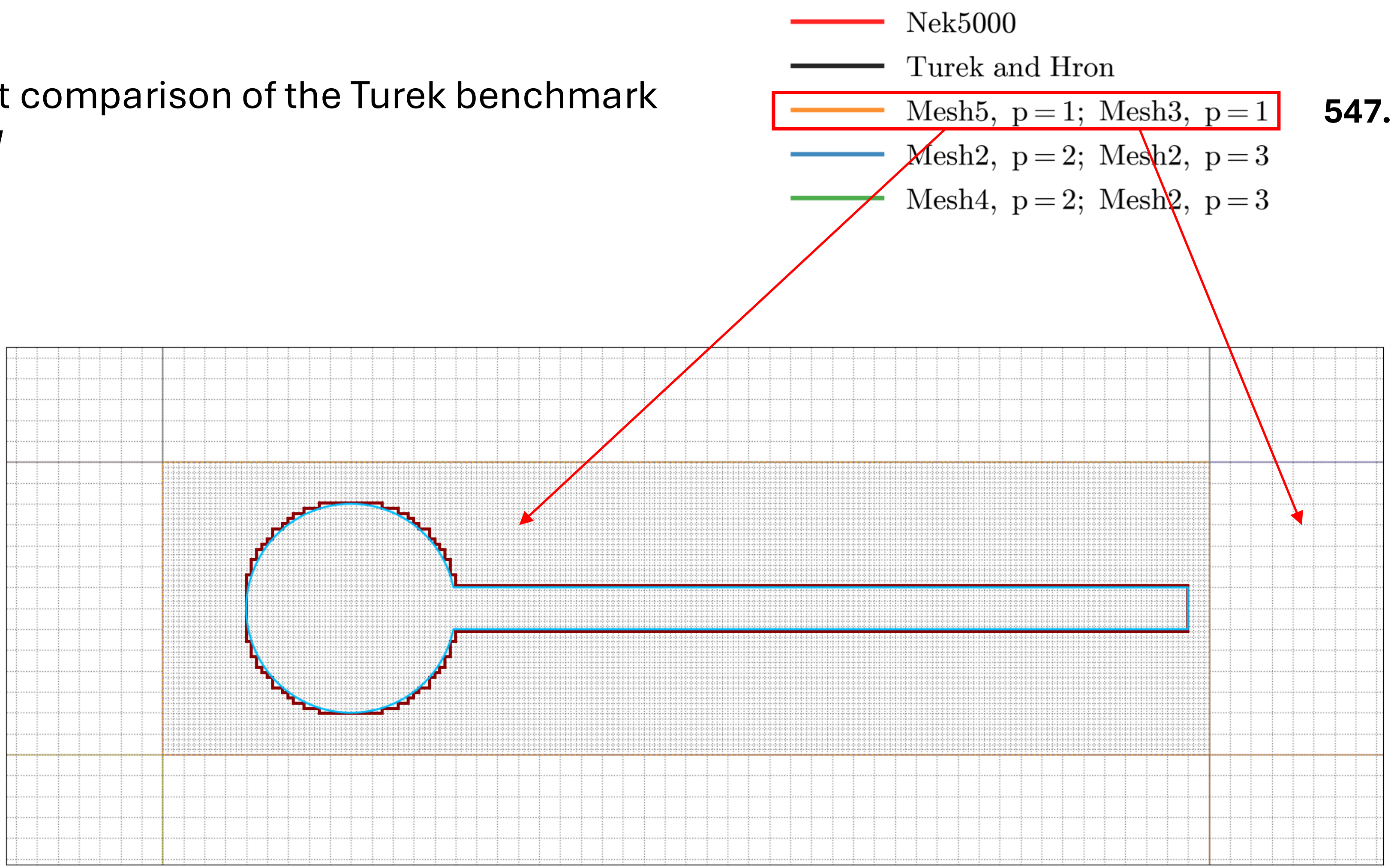

547.848 dofs

SBM-IGA vs Body-fitted FEM

Drag and lift comparison of the Turek benchmark for *t=[9,9.6]*

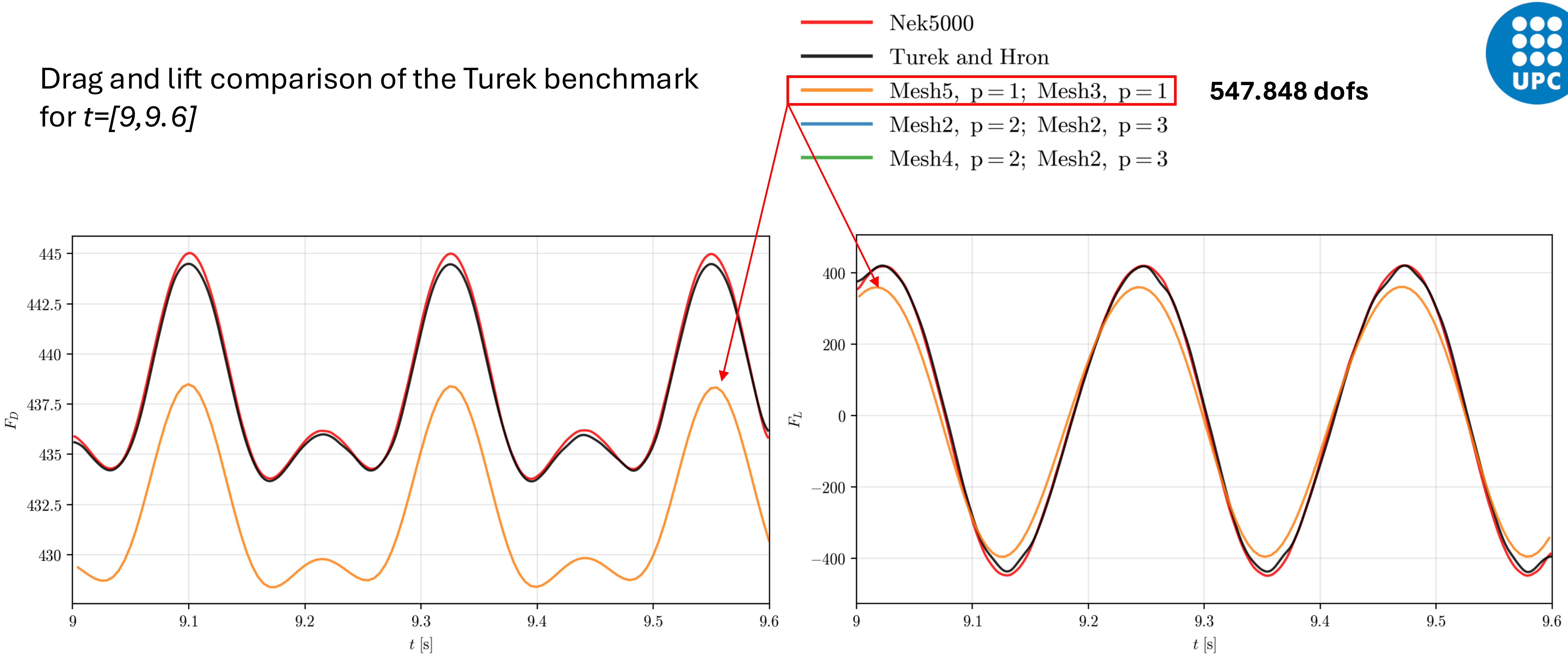

547.848 dofs

Drag

Lift

SBM-IGA vs Body-fitted FEM

Drag and lift comparison of the Turek benchmark for *t=[9,9.6]*

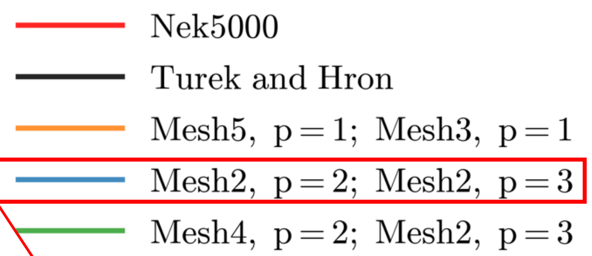

547.848 dofs

44.103 dofs

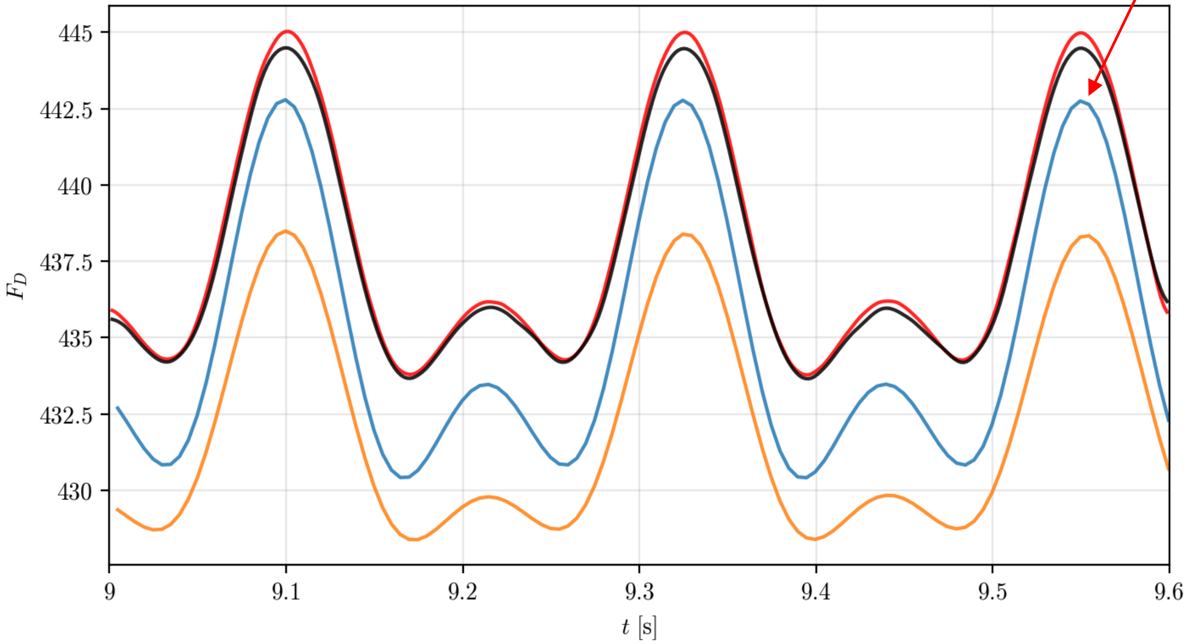

Drag

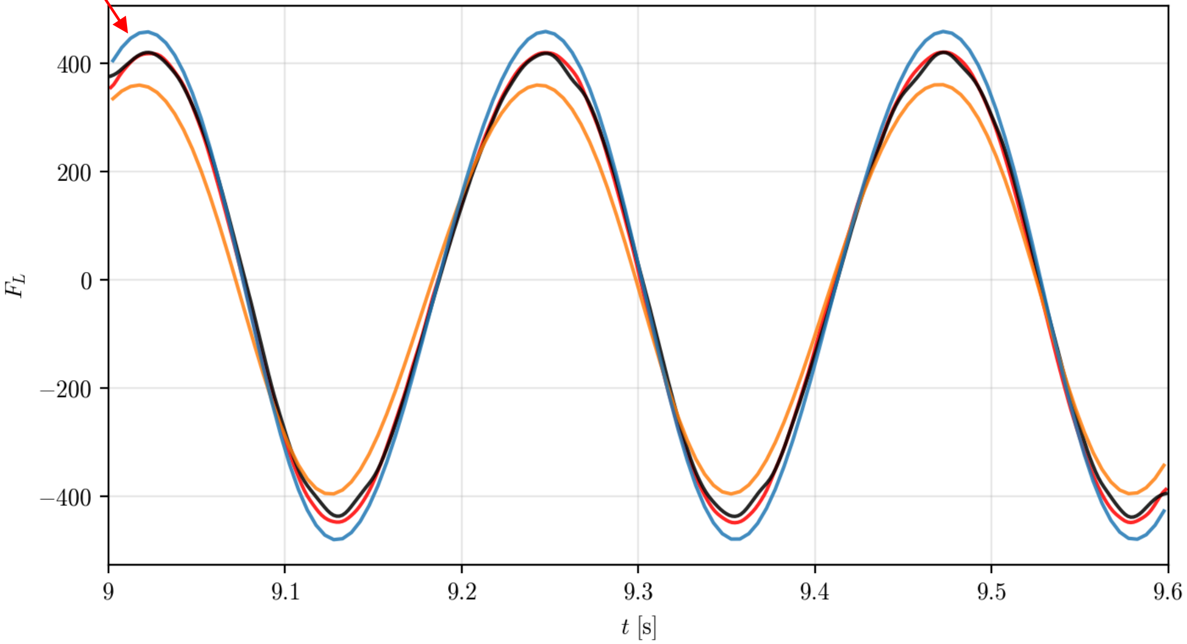

Lift

SBM-IGA vs Body-fitted FEM

Drag and lift comparison of the Turek benchmark for *t=[9,9.6]*

Nek5000

Turek and Hron

Mesh5, p = 1; Mesh3, p = 1 547.848 dofs

Mesh2, p = 2; Mesh2, p = 3 44.103 dofs

Mesh4, p = 2; Mesh2, p = 3 **147.303 dofs**

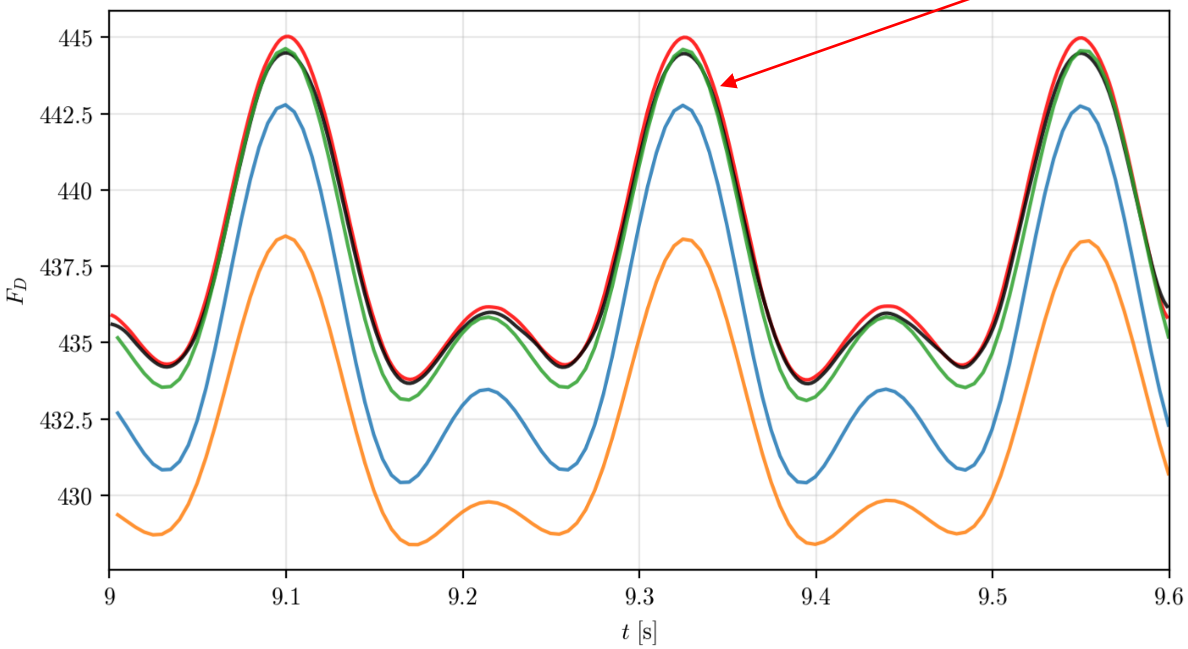

Drag

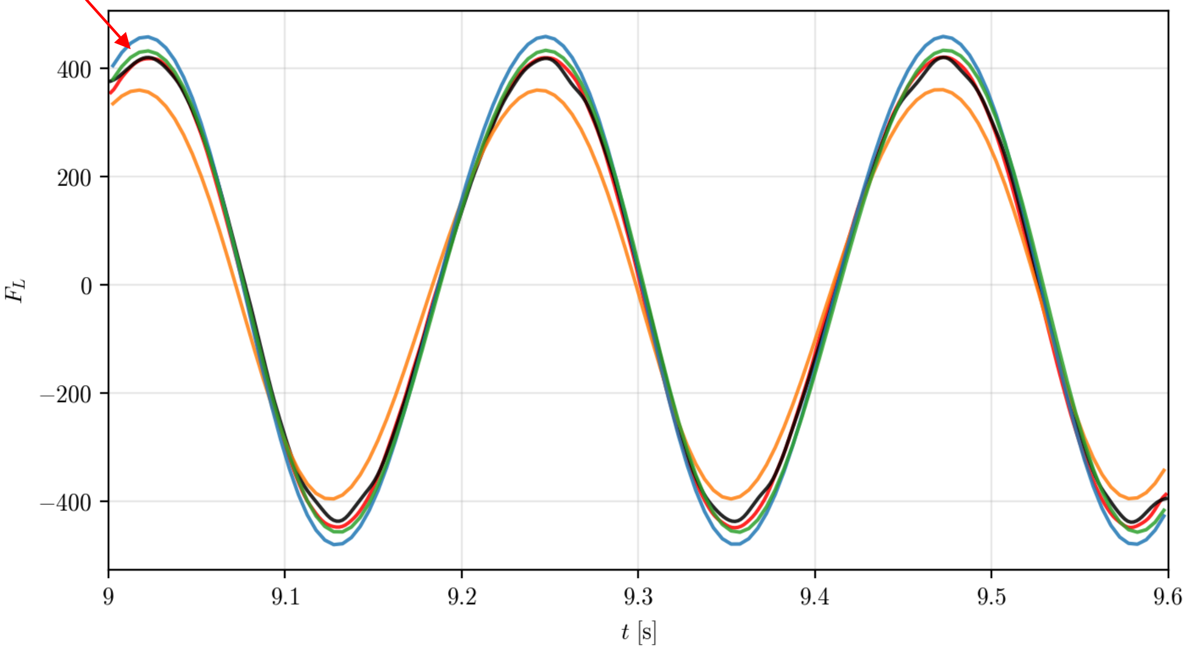

Lift

3D examples

Fluid flow around a sphere

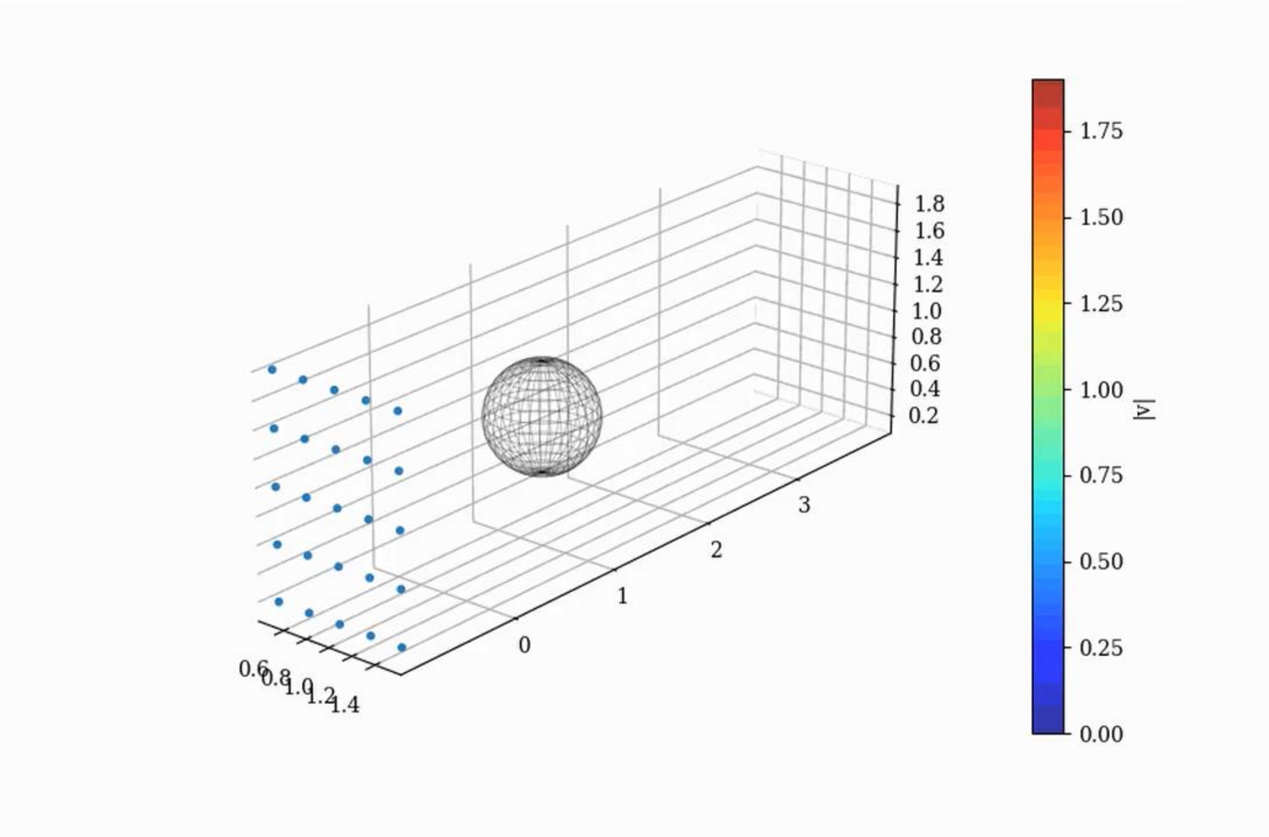

Body-fitted FEM

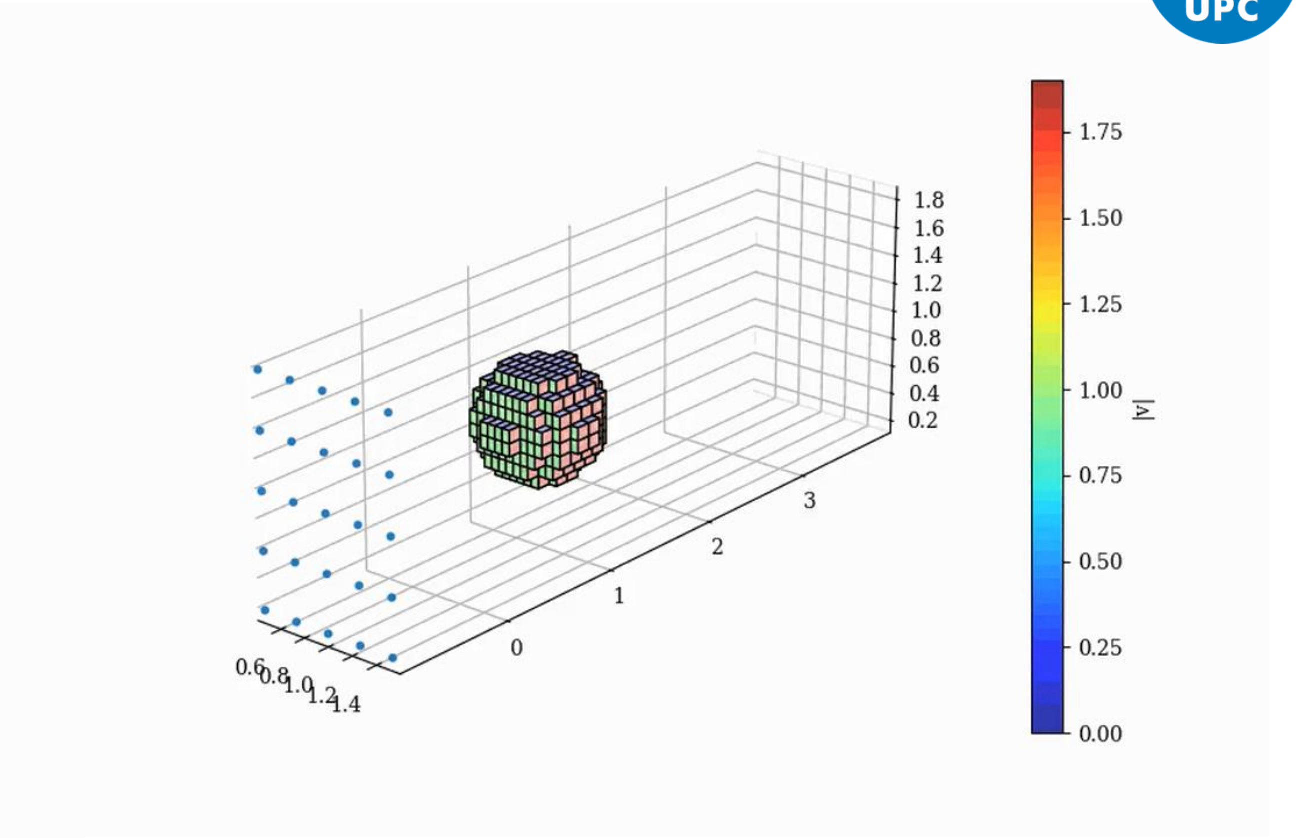

SBM-IGA

3D examples

Fluid flow around a 3D Stanford bunny

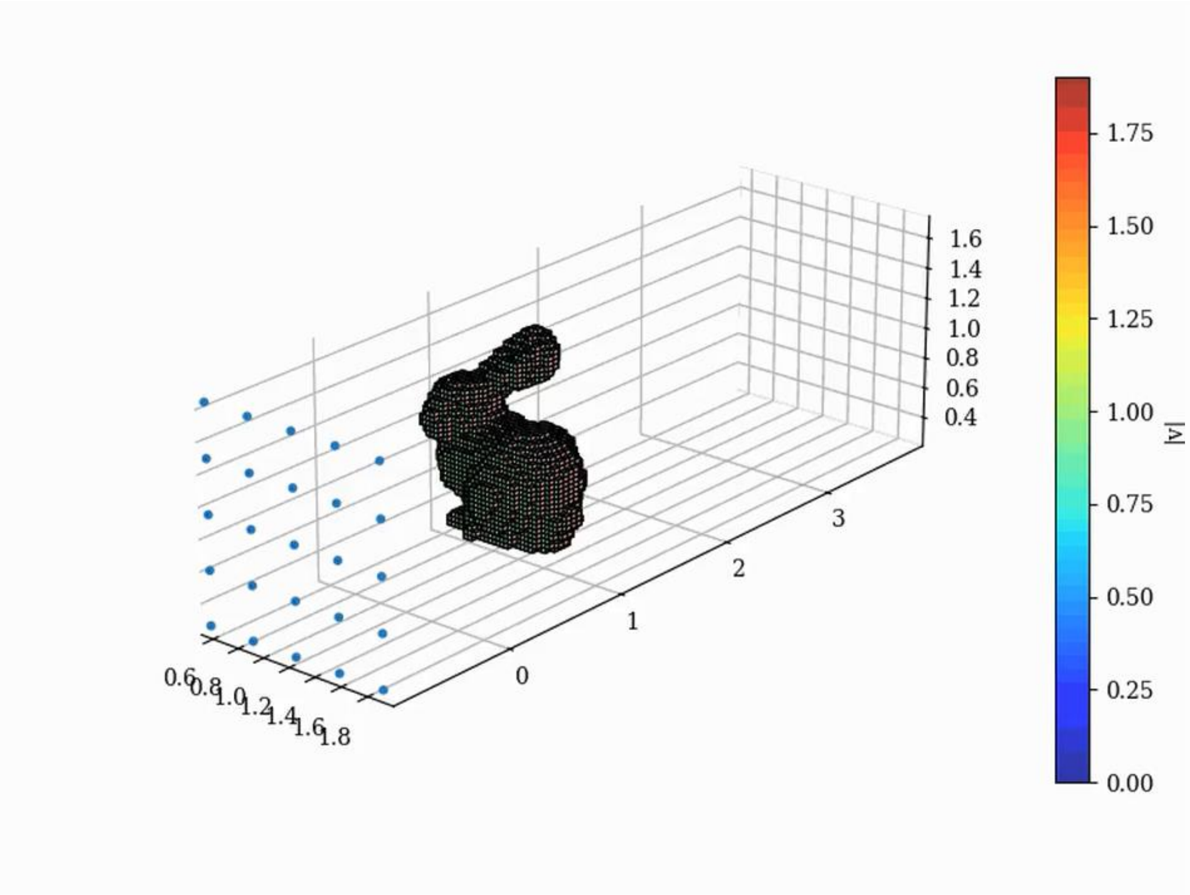

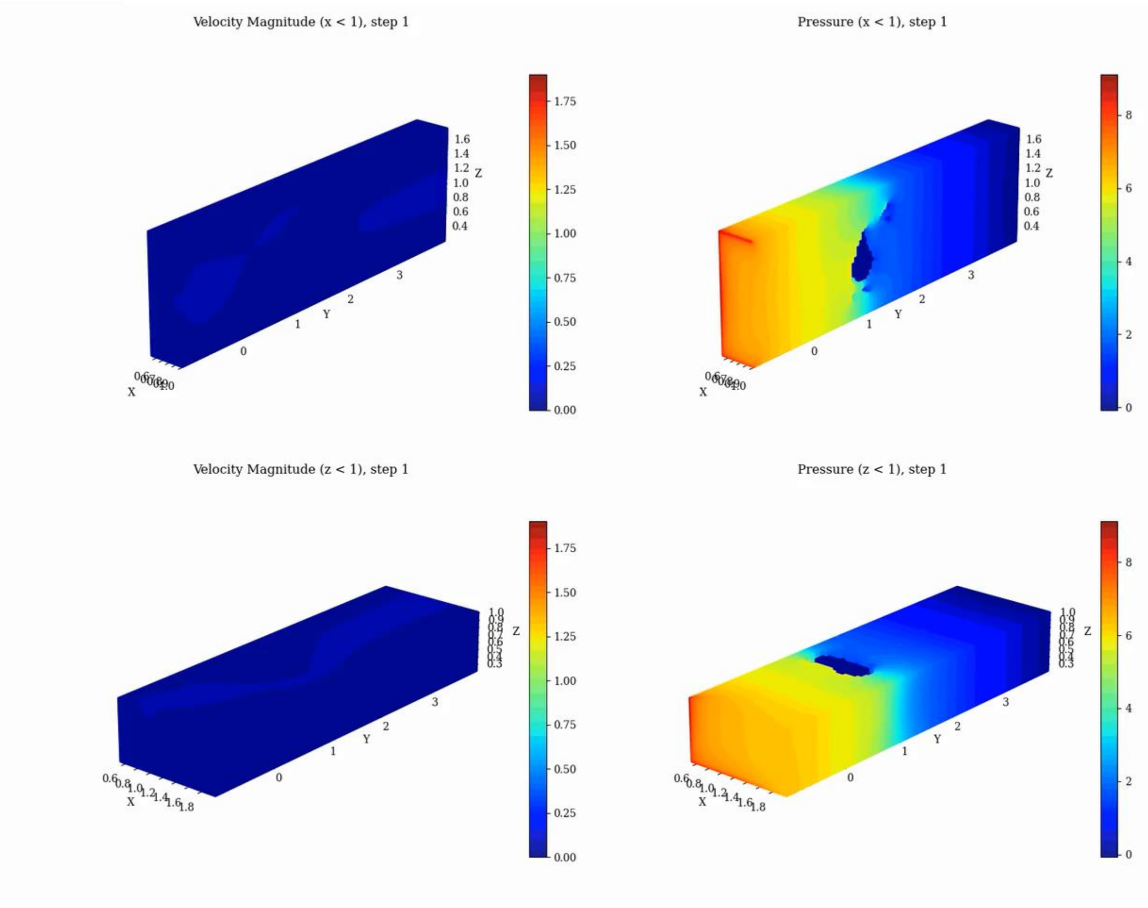

3D examples

Fluid flow around a car

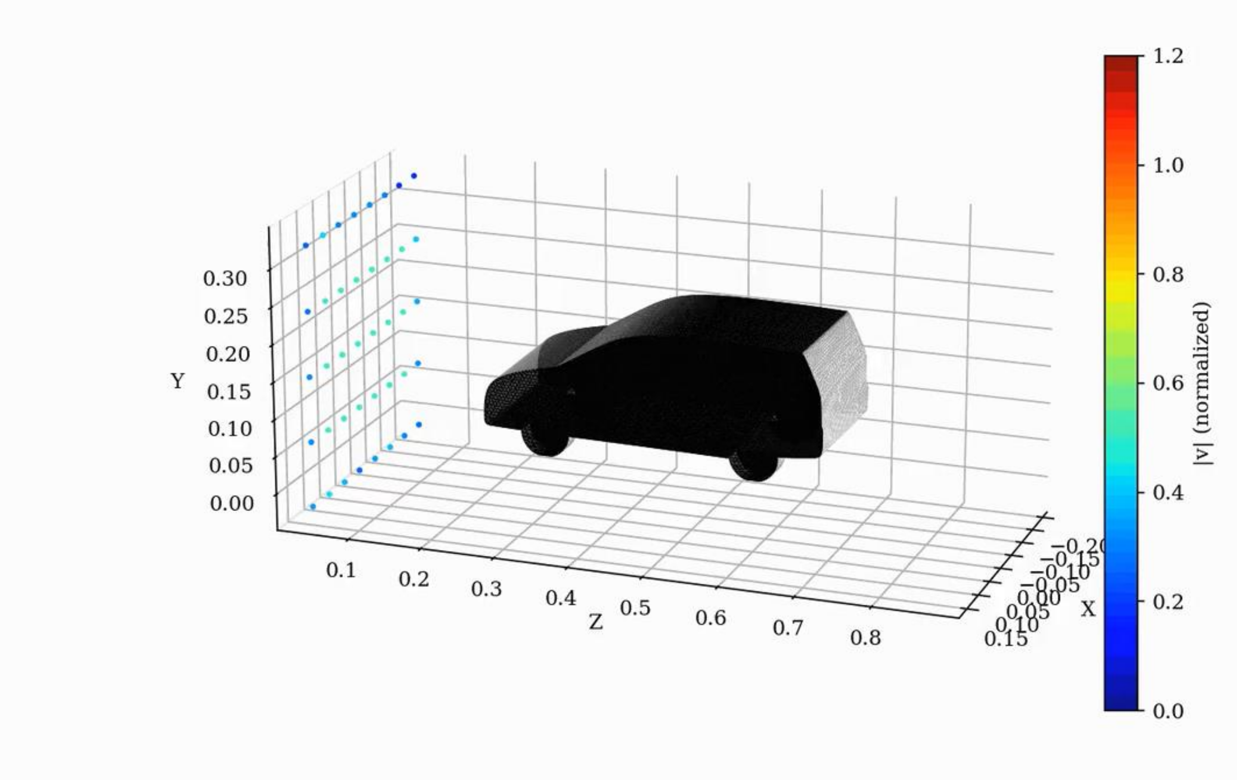

Body-fitted FEM

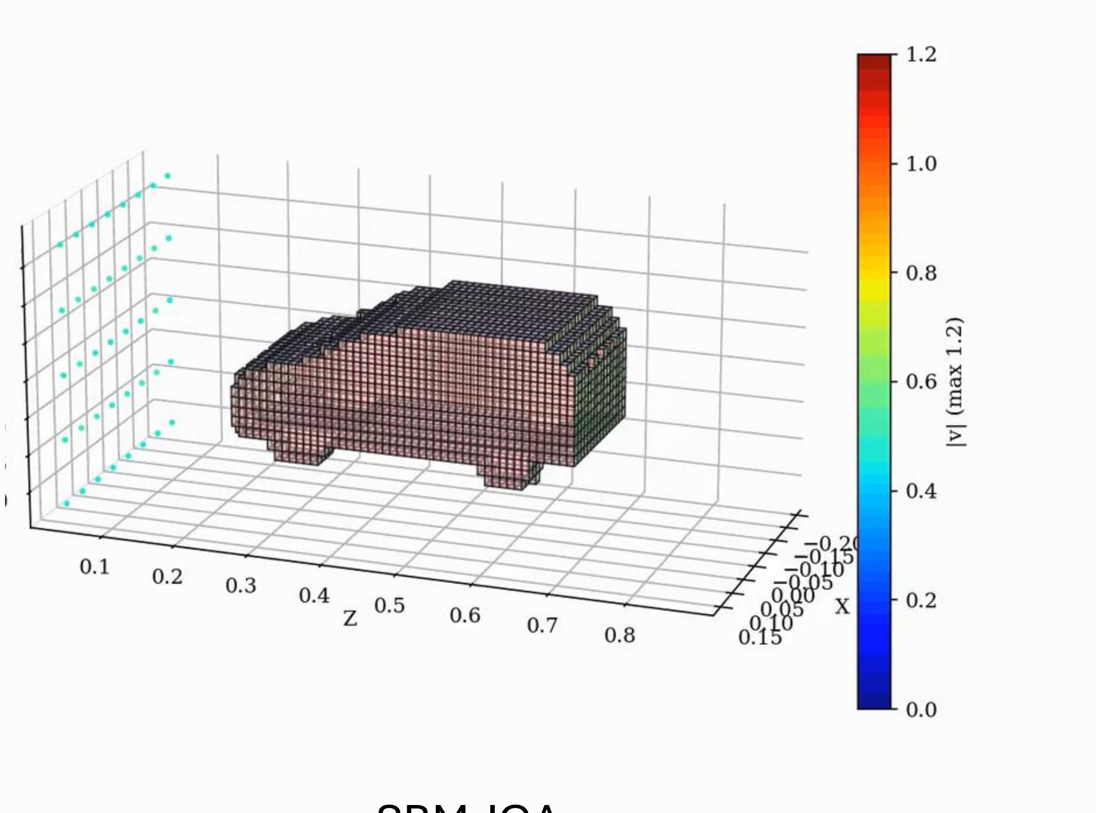

SBM-IGA

Conclusions, limitations and future

This thesis demonstrated that the SBM can be successfully integrated within IGA, resulting in a framework that is:

1. cut-cell-free embedded framework
2. geometrically flexible also in 3D
3. high-order accurate
4. well-conditioned

Conclusions, limitations and future

This thesis demonstrated that the SBM can be successfully integrated within IGA, resulting in a framework that is:

1. cut-cell-free embedded framework
2. geometrically flexible also in 3D
3. high-order accurate
4. well-conditioned

Limitations:

- The optimal treatment of Neumann boundary conditions is still an open issue for classical SBM
- In case of non-Newtonian fluids higher order power of IGA is probably more a disadvantage; local h-refinement and polynomial order reduction is essential
- The Gap-SBM framework has not yet been extended to fully three-dimensional configurations

Conclusions, limitations and future

This thesis demonstrated that the SBM can be successfully integrated within IGA, resulting in a framework that is:

1. cut-cell-free embedded framework
2. geometrically flexible also in 3D
3. high-order accurate
4. well-conditioned

Limitations:

- The optimal treatment of Neumann boundary conditions is still an open issue for classical SBM
- In case of non-Newtonian fluids higher order power of IGA is probably more a disadvantage; local h-refinement and polynomial order reduction is essential
- The Gap-SBM framework has not yet been extended to fully three-dimensional configurations

Future:

- Moving boundary problems
- Fluid Structure Interaction (FSI)
- 3D Gap-SBM & 3D multipatch coupling

Research output and dissemination

Publications

- The Shifted Boundary Method in Isogeometric Analysis, CMAME, 2024
- Isogeometric analysis for non-Newtonian viscoplastic fluids: challenges for non-smooth solutions, CMAME, 2025
- Isogeometric Multipatch Coupling with Arbitrary Refinement and Parametrization Using the Gap-Shifted Boundary Method, CMAME, 2026

Additional ongoing works

- *The Isogeometric Gap-Shifted Boundary Method*
- *Local h-, p-, and k-Refinement Strategies for the Isogeometric Shifted Boundary Method Using THB-Splines*
- *The Shifted Boundary Method for Acoustic Frequency Domain Problems*

Conferences

- ECCOMAS 2024, Lisbon; CEYDA 2024, Bilbao; ISMA 2024, Leuven; NOVEM 2025, Garmisch; YIC 2025, Pescara

Secondments / research visits

- BETA CAE Systems, Thessaloniki, 3-month industrial secondment (2025)
- University of Pavia,1-month research visit (2026)

Acknowledgements

This project has received funding from the European Union's Horizon Europe research and innovation programme under grant agreement No 101073106 Call: HORIZON-MSCA-2021-DN-01.

Views and opinions expressed are however those of the authors only and do not necessarily reflect those of the European Union. Neither the European Union nor the granting authority can be held responsible for them.

Gecko

Design for IGA-type discretization workflows

Funded by the European Union

Thanks for your attention!

Nicolò Antonelli

MSCA

UPC